

Department of Precision and Microsystems Engineering

Experimental quantification of gripper limits determined by product detachment in a practical set up: applied on high-speed case packing of packaged food

B. Cleijpool

Report no : 2021.091

Coach : ir. A.E. Huisjes, ir. V. Peters

Professor : Prof.dr.ir.J.L. Herder

Specialisation : MSD

Type of report : Master's Thesis

Date : 26-nov-2021

Declaration of Authorship

I, Bram CLEIJPOOL, declare that this thesis titled “Experimental quantification of gripper limits determined by product detachment in a practical set up: applied on high-speed case packing of packaged food” and the work presented in it are my own. I confirm that:

- This work was done wholly and mainly while in candidature for a research degree at this University.
- Where any part of this thesis has previously been submitted for a degree or any other qualification at this University or any other institution, this has been clearly stated.
- Where I have consulted the published work of others, this is always clearly attributed.
- Where I have quoted from the work of others, the source is always given. With the exception of such quotations, this thesis is entirely my own work.
- I have acknowledged all main sources of help.
- Where the thesis is based on work done by myself jointly with others, I have made clear exactly what was done by others and what I have contributed myself.

Signed: 

Date: 19-11-2021

“Shoot for the moon, even if you miss you will land between the stars”

DELFT UNIVERSITY OF TECHNOLOGY

Abstract

3mE

High-Tech Engineering

Msc Mechanical Engineering

Experimental quantification of gripper limits determined by product detachment in a practical set up: applied on high-speed case packing of packaged food

by Bram CLEIJPOOL

The detachment of a product from a suction cup gripper is a challenge that emerged in recent years in the high-speed case packing of packaged food. In this industry suction cups are used to temporarily attach a product to a case packing robot. The detachment of products from the suction cup gripper threatens throughput. In some cases, the industry notes robots to operate at only 40 picks per minute. This is 30 % of their maximum throughput.

This study aims to gain a better understanding of the dynamic grasping strength of suction cups. This was done by reviewing the state-of-the-art from industry and state-of-the-practice from literature. It was found that suction cups are the best overall gripper class, and that actuation time poses the main limiting factor for other grippers to perform well in this industry.

Secondly, a six-axis force moment sensor that passes airflow for gripper actuation and without limiting the pull-out load measurement performance was designed, fabricated, and validated. With the current sensor technology, the vacuum hose must be placed over the sensor, leading to the generation of parasitic loads. Passing the airflow through the sensor structure is essential to eliminate loads otherwise induced by the stiff vacuum hose. The sensor was designed using strain gauges and a Maltese cross sensor. Finite Element Modeling and optimization using sequential quadratic programming was used to determine the dimensions of the sensor. The sensor validation showed a maximum measurement error of 8% in the F_z direction. Lastly, with the validated sensor, the dynamic grasping strength of compliant and stiff suction cups was measured using motion paths and products that are typically seen in the packaged food industry. For both the stiff and compliant suction cups, the moment around the axis perpendicular to the plane of motion showed to be a leading factor in detachment of a product from a suction cup gripper. The failure of stiff suction cups is explained by impulse loading, this results in peaks in the load in the horizontal direction and the moment perpendicular to the plane of motion. For the compliant suction cups, the detachment was found to be caused by accelerating downwards while the product was not in the center of the gripper.

These results have led to the recommendation of two gripper designs. The first, is a suction cup-underactuated hybrid gripper. The second design intently provides rotation freedom to reduce the moment loading on the suction cup. The second design requires input-shaping to reduce the vibrations at the end of the motion cycle.

Preface

In front of you lies the thesis "Experimental quantification of gripper limits determined by product detachment in a practical set up: applied on high-speed case packing of packaged food". Detachment describes the loss of contact between a gripper and a product. This project has been performed to fulfill the graduation requirements for the master High Tech engineering at Delft University of technology. I was engaged in researching and writing this thesis from September 2020 to November 2021.

The implementation of robots in the agriculture and food (agri-food) industry is a rapidly growing market, which, according to literature, has a large and growing amount of research funding [1], [2],[3].

The agri-food industry operates as a chain consisting of three main steps; growing and harvesting of food; processing food into products; packing of processed food products. The packing step can be split up into two separate processes; the packing of unpackaged processed food into a container, and packaging containers into cardboard boxes or crates, making the food product ready to be shipped. This research will solely focus on case packing of pre-packaged food, which is often automated with robots.

The case packing of packaged food products has already made large steps towards automation. Nevertheless, the challenge of products detaching from the robotic grippers still remains. To ensure practical relevance while addressing this challenge this study was conducted in collaboration with BluePrint Automation (BPA) as part of the FLeXCRaFT project. FlexCRAFT is a Dutch research initiative which aims to strike a collaboration between industry and academia. This research is funded by BPA as part of their contribution to the FlexCRAFT project. The results of this study are intended to guide engineers in the designing of robotic gripper for high-speed case packing of flexible products.

Knowledge on detachment of flexible products from robotic grippers is limited, making this project challenging. Setbacks as investigating dead-ends in search of a good study strategy in combination with the corona pandemic proved to be a unique personal challenge. Fortunately, fellow graduation students and engineers at BPA were always willing to help me, keeping me motivated and giving me inspiration to spark new ideas.

I would like to thank my supervisors ir. V. Peter, ir. A.E. Huisjes and Prof.dr.ir J.L Herder for their guidance and their excellent support. Knowing that there was somebody to turn to at TU Delft and BPA when enduring challenges, was paramount for the completion of this thesis.

To my other colleagues at BPA and the staff at TU Delft involved in fabrication of the six-axis force moment sensor, I would like to thank you for your help and amazing cooperation.

Debates with friends also benefited me in resolving challenging issues. Especially ing. Rick Koolmees, ir. Lucy Bennett and Jos van Driel deserve thanks for their help.

I would like to thank Rick for helping me with writing the software required for the final part of the research and Lucy for teaching me a lot about scientific writing. The help Jos provided with gluing the strain gauges, setting up the data acquisition system and teaching me how to use the amplifier was essential in the fabrication process of this study.

My girlfriend, family and parents are deserving of particular note. They supported me throughout the entire year of research, from celebrating the ups together to helping me get up again during the downs. Their kind words, thoughts and council have always served me well.

I hope reading this thesis makes you a little wiser.

Bram Cleijpool

Woerden, 26 November, 2021

Introduction

In recent years, a problem regarding detachment of products from robotic grippers during case packing of packaged food has emerged. The high-speed pick and place (P&P) motion induces a dynamic loading which the grippers are not able to withstand, meaning that the product detaches from the gripper [4]. Industry observed that detachment occurs when the case packing robots only operate at 30% of their maximum operating speed. Solving this challenge could lead to a throughput increase of 200%.

There are multiple ways of solving the detachment challenge. For example, the robot path could be optimized for holding capabilities, which has already been done for serial robots considering rigid objects [5]. Extending this work to parallel robots would certainly increase the maximum throughput and would decrease error rate. However, results presented in literature do not show a 200% performance increase [5]. Another option could be to add an extra actuator to the robot platform orienting the object in the most desirable direction, essentially creating a controlled mass-spring-damper system integrated into the robot platform. However, this solution would add moving mass to the robot platform, which is undesirable for high-speed dynamic motions. These two solution directions will therefore not be considered in this work. Another possibility is to change the robot's gripper so that it better suits the requirements for high-speed case packing considering packaged food. This limitation will be the scope of this research because it considers the source of the product detachment from a gripper.

To temporarily attach a product to a robot, suction cup grippers are typically used in the packaged food industry, an example of which is shown in Figure 2a. Suction cups are primarily used in this industry, because they are light and economical, and have an easy on-off control.

To keep up with the increasing demands of the food chain, P&P robots should be operating at their maximum throughput. The maximum throughput is defined as the highest amount of pick and place cycles that can be obtained by one case packing robot per minute without product detachment. In reality, achieving zero detachments is impossible. Therefore, a detachment rate of 0.1% is deemed as an acceptable error rate by industry. To achieve these demands, BPA and other case packing companies typically use delta robots as is shown in Figures 1 and 2b. For these delta robots, a maximum throughput of 120 picks per minute can be achieved for a 1.0 kg load with a P&P distance of 400 mm. To accomplish such a high throughput, grippers on the case packing line accelerate with 100-120 m/s^2 and move with speeds between 5-10 m/s . This performance is comparable to the commercially available and well known ABB flexpicker [7].

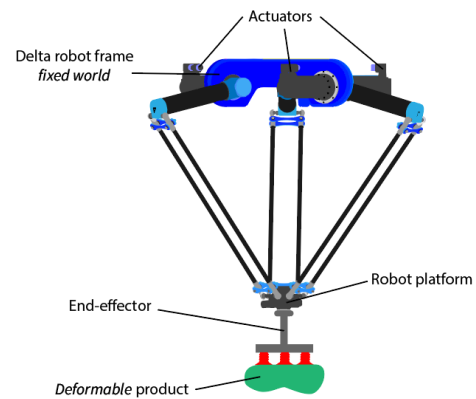
The packaged food industry observed that this maximum throughput is rarely achieved. Some products detached from the gripper at relatively low P&P speeds of 30 to 40



FIGURE 1: Photo of robotic case packing at BluePrint Automation [6]



(A) Image of a standard suction cup based end effector



(B) A drawing of the robots used by BPA

FIGURE 2: Figures show the currently used system

PPM. This effect has also been observed in literature and limits the throughput of case packing lines [5], [8]. An explanation could be the wider application of robots in the food industry [9]. Objects previously packed by dexterous human hands are now packed by robots.

In light of this challenge, this study aims to identify the limitations of robotic grippers under dynamic conditions, including flexible products. The main contribution of this study is a structured approach to determine the pull-out load of grippers in a practical experimental setting. This pull-out load is defined as the load which causes detachment between the gripper and its product. The pull-out load is in this study for the first time considered as a combination of the forces and moments.

This thesis is structured in the following way. Chapter 1 reviews the state-of-the-practice and state-of-the-art grippers. The reviewed grippers are classified and graded to identify their limitations. Chapter 2 details the design, fabrication and validation

of a sensor designed to pass airflow without influencing the measurement performance. This sensor addresses the knowledge gap identified in Chapter 1. Chapter 3 presents measurements into the dynamic grasping strength of suction cups, obtained using the sensor designed in Chapter 2. In the final two sections, the results are discussed and the overall conclusion from all three previous chapters is drawn.

Chapter 1

State-of-the-art robotic grippers and their limitations when applied in the packaged food industry during high-speed case packing

Abstract

A literature review was started in light of an emerging challenge in the case packing industry for packaged food: detachment. The detachment issue was observed by the industry, and it was noted that certain food products detached from the robotic gripper at 30% of the robots maximum operating speed. To address this issue, a review of the state-of-the-art literature and state-of-the-practice by the industry has been performed. This review set out to answer the question: *What are the limitations of state-of-the-art robotic grippers when applied in the packaged food industry during high-speed case packing?* By creating a gripper classification graded according to 10 criteria found during the state-of-the-art literature review, the main limiting factors of each gripper class were determined. Actuation time showed to be the largest limiting factor consisting of 20.8% of the average limitation. Notably, research focusing on reducing the actuation time is very limited. The other most prominent limitations are the capability to hold force, operate in a confined space and the capability to hold moment, contributing to 16.2%, 15.4% and 15.0% of the average limitation respectively. The best overall gripper was selected to be used as the suction cup gripper.

1.1 Introduction

Research in case packing has focused on improving throughput by decreasing cycle times of case packing robots [10]–[12]. This has been achieved through improvement of mechanical design and control of the used robots, for which an assortment of literature exists [11], [13]–[15]. Efficient path planning in combination with advances in motor and robotic vision technology [10], [16], [17] have reduced the cycle times for industrial robots.

An emerging challenge in the automated case packing industry is now seen: detachment of products during manipulation. Detachment is where grippers lose contact with their product before the maximum operating speed is achieved. Detachment threatens throughput; in the worse case, industry notes robots to operate at only 40 picks per minute. This is 30 % of their maximum throughput [4]. However, whilst many challenges in the case-packing industry are clear - such as the combination of very low cycle times and flexible products - research has only very recently identified detachment as a limiting factor [5], [8].

In pursuit of higher throughput, grippers specifically for the application of high-speed packing have been researched by industry. For example, a recent study presented the structured design of an array of suction cups able to pack multiple drug boxes at once [18]. This method reduced the amount of motion cycles a robot had to perform in order to reach the same amount of picks, and is known as 'multi-pick' in the industry. The effectiveness of this strategy is only limited because of the increased robot loading.

Other strategies for dealing with detachment found in the industry include increasing vacuum level, adding more robots to a case packing line and trial-and-error gripper selection. These solutions are not ideal and have limited effectiveness, because they lead to product wrapper damage, increase case packing line cost, and lack structure for guaranteed improvement.

The lack of research about grippers in combination with demands for the high-speed packing of food and the lack of structured implementation of state-of-the-art advances by industry could be the reason for the emergence of the detachment issue [19].

The literature and knowledge on grippers and gripping is, however, extensive. Research is driven by other fields such as fruit and vegetable harvesting, low speed food handling, prosthetic hand design, general industrial automation, marine environment gripping, soft robotics and many more [18], [20]–[25].

The knowledge and designs from these studies can help during development of grippers for high-speed case packing of food. To review the available literature in a structured manner, grippers are grouped by unifying features, creating a gripper classification. Depending on the field of study, these classifications are based on different aspects.

In literature, many classifications fitting the specific needs of certain fields of interest have been presented [20], [26]–[29]. By using a classification, grippers can be compared and graded on a fundamental level. Nevertheless, a gripper classification specially focused on the high speed case-packing of packaged food does not yet exist.

This Chapter focuses on the review of state-of-the-art grippers in literature and state-of-the-practice in industry. This review is used to answer the following question: *What are the limitation of state-of-the-art robotic grippers when applied in the*

packaged food industry during high-speed case packing? By answering this question, the limiting factors for grippers improvement addressing packaged food for the high-speed case packing industry were identified, enabling the determination of knowledge gaps that require further research. In addition, insight was gained into the implementation of state-of-the-art advances by the industry.

This study is performed in three parts: the state-of-the-practice is reviewed to gain a better insight into the problems seen in industry, the literature study is performed to make a gripper classification, and a set of grading criteria is set up with the knowledge gained from reviewing the state-of-the-practice. The different gripper classes are graded with Analytical Hierarchy Process (AHP) using data collected while studying literature required to create gripper classification. By using a grading system, limiting factors for all gripper classes in the high speed case packing of packaged food are determined, thereby answering the research question. Subsequently, the most suited gripper class is determined according to the grading system. The remainder of this paper is structured as follows: in section 1.2 the state-of-the-practise is reviewed, followed by a literature review considering the state-of-the-art in section 1.3. The gripper grading system is presented in section 1.4. The results of these three study steps is discussed in section 1.5. Finally, concluding statements are presented in section 1.6.

1.2 State-of-the-practice review

1.2.1 State-of-the-practice review method

To gain insight into the state-of-the-practice of high-speed case packing for packaged food three questions were answered by reviewing the available data from industry. In this section the method used to answer the questions will be provided.

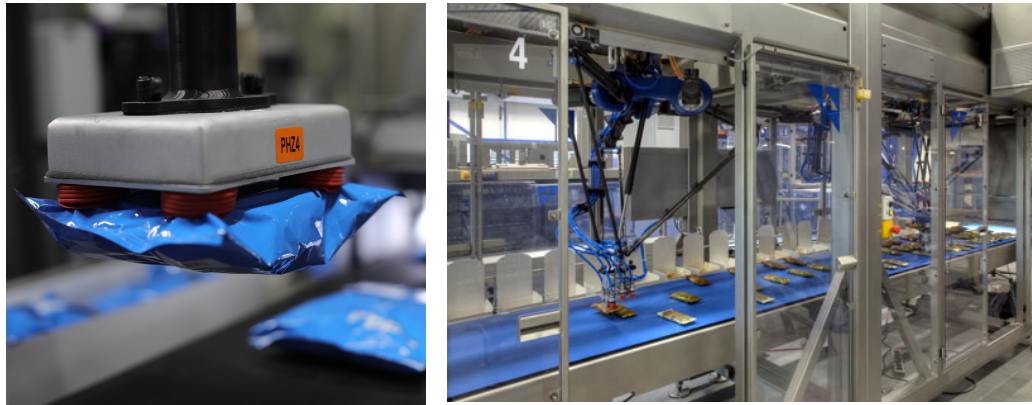
1. What is the current method of case packing packaged food products?
This question was answered by reviewing the modern case packing lines found in the packaged food industry.
2. For which products does detachment occur?
This question was answered by considering the performance data from approximately 200 case packing lines made available by industry. Product groups were determined according to these data. A product group has unifying mechanical characteristics which influence their behavior for high speed case packing. The pick and place speed for each product group was determined according to the considered case packing lines.
3. At what part of the motion path does the error occur?
By review high-speed footage of products breaking off the gripper the error sensitive areas were determined. This insight is used to help set up grading criteria in section 1.4.

1.2.2 State-of-the-practice review results

What is the current method of case packing packaged food products?

The current state-of-the-practice product handling in the packaged food industry is done using parallel robots [9], [30], [31]. Parallel robots, such as delta robots shown in Figure 1.1b, are known for their high rigidity and low moving mass desirable for high speed motion.

Figure 1.1a shows a typical gripper for P&P in the packaged food industry. In this gripper, suction cups are used because they are light, cheap and have an easy on-off control. In addition, they have been used because of tradition. Suction cups have been used in the P&P industry for the past decade without many issues. In lower speed food packing applications other simple one degree control grippers are also found [12], [31], [32].



(A) image of a standard suction cups based gripper (B) Photo of robotic case packing of packaged food from industry [6]

FIGURE 1.1: Figures showing the system currently used by industry

For which products does detachment occur?

From the considered industrial applications five different product groups were determined. The mechanical properties of each product group is distinctly different. The product groups are listed and explained below.

1. **Solid products**, a well defined shape which does not change under load
2. **Elastically deformable products**, a well defined shape in static equilibrium but allows for some elastics deformation under load.
3. **Liquid pouches**, a sealed deformable membrane containing a liquid
4. **One mass in a foil**, a sealed deformable membrane containing one large mass which is able to move freely inside the foil
5. **Masses in a foil**, a sealed deformable membrane containing multiple small masses which are able to move freely inside the foil

For each product class the surface of the object can either be smooth or rough resulting in 10 different product classes. Nowadays, the handling of products with rough surfaces is rare within the high speed case packing industry. Therefore, this study will not consider the requirements for handling products with a rough surface in detail.

Table 1.1 shows the result of the performance data analysis of case packing packaged food products by suction cups from industry. It can be seen that the solid class is the only class that can be moved at the maximum robot operating speed of 120 PPM. Masses in a foil can be moved close to the maximum speed, 100 PPM. One mass in a foil already shows a slight decrease in throughput achieving 80 PPM. The elastic

deformable products and solids seem to behave similarly. A slight decrease in performance is expected due to the flexibility of the product. However, not enough data was available to determine a reliable P&P speed.

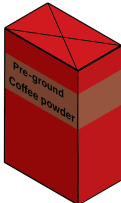
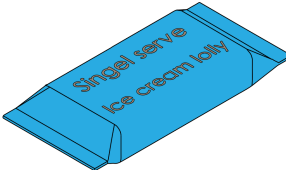
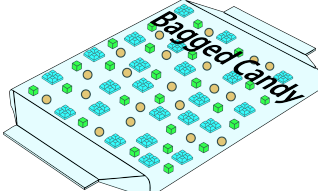
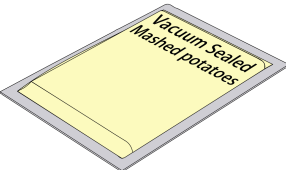
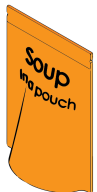
Product group	Example	Expected maximum P&P speed (PPM)
Solid		120
One mass in a foil		80
Masses in a foil		100
Elastic deformable		not enough data
Liquid pouch		40

TABLE 1.1: showing the product classification that was made and the average maximum P&P speed by handling with suction cups, source BPA

At what point in the motion path does the error occur?

By reviewing slow motion footage failure, sensitive regions at the motion path were identified. The first observation is that all product classes detach at the same area. In Figure 1.2, the error sensitive areas are shown in red. The regions rarely showing errors are indicated with green.

Secondly, during the determination of the error sensitive regions two phases were noted: A *grasp* and a *holding phase*. The grasp and holding phase have distinct requirements and can be viewed separately. A good performance in the grasp phase requires a fast actuation time with high precision operating in a confined space. The gripper does only carry the gravity load of the object. In the holding phase the

gripper is required to hold the exerted load generated by the high-speed motion. Following this observation, the case packing manipulation process is categorized by seven consecutive steps that are labelled in Figure 1.2. The first step of the case packing manipulation process starts with a *grasp phase*. The division of the case packing process of seven steps with two phases helps with the determination of grading criteria presented in section 1.4.

1. *Grasp phase*, an object has to be picked from a conveyor belt, labelled 1 in Figure 1.2.
2. *Grasp phase*, the object is moved up horizontally to avoid collision with neighboring objects, labelled 2 in Figure 1.2. Now the object is free from its surroundings, completing the *grasp phase* and starting the *holding phase*.
3. *Holding phase*, the robot moves through a curved spline to ensure a smooth transition to horizontal motion, labelled 3 in Figure 1.2.
4. *Holding phase*, a horizontal motion moves the object near the box, where it needs to be placed, labelled 4 in Figure 1.2.
5. *Holding phase*, the object follows a downward curved spline and is moved above the box, labelled 5 in Figure 1.2. At this stage the object enters the confined space of a box starting another grasp phase
6. *Grasp phase*, the object has to be placed and released in the box, labelled 6 and 7 in Figure 1.2 respectively.

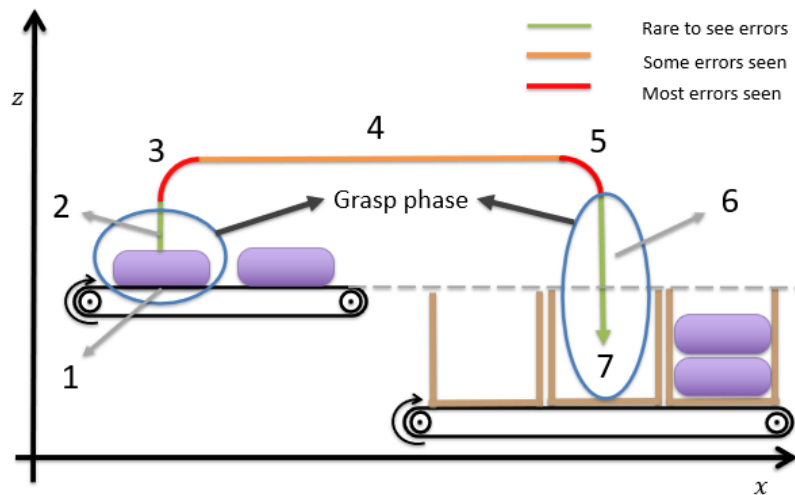


FIGURE 1.2: An overview of a standard the P&P procedure. The line colors show the error sensitive areas of the motion path. The blue circle indicates the grasp phases. The numbers indicate the steps in a P&P procedure: 1 indicates the picking of the object, 2 indicates the obstacle avoidance, 3-5 show the steps achieve the horizontal motion, 6 indicates the movement into the box and 7 indicates the placing

1.3 Literature review

1.3.1 Literature review method

The literature review was performed primarily using the Scopus search engine. Using the the main search query shown in table 1.2. The search was limited to literature in the English language with one of its focus areas labelled as engineering. Furthermore, all micro or nano scale gripper were not considered, because these grippers might not work on a large scale due to scaling laws. These extra filters were added to ensure only relevant literature was reviewed.

The resulting literature was selected based on title, abstract and conclusion. Literature deemed relevant was studied in more detail. The literature presenting relevant data for grading were stored and used during the grading scheme presented in section 1.4.

OR ↓	AND →			
	"end effector"	underactuat*	food	gripp*
	"end-effector"	under-actuat*	industr*	grasp*
	gripper	adaptive	packing	
	grasper	flexible	"P&P"	
	"robotic hand"	soft	prosthetics	
	"scution cup"	industrial	agri*	
			agro	

TABLE 1.2: A table showing the main query used to search literature using the Scopus search engine

1.3.2 Literature review result

Gripper classification

Current gripper literature already presented some classifications. However, considering the high-speed case packing of packaged food an adjusted overview is required to serve the application-field [20], [26]–[29]. Therefore, a new classification considering high-speed case packing for the packaged food industry was made and is shown in Figure 1.3. The classification consists of 5 main branches: Rigid mechanical grippers, Compliant grippers, Pneumatic grippers, Hybrid grippers and Infeasible grippers. Main branches have sub-branches leading to gripper classes. The gripper classification is briefly explained below. The full details of the gripper grading including exemplary pictures can be found in appendix B.

1. *Rigid mechanical grippers*

All mechanical robotic grippers consisting of rigid links and non-compliant parts are placed under this main classification branch. Most traditional robotic grippers fall under this category, which are well established in industry due to their predictability, reliability and availability [33]–[35]. Knowledge and literature on this type of grippers is radially available, due to the many years of research that have already been performed [36].

This gripper type is further subdivided in three gripper classes: Rigid 1 DOF (degree of freedom) grippers [33], [34], rigid fully actuated grippers [37]–[40] and underactuated rigid grippers [23], [41]–[43].

2. *Compliant mechanical grippers*

Compliant mechanical grippers consist of one single compliant structure and

does not contain any traditional rotational or linear joints. In the general classification of compliant mechanisms two main classes are distinguished, lumped and distributed compliance [44]. This classification is also followed in this work resulting in two gripper classes in this main branch: Lumped compliant mechanical grippers [45]–[51] and distributed compliant mechanical grippers [52]–[56].

3. *Pneumatic grippers*

Grippers relying on pneumatic whilst not requiring a mechanical support structure to connect to the object are gathered in this class. This definition was picked to exclude all mechanical grippers using pneumatic cylinders as their actuator from this class.

This gripper type is further divided in vacuum grippers and pressurized air grippers. Vacuum grippers are subdivided in suction cups [26], [57] and structure jamming [58]–[61] gripper classes. Under pressurized air grippers, Bernoulli grippers [62]–[64] and pressurized bellows (also known as soft robotics grippers) [20]–[22], [65]–[67] are classed.

4. *Other grippers*

The literature available on gripping and grippers is more extensive than the gripper classes shown previously. Some other grippers classes were determined but deemed infeasible for high-speed case packing. The gripper classes deemed infeasible are Electro-magnetic grippers [68]–[70], heat based grippers, [71], chemical or nano-scale adhesion based grippers [72], hydraulic grippers [73], [74], and piercing grippers [75]. For a more detailed explanation for their exclusion, see appendix B.

5. *Hybrid grippers*

A hybrid gripper is a combination of two or more of the above mentioned gripper classes [76]–[82]. The goal of a hybrid gripper is to counteract the weak points of one gripper class by combining it with another gripper class that has opposite strength properties. The operating principles of infeasible grippers could even find their place here. In grading the gripper classes, a hybrid gripper can not be placed in one of the other gripper classes. Therefore, this gripper class is excluded from grading. Nevertheless, the importance of this gripper method design should not be underestimated.

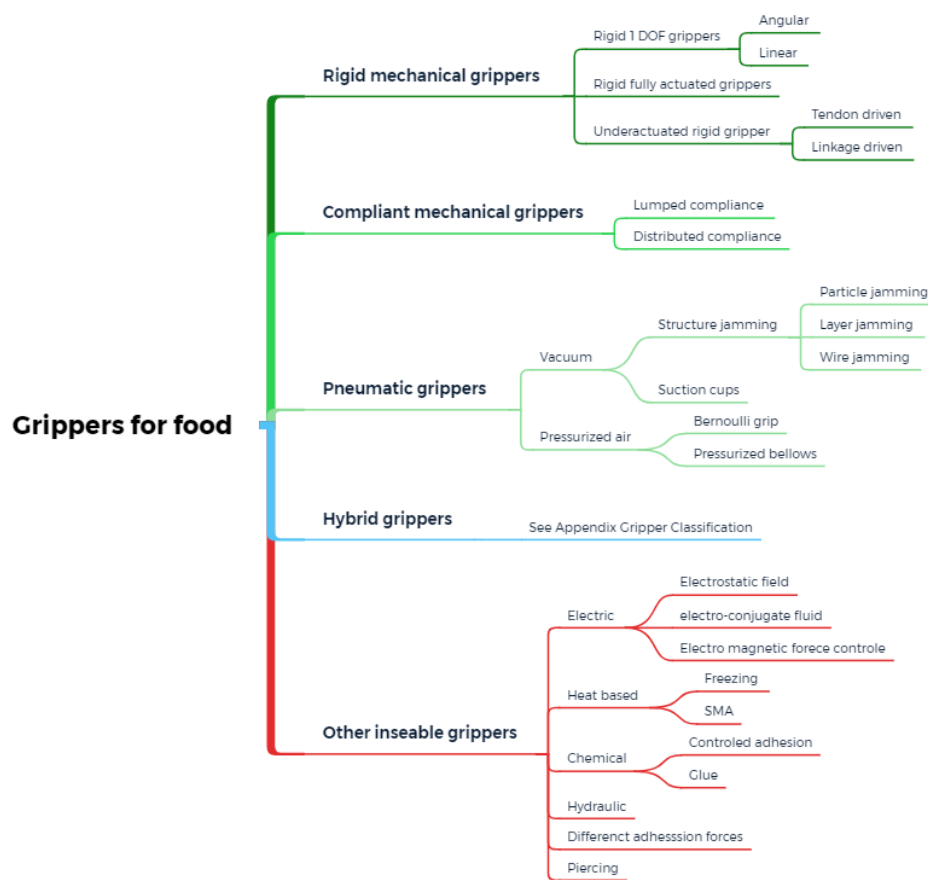


FIGURE 1.3: An overview of the presented gripper classification

1.4 Gripper Grading

To answer the research question, the grading outcome of the different grading classes will be presented here. Important performance criteria noted in literature are: actuation speed, holding capabilities, mass, grasping range, and product damage [83]. These general grading criteria for the packing of food are combined with the insights gained from reviewing the state-of-the-practice in section 1.2.

Ideally, all grippers would be validated using the same or comparable performance metrics. Many gripper development and validation studies do however not report all performance criteria. This is potentially due to a focus on gripper specific metrics rather than a standardised approach. Some steps towards generalizing performance metrics have already been taken [43], [84]. However, this has currently not developed far enough to create a grading system of the gripper classes based on the same or similar performance metrics.

Therefore, the grading outcome will require some approximations and engineering judgement. Where possible, the grading will be based on data available in literature. Improvements for the grading will be discussed in section 1.5.

An asterisk (*) is used to show the grading criteria requiring the authors engineering's judgement or an approximation. Furthermore, different pieces of literature needed to be combined to create a full picture of a gripper class performance. Only literature presenting grippers deemed capable of handling a product of typical size for the packaged food industry were considered. This was done to eliminate the effects of scaling on gripper performance.

For the gripper grading, a four point Harris profile like grading system is used [85], [86]. The gripper classes were graded based on a Harris profile rather than a quantitative point based grading, because common metrics to make a general quantitative comparison are lacking.

The four points on the scale were divided as follows:

1. ++, Exceeds what is required for high speed P&P in the packaged food industry
2. +, Meets what is required for high speed case packing in the packaged food industry
3. -, Requires a slight improvement to meet what is required for high speed case-packing in the packaged food industry
4. --, Does not meet what is required for high-speed case packing in the packaged food industry

1.4.1 Grading criteria

Following literature and the determined holding and grasping phase, ten grading criteria were determined. The grading criteria will be presented in three categories: Criteria specific to the grasp phase, criteria specific to the holding phase and criteria considering the overall packing process. The full reasoning behind the determination of the grading criteria and their grading can be found in appendix C.

For the grading, one main reasoning was used regarding improvement of the current system. For any significant improvement of the current system, the amount of robots required to do a task should be reduced with at least one. The maximum P&P speed of one robot with an easy product is 120 PPM as shown in section 1.2. Achieving the same PPM for most challenging products that are limited to 40 PPM due the end defector limitations, 3 robots are required. A significant improvement could be made if two robots operating at 60 PPM could be used to achieve the same result. This would require an increase of 20 PPM. This train of thought will be the leading consideration for the grading.

Grasp phase grading criteria

- A **Actuation time:** the actuation time of the gripper is graded as the sum of the opening and closing time of the gripper. Since the robot performance is known and will not be altered in this research, the actuation time determines the theoretical maximum P&P speed considering a perfectly connected load. This knowledge was used to calculate the actuation time that still allows a case packing speed to increase to 60 PPM.

- B Grasping range**, the grasping range in this work is considered as the theoretical maximum object range that can be picked by the gripper. This is calculated as the difference of the maximum and minimum object size that can be picked. In an industrial setting gripping range is required to correct for possible errors in robot accuracy. The robots considered in the state-of-the-practice review enter an error mode when the measured and expected position deviate more than 5mm . This value is used for grading the gripper classes.
- C Operating in confined space***, to achieve a faster case packing speed products are often not placed inside a box, but are dropped as the robot hovers above a box. This is only possible for impact resistant objects. Not all packaged food products are impact resistant, some packaged food products will break or crack when dropped. These products need to be carefully placed inside the box instead. This in turn means the gripper has to be able to operate in the confined space of a box.
- All grasping gripper are assumed to use an enveloping grasp during the holding phase. A pinch type grasp does not give the required holding force during the holding phase. In the grasp phase, a pinch grasp is allowed since the forces are significantly lower compared to the holding phase. The ability transition behavior between the grasp and holding phase are used to grade this criteria.

Holding phase grading criteria

- D Force holding capabilities**, the pull-out force is defined as the maximum force that is required to fully detach a product from the gripper considering the weakest loading direction. This grading criteria is well documented in literature. In literature, different performance metrics for holding capabilities for finger based grippers can be found [43], [87]. The applicability of these performance metrics are usually limited to a specific gripper class and not to all gripper classes. Even though dimensionless performance metrics are available for some gripper classes there is no dimensionless performance criteria applicable for all gripper classes. Therefore, the pull-out force was used as a grading criteria in this paper. According to Newton's second law the required force was determined.
- E Moment holding capabilities***, in the dynamic load case in high-speed case packing the moment a gripper can withstand around any axis becomes of importance. First of all, objects have to be rotated 180 degrees during the pick and place motion, which requires considerable angular acceleration. Furthermore, if there is any eccentricity between the object's center of mass and the center of the gripping location a purely translational acceleration will also include a moment. The measurement of the moment loading causing product loss is poorly documented in literature and no generalized grading criteria was found. To still grade this important criteria an approximation based on the author's judgement has to be made.
- F Gripper mass**, the gripper mass is defined as the mass of the gripper measured in kg under standard condition. The gripper mass is an important measurement for the dynamic response of the system. In addition, the maximum acceleration of the case packing robots is depended on the moved mass. The moved mass is the combined mass of the gripper, the robot platform and the

gripper object. The platform and object mass are constant. Therefore, the gripper mass determines the theoretical maximum pick and place speed. This was used to determine what gripper mass still allowed for a pick and place speed of 60 PPM.

General grading criteria

G Contact pressure, the available data in literature was not sufficient to make a grading based on literature. Similar to point **E**, the authors divided four grading intervals to obtain a fair grading. These intervals were based on the reduction of contact pressure.

Ideally, the maximum contact pressure of a gripper is of interest when handling fragile products. It would be an ideal measurement outcome to estimate product damage and it is also used in other fields to estimate wear or failure [88], [89]. However, measurements of contact pressure were only available for some gripper classes.

H Life time, a good measurement for the life time of a gripper is the amount of operational hours that 99% of the grippers are expected to achieve. If a gripper breaks during operation the case packing line has to be stopped to replace the gripper. As the case packing stops, the food processing step is also has to be halted, this will often results in perished food products.

For many gripper classes the lifetime is unknown, making it impossible to grade this criteria based on literature. Therefore, grading of life time in this work will be completely done based on the author's engineering judgment.

I Financial cost *, the financial cost of a gripper is defined as the financial investment that has to be made to obtain a certain gripper. The financial cost is interesting from a business point of view. A cheaper gripper with similar performance will result in higher profits. Moreover, considering replacing human case packing lines makes the cost of the robotic case packing line and its gripper to become important. If a robotic line would be more expensive than a human operating, whilst having the same performance then it would not be beneficial to invest a robotic line.

The data available on the cost of state-of-the-art grippers is highly limited. Therefore, the author has set up 4 grading questions for this grading criteria, which are presented in table 1.3.

J Control complexity *, when building a case packing line every extra control variable will create a more complex and error sensitive process. Less control variables of a boolean data type are desired. For the grading, four levels of control complexity were determined as is shown in table 1.3. The four levels of control complexity correspond to the four grading intervals.

Grading intervals Grading criteria	Grading method			
Actuation time	Actuation time t_{act} from literature	$t_{act} < 50 \text{ ms}$	$50 \text{ ms} < t_{act} < 550 \text{ ms}$	$550 \text{ ms} < t_{act} < 1050 \text{ ms}$
Grasping range	Actuation range (Δx) from literature	$\Delta x < 5 \text{ mm}$	not required	not required
Operating in confined space *	Required contact surface for gripping	No gripper parts located outside the product top surface	Using the top edge to grab a product	Grippers using multiple surfaces to hold the product, yet able to reconfigure from enveloping grasp to a pinch
Force holding capabilities	pull-out force($F_{pull-out}$) from literature and newtons second law	$F_{pull-out} > 72 \text{ N}$	$72 \text{ N} > F_{pull-out} > 32 \text{ N}$	$32 \text{ N} > F_{pull-out} > 8 \text{ N}$ $8 \text{ N} > F_{pull-out}$
Moment holding capabilities	Grading questions on grasp type and required deformation for contact loss	Grasp type gripper requiring plastic deformation for product loss	Grasp type gripper requiring elastic deformation for product loss	Grippers requiring frictional forces to hold an external moment
Gripper mass	Gripper mass ($m_{gripper}$) from literature	$m_{gripper} < 0.6 \text{ kg}$	$0.6 \text{ kg} < m_{gripper} < 1.5 \text{ kg}$	$1.5 \text{ kg} < m_{gripper} < 2.0 \text{ kg}$ $2.0 \text{ kg} < m_{gripper}$
Contact pressure *	Grading questions on contact type	A contact surface	A line contact	Multiple contact points Three or less contact points
Life time *	Engineering judgement	-	-	-
Financial cost *	Grading questions on the availability and wide-spread usage of grippers	Grippers widely available on the market. Having a large catalogue with different tested models	Grippers used by industry and available from vendors	Grippers not available on the market or explicitly known for their high cost
Control complexity *	Grading questions on the requirement of sensor and control variables	Requiring no sensors and one boolean control variable	Requiring no sensors and multiple boolean control variables	Requiring specialized control with sensors and boolean control variables

TABLE 1.3: Showing the four grading intervals for each grading criteria

1.4.2 Weight factors

Before finalizing the grading it is important to determine the importance of each grading criteria. This will be done by introducing weight factors. To ensure all grading results will yield a positive value, the 4 point grading scheme is ranged from 0 to 3. By using normalized weight factors the score ranges from 0 to 3, low to high respectively.

No literature on grading criteria and weight factors for high-speed case packing is available. Therefore, a set of grading factors will be proposed in this chapter. The well known Analytical Hierarchy Process (AHP) was used to determine the weight factors [90]. This method was picked because it is easy to understand and because it is efficient [91]

The weight factors presented here are the result of the average grading of six engineers working in the high speed case packing industry. An easy and efficient method such as AHP is essential when considering multiple experts. Table 1.4 shows the determined weight factors. Appendix C briefly explains the AHP grading method and shows the opinion of the interviewed engineers.

1.4.3 Grading

Combining the weight factors and grading criteria, the gripper classes were graded using data obtained from the state-of-the-art literature. Appendix A.1 shows the data set that was made for the grading. The result of this grading is shown in table 1.4.

Considering the definition of the four points of the grading scale presented in section 1.4, each minus or double minus sign indicates a limitation. For example, a limitation caused by the grading criteria financial cost indicates that the financial cost of the gripper class is too high, thereby limiting its application in the field of high speed case packing. More specifically, the columns of table 1.4 show the degree of limitation stemming for each grading criteria. Additionally, the limitations for the specific gripper classes can be seen in the rows of table 1.4.

	Actuation time	Grasping Range	Operating in confined space	Force holding	Moment Holding	Gripper mass	Contact pressure	Life time	Financial cost	Control complexity	Weight average gripper score
WF	0.138	0.024	0.102	0.181	0.181	0.055	0.162	0.055	0.425	0.060	
Rigid 1 DOF	+	++	--	++	++	+	--	++	++	++	2.0
Rigid fully actuated	+	++	-	++	++	-	-	--	--	--	1.8
Under actuated rigid	-	++	-	+	++	+	-	+	+	++	1.9
Lumped compliant	-	++	-	+	++	++	-	-	--	++	1.8
Distributed compliant	-	++	--	+	++	+	+	+	--	++	1.8
Suction cups	++	++	++	++	-	++	++	-	++	++	2.5
Structure jamming	--	++	+	+	+	+	++	-	+	+	1.9
Bernoulli	++	++	++	--	--	++	++	+	-	++	1.8
Pressurized bellows	-	++	--	-	-	++	++	+	++	++	1.6

TABLE 1.4: The results of the gripper grading including weight factors in the second row and the average gripper score in the final column

To draw any more meaningful conclusions a numerical value describing limitation has to be determined. This value is named the weight limitation score (WLS) and is calculated according to equation 1.1. When the gripper scores ++ or 3 points then there is no limitation posed by that grading criteria. In this case the WLS is 0.

$$WLS(i, j) = W(j) \cdot (3 - GS(i, j)) \tag{1.1}$$

Here:

$W(j)$ = The weight factor of the j 'th grading criteria

$GS(i, j)$ = The considered gripper class (i) and grading criteria (j)

The degree of limitation for the different grading criteria can be derived from WLS and can be calculated for each gripper class. This is done by dividing the WLS of one criteria by the total WLS for that gripper class. This calculation is mathematically shown in equation 1.2.

$$\text{degree of limitation}(i, j) = \frac{WLS(i, j)}{\sum_{k=1}^{10} WLS(i, k)} \cdot 100 \quad (1.2)$$

The degree of limitation is presented in table 1.5. The bottom row of table 1.5 shows the average calculated limitation.

Limitation for	Actuation time(%)	Grasping Range (%)	Operating in confined space (%)	Force holding (%)	Moment Holding (%)	Gripper mass(%)	Contact pressure (%)	Life time (%)	Financial cost (%)	Control complexity (%)
Rigid 1 DOF	14.0	0.0	31.1	0.0	0.0	5.6	49.3	0.0	0.0	0.0
Rigid fully actuated	14.4	0.0	0.0	0.0	0.0	11.5	0.0	26.2	19.7	28.2
Underactuated rigid	32.9	0.0	12.2	32.3	0.0	3.3	19.3	0.0	0.0	0.0
Lumped compliant	16.8	0.0	12.4	22.0	0.0	0.0	19.7	13.6	15.3	0.0
Distributed compliant	20.8	0.0	23.0	27.3	0.0	12.5	12.2	4.2	0.0	0.0
Suction cups	0.0	0.0	0.0	0.0	82.9	0.0	0.0	17.1	0.0	0.0
Structure jamming	43.5	0.0	10.7	19.0	6.3	5.8	0.0	3.9	4.4	6.3
Bernoulli	0.0	0.0	0.0	45.3	45.3	0.0	0.0	2.3	7.0	0.0
Pressurized bellows	44.6	0.0	49.4	0.0	0.0	0.0	0.0	6.0	0.0	0.0
Average limitation	20.8	0.0	15.4	16.2	15.0	4.3	11.2	8.2	5.2	3.8

TABLE 1.5: The degree of limitation calculated for each gripper class

1.5 Discussion

This work set out to identify the limitations of state-of-the-art robotic grippers when applied in high-speed case packing for the packaged food industry. The results show that actuation time, pull-out force, operating in confined space and holding capabilities for moments are the four most prominent limiting factors for the average overall gripper classes. These four main limiting factors take up 20.8, 16.2, 15.4 and 15.0 % of the limitations respectively, forming over 65% of the total limitation as can be seen in table 1.4. The only criteria forming no limitation and achieving a CS of 0 % is the grasping range, meaning every gripper class is able to achieve the required grasping range.

Furthermore, when considering the rows of table 1.5 the limiting factors for each gripper class are identified. For future design of robotic grippers for the high speed case packing industry this is the most interesting information. The research question could in that case be answered specifically for one gripper class. For example, for the rigid 1 DOF grippers shown in the first row of table 1.5 14% of the limitations come from actuation speed, 31% from operating in confined space, and 49.3% from contact pressure. Therefore, for future research it would be advisable to focus on reducing the contact pressure, which has already been tried to some extent [92].

Additionally, the final column of table 1.4 shows the score of each gripper class. From this score it can be concluded that suction cups are the overall best solution with 1 DOF rigid grippers as the second best option. Suction cups are already the state-of-the-practice showing the choice made by industry is in agreement with the data from literature.

An interesting notation is that the research effort into suction cups is not as extensive as the research into other gripper classes. However, in recent years a newly gained research interest can be noted [5], [93]–[96].

The 1 DOF rigid grippers have also seen some application for packing of naked food. Some good examples are: A recent gripper made by Marel, designed to handle fresh fish fillets [31]; An older gripper presented by applied robotics used to handle raw chicken filets [32]; Or hybrid gripping designs in recent literature combining a 1 DOF rigid with compliant gripping [97], [98].

Next to answering the research question new insights were also gained during this literature study. Firstly, when the results are viewed together an interesting and unexpected observation is made. The best overall gripper class, the suction cup grippers, does not follow the same limiting factors as other grippers. They perform excellently for actuation time, holding force and operating in confined space, while they perform poorly for holding moments.

Secondly, product grouping shows that the mechanical properties of products are of great influence on the performance during high speed case packing. A factor 3 difference in throughput is found between the best and the worst performing product class. Liquid pouches are found to pose the largest challenge and can be considered as the worst product class to handle via mechanical grippers. Finally, an important observation in the reviewed literature is that no literature on designing minimal actuation time for a gripper is available. Only one paper was found that considered the actuator design to minimize the actuation time [99]. Mechanical design for maximizing actuation speed of the gripper is however not considered in this work. This shows the first literature gap discovered during the literature search. This literature gap indicates a promising future for the improvement of grippers in the high speed case packing industry. Actuation time is found as the main limiting factor for most gripper in this field. Since limited research is performed on this topic a large improvement can be expected, enabling other gripper classes to become feasible of high speed case packing. Looking back at the design of a hybrid gripper and precisely knowing the limitations allow for a minimalist design achieving a better actuation time.

Considering the trustworthiness of the result several improvements can be made. Firstly, the grading is not fully based on literature of measured data. Especially the grading of life time, financial cost and break out load should be looked at critically. Lack of available information for gripper comparison reveals a second large literature gap. This is particularly problematic for the criteria with a high weight factor, such as the force and moment holding capabilities. For finger based grippers the holding moment is rarely measured. Also, the failure load for suction cups under dynamic load considering flexible products is not considered in literature. In order to achieve more trustworthy grading these gaps should be addressed.

Secondly, the state-of-the-practice was also reviewed using limited available data. This could be improved by considering more companies operating in this field. If the problems found here do also occur at other companies then the implicating of this literature becomes more significant. On the other hand, if other companies do not face this issue then this work has considered an issue that has already been solved

by industry.

Furthermore, it should be noted that the weight factors presented here are based on the judgement of a small group of 5 engineers. To obtain a more trustworthy grading a more thorough stakeholder analysis should be performed in the field of high speed case packing for food. Each stakeholder should be included in the weight factor determination to increase the validation of the the grading criteria.

Finally, the AHP method has received some critique in literature, which has also been contested [91], [100]. The AHP method has certain disadvantages but also offers a simple, justifiable, appropriate, efficient and important technique for settling on better choices [91]. Because the grading should take into account a large set of experts in this field, also including mechanics with limited academic experience, a simple and efficient method is necessary to include many opinions regarding grading.

The knowledge gained in this study should be used to guide future work aimed at improving the performance of high speed case packing lines. If no improvements are made onto the current system then the performance will keep decreasing. More challenging products that are still handled by dexterous human hands will also be packed using robotic case packing lines. However, the current system is not capable of handling these products anywhere near the maximum throughput.

For future work it is recommended to identify the limiting factors of the current system in more detail. Simultaneous research into improving the actuation time of all gripper classes is recommended. Looking into a hybrid suction cup gripper is recommended as the most promising solution direction.

1.6 Conclusion

This study focused on finding the limitation factors for grippers when applied to case packing packaged food with high-speed by using the reviewed state-of-the-practice by industry and state-of the-art in literature. A gripper classification has been made and limitations are identified using performance criteria. Those criteria are established to different regions of the case packing motion path.

The limitation for different gripper classes were determined. On average 65% of the limitations were found to come from four aspects. Actuation time showed to be the largest limiting factor with 20.8% of the average limitation. Interestingly, the research focusing on reducing the actuation time is very limited. The other most prominent limitations are the capability to hold force, operating in a confined space and capability to hold moment, contributing to 20.8%, 15.4% and 15.0% of the average limitation respectively.

For the grading, limited data was available, reducing the trustworthiness of the result. Nevertheless, the structured approach that has been used can be extended upon and has provided new insights. The limitations and strengths of different gripper classes are better understood. Therefore, the structured selection of hybrid grippers for the high-speed case packing industry considering packaged food products is possible.

Another main observation is that the usage of suction cups is widespread, while their research effort into their limitations remain lacking.

Furthermore, the mechanical properties of packaged food products have shown to have large effect on the maximum case packing speed. A factor 3 deference in throughput is seen between the easiest and most challenging product to pack. Based

on these conclusions, practitioners should consider to improve the available data used for gripper grading and to start with the design of a hybrid gripper.

Chapter 2

Design, fabrication, and validation of a six axis force moment sensor that passes airflow for gripper actuation and without limiting the pull-out load measurement

2.1 Abstract

Detachment of a product from a suction cup gripper is a recent challenge during high-speed case packing of packaged food products. To investigate this limitation, dynamic load measurements during the case packing process are required. This study outlines the design, fabrication, and validation of a six-axis force moment sensor that passes airflow for gripper actuation, without limiting the pull-out load measurement performance. With the current six-axis force moment technology the stiff vacuum hose, used for suction cup actuation, must pass around the sensor. The integration of the airflow passage into the sensor structure eliminates the loads induced by passing the stiff vacuum hoses around the sensor. In the design process, strain gauges were identified as the most suited transducer using a Maltese cross sensor structure. Optimization was used to obtain the final design dimensions, meeting the requirement of the high-speed case packing industry. When using the fabricated sensor on the case packing system the acceleration at which detachment of the product from the suction cups occurred did not change. Therefore, the sensor proved to be able to pass airflow without limiting gripper performance. The airflow integration is not limited to suction cups, as other pneumatic grippers could also benefit from this six-axis force moment sensor design. The most notable sensor validation results showed the sensor achieved a maximum cross-coupling of 25.6%. The maximum measurement error was measured to be 8% in the F_z direction while striving for 5%, which is at least in part explained by manufacturing and calibration errors. Only the F_z direction achieved an unsatisfactory error performance; all other directions including their cross-coupling achieved an error lower than 5%. Therefore, the sensor was still deemed usable for measuring the dynamic load during high-speed case packing. Nevertheless, re-fabrication of the sensor is advised to produce a sensor that entirely falls within design specifications.

2.2 Introduction

Product throughput is directly affecting the profit made in the high-speed case packing for packaged food products. To obtain a high throughput with limited factory space, robot productivity should be maximized. Chapter 1 concluded that for high-speed case packing, suction cup grippers are highly applicable. However, the detachment of products from the suction cups gripper has shown to be hindering throughput and robot productivity.

Chapter 1 showed that the mechanical properties strongly influence the packing speed at which the objects detach from the suction cups gripper. The cause of detachment is not yet well understood; in order to solve this, more information is required about the failure load just before detachment occurs.

The failure load is poorly documented in literature. Some studies looked at quasi-static load cases considering rigid products [101]–[105]. The most influential of these studies, by Mantriota, attempted to model and measure the failure loads for suction cup grippers in the static case using rigid products [95], [101], [106]. Despite this, detachment is still an issue. This could be because static assumptions are not suitable for highly dynamic systems in practice, especially when considering flexible products. Therefore, a method is required that measures failure modes of suction cup grippers used in dynamic systems involving flexible products.

Using a six axis force moment F/M sensor, the interaction between the product and the gripper can be studied in more detail. F/M sensors, also known as force torque (F/T) sensors, are devices that are designed and used to measure an applied load vector. A six-axis F/M sensor is a device able to measure force and moment around all three axis of a Cartesian reference frame, referred to as F_x , F_y , F_z , M_x , M_y and M_z respectively. Since the failure is not well understood, it is desirable to measure in all six load directions during case packing at maximum speed.

The application of a vacuum gripper with the current sensor technology requires passing a vacuum hose around the sensor, creating a parallel path between the gripper and the fixed world, causing part of the load to be received by the vacuum tube. Furthermore, during dynamic loading, the vacuum tube will exert undesirable loads to the sensor.

This issue is addressed by the integration of airflow passage into a sensor structure without influencing the load measuring capabilities. To the best of the authors knowledge, no F/M sensor proposed in literature or available for sale has considered this integration of passing airflow in the structure of an F/M sensor. Design requirements of case packing for packaged food have also not yet been considered in previous studies on multi axis F/M sensor design.

This chapter is structured as follows: the concept generation and selection is presented in section 2.3, followed by design process in section 2.4 and 2.6. The fabricated sensor is validated in section 2.8. In section 2.9, the results are discussed and concluding statements on the final design are given.

2.3 Concept generation and selection

In this section, design decisions leading up to design process are presented. Firstly, design requirements and sensor placement are discussed. Secondly, transducer selection is reasoned. Following transducer selection, sensor structure is chosen according to available literature on multi-axis F/M design. Next, picked sensor structure is considered in more detail. Finally, transducer placement on sensor structure is given. A more detailed discussion of the sensor selection process can be found in appendix D.

2.3.1 Design requirements

The design of the six axis F/M sensor will have to meet requirements specific to the high-speed case packing for packaged food. These requirements are listed here and are briefly explained.

1. Sensor mass, the sensor mass is limited to 450 grams. By adding this much weight to a standard gripper, the case packing robots are still able to reach their maximum acceleration. This weight is also typical for light weight F/M sensors in industry [107]
2. Minimum sensor load, the minimum load the sensor has to be able to withstand is determined by using simple models that are also used by suction cup vendors and design studies [18]. Because of the observed detachment challenge discussed in chapter 1, these methods are known to be off. Therefore, a safety factor of two is introduced, leading to a minimum sensor loading of 360 N and 36 Nm
3. cross-coupling, the cross-coupling or cross talk of the sensor needs to be low, allowing for initiative data interpretation. From literature, a cross talk of 5-10 % is to be expected [108]. Since this research is focused on adding the additional feature of passing airflow, a maximum cross-coupling of 5 % is set a design bound, achieving a performance similar to the best validated state-of-the-art sensor designs.
4. Manufacturability, The most advanced manufacturing technique available is a 5 axis CNC mill. Using this machine or a traditional lathe and mill, the sensor should be manufactured. This constraint causes minimum inside radii in the design.
5. Suitability, the sensor has to fit the robot platform and needs to be able to connect a gripper, resulting in a 25mm axis ending in a 25mm axis connection.
6. Moment to force ratio, a sensor suited for industry is desired to have a moment to force ratio of 10% for the x and y direction. [109].
7. Transducer overload, the selected transducers should not be overloaded, a minimum of 10^8 load cycles at maximum load is set.

The following criteria are based on achieving the same performance as accepted shelf sensors by industry.

8. Measurement error, the measurement error obtained by off-the-shelf F/M sensor is $> 5\%$ of full scale at maximum load [107]. This bound was also set for the design in this work.
9. Hysteresis, the hysteresis or the relative repeatable error of the sensor has to be low [110]. The maximum hysteresis error was set to 2% of the full scale, being the same value found in the shelf sensors [107].
10. Eigenfrequency, the eigenfrequency of the sensor needs to be sufficiently high to not cause vibrations during the measurement. The case packing robot has seen ongoing upgrades, therefore the eigenfrequency is not well known. To set a generally acceptable level, the eigenfrequency was set to 2000Hz.
11. Robot loading, the addition of the sensor should not overload and damage the mechanical structure of the test platform, shown in figure 2.1a. The test platform has not been tested to its failure point. Therefore no exact bound can be placed on this design requirement.

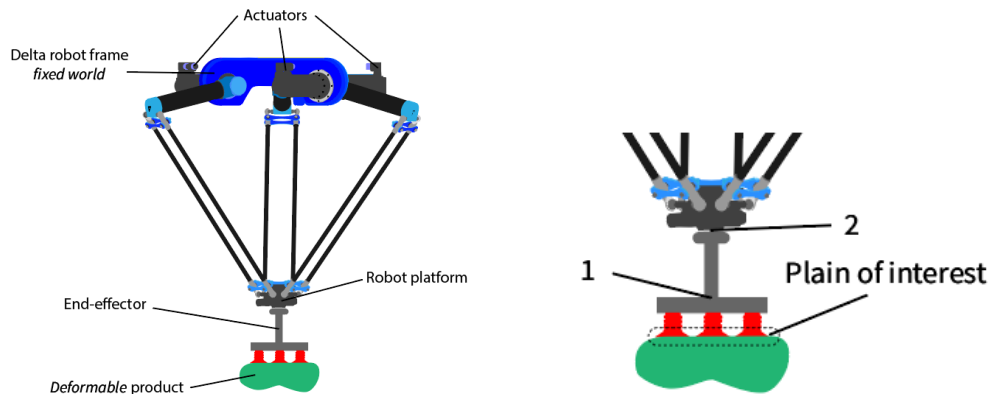
2.3.2 Sensor placement

Ideally, the sensor should be placed directly at the point where the load needs to be known. This plain of interest is between the gripper and the product, as shown in figure 2.1b. Measuring directly at this interface is challenging and will likely influence the gripper behavior. Also for each gripper class determined in chapter 1 the plain of plains of interest are different. Leading to a gripper specific sensor design. Moreover no sensor capable of performing such measurements was found available on the market or in literature. Placing the sensors at another location requires a correction calculation.

The best practical location to place the 6 axis F/M sensor is the location labelled 2 in figure 2.1b. This location places the sensor directly under the robot platform, minimizing the additional load added by the mass of the sensor during acceleration. Moreover the sensor can be designed as an extension of the robot platform. This allows the connection of any previously designed gripper to the sensor.

Another interesting location to place the sensor is labeled 1 in figure 2.1b, places the sensor as close as possible to the suction cup grasp plane, minimizing the correction that has to be made for the sensor displacement. This location will result in a gripper specific sensor design, making the sensor only applicable to one gripper class.

Placing the sensor in between location 1 and 2 is undesirable. This location would not gain the benefits of the design as an extension of the robot platform. However, the amount of correction required caused by the sensor displacement will increase.



(A) Overview of the measurement set up

(B) Overview of the measurement set up

2.3.3 Transducer selection

To measure the applied load to a six axis F/M sensor a transducer is required. Measuring transducers convert one form of energy into another form which is more easily processed. Transducers used to measure force do that often indirectly by measuring the elastic deformation of a structure. Since this deformation is driven by an external load, this method can be used to establish this applied load.

Many different available transducers can measure loads or deformations. The considered transducers for this design have at least a proof of principle in literature. Examples of considered, but infeasible transducers are force sensitive resistor [111], [112], capacitive measurements [113]–[115] [116], [117], optical [118] and fluid pressure [119]. Their infeasibility is caused by too large errors, low measuring range, large deformations, incapability to measure moments and physical size.

Strain gauges were selected as the transducer for the developed force torque sensor. Strain gauges have a slight change in resistance when they are subjected to a strain. By measuring the strain of a loaded structure, strain gauges can be used to determine an external load. Strain gauges are well developed and are accepted in industry due to their ability to be applied in dynamic and static load cases, their repeat ability, smallness, low hysteresis and low cost [109].

Other feasible transducers were piezoelectric transducers and piezoresistive transducers. Piezoelectric transducers generate a voltage when compressed. This effect has been used to design a multi axis F/M sensor [120]. As apposed to other transducers, this transducer does not fail under high loads, and is most suited for measurements in the kN range [120]. This is not the load range seen in high-speed case packing. Piezoresistive transducers behave similarly to stain gauges, their resistance changes when experiencing a strain. [112], [121]. They can therefore be used as a replacement for strain gauges. However, they perform slightly worse than traditional strain gauges [122].

Appendix D explains selection process, the working principle and usage of strain gauges in more depth.

2.3.4 Sensor structure

The sensor structure has to be selected according to the design requirements presented in section 2.3.1. Many different sensor structures using strain gauges have been designed, fabricated and validated. These sensor structures have not yet been

considered the requirements for the high-speed case packing of packaged food. However, the results of previous works can guide the concept selection of this design. For the selection multi-axis F/M sensor based on the strain gauges transducer presented in literature were considered. The structure consideration was not limited to 6 axis F/M sensors, because a structure used for lower amount of measuring axis could be extended to six axis.

The list of considered sensor structures consist of E-type membrane structure [123], platform based structure [124], [125], a circular spoke membrane structure [126], a parallel plate structure [127], [128], a parallel beam structure [129], a stack of multiple load cells [130], [131], T-shaped bars [132], 3 beam structure (commercially available sensors) [133], multi-spoke wheel structure [134], [135], the Maltese cross structure [108]–[110], [136], [137] and the sliding joint Maltese cross structure, an adaptation to the traditional Maltese cross structure [137], [138]. Table 2.1 gives an overview of all the considered structures.

From the considered sensor structures, one has to be selected for further detailed design. The final sensor structures was selected based on 5 criteria defined according to the design criteria presented in section 2.3.1. The selection of the sensor structures was done using simple questions, a full grading scheme was not required, because the Maltese cross sensor structure clearly outperformed the other sensor structures. The 5 criteria are explained below and the review of the sensor structures can be found in table 2.1. The 6'th and 7'th column provides information on the publishing year and the source of the most recent publication.

1. Passing airflow

Passing airflow through the sensor structure is unique and has to the best of the author's knowledge not yet been implemented in a multi-axis F/M sensor and can therefore not be directly reviewed from literature. The author's engineering judgement will be used to label this criteria either likely or unlikely. Where likely means the sensor structure is expected to be modifiable to allow the passage of airflow, and where unlikely indicates the opposite.

2. Coupling

Coupling cause strain to be measured in a measuring direction while no load is applied on that direction. Mechanically decoupled sensors measure strain in only one transducer bridge when a pure load is applied in one of the principle measuring directions. Mechanically coupled sensors on the other hand measure strain in multiple bridges if a load is applied in one of the principle measuring directions. Mechanically decoupled sensors require less complex calibration procedures, but have more complex mechanical designs [108], [139]. More information on the difference between coupled and decoupled sensors, and the studies performed to obtain decoupled sensors can be found in Appendix D. The remaining cross-coupling of mechanically decoupled sensors tend to be too large to truly be decoupled, making them slightly coupled [108], [139], [140].

The coupling review criteria checks whether a sensor structure is slightly or strongly mechanically coupled. Mechanically decoupled or slightly coupled sensors are preferred over strongly mechanically coupled sensors.

3. Detailed design

For the detailed design, a literature review was performed to find a structured

and proven design method for each sensor structure. The availability of a structured and proven design method will lead to an easier and more feasible design.

4. Case packing compatible

The case packing compatible criteria considers if the sensor structure is compatible for usage during high-speed case packing. Sensors that are designed to be attached to or integrated in a robot are labeled compatible, while sensor structures designed to function as a stationary multi-axis scale are labeled incompatible.

5. Error

Commercially available multi-axis sensors are expected to measure loads with a maximum error of 3-5% at their rated load [107], [109]. This review criteria will look at the maximum measurement error for each sensor structure. A sensor is deemed usable if the error rate at its rated load is below 5%. In specific load cases much larger errors can be found, which is one of the driving factors for active research into the multi-axis F/M sensor [109]. Nevertheless, 3-5% cross-coupling error is what can be expected from a fully developed and commercially available multi-axis F/M sensor. Designing a sensor with a lower error rate than the industrial average is highly unlikely and is not expected.

Sensor Structure	Coupling	Design method	Passing airflow	P&P compatible	Error	Year
E-type membrane	slight	available	likely	yes	>5%	2010
Platform	strong	available	unlikely	no	>5%	2016
circular spoke	strong	available	unlikely	yes	>5%	2014
parallel plate	slight	available	unlikely	yes	>5%	2002
parallel beam	slight	available	unlikely	yes	>5	2007
load cell stack	unknown	available	unlikely	yes	>5	2005
T-shaped bars	strong	available	unlikely	yes	Unknown	2002
3 beam structure	strong	available	likely	yes	>5%	2021
Multi spoke wheel	strong	available	likely	yes	>5%	2016
Maltese cross	slight	available	likely	yes	>5%	2021
Sliding joint Maltese cross	near perfect	available	unlikely	no	>5%	2021

TABLE 2.1: A summary of the considered sensor structures and their considered criteria

The Maltese cross structure is expected to assumed to be able to pass airflow during and is shown in Figure 2.2. It was first proposed by B.Shimano V. Scheinman in 1971 [141]. In 1977, B.Shimano and B. Roth further extended on the previous work outlining the mathematics and calibration process of a Maltese cross sensor [110]. This sensor structure is very close to being mechanically decoupled and is still part of active research. Furthermore, it is inherently sensitive for forces, it is sufficiently strong and compact, and has a low weight and low non-linear, non-repeatable and hysteresis errors. [109], [110]. This performance is explained by its symmetric and monolithic design.

As shown in figure 2.2 the sensors structure consists of 4 strain measuring beams, 4 thin plates, a central connection block and a connection rim. By measuring the strain of the strain measuring beams, the applied force can be determined. Unrestricted relative motion between the central block and connecting rim is required for proper functioning of this sensor. A more detailed explanation of the working principle of the sensor can be found in Appendix D.

All other considered sensors were either not suited to pass airflow, were too large to be added to a dynamical moving robot platform or were discarded noticing other

research with better performing sensor structures.

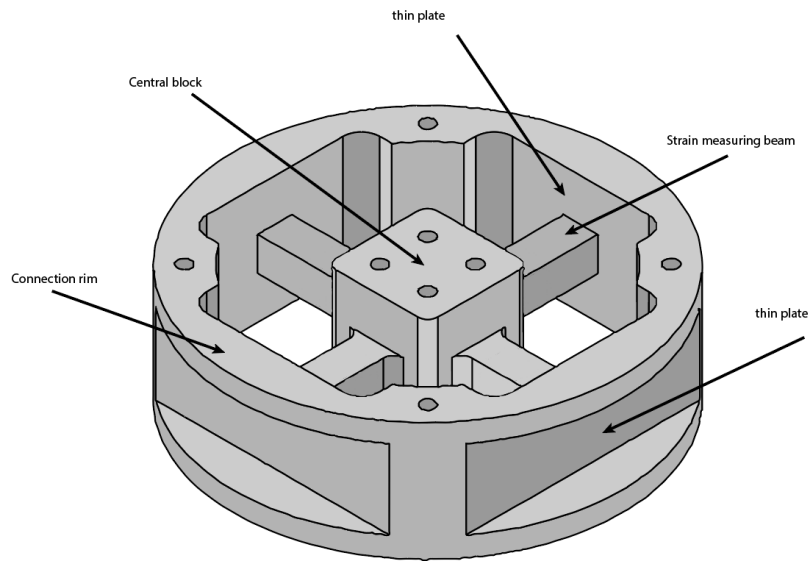


FIGURE 2.2: An overview of a Maltese cross sensor structure

2.3.5 Transducer placement

The determination of the strain gauge arrangement was done in three steps: Selecting measuring circuit, arranging strain gauge and positioning strain gauge.

Measuring circuit

Different measuring circuits can be used to measure loads using strain gauges. The Wheatstone bridge is a typical circuit used to measure deformations using strain gauges [109]. In literature, full bridge Wheatstone circuit are most often used [109]. Half Wheatstone bridges have also been used sometimes [133], [140]. This is for example done to allow for the integration of a small scale data accusation system (DAQ) into the sensor [133]. This however resulted in a decrease in performance, because less strain gauges are used to measure the strain. In this research, the DAQ system will be placed next to the robot, so that space is not an issue, allowing the usage of a full Wheatstone bridge circuit.

Stain gauge arrangement

In literature, different strain gauge arrangements can be found. Some strain gauge arrangement use more measurement bridges than load directions, which almost always result in mechanically coupled sensors by design [110]. In more modern research, effort nearly managed to mechanically decouple sensors with one measurement bridge per load component [108], [109], [139], [142].

Two of these works critically noted that the previously attempted strain gauge arrangements did not maximize the sensitivity for measuring moments, but only for measuring forces [108], [142]. Measurement sensitivity is related to the location of a strain gauge on the strain measuring beams. In previous works, strain gauges were

placed behind each other, placing the force measuring strain gauge in the most sensitive location. Using double parallel strain gauges, such as the DY43-3/350 strain gauges from HBM, a novel arrangement was proposed, as shown in figure 2.3. In this novel arrangement, the strain gauges can be placed next to each other, positioning both the force and moment measuring sensor in the most sensitive location. Hence, this arrangement will be used in this study as well.

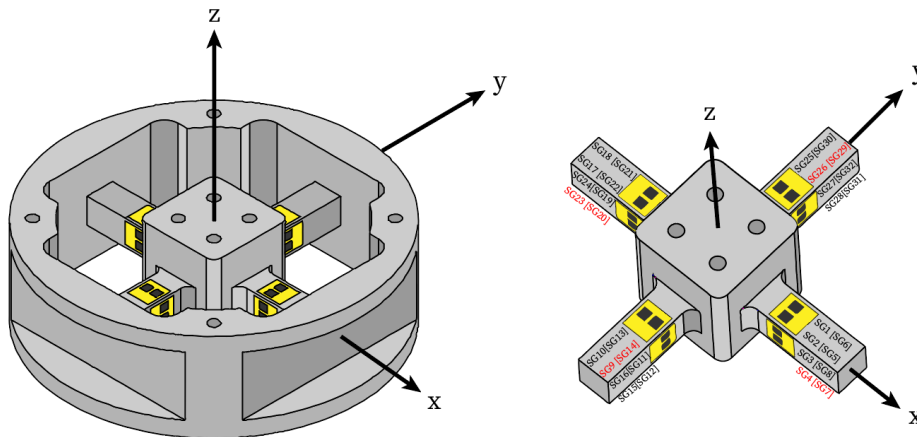


FIGURE 2.3: The strain gauge arrangement proposed and numbering used in [139]. Red indicates strain gauges which are not used, black indicates active strain gauges, square brackets indicate strain gauges on the opposite side of the beam

This strain gauge arrangement uses 16 double parallel DY43-3/350 strain gauges from HBM of which 24 strain gauges are active. This arrangement creates a theoretically nearly decoupled sensor with one measurement bridge per load direction. Because of the chosen sensor structure, the cross-coupling terms C_{51} and C_{42} remain significant [108], [109], [139]. This cross-coupling effect is mostly caused by the behavior of this sensor structure and not by the placement of the strain gauges. The cross-coupling term C_{51} refers to the measurement in strain in the F_x direction when a moment purely around y is exerted. The deformation mode of a pure moment around the y axis is shown in figure 2.4. The C_{42} is the same cross-coupling effect, only in that case between M_x and F_y . A more detailed explanation on cross-coupling and the measurement principle of this sensor can be found in appendix D.

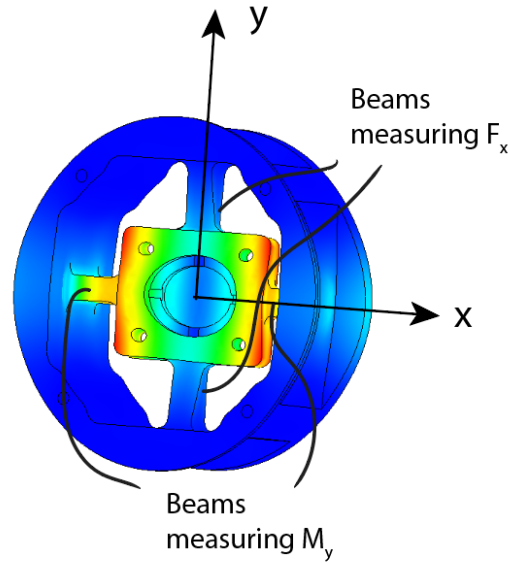


FIGURE 2.4: The deformation mode for a moment around the y axis

Equation 2.1 shows the equation used to calculate measured strain specific to each of the load direction [108]. These equations can be set up following the explanation presented in appendix D section D.4.1.

$$\begin{aligned}
 \epsilon_{Fx} &= \frac{1}{4}((\epsilon_{28} - \epsilon_{31}) + (\epsilon_{15} - \epsilon_{12})) \\
 \epsilon_{Fy} &= \frac{1}{4}((\epsilon_8 - \epsilon_3) + (\epsilon_{19} - \epsilon_{24})) \\
 \epsilon_{Fz} &= \frac{1}{4}((\epsilon_1 - \epsilon_6) + (\epsilon_{18} - \epsilon_{21})) \\
 \epsilon_{Mx} &= \frac{1}{4}((\epsilon_{25} - \epsilon_{30}) + (\epsilon_{13} - \epsilon_{10})) \\
 \epsilon_{My} &= \frac{1}{4}((\epsilon_{17} - \epsilon_{22}) + (\epsilon_5 - \epsilon_2)) \\
 \epsilon_{Mz} &= \frac{1}{4}((\epsilon_{32} - \epsilon_{27}) + (\epsilon_{16} - \epsilon_{11}))
 \end{aligned} \tag{2.1}$$

Strain gauge placement

The location of a strain gauge on the strain measuring beams determines the sensitivity of the sensor. The closer the strain gauges are placed to the central block, the higher the measured strain. However, the deformations near the ends of the strain measuring beams are known to show non-linear effect from literature [108]. Placing the strain gauges in this non-linear area will result in loss of linearity of the sensor. Figure 2.5 shows the measured strain in the bridge circuits for different locations of the strain gauge. This figure was made for the most compliant version of the sensor which is expected to show the most non-linear effects.

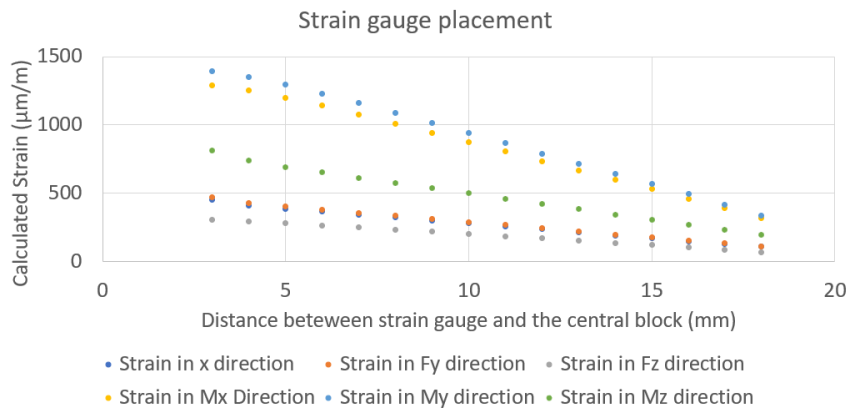


FIGURE 2.5: Measured strain for different positions of the strain gauge on the strain measuring beams

Because of the the manufacturing process, the inner corners can not be cut at 90 deg. For this reason, the strain gauges can not be placed directly against the central block, as can be seen in figure 2.5. Only the first point, which places the strain gauge directly against rounded corners, shows a slight deviation from the linear line. The deviation from the linear line is however not as strong as the effects found in literature [108], [129], [143]. This is likely because the strain gauges can physically not be placed close enough to the central block to cause the non-linear effects. The strain gauges will be placed at the smallest distance from the central block where no deviation from the linear line is observed. This is at 4mm from the central block.

2.3.6 Detailed design

Before starting the design of the sensor, the design method and goal have to be determined. This was done by considering the design methods and goals of previous studies

Design methods

Some researchers in this field critically observe a division in research methods concerning the structural design of the multi-axis F/M sensors. They classify two groups of research [109], [124], [139]. The first group considers case specific designs following a trial-and-error design strategy based on the designers experience, resulting in a sensor with high production cost. This is not or hardly generalized for other fields. The second group aims to create a general and structured design method, aiming to create a generally applicable sensor with low production cost. Other researches and industries can follow the proposed design methods to create a sensor fitting their needs.

In the structured design method, two focus areas can be distinguished. The first method attempts to model the sensor using analytical models. Strain is for example modeled, based on Timoshenko beam theory [126], [137], [143]–[145]. Also, analytical models to calculate the eigenfrequency have been proposed [146]. The second method follows a numerical approach using finite elements method (FEM) models [108], [109], [139].

The analytical models are computationally less expensive compared to FEM models. However, the errors with respect to reality are larger [143]. Furthermore, when

another design requirement is added an analytical model for this requirement has to be determined. In standard FEM software this is often already implemented. Both structured design methods used optimization to obtain the final design parameters. Particle swarm optimization has seen some usage [147]. However, in this case the optimization problem is constrained and expected to be non-linear. For such problems SQP is often used [148]. In literature, SQP has also proven to be well suited for this type of optimization problem [108], [109], [134], [139], [143].

The FEM analysis and optimization using the SQP algorithm has proven to be most successfully in recent literature and was also followed in this work. Using this method, sensor designs with near zero cross-coupling, low measurement error, high moment to force ratio and a good sensitivity were considered [109], [139]. This design method will also be used in this design.

Optimization objective

All design criteria found in literature can be used with the chosen design strategy, FEM and optimization. However, considering only one design aspect during optimization is viewed as too trivial for the application in the the high-speed case packing. Because of, for example, the highly dynamic motion during measurements, not only the cross-coupling error, but also sensor sensitivity, sensor resonance frequency, mass and stiffness are of importance. If one of these aspects does not meet the required criteria, the designed sensor will lose its usability. A combination of design criteria is needed to ensure that all design aspects are taken into account. This design will extend on what has been presented in literature by combining different design criteria in one optimization scheme.

The objective of the optimization will be to maximize sensor sensitivity while setting constraints to the other important design aspects. The constraints were set according to the design requirements presented in section 2.3.1. In descending order of priority the constrains are: maximum stress, cross-coupling error, maximum strain, minimum strain, eigenfrequency and sensor mass. During optimization all constrains will be treated as equally important. However, during validation it is valuable to know which constrain are most important. Separately these objectives have been considered in literature for both FEM and analytical modeling [108], [109], [139], [140], [142], [143], [146], [147], [149]–[151].

2.4 Design process

The design process of the sensor was performed in two separate parts. Firstly, the airflow passage was designed. Secondly, the dimensional design, largely influential for the sensor performance, was designed. This separation was made to ensure a decoupling between the airflow passage properties and the measuring capabilities. Furthermore, the viability to modify the sensor structure in order to pass airflow is checked a priori. This section will firstly go into the design of the airflow followed by the structural design of the sensor.

2.4.1 Airflow passage

This section explains the train of thought and the design steps taken to design the airflow passing part of the sensor design. The design starts at the minimal sensor

structure as depicted in figure 2.6a. The first step in the design is the connection of the sensor to the robot platform. The robot platform is used for testing connects to its various end effectors using a round hollow steel tube. This tube is used to provide the airflow required for the suction cup grippers. A hole with the correct fit is inserted in the central block of the sensor, as can be seen in Figure 2.6b. A seal is required here to ensure there will be no leaks in the system. A rod type seal with an o-ring compression of 20% was designed for this seal, the o-ring is depicted as a black rim in Figure 2.6b. This design enables the sensor to be connected to the robot in a similar manner as the robotic grippers.

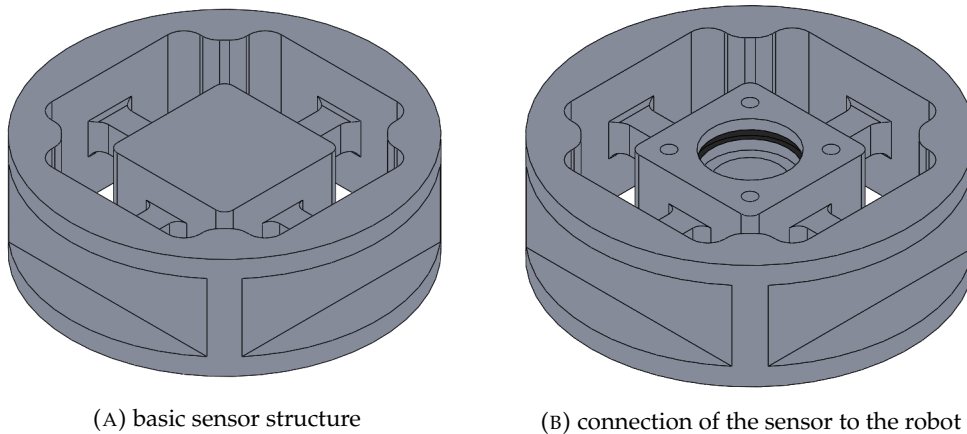


FIGURE 2.6: Showing the starting point and first step of the design of the airflow passage

The second step in the design of the airflow path is to connect the central block and connection rim for airflow. To allow for a maximum measurement sensitivity and minimal cross-coupling the sensors, the connection rim and central block should only be connected by the strain measuring beams and thin plates. These observations lead to the conclusion that the air passage should ideally be passed through the measuring beams, as shown in Figure 2.7.

The area of these tubes is much lower than the area of a normal vacuum hose. This raises the question, what diameter is sufficient to pass enough air through to ensure that a fair measurement can be performed. The main reason for having a large area in a vacuum tube is to allow for a fast actuation time. During testing, this is not of interest. If a suction cup requires a longer time to create a proper seal, the load during the P&P motion can still be studied. However, since no suction cup will create a perfect seal, every product has a certain amount of leakage flow. If the integrated airflow passage is not able to pass this amount of flow, the vacuum pressure will decrease, leading to an unfair comparison of the load during the motion of the robot. To check if this design constraint could be met, four small pieces of Festo pneumatic tubing with a length of 30 mm and a diameter of 4mm were connected to a typical end effector. This set up simulated the 4 strain measuring beams in the sensor design. This set up was able to hold the product without any noticeable decrease in performance. As long as holes in the strain measuring beams are at least 4 mm in diameter with a length of less than 30 mm, the sensor structure is expected to allow sufficient airflow passage.

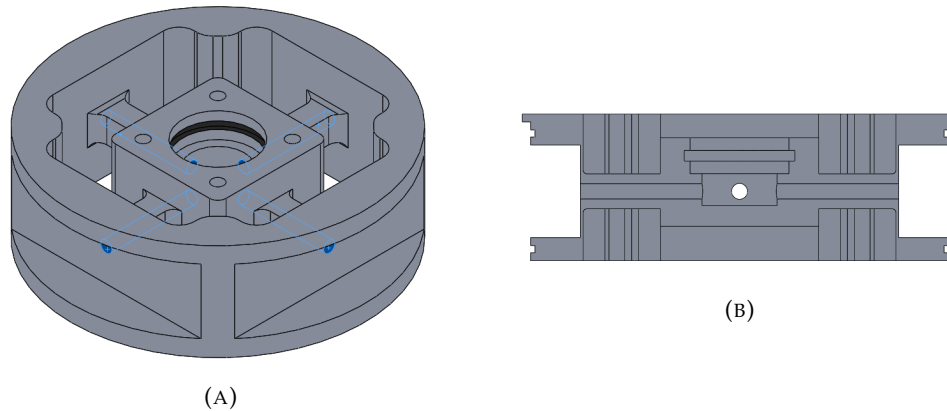


FIGURE 2.7: Connection of the vacuum flow from central block to connection rim

In the third design step, the supplied vacuum pressure was sealed in 4 separate chambers by adding a ring around the sensor as is depicted in Figure 2.8b. This ring is made as a separate part and will be press fitted to the main sensor body. An end stop for this ring was created by adding a small protruding rim. To ensure an air tight seal, two piston type seals were added to the connection rim. The o-rings were designed to have an o-ring compression of 20% and a 5% o-ring diameter stretch to keep the o-ring located in its groove. The two piston seal o-rings are depicted in black in Figure 2.8a.

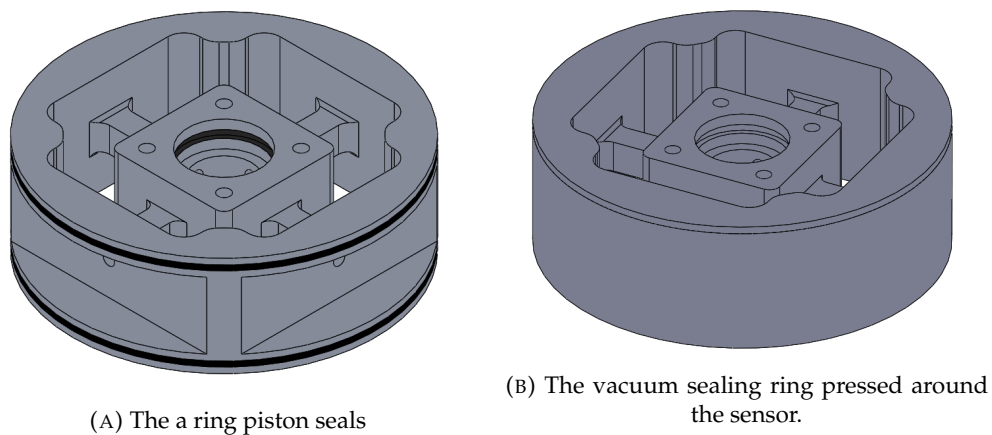


FIGURE 2.8: The addition of a vacuum sealing ring using two piston seals. This vacuum sealing ring ensures no unwanted opening for the air flow.

In the fourth step, four slots were added to the bottom part of the main sensor body. The slots are depicted in Figure 2.9 and are used to pass the airflow to the final parts of the airflow integration design.

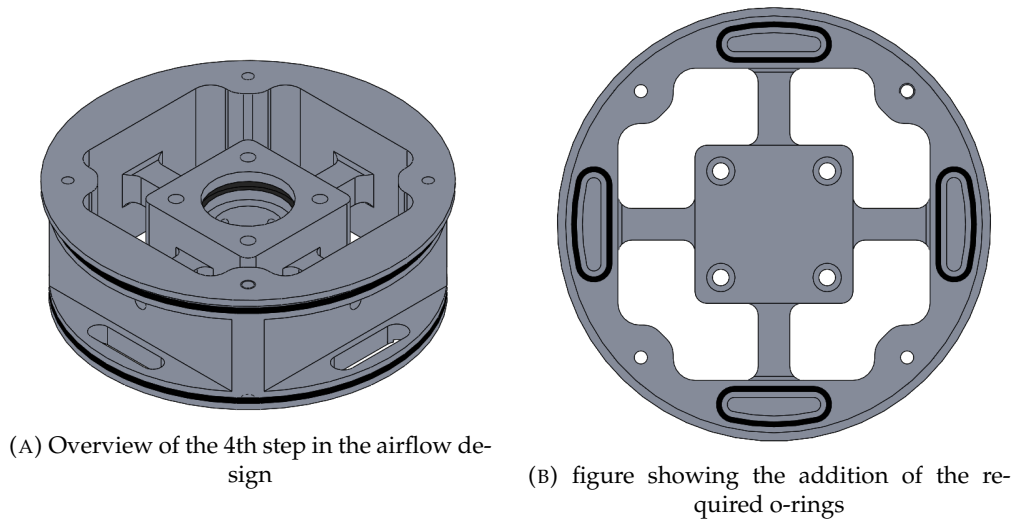
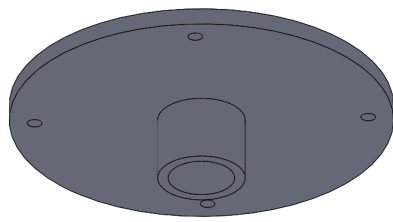
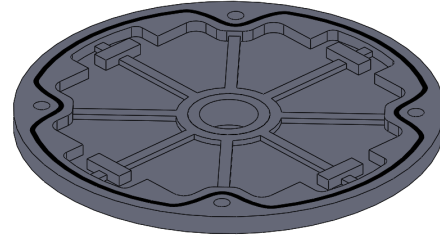


FIGURE 2.9: Addition of slots to the sensor design to pass the air flow to the gripper connection platform

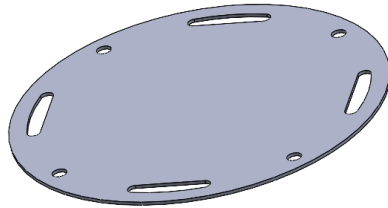
In the final step of the design, a new chamber consisting of two parts is designed. This chamber connects to the four slots added in step four and the robotic grippers, joining the sensor and robotic gripper together. The bottom part of the chamber, depicted in Figure 2.10a, ends in a hollow tube similar to the tube coming from the robot platform. To this tube, all previously designed grippers can be attached. To complete the chamber, the top part is added, which consists of a simple plate that functions as a lid for the bottom part. The top part and the designed chamber are shown in Figure 2.10c and 2.10d respectively. To ensure an air tight seal between the bottom and top parts, an o-ring is added, shown in black in Figure 2.10b. The same is applicable for the seal between the top part and the main sensor body. This seal requires four o-rings as is depicted in Figure 2.9b. To ensure sufficient stiffness, spokes were added to the bottom plate. As a final addition, four supporting blocks are added to the bottom plate. These support blocks create the required o-ring sealing pressure for the o-rings between the top plate and the sensor main body.



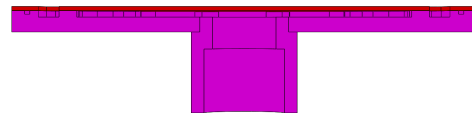
(A) View of the gripper connection axis of the sensor



(B) View of the milled structure and seal in the bottom connector



(C) The vacuum sealing plate



(D) The combination of the bottom connector and the top vacuum sealing part

FIGURE 2.10: Overview of the two elements of the bottom vacuum chamber

This finalizes the design of the airflow passage integration into the sensor structure. A visual summary of the design steps can be found in Figure 2.11. Because of the addition of the additional parts required to pass the airflow through the sensor, the design is theoretically no longer monolithic. However, the strain measuring main sensor body remains monolithic in design and will keep the beneficial effects associated with monolithic designs.

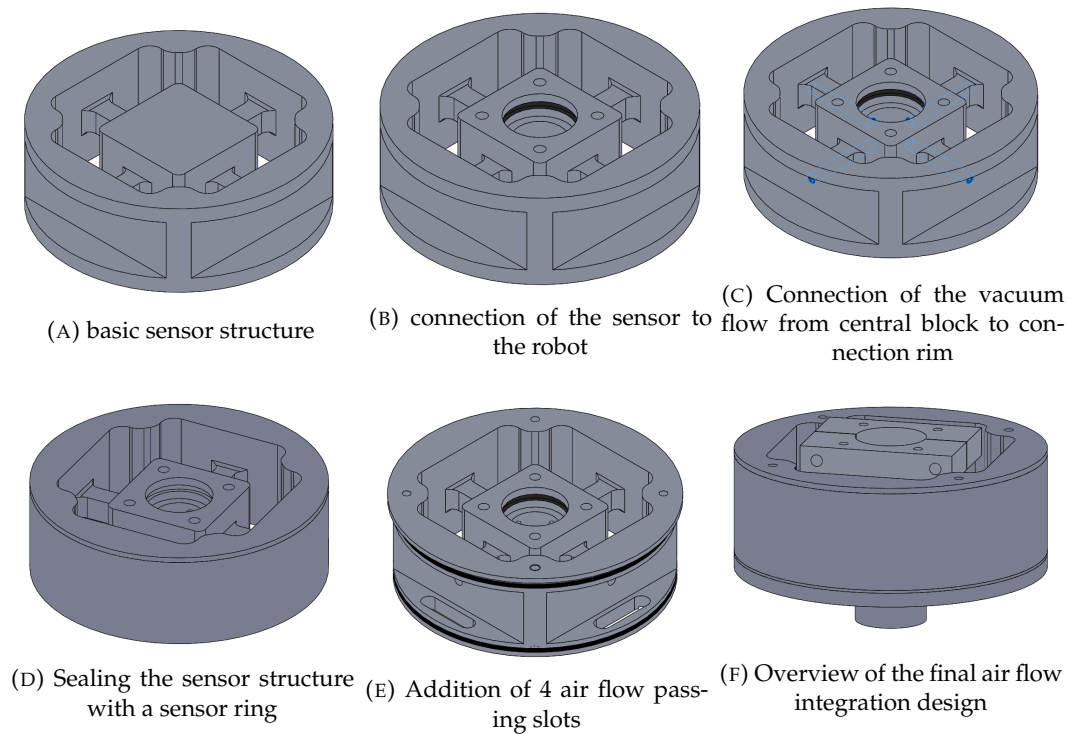


FIGURE 2.11: A step by step overview of the design process of integration of the air flow tubing into the sensor structure

A cross sectional view of the sensor is shown in Figure 2.12 and will be used to explain the sensor combined sensor operation. For extra clarity, the sensor components have been colored. The sensor is attached to the robot platform in a similar manner as a robotic gripper. The tube from the robot platform is inserted in the connection hole, labeled 1 in Figure 2.12. This connection requires a separately designed clamp, which is also depicted in Figure 2.12. The connection interface to the sensors, labeled 2 in Figure 2.12, is designed as a copy of the connection interface of the robot platform. Due to this design decision all previously design robotic grippers can be measured using this sensor. The separate vacuum chamber required for the connection interface is attached to the sensors main body using 4 bolts. These bolts clamp the bottom plate, labelled 3 in Figure 2.12, to the main sensor body.

The blue arrow indicate the airflow through the sensor structure. To create an air tight seal o-rings were added at each interface with the outside air. The selection and design of the o-rings and their grooves are essential to ensure a proper seal and require special design effort.

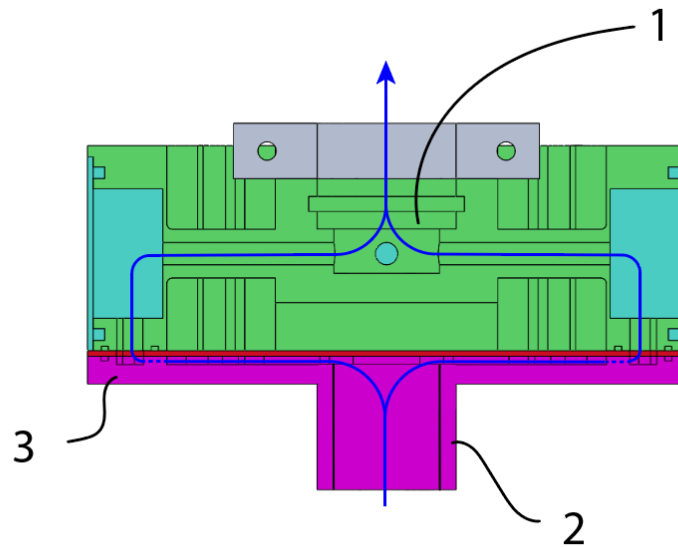


FIGURE 2.12: The cross sectional view of the designed sensor. Label one shows the connection point to the robot, label 2 shows the connection point for a gripper, label 3 shows the vacuum chamber that has to be clamped to the sensors main body. The blue line indicates the airflow path.

2.5 Structural Design

In this section, the structural design of the sensor is explained while using the selected SQP optimization technique. This section will start with explaining the optimization scheme, cost function and constraints to meet all the set requirements. The neglect of the design aspects important for dynamic robot motion in literature is addressed here. After the explanation of the optimization scheme, the used FEM model is briefly discussed. Then the optimization outcome is presented after which the final design is validated using the FEM model.

Design variables

For the optimization, five design variables are selected. Some designs in literature have considered nearly all possible parameters as a design variable, while other designs only considered a few variables [109],[139]. Choosing more design variables is expected to result in a better functioning sensor since more aspects of the sensor can be optimized. However, this will drastically increase the computational effort of the optimization scheme.

Due to the available manufacturing method of CNC milling as apposed to edm wire cutting, some curvatures were set a priori. In this work, only the most influential design parameters were considered as shown in Figure 2.13. These parameters directly influence the stiffness of the sensor. Figure 2.13 shows the Maltese cross sensor in its original shape. In the optimization, the airflow passing aspects are included.

The design variables are grouped in vector $\vec{X} = [b, h, H, L, t]$. Here, the first variable (b) is the strain measuring beam width. The second variable (h) is the strain beam

Design variable	Upper bound	Lower bound
b	8 mm	15 mm
h	8 mm	21 mm
H	15 mm	25 mm
L	13 mm	25 mm
t	0.7 mm	3 mm

TABLE 2.2: Table showing the design variable bounds used during optimization

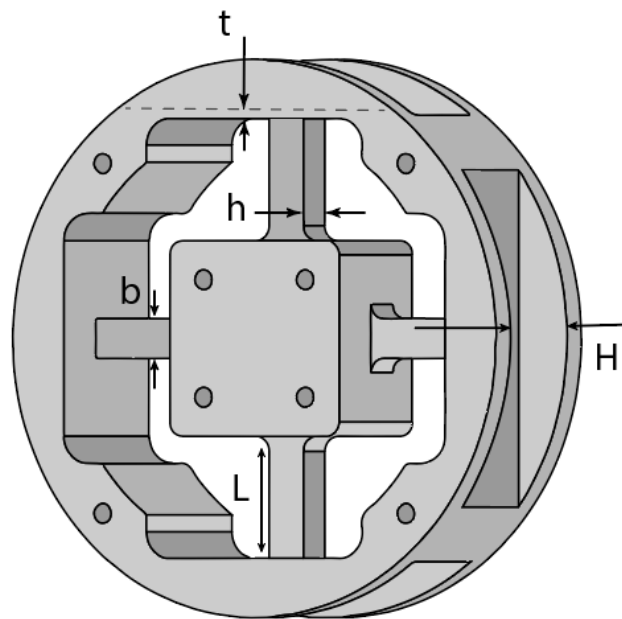


FIGURE 2.13: A visual overview of design variables of the mechanical sensor design

height. The third variable (H) is the height of the thin plate. The fourth variable is the length of the strain measuring beams (L). The fifth and final design variable is the thickness of the thin plates (t).

Table 2.2 shows the bounds set for the design variables. Most of the upper and lower bounds were set according to physical constraints or literature. The bounds for H and the the upper-bound for L and t were set to limit the range of the optimizer because no meaning-full physical limitation could be defined. If the optimizer hits one of these bounds, the bounds should be adjusted accordingly.

Optimization work flow

The work flow of the optimization scheme is shown in Figure 2.14. The optimization scheme used in this work is inspired by the successful designs presented in literature [108], [109], [139]. Some changes have been made to have an easier implementation in industry. For example, Solidworks was used to model the sensor structure, the

software package COMSOL for FEM analysis, and Matlab for optimization calculations. These software packages offer training and customer support, are well established in industry and offer many options for extension on the optimization scheme. By using the appropriate professional software packages, the optimization scheme is applicable in a wider part of industry without requiring extensive knowledge of mechanical design theory or optimization.

An optimization sequence starts by picking a set of starting dimensions stored in COMSOL. The model is build by Solidworks and passed on to COMSOL. COMSOL runs the FEM analysis and calculates the quantities required to calculate the cost function and constraints. These values are passed on to MATLAB, which calculate the cost function and constraints, if the optimization stop criteria are not met, Matlab updates the design variables which are passed to COMSOL, which updates the Solidworks model, starting the next optimization loop.

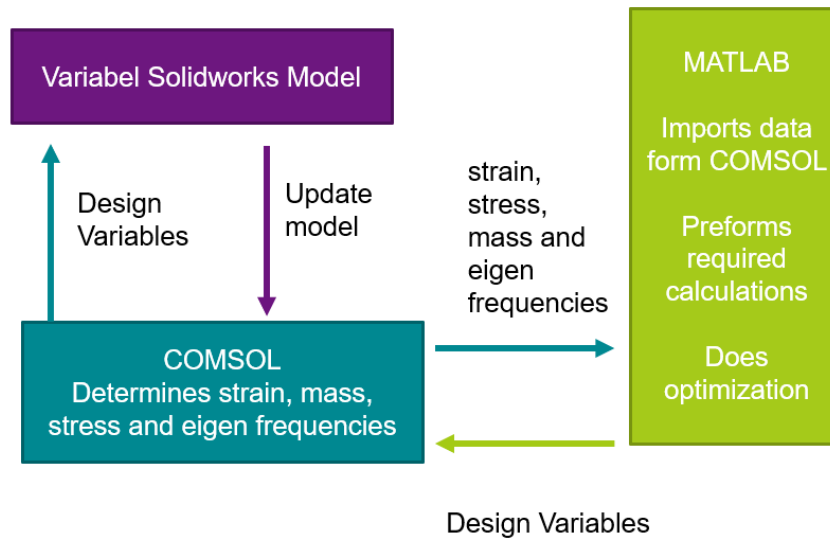


FIGURE 2.14: Overview of the optimization method

Optimization problem

To perform the optimization in Matlab, the optimization problem should be fully determined. This is done by determining the cost function and constrains. The optimization goal will be defined as the average sensor sensitivity over six measuring bridges when the combined maximum load is applied. The combined maximum is defined as the load case where all 6 load directions are at their maximum. The cost function is physical defined as the negative average absolute strain measured at the maximum load. Minimizing this function will maximize the average measured strain at combined maximum load. To limit the magnitude of the cost function to be around one, the cost function was divided by 200 to obtain $f_{opt}(\vec{X})$, which is shown in equation 2.2 and was used during optimization.

$$f_{opt}(\vec{X}) = - \frac{|\epsilon_{Fx}| + |\epsilon_{Fy}| + |\epsilon_{Fz}| + |\epsilon_{Mx}| + |\epsilon_{My}| + |\epsilon_{Mz}|}{6 \cdot 200} \quad (2.2)$$

In this calculation it is assumed that the coupling effects are small compared to the

true measured strain. The measured strain in one bridge under the combined maximum load will be nearly identical to the measured strain in this bridge when a pure load in its measuring direction was applied.

Next to the cost function, constraints are added to the design to take other important design considerations into account. These design criteria are deliberately not added to the cost function to prevent any priority issues in a combined cost function. The constraints for the cross-coupling, sensor mass, life time, eigenfrequency and stiffness were set according to the design requirements. Additional constraints were added to ensure no geometrical errors would occur in the sensor structure. The mathematical overview of the optimization problem is shown in equation 2.3

To ensure a sufficient signal in each measuring direction, a minimum strain was set to each of the six measuring bridges. The minimum strain ϵ_{min} is set to $300 \frac{\mu m}{m}$, which is slightly lower than values used in literature [139]. Since more constraints are added compared to other designs, less strict bounds have to be set to find a design that meets all constraints.

To provide sufficient life time, a maximum strain at the strain gauges and maximum stress constraint had to be set. The life time constraints were set to the 6 individual loading conditions and not the combined maximum load. The combined maximum load rarely happens in practice. Setting the life time constraint of the sensor to this level will result in an unnecessary decrease in measuring performance.

To provide sufficient life time, a maximum strain was set according to the data sheet. A maximum cyclic strain of $\pm 900 \frac{\mu m}{m}$ is allowed for the desired fatigue life [152]. It is assumed that all 4 strain gauges in the Wheatstone bridge measure about the same strain. Following this reasoning, this constraint is set for all 6 measurement bridges and not for each strain gauge individually.

The maximum stress was set to $150 Mpa$ to limit the fatigue of 7075 T6 aluminium [153], ensuring sufficient life time.

$$\begin{aligned}
 & \min_x f_{opt}(\vec{X}) && (2.3) \\
 \text{subject to:} & && \\
 & 8 \text{ mm} < b &< 15 \text{ mm} \\
 & 8 \text{ mm} < h &< 21 \text{ mm} \\
 & 15 \text{ mm} < H &< 23 \text{ mm} \\
 & 15 \text{ mm} < L &< 25 \text{ mm} \\
 & 0.7 \text{ mm} < t &< 3 \text{ mm} \\
 & \epsilon_{min} < \epsilon_{F(i)} < \epsilon_{max} & i = 1, \dots, 6 \\
 & 2000 \text{ Hz} < \omega_n && \\
 & 0.9 \cdot h < H && \\
 & m &< 450 \text{ g} \\
 & CC_{15} &< 5\% \\
 & CC_{24} &< 5\% \\
 & \sigma_{maxF(i)} &< \sigma_{Fatigue} & i = 1, \dots, 6
 \end{aligned}$$

FEM and mesh setting

Similarly to picking the correct optimization algorithm, the FEM analysis should also be considered carefully. Firstly, the model excluded geometric nonlinearities because the deformations are very small. The validity of this exclusion was validated by performing a test calculation with and without geometric nonlinearities. No significant difference was found between the test calculations.

Secondly, the correct material and boundary conditions have to be selected. The material 7075-T6 aluminium is part of the standard COMSOL material library. For the boundary conditions, either the central block or the outer rim has to be fixed. The part that is not fixed is used to be applied with the external load.

The connection rim was constrained using a fixed boundary condition. The central block is used to exert the external loads, because in COMSOL only forces can be applied, while moments have to be created by applying two anti parallel forces. As the length of the strain measuring beam changes, the position of the mounting holes in the connection rim change accordingly. The location of the connection holes in the central block do however not change position. The holes in the central block provide a constant moment arm for the anti parallel forces.

Thirdly, a proper mesh should be created. The model is changing in size and shape with each iteration of the optimizer. The mesh needs to be automatically generated for any set of design variables. The mesh was designed for the most demanding set of design variables $\vec{X} = [b, h, H, L, t] = [8, 8, 25, 0.7, 25] \text{ mm}$. When values of strain measuring beams length and thin plates height were taken as small as possible, a finer mesh was required. When values of strain measuring beam length and thin plate height were picked as large as possible, a larger thin plate and slender longer beams were created that required harder geometries to mesh properly. A mesh sufficient for the most demanding design variables is expected to also achieve the desired performance on less demanding design variables.

To mesh the sensor structure, the sensor was divided in 6 domains. Each domain has its own mesh size. Areas requiring more detail are meshed finer than areas which do not require the same level of detail. In this manner each domain can be meshed with just the right amount of detail. The selected domains from fine to course are the thin plate, the strain gauge surface, the milled corners, the strain measuring beams, the central block and the connection rim.

To study which level of detail was required, a mesh convergence and quality study was performed. In this study the mesh is iterative refined. At each iteration the strain matrix was calculated [139]. COMSOL also offers a mesh quality statistic, this was used as a second check for the selected mesh. To determine the mesh quality, a quality measure had to be picked. For this work, the standard skewness measure was picked, but other quantities can also be used [154]. Appendix E gives a more in depth explanation and shows the results of these studies.

Lastly, the measured strain can be compared to designs found in literature. The strains calculated using the model were compared to those found in literature as is shown in Table 2.3. For this comparison only the diagonal terms of the strain matrix were considered. The load applied and dimensions to the sensor were similar to the load applied in literature. It is concluded that the result of the simulation is likely to be correct, because the calculated strain and the strain from literature are in the same order of magnitude.

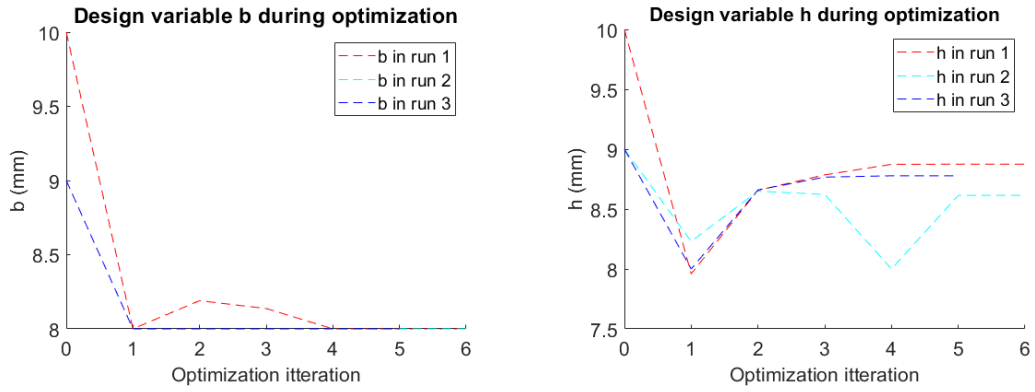
Measuring direction	strain from design $\frac{\mu m}{m}$	strain from [139] $\frac{\mu m}{m}$	strain from $\frac{\mu m}{m}$ [143]
ϵ_{Fx}	429.1	350.0	174
ϵ_{Fy}	428.1	350.1	174
ϵ_{Fz}	301.3	437.8	1872
ϵ_{Mx}	1302.3	859.9	1375
ϵ_{My}	1302.1	859.9	1375
ϵ_{Mz}	734.26	486.2	1486

TABLE 2.3: Comparing the diagonal elements of the strain matrix strain

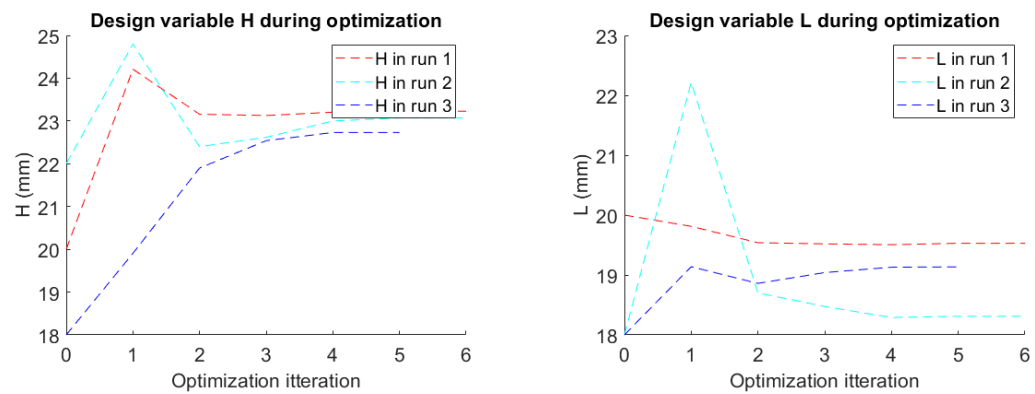
As an extra conformation, the mesh quality and the convergence study were also studied for several different sets of design variables.

2.5.1 Optimization results

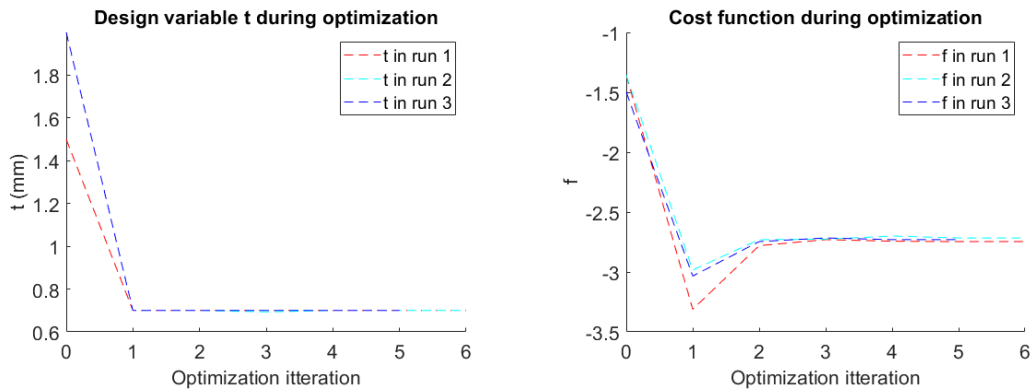
For illustration purposes, Figure 2.15 shows the results of three optimization calculations all considering different starting variables. In the design of the sensor many more optimization runs were performed, showing similar behavior to the plots in 2.15 Figure 2.15a through 2.15e, and showing the convergence of the design variables. Figure 2.15f shows the corresponding value of the cost function. The infeasible design points are labelled with an x in Figure 2.15f. From these calculations the final sensor dimensions were picked as $\vec{X}_{final} = [8, 8.75, 23.25, 19.5, 0.7] mm$. The results show that multiple design variables sets achieve nearly the same cost function as is reported in literature [109].



(A) The change of the design variable b for five different optimization runs. A different set of design variables is used for each optimization run
 (B) The change of the design variable h for five different optimization runs. A different set of design variables is used for each optimization run



(C) The change of the design variable H for five different optimization runs. A different set of design variables is used for each optimization run
 (D) The change of the design variable L for five different optimization runs. A different set of design variables is used for each optimization run



(E) The change of the design variable t for five different optimization runs. A different set of design variables is used for each optimization run
 (F) The change of the cost function for five different optimization runs. A different set of design variables is used for each optimization run

FIGURE 2.15: Results of the optimization runs

2.6 Analysis of the final design

To compare to the fabricated sensor and to verify if the most important constrains were met, the final design was analysed to determine mass, maximum stress, eigenfrequency, strain matrix and cross-coupling matrix. The evaluation of these constrains was done using the FEM model. The results are shown below and indicate

that the most important criteria are met.

2.6.1 Maximum von Mises stress

The maximum von mises stress was found under a M_y and M_x loading. For this load case, a maximum stress of 149MPa was calculated using the FEM model. The maximum stress calculated under the six different load cases are shown in Figure 2.16

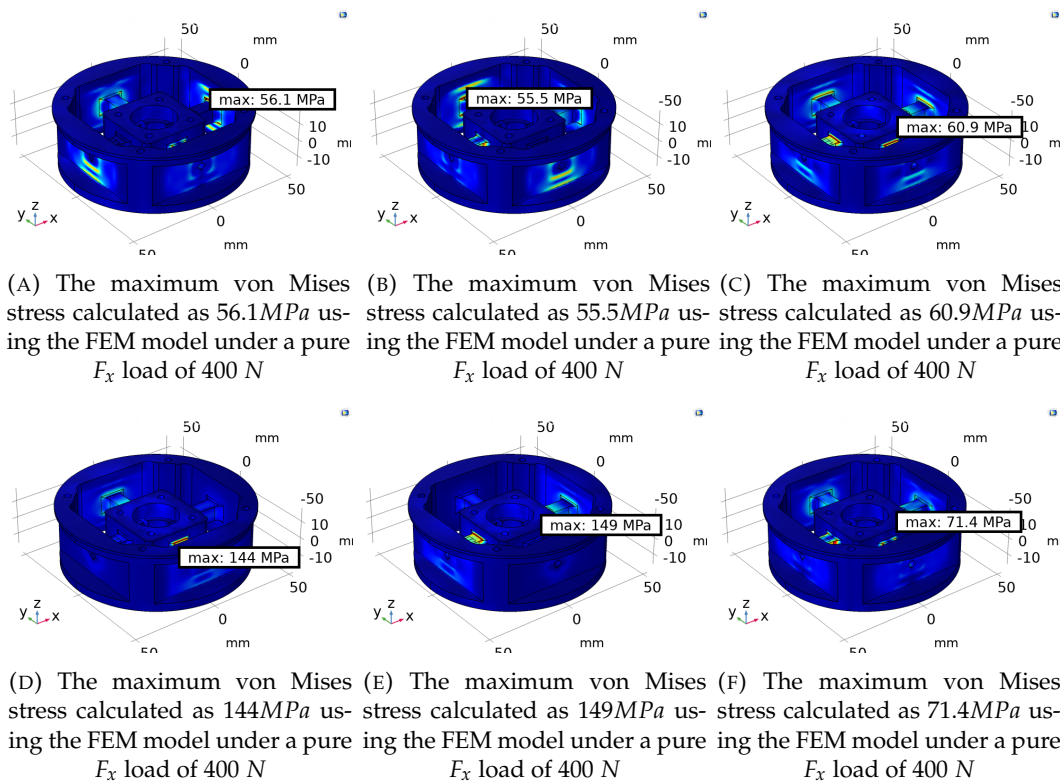


FIGURE 2.16: The von Mises stress for the six load conditions at maximum intensity, calculated using the FEM model

2.6.2 Mass and eigenfrequency

Following the COMSOL model, the total sensor mass, including the airflow integration parts, was determined to be 449.6g . The eigenfrequency of the sensor while constraining the central block was found to be 2006Hz . More details on the determination of the eigenfrequency can be found in appendix E. Figure E.7c shows the corresponding eigenmode.

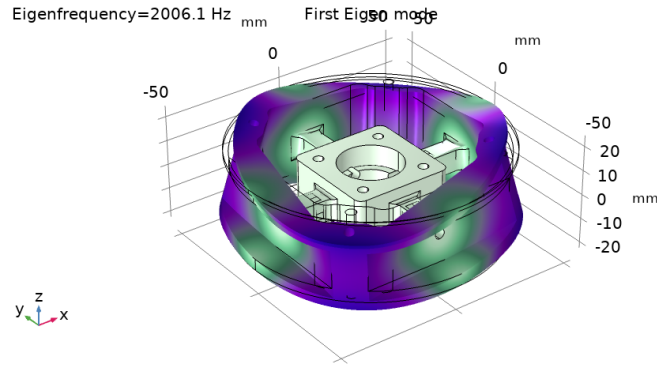


FIGURE 2.17: The first eigenmode calculated by COMSOL, considering the sensor main body with connection points fixed on the central block

2.6.3 Strain and cross-coupling matrix

From the FEM analysis, the theoretical strain and cross-coupling matrix can be calculated. During sensor validation, these results can be compared to see if the fabricated sensor matches the design. The method for calculation the cross-coupling is well documented in literature and is also explained in appendix D [109], [139]. This comparison gives insight into the error sources of the fabricated sensor. The strain matrix from the FEM model is shown in Table 2.4. For the strain matrix it can be seen that the minimum and maximum strain constraints, 300 and 900 $\frac{\mu m}{m}$ respectively, are met.

Applied pure load	F_x	F_y	F_z	M_x	M_y	M_z
Bridge circuit	$S_{ij}(\mu m/m)$	$S_{ij}(\mu m/m)$	$S_{ij}(\mu m/m)$	$S_{ij}(\mu m/m)$	$S_{ij}(\mu m/m)$	$S_{ij}(\mu m/m)$
S_{F_x}	313.5	0.0	0.0	0.0	-10.9	0.0
S_{F_y}	0.0	312.6	0.0	-11.0	0.0	-0.1
S_{F_z}	0.0	-0.4	363.2	-8.0	0.0	0.0
S_{M_x}	0.0	0.0	0.0	895.0	0.0	-0.5
S_{M_y}	0.0	0.0	0.0	0.0	895.0	-0.5
S_{M_z}	0.0	0.0	0.0	-0.1	0.0	543.6

TABLE 2.4: The strain matrix calculated by the FEM model for the final sensor design

Applied pure load	F_x	F_y	F_z	M_x	M_y	M_z
Axis of reading	$CC_{ij}(\%)$	$CC_{ij}(\%)$	$CC_{ij}(\%)$	$CC_{ij}(\%)$	$CC_{ij}(\%)$	$CC_{ij}(\%)$
F_x	-	0.0	0.0	0.0	-3.5	0.0
F_y	0.0	-	0.0	-3.5	0.0	0.0
F_z	0.0	-0.1	-	-2.2	0.0	0.0
M_x	0.0	0.0	0.0	-	0.0	-0.1
M_y	0.0	0.0	0.0	0.0	-	-0.1
M_z	0.0	0.0	0.0	0.0	0.0	-

TABLE 2.5: The cross-coupling matrix determined from the FEM model for the final sensor design

2.7 Sensor Fabrication

Now the sensor is validated and all design requirements are met according to the FEM Model, the sensor was fabricated according to the optimized design vector

$X_{final}^{\vec{}} = [8, 8.75, 23.25, 19.5, 0.7] \text{ mm}$. Figure 2.18 shows the designed sensor in Solidworks attached to the case packing robot after fabrication.

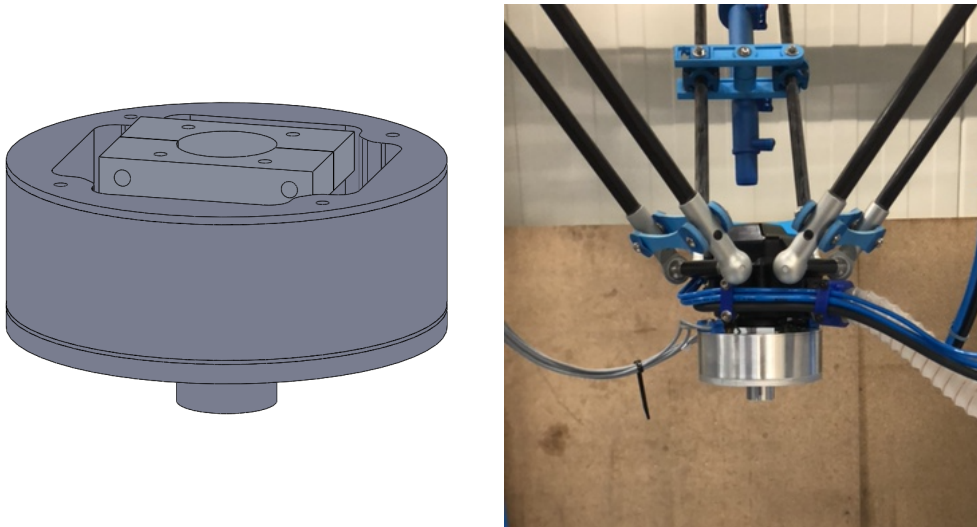


FIGURE 2.18: The designed sensor in Solidworks and the sensor attached to the case packing robot after fabrication

2.8 Sensor validation

In this section the steps taken to validate the sensor are explained. The sensor starts off with calibration of the sensor and is followed by the validation of the design requirements.

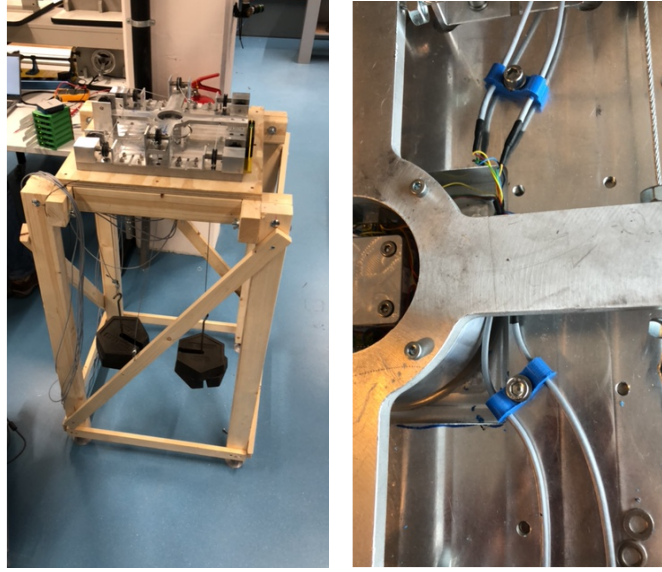
2.8.1 Calibration

For sensor usage, a calibration process is required. Despite design efforts, the creation of a decoupled sensor was unsuccessful. Initial testing showed that the sensor had significant coupling as can also be seen in Table 2.6. The method for cross-coupling calculation is well documented in literature and is also explained in appendix D [109], [139].

For coupled sensors the least squares (LS) method is the main calibration method used to combat cross-coupling errors [108], [110], [155]. This method was also the basis of the calibration process used in this study and is further explained in section 2.8.1.

For the calibration a set up calibration jig was designed and fabricated. The goal of this calibration jig is to repeatably apply six independent loads. For an intuitive calibration process, applying a pure load is preferable. In literature, some examples of calibration jigs for Maltese cross sensors can be found [108], [156]. Figure 2.19a shows the fabricated calibration jig. The central block of the sensor is fixed to the center of the calibration jig. To the outer-ring a load applying cross was connected, which can be seen in Figure 2.19b. The load applying cross and the rollers on the calibration jig are used to exert a load on the sensor. One end of a metal cable is attached to the calibration cross, while the other end is passed over a roller. By

attaching a known mass to the cable, the sensor can be loaded as desired. To reduce damage risk, the sensor was loaded to at most 75% of its maximum load capacity during calibration.



(A) Visual overview of the calibration jig (B) Figure showing the load applying cross

Applied pure load Axis of reading	F_x CC _{ij} (%)	F_y CC _{ij} (%)	F_z CC _{ij} (%)	M_x CC _{ij} (%)	M_y CC _{ij} (%)	M_z CC _{ij} (%)
F_x	-	-0.1 ± 0.8	0.5 ± 1.0	4.8 ± 1.3	5.6 ± 1.7	-1.9 ± 2.7
F_y	-2.1 ± 0.8	-	5.1 ± 3.5	-15.7 ± 0.8	16.5 ± 1.4	25.6 ± 2.7
F_z	-0.6 ± 1.8	-1.5 ± 0.5	-	5.4 ± 1.1	-7.8 ± 7.2	9.5 ± 1.0
M_x	0.9 ± 0.2	0.9 ± 0.7	0.2 ± 1.2	-	0.3 ± 0.4	0.1 ± 0.5
M_y	-1.6 ± 0.7	0.0 ± 0.3	-0.3 ± 5.2	-0.6 ± 0.3	-	-2.3 ± 0.8
M_z	-0.2 ± 2.5	1.8 ± 1.9	1.0 ± 0.8	4.7 ± 0.6	-0.7 ± 1.5	-

TABLE 2.6: The cross-coupling matrix determined from the fabricated sensor that is used to check the requirement of the least squares calibration method. The data is presented as the average value and is followed by its standard deviation taken over 24 measurements

Least squares calibration method

The basic principle and an additional suggested method of implementation of the LS method was already suggested by the first design papers on Maltese cross sensors [110]. The LS method requires applying six independent loads to the sensor that resolve in a single point of which the location is known [110]. From these six loads, the six columns of the compliance matrix are calculated. The compliance matrix (C) for this sensor is a six by six matrix, which is used to translate the sensors output voltage to a measured load as is shown in equation 2.4. This error reduction technique will only be capable of performing linear error reduction.

$$\vec{F} = C^{-1} \cdot \vec{V} \quad (2.4)$$

For each of the six applied load vectors, equation 2.4 has to apply. Re-writing this equation results in the matrix equation required for this calibration method. During

the calibration process, three indices i, j and k are used to distinguish different forces, strain gauge voltages and compliance matrices entries.

C_{jk} = the component of the compliance matrix that will be solved for

v_{ij} = the amplified output voltage the j 'th strain gauge bridge,
due to the application of the i 'th load

f_{ik} = the k 'th component of the i 'th independent load

For the designed sensor:

$$i = (1, \dots, 6)$$

$$k = (1, \dots, 6)$$

$$j = (1, \dots, 6)$$

As an example, take $i = 2$ and $j = 1$, referring to the output voltage of the F_x strain gauge bridge due to a load in the F_y direction. This output voltage is only a function of the second row of the compliance matrix and the applied load vector according to equation 2.4. This insight can mathematically be written as the relationship shown in equation 2.5 [110].

$$v_{ij} = C_{j1} f_{i1} + \dots + C_{j6} f_{i6} \quad (2.5)$$

This equation can be summarized as a matrix equation shown in equation 2.6, which has to be solved 6 times to find the compliance matrix [110].

$$\begin{bmatrix} v_{1j} \\ v_{2j} \\ v_{3j} \\ v_{4j} \\ v_{5j} \\ v_{6j} \end{bmatrix} = \begin{bmatrix} f_{11} & f_{12} & f_{13} & f_{14} & f_{15} & f_{16} \\ f_{21} & f_{22} & f_{23} & f_{24} & f_{25} & f_{26} \\ f_{31} & f_{32} & f_{33} & f_{34} & f_{35} & f_{36} \\ f_{41} & f_{42} & f_{43} & f_{44} & f_{45} & f_{46} \\ f_{51} & f_{52} & f_{53} & f_{54} & f_{55} & f_{56} \\ f_{61} & f_{62} & f_{63} & f_{64} & f_{65} & f_{66} \end{bmatrix} \begin{bmatrix} C_{j1} \\ C_{j2} \\ C_{j3} \\ C_{j4} \\ C_{j5} \\ C_{j6} \end{bmatrix} \quad (2.6)$$

Proposed improvements

In this study several improvements are proposed with respect to the state-of-the-art. Firstly more measurements are performed to calculate the cross-coupling and error matrix with respect to literature. Most papers using the LS calibration method only present one cross-coupling and error matrix [108], [157]. By presenting the data in this manner, it is implicitly assumed that there is no deviation from the mean measurement, which is an invalid assumption. The LS method even has a relatively high standard deviation compared to other calibration methods [155]. In this work, the error of the sensor will be considered as a mean error with a standard deviation. The maximum error will be considered as the largest absolute bound on the 95% confidence interval. The same holds for the cross-coupling and measurement error after calibration.

In literature, the calibration jig is often assumed to exert a pure load [108], [139]. This is however not true for most of the time and will result in the introduction of unnecessary errors. The focus of the calibration process in this work is to determine the applied load more precisely, reducing the errors introduced by the calibration setup. This is possible because the non-pureness of the applied loads should not and does not have to be neglected using the LS method. Using this improvement, the necessity of precise weight calibration is also eliminated.

For the application of each of the six loads two attachment points are used. Figure 2.20 shows the manner in which calibration loads are applied.

Since the weights are precisely measured, the error caused by a difference in mass can be calculated. The weight difference between the two points of load application is indicated using Δm_i .

Furthermore, the load applying cross is attached to the top of the sensor, displaced in z direction with respect to the measuring frame of the sensor. This displacement is labeled r_z and causes a moment to be applied simultaneous to the application of a force in x and y direction. Both the error due to difference in calibration masses and non-pureness of the load are reduced via this proposed method. The loads applied during calibration are shown in equation 2.7

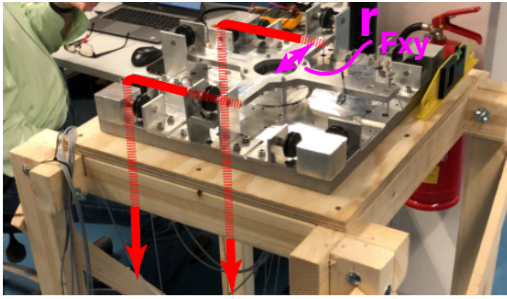
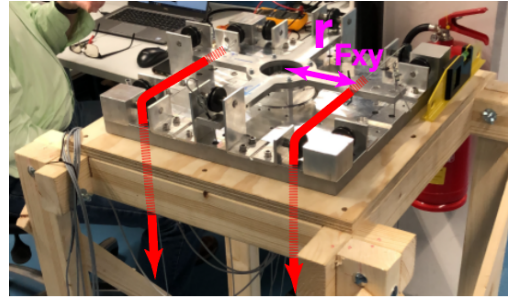
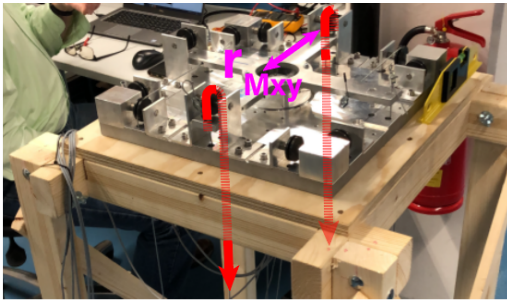
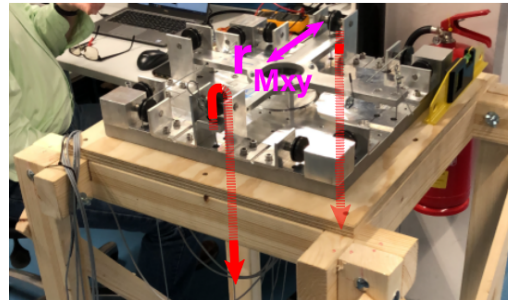
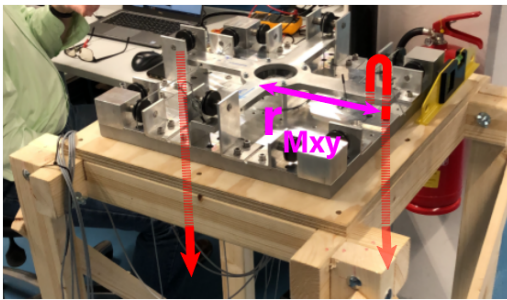
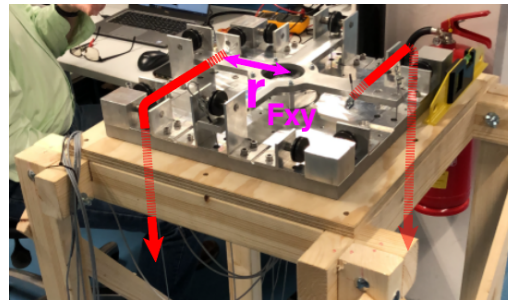
(A) The application of a load mainly in the F_x direction(B) The application of a load mainly in the F_y direction(C) The application of a load mainly in the F_z direction(D) The application of a load in the mainly M_x direction(E) The application of a load in the mainly M_y direction(F) The application of a load in the mainly M_z direction

FIGURE 2.20: Figures showing how the 6 different loading conditions are obtained using the calibration table. Equation 2.7 shows how the loads are considered during the calibration process.

$$F_{xSensor} = \begin{bmatrix} F \\ - \\ - \\ - \\ F \cdot r_z \\ \Delta F \cdot r_{Fxy} \end{bmatrix} \quad F_{ySensor} = \begin{bmatrix} - \\ F \\ - \\ - \\ -F \cdot r_z \\ \Delta F \cdot r_{Fxy} \end{bmatrix} \quad F_{zSensor} = \begin{bmatrix} - \\ - \\ F \\ \Delta F \cdot r_{Fxy} \\ - \\ - \end{bmatrix} \quad (2.7)$$

Under the assumption that the total load on the sensor F is mostly divided evenly over the two cables.

$$Mx_{Sensor} = \begin{bmatrix} - \\ - \\ \Delta F \\ F \cdot r_{Mxy} \\ - \\ - \end{bmatrix} \quad My_{Sensor} = \begin{bmatrix} - \\ - \\ \Delta F \\ - \\ F \cdot r_{Mxy} \\ - \end{bmatrix} \quad Mz_{Sensor} = \begin{bmatrix} - \\ \Delta F \\ - \\ - \\ - \\ F \cdot r_{Fxy} \end{bmatrix}$$

Finally, the LS method is known as a manual and labor intensive process [155], mostly because the sensor has to be loaded and unloaded manually. This is often done in a step wise manner, required to determine the linearity of the sensor [108], [139]. Since the cross-coupling is defined at the sensor's rated load, only one of the loading intervals is used to calibrate the sensor.

As mentioned in section 2.3.4, the Maltese cross sensor is known for a good linear behavior, this was also validated for this sensor. As an example, Figure 2.21 shows that the linear behavior of the sensor in the F_x direction is excellent. The other directions show the same behavior.

Because of this excellent linear behavior, any load can be linearly scaled to the sensor's rated load. With this insight, any sensor load can be scaled to the sensor's rated load enabling the calibration, cross-coupling calculation and measurement error determination. This reduces the amount of calibration process that has to be performed before a meaningful standard deviation and mean can be calculated. A step wise overview of the calibration process is shown below. Measurements 2 through 7 were performed three times in positive and three times in negative direction resulting in a total of 24 calibration measurements.

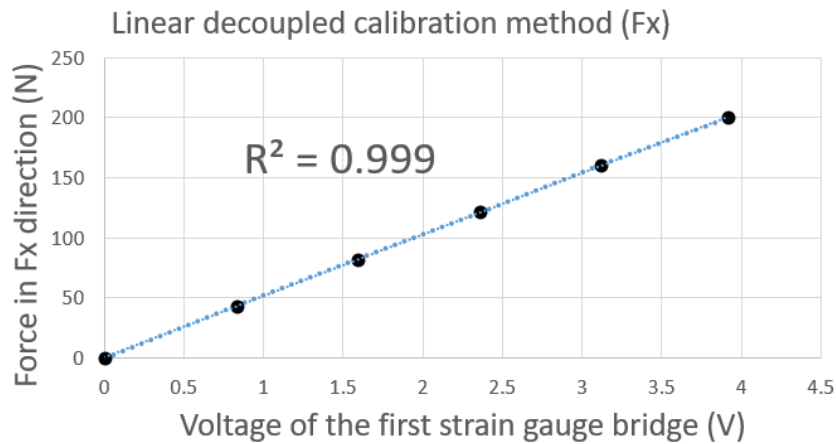


FIGURE 2.21: Showing the excellent linear behavior of the sensor in F_x direction

Because of the excellent linear behavior of the sensor, each load interval is used to calculate the compliance, cross-coupling, and measuring error matrix. Apposed to only using the maximum load for these calculations.

1. The zero offset of the amplifiers need to be adjusted so that the 0 volt measurement is placed at the unloaded position.

2. The maximum calibration load has to be applied to the sensor. The amplification factor of the amplifier is set such that the design load will still be measurable by the sensor.
3. Different load intensities ranging from 0 to the calibration load have to be added to the sensor. The voltage at each load intensity level is precisely registered.
4. Apply a calibration load in a step wise manner to the sensor and note the directions that will be effected by Δm_i and r_z . In this work, four load intervals were used to apply moments and six loads intervals were used to apply a force.
5. For each load interval note the applied load and the achieved voltage levels at the corresponding load.
6. For each load interval scale the applied load to the maximum load and scale the measured voltage accordingly.
7. Use this data to populate the voltage vector and force matrix from equation 2.6.
8. Repeat step 2 to 4 for all six load directions to complete the data acquisition process of the calibration method.
9. With the gathered data four cross-coupling matrices can be made because only four load intervals were used for the application of moment.

2.8.2 Fabricated sensor validation

In this section the measurements performed to validate the design requirements are presented. A brief explanation of the method used to validate each design requirement is given, a more detailed explanation is given in appendix E. The design requirements that were validated are the measurement error, the strain, the mass, the hysteresis, final dimensions and strain gauge placement.

Passing airflow

The passage of airflow through the sensor was validated by measuring the cycle time at which product detachment occurred. If the sensor negatively influences the suction cup gripper performance, the cycle time causing product detachment will increase. A lower cycle time will required a higher acceleration and velocity, increasing the loading of the suction cup gripper. In this test is no difference in cycle time of the critical path was found. Figure 2.22 showed the test setup that was used to determine the cycle times.

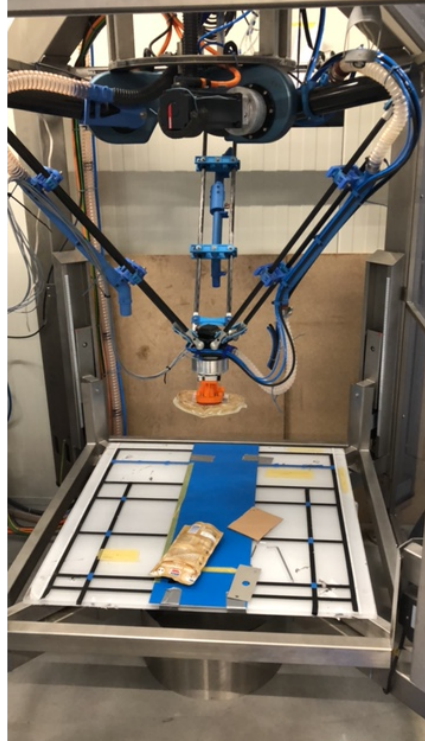


FIGURE 2.22: The test set up used to validate the airflow passage through the sensor structure. The test compared the cycle time with and without the addition of the sensor and found no difference in cycle time of the critical path.

Measurement errors

The error is calculated as the difference between the measured load and the applied load with respect to the sensor's rated load. The corrected measurement error is shown in Figure 2.7. For the sensor without correction, the error was expected to be at least as large as the cross-coupling presented in Table 2.6.

Applied pure load	F_x	F_y	F_z	M_x	M_y	M_z
Axis of reading	$\overline{CC_{ij}(\%)}$	$\overline{CC_{ij}(\%)}$	$\overline{CC_{ij}(\%)}$	$\overline{CC_{ij}(\%)}$	$\overline{CC_{ij}(\%)}$	$\overline{CC_{ij}(\%)}$
F_x	0.1 ± 1.6	0.0 ± 0.4	0.0 ± 0.56	0.1 ± 0.9	0.1 ± 0.9	0.0 ± 1.5
F_y	0.0 ± 0.3	0.1 ± 1.4	0.1 ± 0.44	0.0 ± 0.53	0.2 ± 0.5	0.1 ± 1.47
F_z	0.0 ± 0.3	0.0 ± 0.2	0.4 ± 3.3	0.0 ± 0.75	0.3 ± 1.6	0.1 ± 0.7
M_x	0.0 ± 0.1	0.0 ± 0.6	0.0 ± 0.63	0.1 ± 2.8	0.1 ± 0.3	0.0 ± 0.4
M_y	0.0 ± 0.5	0.0 ± 0.1	0.1 ± 4.0	0.0 ± 0.2	0.1 ± 1.6	0.0 ± 0.4
M_z	0.0 ± 1.4	0.0 ± 1.2	0.0 ± 0.5	0.0 ± 0.3	0.0 ± 0.9	0.1 ± 2.2

TABLE 2.7: The remaining errors after the LS calibration method. The data is presented as the average followed by its standard deviation taken over 24 measurements.

Strain matrix

The design of the sensor considered the strain of the strain gauges, during the measurements, amplifier output voltages were measured. To compare the designed and the fabricated sensor, the relationship between voltage and strain has to be determined. This was done using a shunt resistance on one of the strain gauges. Table shows the relationship between voltage and strain for each of the six measuring

bridges. Table shows the resulting average diagonal terms of the strain matrix. The error in the measured strain stems from the errors already made during the voltage measurements.

Measuring bridge direction	$\frac{\text{strain}}{\text{voltage}} \frac{\mu m}{m V}$	measured strain $\frac{\mu m}{m}$
F_x	36.7	296.5 ± 18.3
F_y	33.6	265.1 ± 16.8
F_z	42.2	417 ± 10.5
M_x	93.0	916.4 ± 46.5
M_y	89.9	888.0 ± 44.9
M_z	39.8	502.8 ± 19.9

TABLE 2.8: The relationship between measured voltage and strain

Sensor mass

The mass of the sensor was measured to be 480 grams, with a precision of $\pm 1g$.

Hysteresis

The hysteresis was calculated by considering the difference between the measured load before and after applying calibration loads measuring. The hysteresis is defined with respect to the rated load (FS). Table 2.9 shows the hysteresis measurements for the six calibration measurements.

Measuring bridge direction	Upper bound of the 99.7% Hysteresis error confidence interval
F_x	1.5 % FS
F_y	2.4 % FS
F_z	1.6 % FS
M_x	1.6 % FS
M_y	1.5 % FS
M_z	1.3 % FS

TABLE 2.9: The relationship between measured voltage and strain

Final dimensions and strain gauge placement

The final dimensions and strain gauge placement were measured using a caliper and micrometer. Figure 2.23 shows the measured variables, their measured value is shown in table 2.10. The strain gauge placement is shown in Figure 2.24 and Table 2.11

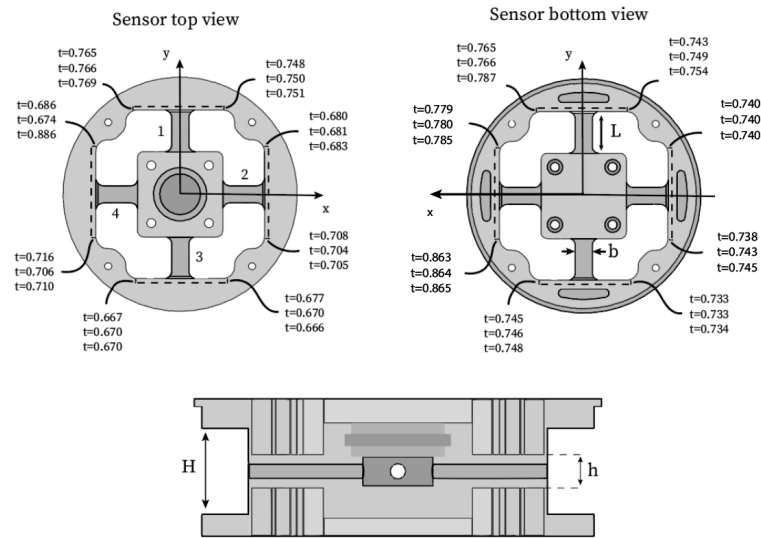


FIGURE 2.23: The measured variables the fabricated sensor using a caliper and micrometer

variable	Designed (mm)	Beam 1 (mm)	Beam 2 (mm)	Beam 3 (mm)	Beam 4 (mm)
b	8.0	8.2	8.2	8.2	8.2
h	8.75	8.75	8.75	8.75	8.75
H	23.25	23.25	23.25	23.25	23.25
L	19.50	19.50	19.50	19.50	19.50
t	0.70	see figure 2.23	see figure 2.23	see figure 2.23	see figure 2.23

TABLE 2.10: Dimensions of the design variables of the fabricated sensor

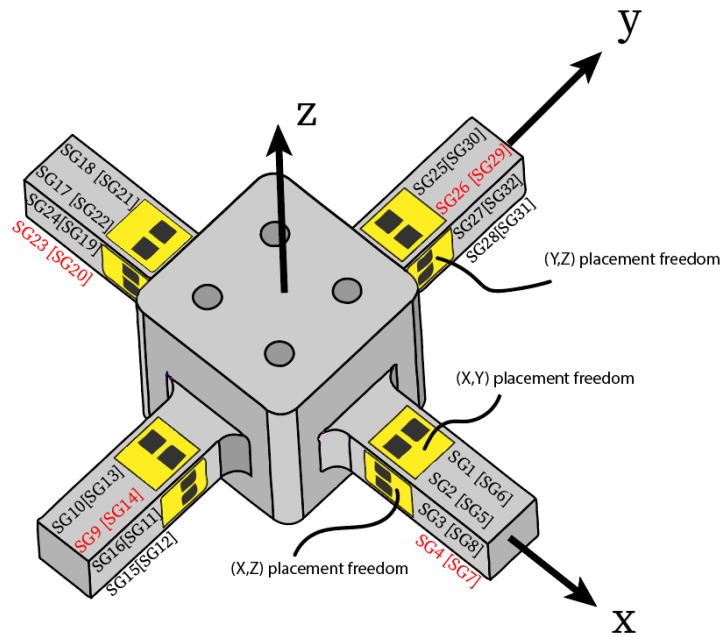


FIGURE 2.24: Showing the possible strain gauge placement errors. A placement error is only possible in two directions, because the strain gauges are constraint to the surface of the strain measuring beam.

Strain Gauge Nr.	Intended position (x,y,z) mm	Measured position (x,y,z) mm
1 and 2	(4.0,0,-)	(2.8,0,-)
3 and 4	(4.0,-,0)	(3.9,-,-0.3)
5 and 6	(4.0,0,-)	(3.8,0,-)
7 and 8	(4.0,-,0)	(3.8,-,-0.3)
9 and 10	(0,4.0,-)	(0,3.5,-)
11 and 12	(-,4.0,0)	(-,3,-0.3)
13 and 14	(0,4.0,-)	(0,2.65,-)
15 and 16	(-,4.0,0)	(-,4.5,-0.3)
17 and 18	(4.0,0,-)	(3.6,0,-)
19 and 20	(4.0,-,0)	(3.5,-,-0.3)
21 and 22	(4.0,0,-)	(3,0,-)
23 and 24	(4.0,-,0)	(3,-,-0.3)
25 and 26	(0,4.0,-)	(0,2.7,-)
27 and 28	(-,4.0,0)	(-,3.4,-0.3)
29 and 30	(0,4.0,-)	(0,3.1,-)
31 and 32	(-,4.0,0)	(-,4.1,-0.3)

TABLE 2.11: The intended and achieved strain gauge location after fabrication measured using calipers in the frame of reference shown in Figure 2.24. A bar (-) is used to indicate the constraint coordinate. The location which this table refers to is the mid point of the side facing the central block. The rotational error was not included in this table

These errors were added to FEM model, for the model including the fabrication error the following cross-coupling matrix was calculated. The rotational error were

not included in this model because they were to challenging to measure.

Applied pure load	F_x	F_y	F_z	M_x	M_y	M_z
Axis of reading	CC _{ij} (%)	CC _{ij} (%)	CC _{ij} (%)	CC _{ij} (%)	CC _{ij} (%)	CC _{ij} (%)
F_x	-	0.1	1.8	9.0	7.3	1.0
F_y	0.6	-	4.4	-3.5	19.5	8.3
F_z	0.5	0.8	-	2.3	-2.3	0.7
M_x	0.3	-1.7	0.0	-	0.0	0.5
M_y	1.4	0.1	3.0	0.1	-	-0.1
M_z	0.3	-1.4	-1.1	1.5	0.1	-

TABLE 2.12: The cross-coupling matrix calculated by the FEM model for the final sensor design

2.9 Discussion and Conclusion

In this study a sensor that can pass airflow in sake of gripper actuation was designed, tested, and validated. The integration of airflow into the sensor structure did not diminish the sensors capability to measure loads. The throughput at which products detach from the gripper is unchanged with the addition of the sensor. The fabricated sensor showed a maximum cross-coupling and measurement error of 31% and a 8% respectively, in which the error is determined as the largest absolute bound of the 95% confidence interval. This large cross-coupling is, at least partly, explained by error made during fabrication.

This work was performed in three parts. In the first part, the design criteria, appropriate transducer, sensor structure and design strategy was was selected. In the second part the sensor is designed using SQP optimization and FEM simulation according the design criteria. In the second section, the FEM simulation is used to validate the final design dimensions. In the third and final part the fabricated sensor is calibrated and validated. In the discussion, the three steps are considered separately.

Reflecting on the design decision, the transducer, sensor structure, design method and design criteria worked well. The strain gauges are capable of measuring the load to a sufficient degree. The measurement error stemming from position error of the strain gauges would also be an issue for other feasible transducers. The sensor structure passed airflow through the structure without influencing the cycle time at which a product detaches from the gripper, while also achieving sufficient load measuring capabilities. The design strategy of FEM simulation resulted in the calculation of a optimized sensor structure in one to two hours, using a decent laptop (Lenovo YOGA 730-15IWL, 16 GB ram). The FEM model also allowed the effects of fabrication errors to be taken into account during the validation process, as shown in Table 2.12. Analytical models would have achieved faster optimization times. Since the optimization of a sensor structure has to be computed a limited amount of times this benefit is small.

The design criteria can be improved upon for future sensor design. Firstly, one of the design criteria enforced that the sensor had to be fabricated using the manufacturing technique that was available, 5 axis CNC milling. In future work this manufacturing technique should be avoided. Due to end mill deflection, the sensor had to be manually turned during manufacturing. This caused miss alignment in the sensor structure, decreasing the sensors performance. EDM wire cutting is advised for future work.

Secondly, some design criteria were set similar to of the shelf available sensors. This

was done because not enough information was available about the robotic system the sensor was designed for. This knowledge gap can be filled using the sensor validated in this work. For example, the eigenfrequency of the robot has been determined using this sensor. With this knowledge the eigenfrequency of the sensor can be set to ten times the robot frequency [151].

In the second step of this study, the design step, some key observations were made. First, the optimization scheme was calculated for several different starting condition. Firstly, different starting points of the optimization resulted in different final design variables, with nearly the same objective function. In literature, the design proposed by H. Akbari et al. also presented this behavior [109], while another design by M. Kang et al. [139] showed the optimizer ending at the same design variables for different starting point. One main difference between these studies is the introduction of the strain measuring beam length as one of the design variables. This might indicate that the introduction of strain measuring beam length causes multiple local minima with nearly the same objective function. Further evaluation of the convexity of this problem is required to verify this explanation.

Secondly, an observation was made which can be used to reduce the computational time of the optimizer. The design variables b and t converged to their lower bound for every optimization run that was performed. The change of b and t for three different sets of starting design variables are shown in Figure 2.15 Since the design variables b and t are optimal at their upper and lower bound, these design variables can be made fixed in the optimization scheme. Removing two out the five design variables is expected to reduce the computational time by 30-40%.

During the validation of the sensor using the FEM model points worth special attention were noted. In the analysis of the FEM model the cross-coupling is far lower than expected during the design stage. Initially it was expected that the 5% cross-coupling would be challenging to obtain. The paper presented by Kebede et al. proposing the strain gauge arrangement used in this design, reported a principle cross-coupling error of 10 – 11% for C_{15} and C_{24} [108]. For this design the cross-coupling is calculated to be 3.5%. The paper presented by kebede et al. does not go into detail about the design process of their sensor. However it is stated that the structural design was based on the structured design method proposed by Kang et al. [139]. Kang et al. were the first to identify the principle coupling terms and minimized C_{15} and C_{24} in there design.

An explanation could be the addition of strain measuring beam length to the set of design variables. In literature designs using beam length as a design variable have also achieved low cross-coupling [109]. The added holes in the center of the beams and the milling radii were not influential. These features were removed from the FEM model, which show not to cause an increase in performance.

Compared to the work presented by Kang et al., which uses a different strain gauge arrangement and focuses on minimization of the cross-coupling terms the results are more logical. Kang et al. found a cross-coupling of 2.5% for C_{15} and C_{24} , in this design 3.5% is found which is logical since optimizer did not focus on minimization of cross-coupling [139].

Also notable, is the CC_{34} is non zero and not the same as CC_{35} in the FEM model are not the same. Due to the symmetrical sensor structure these two terms were expected to be the same, as can be seen in table 2.12 this is not the case. After further investigation this difference was cause by the asymmetrical strain gauge arrangement. The strain gauges used to measure the force in the z are deformed by a twist

when a moment is applied around the x axis. When a moment is applied around the y axis this is not the case.

One of set unused of strain gauges, SG_6 , SG_{14} , SG_{26} and SG_{29} could also be used to measure the force in the z direction. When this set of strain gauges is used to measure the force in the z direction the CC_{35} and CC_{34} switch their cross-coupling value. This is in agreement with the explanation presented above. Even when suppressing the air flow passing passage changes, essential restoring the sensor to its originally shape, this cross-coupling factor is still apparent. Because the two strain gauge bridges can be used to measure the force in the z direction this cross-coupling might be combated by taking the average over these two measurements.

In the final step in this study the sensor was calibrated and validated. During the calibration is was noted that the LS method is sensitive to human error. The error in the calibration table and its human operator might be larger that the error in the sensors measuring capabilities. However, since these error are part of the calibration these also carry over to the performed measurements. When applying a load to the sensor the cables used to apply the load need to be perfectly perpendicular to the load applying cross. If this is not the case the load is not applied as expected, this causes error in the calibration process. After having re-performed the calibration the standard deviation in the cross-coupling terms and measurement was reduced by 1-3%. Yet this issue still remains and explains the maximum measurement error of 8%.

Furthermore this study proposed three improvements to the calibration process with respect to literature. In this study the known non-pureness of the applied loads is including in the sensor calibration. When this improvement is removed, not taking into account the non-pureness, the cross-coupling terms increase drastically. The second improvement uses the linearity of the sensor to reduce the amount of measurements required for a good calibration. The effect of this improvement can be seen in the average measurement error presented in table 2.7. Since the sensor behavior is strongly linear using a linear correction method no average error is expected. In literature however often only one measurement is performed for calibration and another for the error determination. This method essential takes two samples from a random pool. This gives a unfair view of the sensor performance. A more fair view of sensor measurement error and cross-coupling the mean and standard deviation should be considered. Defining the error and cross-coupling as absolute maximum bound of the 95% confidence interval is the third proposed improvement. If the error would have been computed using method presented in literature instead of proposed method, odds are that the sensor would have appeared to meet the requirements.

When considering the sensor validation results it can be seen that the design constraints are not met. The design requirements that are not met are the minimum strain, the mass, cross-coupling and the measurement error. The design mass is exceed by 30 gram because the vacuum sealing ring had to be manufactured with twice the designed thickens. The bolt required for the sensor assembly were also neglected during the design stage. The validation of the remain requirements can be at least partly explained by errors made during fabrication. Figure 2.23 shows the measurements of the design variables after fabrication. The most influential milling errors can be found in the thickness of the thin plates. These errors are caused by rotating the sensor half way trough the milling process. This rotation is required because of end mill length limitations. Another error was made during the placement of the strain gauges. The strain gauges were not placed at the intended location as can be seen in figure 2.24 and table 2.11. Due to a relative location difference of the

strain gauges in a measuring bridge cross-coupling is inevitably introduced. A difference in measured strain is also explained by misplacing the strain gauges. For future work a strain gauge placement guide is recommended, placing strain gauges at an exact distance by hand requires expertise. The placement guide should provide straight reference surfaces at the strain measuring beams. A "U" shaped part could be milled with the inner dimensions of the strain measuring beams. This placement guide can be slid over the strain measuring beams and is placed against the central block. The length of the "U" shaped guide determines where the strain gauges are placed. The straight reference edge at a fixed location helps placement.

When the measured error's are included in the FEM model the errors seen in reality are also introduced in the FEM model. The errors are not identical, however the direction and location at which the cross-coupling matrix changes is the same as seen in the fabricated sensor. Measuring the strain gauge placement and dimensional errors exactly is challenging, an exact corresponds to reality is therefore also not expected. The rotational errors are for example not taken in account.

The design constraint coinciding eigenfrequency was not measured because the required equipment was not available. This design requirement is however checked because, no sensor vibration issues were faced during on machine testing. The violation of the error, hysteresis and mass constraint is only small and well known. The main sensor loading can be oriented in a the most favorable direction. Furthermore, the most important design criteria of passing airflow is met. This lead to the conclusion that this sensor has sufficient performance for load measurements during high-speed case packing.

For future research it is recommended to re-fabricate the sensor to achieve a sensor within design specification. This sensor could however already be used to measure the failure mode of suction cups under the dynamic loading seen in high-speed case packing.

Chapter 3

Experimental determination of the dynamic grasping strength of suction cups when applied in high-speed case packing

3.1 Abstract

In this study, the dynamic grasping strength of a suction cup gripper was experimentally studied for the first time. The limit of the dynamic grasping strength is defined as the load at which a product detaches from the suction cup gripper under dynamic motion paths. The product and motion path considered were based on case packing operations in the food industry. This was determined by measuring the load exerted on suction cups during high-speed case packing operations in the packaged food industry. The limit of the dynamic grasp strength was determined using an earlier designed six-axis force moment sensor. This sensor was specially designed to pass airflow through the sensor structure without limiting the pull-out load measurement capabilities. During the robot motion, the load on the sensor was measured. To transform this measured load to the load on the suction cup, the load measurements were combined with Apriltag tracking from captured high-speed video imagery. This tracking was required to measure the product displacement and rotation induced by the high-speed motion during case packing. From the resulting measurements, the dynamic grasping strength limit for stiff and compliant suction cups was determined. Remarkably, the location where detachment occurred in practice does not comply with the current understanding and current models of suction cup grippers. Compliant suction cups performed better than stiff suction cups because of their ability to rotate the product. The rotation of the product results in a more desirable load in the suction cups. The measurements on stiff suction cups showed force peaks in the horizontal direction and the moment perpendicular to the plane of motion. These peaks occur after changing the direction of robot acceleration. The change in acceleration causes the product to rotate from one side of the gripper to the other. Due to the stiffness of the suction cup, this rotation stops suddenly, resulting in an impulse loading. For compliant suction cups, the detachment of the product is caused by an increased moment loading. As the object is decelerated in the horizontal direction, it swings past the gripping center of the suction cup gripper. At this point, a downward acceleration is started to place the object. This combination causes for an increase in moment loading perpendicular to the plane of motion.

3.2 Introduction

Measuring the load during the high-speed case packing of flexible food products provides the limits of suction cups in a dynamic case. The capability to hold a product under a dynamic load is referred to as dynamic grasping strength in this study. Knowing the dynamic grasping strength is required to improve the design of suction cup based grippers in a structured manner.

The research effort into suction cup modeling and grasping strength measurements have mainly coincided quasi-static load cases of rigid objects. The research is driven by interests such as general industrial application, wall climbing robots, robotic vacuum gripper design and gripper pose planning. [101], [158]–[162].

In the early 2000's, Mantriota observed that the models and measurements into suction cups failure loads was lacking compared to their widespread use in industry [101]. In response, a suction cup model was proposed considering the two most prominent suction cup failure modes, namely sliding of an object over the suction cup surface and full detachment of the object from the suction cup [90], [102]. This model only considered the suction cup edge to be load bearing, but this model was later extended to also include a contact surface and was validated by performing measurements on the grasping strength of a suction cup on different materials [101], [106], [163]. The largest deviation between a measurement and a model was 15% for slightly porous cardboard sheets. Other more extensive research on the failure of passive suction cups also concluded that Mantriota proposed model and assumptions are likely to be valid [104]. Mantriota's models has been considered, directly used, or adapted in later studies [95], [164].

In more recent studies, more complex and promising models and simulations of suction cup grasping strength have been presented [5], [160], [165]–[167]. The validation of these models is however lacking, because often only the axial loading is considered during validation if any validation is preformed at all.

These studies have brought the failure load estimation of suction cups a long way. However, from the available literature a gap can be identified which limits the structural improvement of suction cup based robotic grippers. The measurements of failure load of suction cups has not considered dynamic loads. Induced by for example the case packing flexible products, this work aims to fill this literature gap. The current literature on modeling and model validation of suction cups grasping strength only consider quasi-static loading. These results and conclusions found for the quasi-static load cases are assumed to be directly applicable for dynamic load cases simply by taking newtons second law into consideration [101], [159]. Models or measurements of suction cups failure have not yet focused solely on dynamic load cases.

Furthermore, previous work showed that mechanical properties of packaged food products strongly influence the maximum throughput. This study will therefore consider the products found in the packaged food industry. These products are vastly different from the products considered in previous suction cups modeling or measurement literature. In current literature, plates, slabs or blocks of stiff materials such as glass pains, concrete blocks or stamped sheet metal are considered [5], [101], [160], [165]–[167]. As concluded in chapter 1 these products behave very differently under dynamics loading compared to the flexible food products that are most often contained is a loose foil.

This study will focus on measuring the grasping strength on suction cups grippers using the sensor of chapter 2. This study sets out to answer the following question: *What is the failure mode of suction cups under dynamic load while case packing flexible food products ?*

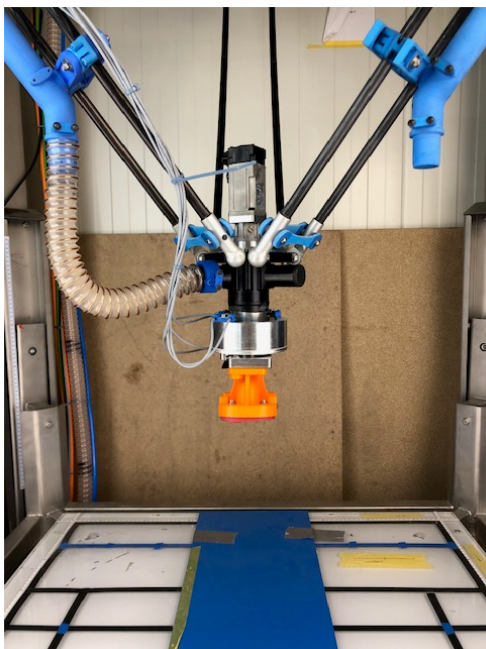
Section 3.3 outlines the method. Section 3.4 presents the measurements results. In section 3.6 the results are discussed. Concluding statements are given in section 3.7.

3.3 Method

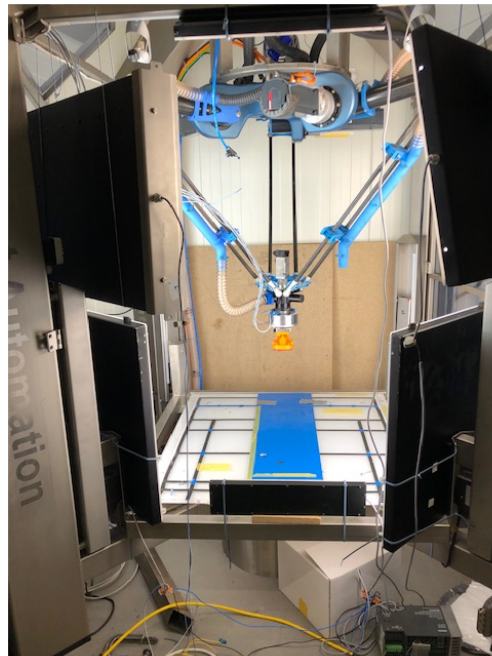
To determine the dynamic grasping strength, the measurement procedure will be presented, where after the correction calculations are given, after which the considered products and grippers are explained.

3.3.1 Measurement set up

To determine the dynamic grasping strength of suction cups, the load on the suction cups during the high-speed case pacing motion has to be determined. For these measurements the novel six-axis force torque sensor from chapter 2 was used in combination with high-speed imagery. This sensor can pass airflow without influencing the load measuring capabilities of the sensor. Details on the design, fabrication and validation of this sensor can be found in chapter 2. For capturing high-speed imagery the PROMON U1000 color camera made by company AOS was used at a frame rate of 250 FPS. An overview of the complete measurement setup is shown in figure 3.1b.



(A) Sensor and gripper placement during the measurements



(B) Overview of the complete measurement set up

FIGURE 3.1: Overview of the setup used during the measurements

The six-axis F/M sensor is mounted between the robot platform and the robotic gripper, as shown in Figure 3.1a. During the motion of the robot the load is measured at the measuring frame of the sensor.

By performing two separate measurements the load on the suction cups is determined. In the first measurement a delta robot is used to move a product using a predetermined test path. In the second measurement only the sensor and selected gripper are moved. The difference between these two measurements is the contribution of the product to the measured load and can be used to find the load on the suction cups.

For a fair comparison all measurements were performed using the same robot path. The path picked for the measurements resembles the motion paths of practical industrial implementations.

As shown in Figure 3.2 the shape of the path is determined according W_{Path} , H_{Path} and R_{Path} , the width height and radius of the path respectively. The review of the case packing industry as presented in chapter 1 was used to determine these parameters as $W_{Path} = 700 \text{ mm}$, $H_{Path} = 100 \text{ mm}$ and $R_{Path} = 100 \text{ mm}$. The motion constraints consist of a jerk, acceleration limit.

The delta robot is controlled using a Beckhoff PLC with Beckhoff AX8000 series motor drivers. In the control software, a robot path is generated according to three path shaped parameters and three motion constrains.

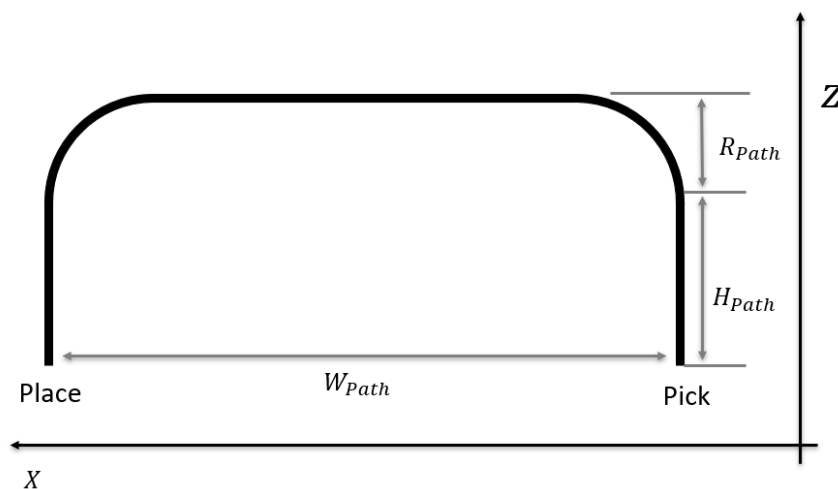


FIGURE 3.2: The robot path taken during all tests. The parameters used to determine the path are the width, $W_{Path} = 700 \text{ mm}$, the height, $H_{Path} = 100 \text{ mm}$ and the radius of the path $R_{Path} = 100 \text{ mm}$. The labels Pick and Place are used to indicate pick and place locations respectively.

Measurement procedure

The measurement procedure starts with the selection of a product that will be studied. Hereafter, a gripper design has to be selected. Testing different grippers on the same product can give meaningful insight into different failure modes. Many aspects are influential on the detachment load of suction cups. One of the main contributions is expected to be the compliance of the suction cup gripping surface. A more compliant suction cup gripping surface is able to conform to the surface of the product better. This is expected to increase the holding capabilities.

At the start of a measurement the product is manually attached to the gripper at the location, shown as pick in Figure 3.2. The attachment is done manually to ensure the sensor will not be overloaded when the robot experiences first contact with the product. Next, the motion constraints, which cause the product to break away from the gripper, are determined. For each combination of product and gripper, measurements just below the critical motion constraints and above the critical motion constraints are tested. During these tests the load at the sensor is measured and high-speed imagery is recorded. These two measurements together determine the transition from subcritical to supercritical gripper load. Furthermore, the acceleration recorded by the motion control is stored to verify the correct motion constraints that were achieved during the measurements.

To ensure that the required frame transformations can be applied correctly, the load measurements without product, the load measurements with product, and the high-speed footage are manually synchronized. The rising edge of the load was synchronized with the first frame in which motion was detected. After the transformation the data can be interpreted by comparing the measured load with and without the product.

Measurement procedure described in a step-wise manner:

1. Select a product to be studied
2. Select one or more grippers for the selected product
3. Determine the critical load for each product and gripper combination
4. Measure the load and record the high-speed video for the subcritical path with a product attached to the gripper
5. Measure the load for the subcritical path without a product attached to the gripper
6. Measure the load and and record the high-speed video for the supercritical path attached to the gripper
7. Measure the load for the supercritical path without a product attached to the gripper
8. Synchronize the data, the first video frame is synchronized on the rising edge of the measuring loads
9. Perform the required transformations to translate the measured force of the suction cup frame of reference.
10. Interpret the resulting load

Considered products and grippers

In this study, 2 products were measured according to the procedure. Chapter 1 found that the product classes showing the most challenges were the liquid pouches and the single mass in a foil. From both product classes one product was selected to study.

For the liquid pouches, soup in a pouch was selected because of its high weight that enables it to achieve a large signal to noise ratio during measurements. From the single mass in a foil, single serve ice cream was selected due to its industrial relevance. A single mass in a foil is challenging to case pack because its height to

width ratio is large. This reduces the amount of vacuum force compared to the product mass. Furthermore, the center of mass is located further below the suction cup increasing the moment loading during acceleration

Two different grippers are used in their industrial applications. For liquid pouches an array of compliant suction cups is used and for single masses in a foil a stiff rim of Linatex is used. In this study, this difference is further explored by using both types of grippers for both the liquid pouch and the single mass in a foil, resulting in 4 different gripper and product combinations. In Figure 3.3 the four considered grippers and their products are shown.

The compliant suction cup grippers use PIAB BL40-5 suction cups in this study. For the soup, eight suction cups are used and for the single serve ice cream, 2 suction cups are used.

The stiff suction cup for soup consists of two vacuum surfaces of 60 X 55 mm with round corners and for the single serve ice cream a vacuum surface of 25X95 mm with rounded corners is used.



FIGURE 3.3: The four considered grippers and their respective products

3.3.2 Required transformations

Since the load at the suction cups is of interest, the load measured in the sensor's frame of reference should be transformed to the suction cup's frame of reference. Figure 3.4 shows the sensor's frame of reference in blue and the suction cup's frame of reference in red. When considering an array of suction cups the reference frame

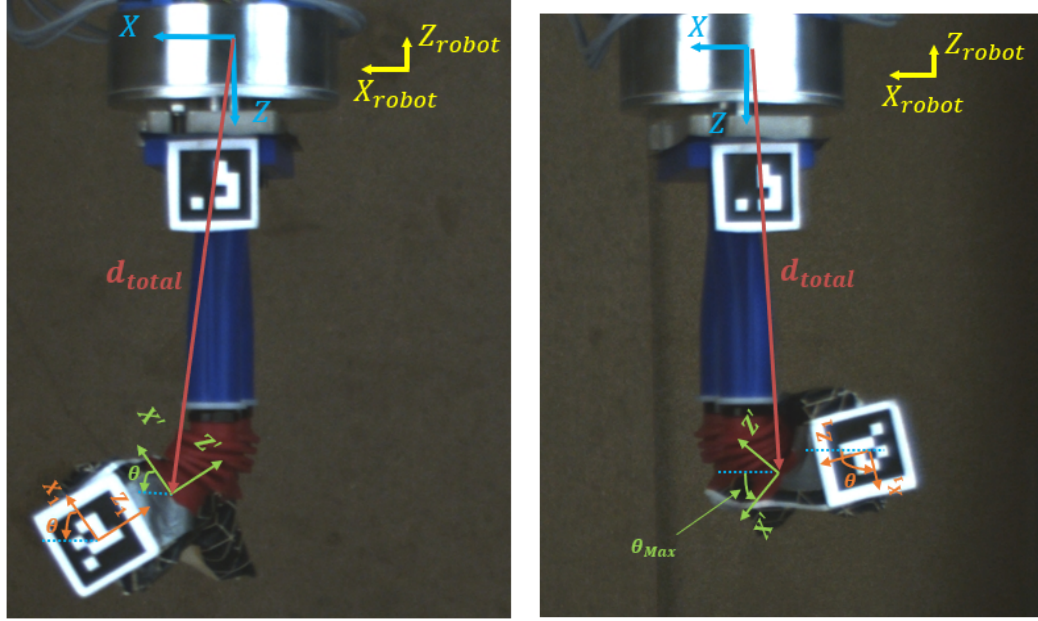
is placed in the center of the array.

The transformations required to obtain the load of the suction cups consist of three consecutive steps [110]. Firstly, the sensor output voltage, V_{sensor} , was converted to a measured load. This was done using the calibration matrix, determined in chapter 2. Secondly, the origin of the sensor's frame of reference is translated to the origin of the gripper's frame of reference. Finally, for compliant suction cups the translated frame of reference is also rotated to achieve the suction cups frame of reference. For the stiff suction cups the rotation angle is set to 0 degrees.

Furthermore, translation and rotation of compliant suction cups are affected by the motion of the robot. For the stiff grippers the translation is constant and the rotation is zero. To track the translation and rotation of the compliant grippers, high-speed video footage was recorded during the pick and place motion. To automate the determination of translation and rotation Apriltags were used. These tags are shown in Figure 3.4. The position and rotation of these tags can be automatically detected in video frames.

This results in a displacement vector $\vec{d} = [d_x, d_y, d_z]^T$ and a rotation angle θ . Here, d_x , d_z and θ are time varying and d_y could be a constant displacement out of the plane of motion. d_y was 0 for all performed measurements in this study. The standard output from the tag tracking software is the rotation angle and pixel location of the Apriltags' center. For small rotations this data can directly be used to determine the rotation angle and displacement vector as shown in Figure 3.4a. For larger rotations the compliant suction jams and loses its compliance. At this maximum rotation angle, θ_{max} , the suction cup's reference frame of rotation stops following the products rotation angle and remains equal to θ_{max} . After the measured angle exceeds θ_{max} , the angle used in the correction calculation was set equal to θ_{max} .

Finally, the data is filtered using a low pass filter, for which the requirements will be discussed in section 3.6



(A) Showing the determination of the rotation angle and displacement vector for small rotations following the Apriltag location
 (B) Showing the effectors of large deformation during the determination of the rotation angle and displacement vector.

FIGURE 3.4: Figure showing the measurement frame of the sensor and the reference frame of interest at the suction cup

For each of the transformations a matrix is used. These matrices are labelled C^{-1} , D and R respectively. Equation 3.1 shows the full transformation. For compliant grippers the translation and rotation matrices are time varying. Their definition and determination does however not change from the method presented by B.Shimano and B.Roth [110]. Equation 3.2 and 3.3 show the translation and rotation matrix. The total rotation matrix is made up of two rotations. The first rotation, R_1 , aligns the sensor's frame of reference with the robot's frame of reference. The second rotation, R_2 , is the rotation of theta around the y-axis. The displacement d_{total} is measured in the robot's frame of reference. Therefore, the multiplication with the displacement correction matrix D has to be preformed after R_1 and before R_2

$$F' = R_2' D R_1' C^{-1} V_{sensor} \quad (3.1)$$

$$D = \begin{bmatrix} 1 & 0 & 0 & 0 & 0 & 0 \\ 0 & 1 & 0 & 0 & 0 & 0 \\ 0 & 0 & 1 & 0 & 0 & 0 \\ 0 & -d_z & d_y & 1 & 0 & 0 \\ d_z & 0 & -d_x & 0 & 1 & 0 \\ -d_y & d_x & 0 & 0 & 0 & 1 \end{bmatrix} \quad (3.2)$$

$$R_1' = \begin{bmatrix} R_1 & 0 \\ 0 & R_1 \end{bmatrix} \quad \text{and} \quad R_2' = \begin{bmatrix} R_2 & 0 \\ 0 & R_2 \end{bmatrix} \quad (3.3)$$

Where:

$$R_1 = \begin{bmatrix} 1 & 0 & 0 \\ 0 & -1 & 0 \\ 0 & 0 & -1 \end{bmatrix}, \quad R_2 = \begin{bmatrix} \cos(\theta) & 0 & \sin(\theta) \\ 0 & 1 & 0 \\ -\sin(\theta) & 0 & \cos(\theta) \end{bmatrix}$$

To determine the load on the suction cup, equation 3.1 has to be calculated twice, once for the measurement with product and once for the measurement without product. The difference between these load measurements is the contribution of the product to the total measured load expressed at the suction cup's frame of reference. These loads expressed in the suction cup's reference frame are filtered with a low pass filter placed at 30 Hz.

3.4 Results

For each product-gripper combination the subcritical and supercritical load were measured 3 times. During these measurements the same trends were seen. Therefore, only one measurement for each product-gripper combination is presented here. In the plots showing the measured loads and the set acceleration, three dashed lines are shown. These lines are used to discuss the results in section 3.6. The line labelled 0 refers to the state before motion, label 1 refers to the state where models predict detachment of a product from the suction cup gripper, and label 2 refers to the state where detachment of the product from the gripper occurs in practise. The lines are used for explanatory purposes, their exact position is not of importance.

The measurements are presented in the following manner:

1. The motion constraints for the gripper-product combinations are provided in table 3.1.
2. The set acceleration, and the uncorrected and unfiltered load measurements are presented for the compliant soup gripper. The robot acceleration is presented in Figure 3.5a and Figure 3.6a. The corresponding load measurement with and without a product attached to the gripper are presented in Figure 3.5b and Figure 3.6b. These figures show that the measured force follows the expected acceleration path shape. Additionally, the misalignment between the sensor's and robot's frame of reference can be seen in Figure 3.5b. For the other grippers the same behavior was seen and are therefore not presented.
3. The corrected load measurements expressing the force exerted on the suction cup gripper by the product is presented for all 8 motion paths. In these figures, 3 lines are marked for discussion in section 3.6. The product orientation at the lines is shown here as well.

To present the data more clearly not all six load measurements are presented. Only the force in F_x , F_y , and F_z are shown.

The grippers were oriented such that their weakest side was placed in the direction of horizontal acceleration. Therefore, the forces in the y direction and moments around the x axis are less influential and are small. Because the axial rotations are introduced in pick and place motion cycles, the moment around the z axis is also introduced in these motion cycles.

4. The remaining vibration after performing a pick and place motion without applying a low pass filter are shown in Figure 3.11

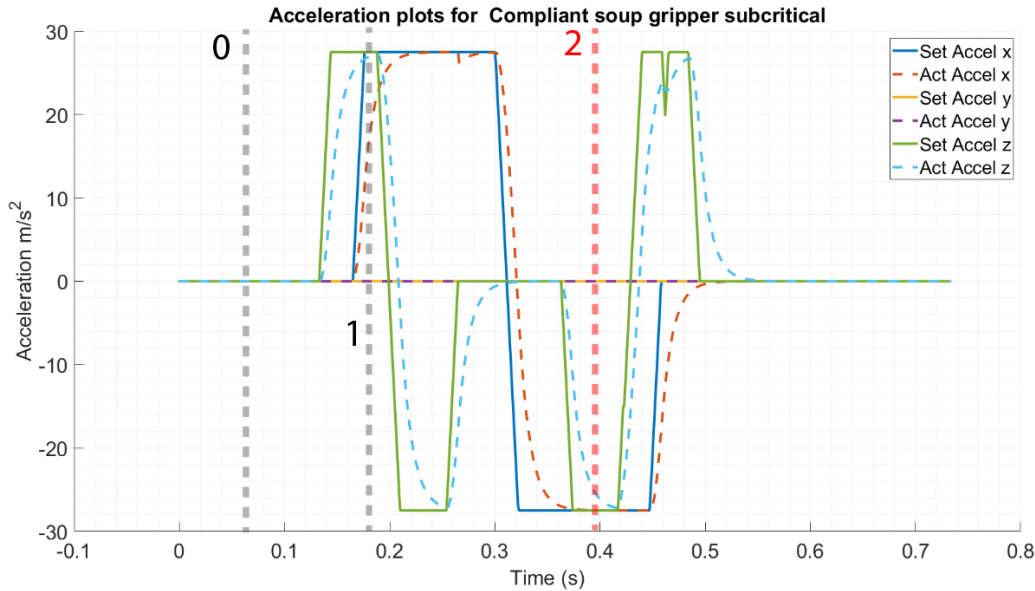
3.4.1 The motion path parameters

Gripper	Product	Path type	Jerk $\frac{m}{s^3}$	Acceleration $\frac{m}{s^2}$	Velocity $\frac{m}{s}$
Stiff	Soup	Subcritical	2250	23	10
Stiff	Soup	Supercritical	2500	30	10
Compliant	Soup	Subcritical	2500	27	10
Compliant	Soup	Supercritical	2500	45	10
Stiff	Ice Cream	Subcritical	2500	35	10
Stiff	Ice Cream	Supercritical	3000	50	10
Compliant	Ice Cream	Subcritical	2500	35	10
Compliant	Ice Cream	Supercritical	3000	50	10

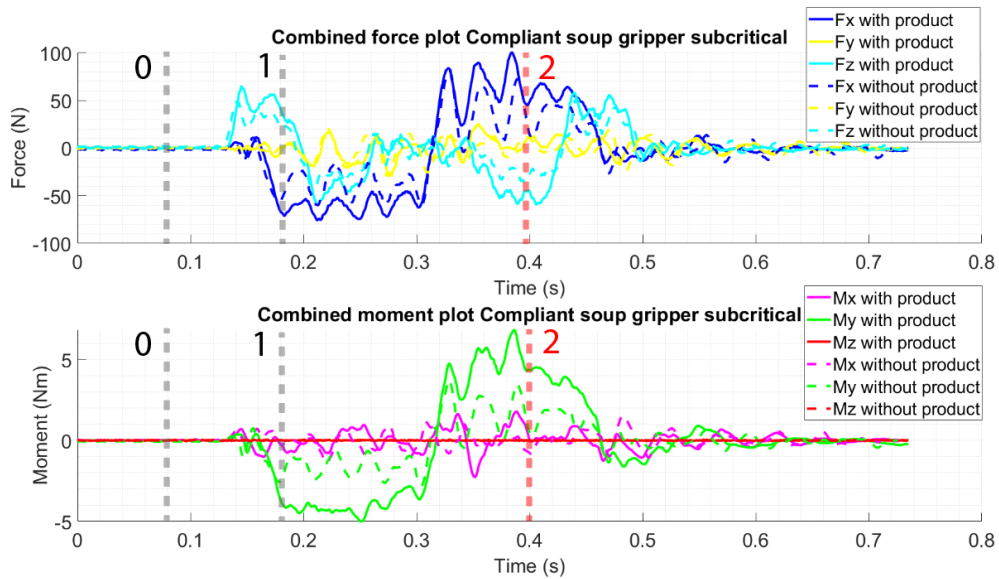
TABLE 3.1: The motion constraints for the gripper-product combination. This table show the transition from subcritical to supercritical motion constraints.

3.4.2 Unfiltered and uncorrected load measurements

Unfiltered and uncorrected subcritical load measurements for the compliant soup gripper and the corresponding acceleration path



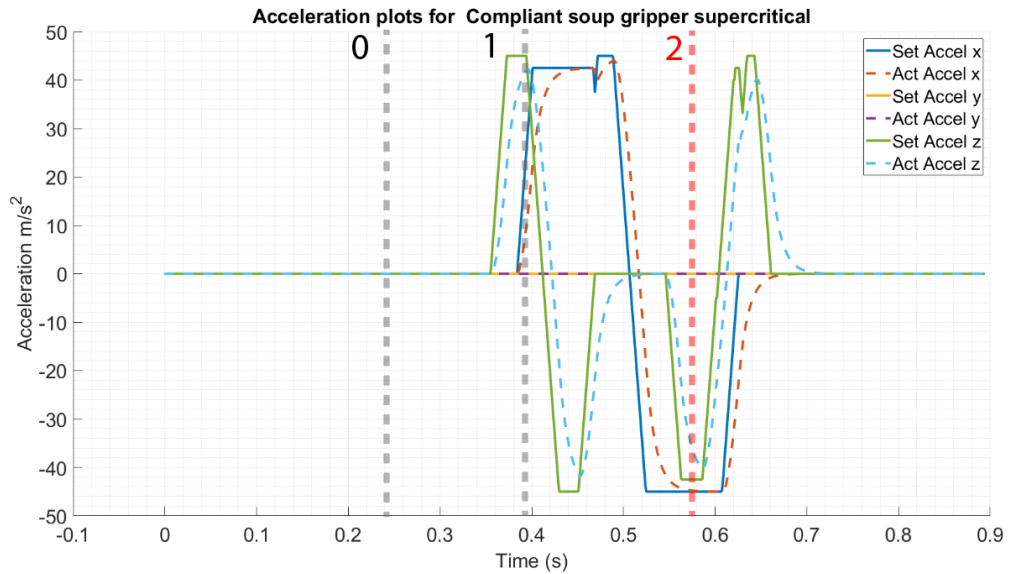
(a) The acceleration path generated by the Beckhoff motion controller for the subcritical motion path of the compliant soup gripper.



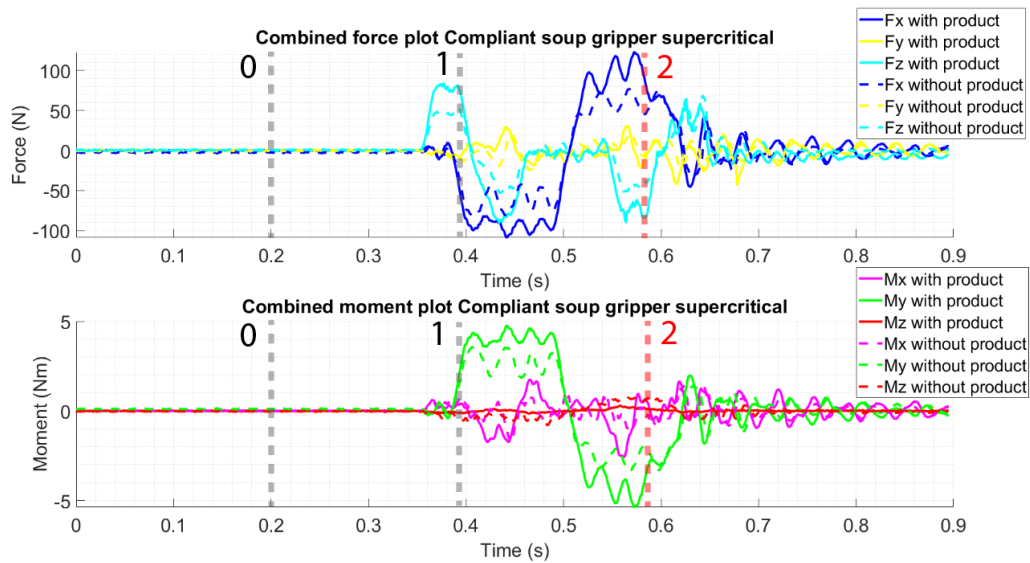
(b) Showing the subcritical load measurement with and without soup attached to the compliant gripper. The measured load at the sensor is not corrected and not filtered. It can be seen that the measured force follows the acceleration path as expected. Furthermore, there exists a misalignment in the axis.

Figure 3.5: Showing the subcritical robot acceleration path and the measured loads for soup with a compliant gripper. For a subcritical motion path the dynamic grasping strength of the gripper is just sufficient to hold the object. The labels 0, 1, and 2 refer to the state before motion, the state where models predict detachment between the gripper and the product, and the state where the product detaches from the gripper in practice respectively.

Unfiltered and uncorrected supercritical load measurements for the compliant soup gripper and the corresponding acceleration path



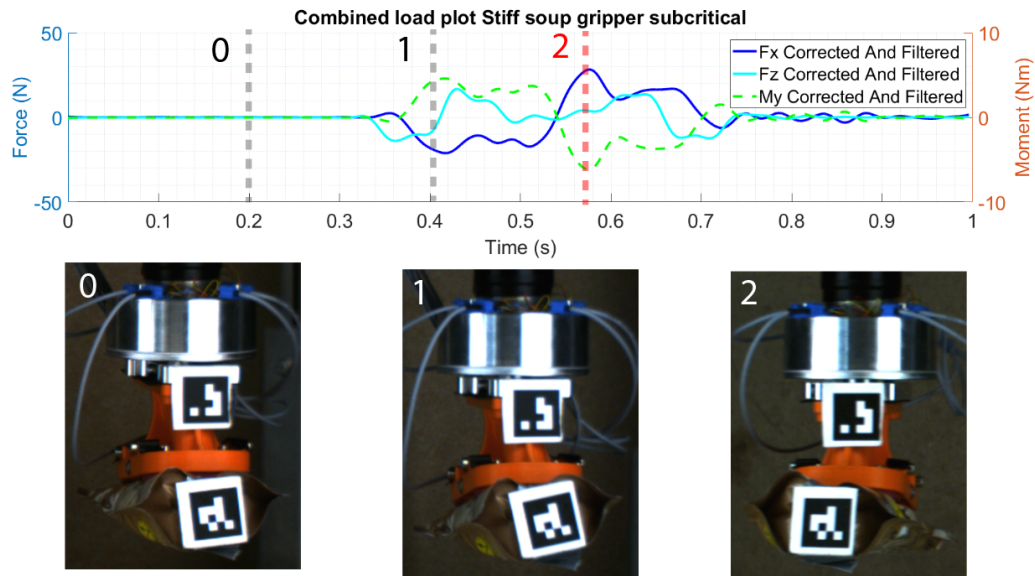
(a) The acceleration path generated by the Beckoff motion controller for supercritical motion path of the compliant soup gripper.



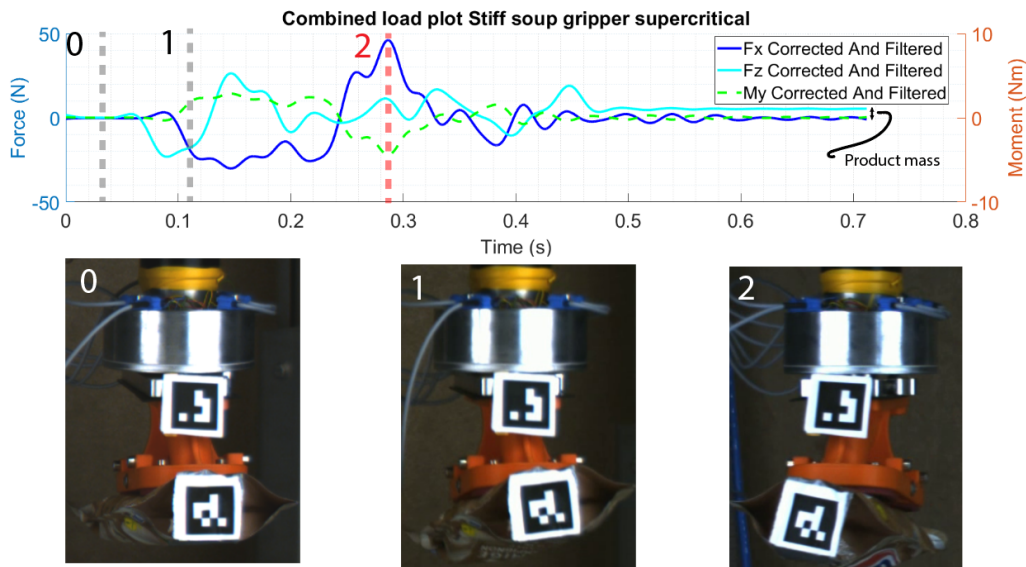
(b) Showing the supercritical robot load measurement with and without a product attached to the gripper for soup with a compliant gripper. The measured load at the sensor is not corrected and not filtered. It can be seen that the measured force follows the acceleration path as expected. However there exists an misalignment in the axis. After the line that is labelled 2, the dynamic holding strength of the gripper is insufficient and the product detaches from the gripper. After this point in time the measured load with and without product overlap as expected.

Figure 3.6: Showing the supercritical robot acceleration path and the measured loads for soup with a compliant gripper. For a supercritical motion path the dynamic grasping strength of the gripper is just insufficient to hold the object. The labels 0, 1, and 2 refer to the state before motion, the state where models predict detachment between the gripper and the product, and the state where the product detaches from the gripper in practice respectively.

3.4.3 Stiff soup gripper



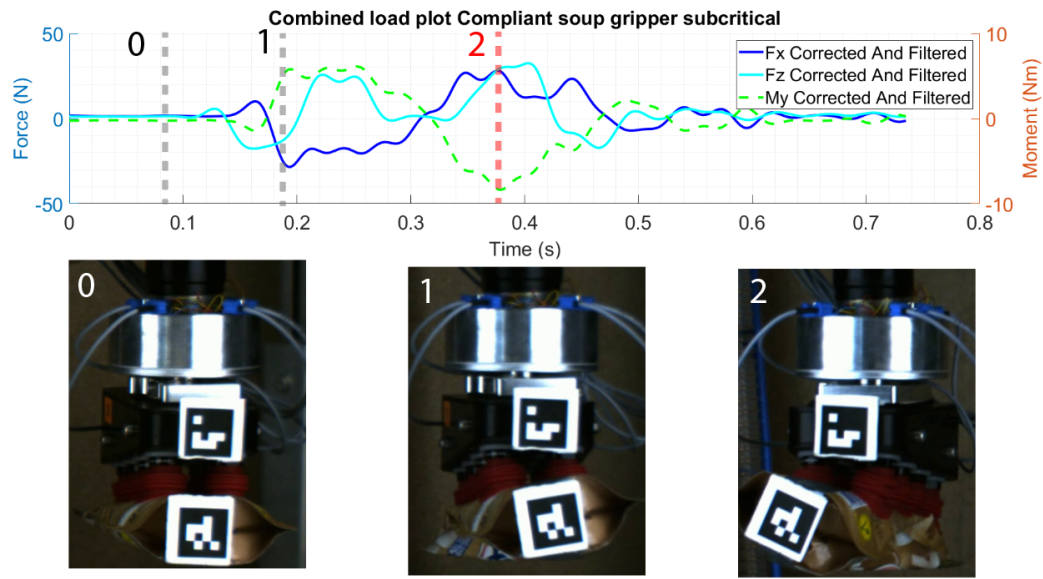
(a) The corrected and filtered force and moment measured for the stiff soup gripper with a subcritical acceleration path.



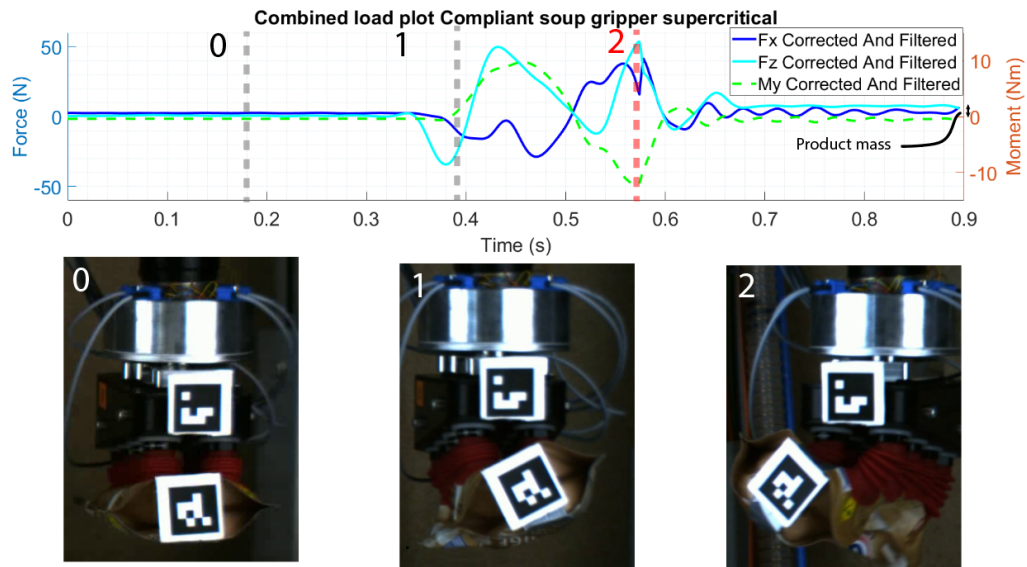
(b) The corrected and filtered force and moment measured for the stiff soup gripper with a supercritical acceleration path. In the picture showing the orientation labelled 2, the product just detached from the gripper. Note the arrow placed between the 0 line and F_z , indicating the loss of the product.

Figure 3.7: The corrected and filtered force and moment measured for the stiff soup gripper with a supercritical acceleration path. The labels 0, 1, and 2 refer to the state before motion, the state where models predict detachment between the gripper and the product, and the state where the product detaches from the gripper in practice respectively. In the picture showing the orientation labelled 2, the product just detached from the gripper.

3.4.4 Compliant soup gripper



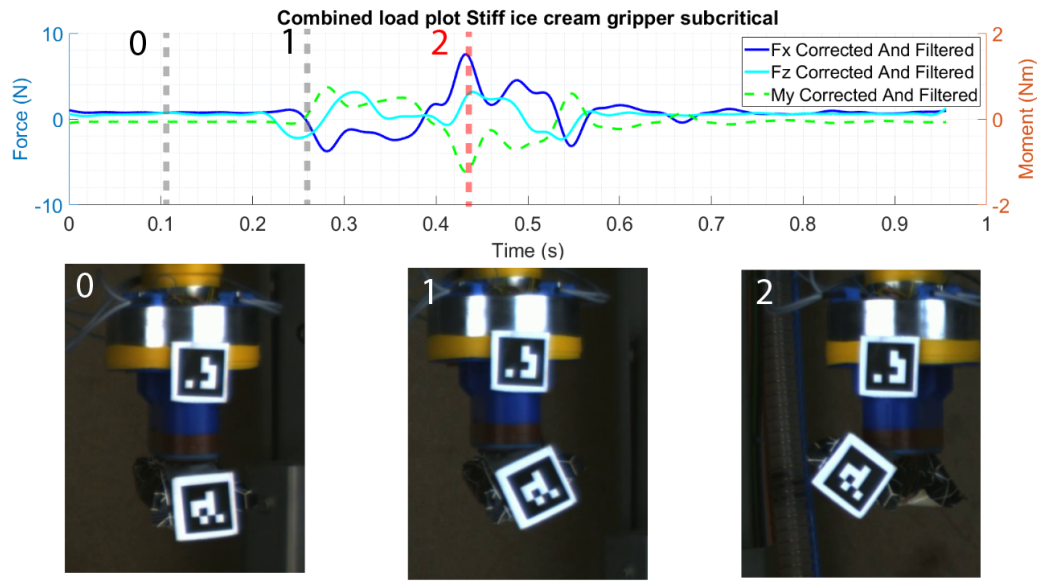
(a) The corrected and filtered force and moment measured for the compliant soup gripper with a subcritical acceleration path.



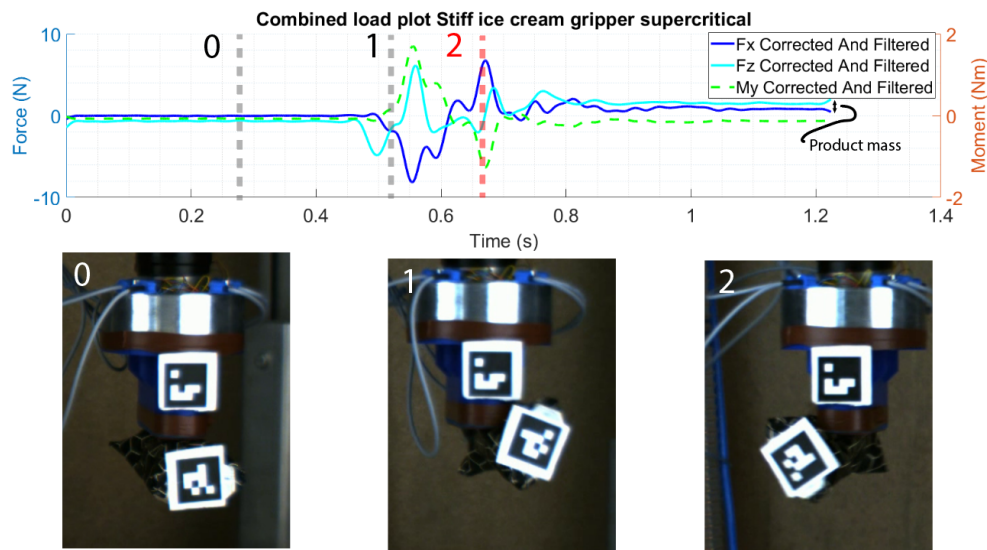
(b) The corrected and filtered force and moment measured for the compliant soup gripper with a supercritical acceleration path. In the picture showing the orientation labelled 2, the product just detached from the gripper.

Figure 3.8: The corrected and filtered force and moment measured for the compliant soup gripper with a supercritical acceleration path. The labels 0, 1, and 2 refer to the state before motion, the state where models predict detachment between the gripper and the product, and the state where the product detaches from the gripper in practice respectively. In the orientation labelled 2 the product just detached from the gripper. Note the arrow placed between the 0 line and F_z , indicating the loss of the product.

3.4.5 Stiff ice cream gripper



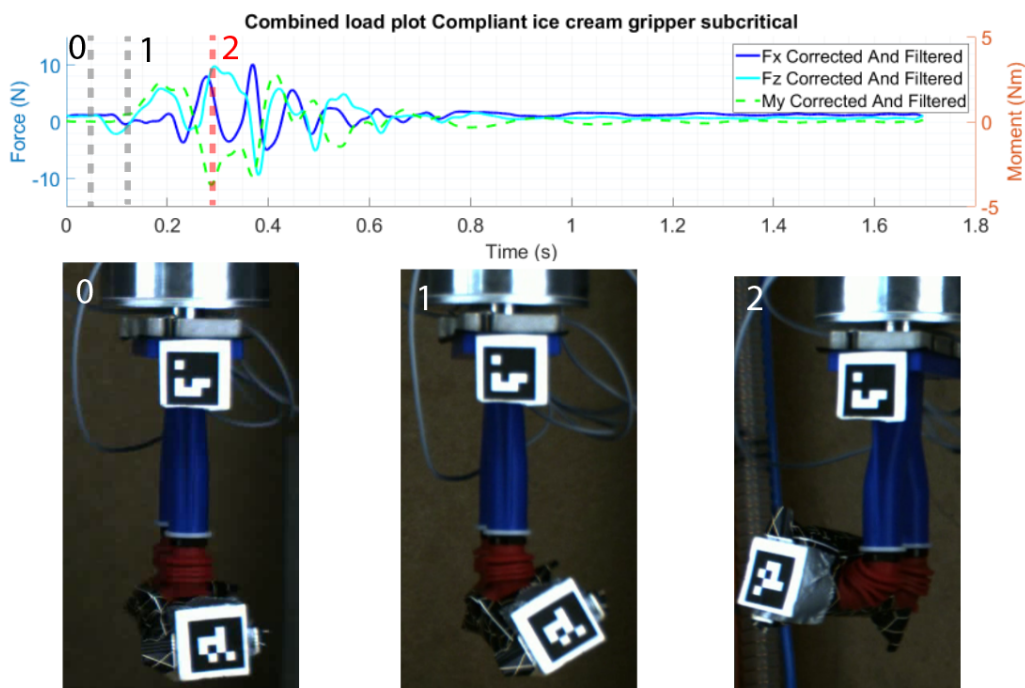
(a) The corrected and filtered force and moment measured for the stiff ice cream gripper with a subcritical acceleration path.



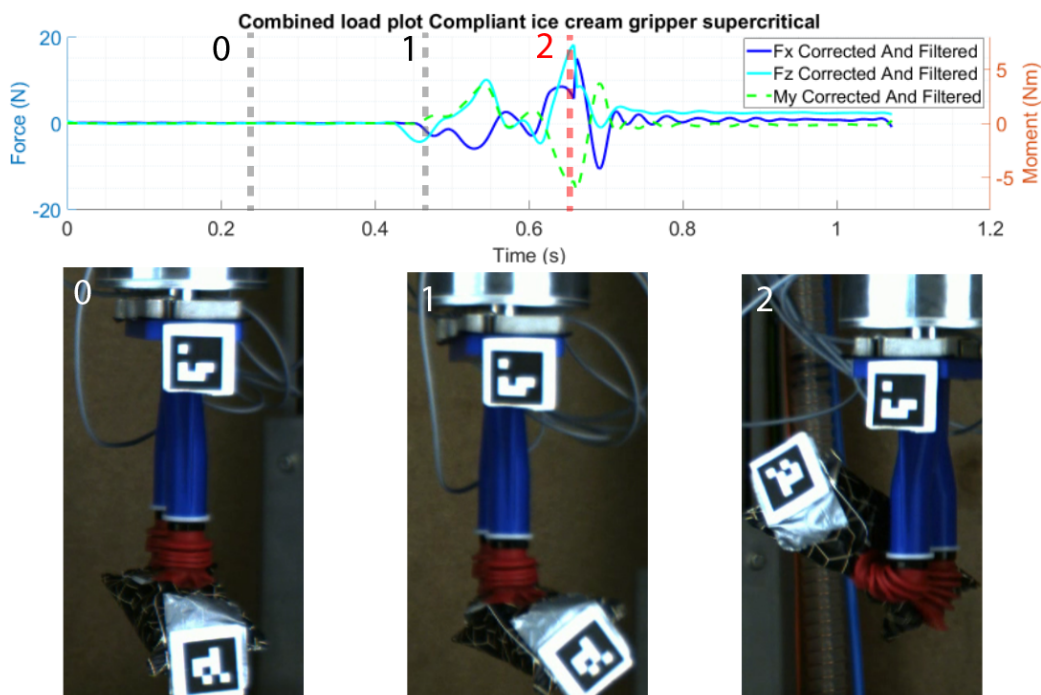
(b) The corrected and filtered force and moment measured for the stiff ice cream gripper with a supercritical acceleration path. In the picture showing the orientation labelled 2, the product just detached from the gripper.

Figure 3.9: The corrected and filtered force and moment measured for the stiff ice cream gripper with a supercritical acceleration path. The labels 0, 1, and 2 refer to the state before motion, the state where models predict detachment between the gripper and the product, and the state where the product detaches from the gripper in practice respectively. In the picture showing the orientation labelled 2, the product just detached from the gripper. The mass of the ice cream is so small that the loss of the product can not be seen at the scale of the plot.

3.4.6 Compliant ice cream gripper



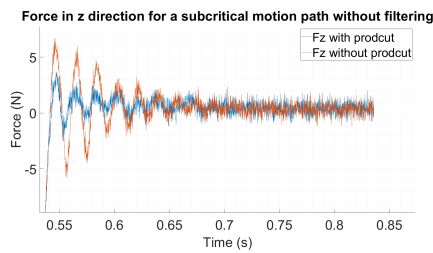
(a) The corrected and filtered force and moment measured for the compliant ice cream gripper with a subcritical acceleration path.



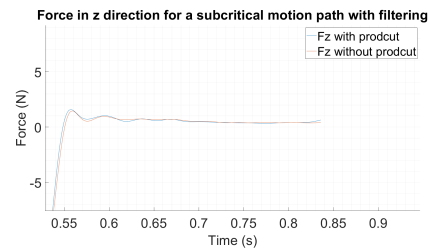
(b) The corrected and filtered force and moment measured for the stiff ice cream gripper with a supercritical acceleration path. In the picture showing the orientation labelled 2, the product just detached from the gripper. The mass of the ice cream is so small that the loss of the product can not be seen at the scale of the plot.

Figure 3.10: The corrected and filtered force and moment measured for the stiff ice cream gripper with a supercritical acceleration path. The labels 0, 1, and 2 refer to the state before motion, the state where models predict detachment between the gripper and the product, and the state where the product detaches from the gripper in practice respectively. In the picture showing the orientation labelled 2, the product just detached from the gripper.

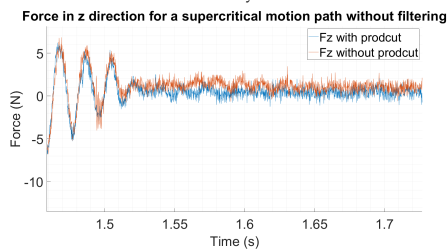
3.4.7 Remaining vibrations after a pick and place motion



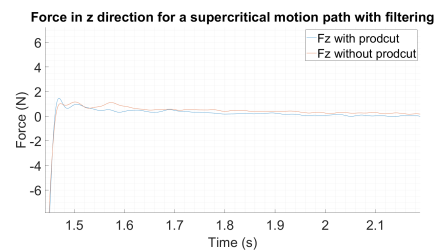
(a) The remaining vibrations after finishing a pick and place motion measured for the stiff single serve ice cream gripper, using the subcritical motion path without filtering. It can be seen that the addition of an object to the gripper has dampened the remaining vibrations. This is not expected because the product adds additional load to the system.



(b) The remaining vibrations after finishing a pick and place motion measured for the stiff single serve ice cream gripper, using the subcritical motion path with filtering. It can be seen that the filtering has removed the remaining vibrations.



(c) The remaining vibrations after finishing a pick and place motion measured for the stiff single serve ice cream gripper, using the supercritical motion path without filtering. It can be seen that the remaining vibrations overlap nicely. In the supercritical motion path the product has detached from the gripper, resulting in a loss of the dampening effects as seen in Figure 3.11a. Additionally, the change of force in the z direction due to detachment of the product can be seen.



(d) The remaining vibrations after finishing a pick and place motion measured for the stiff single serve ice cream gripper, using the supercritical motion path with filtering. It can be seen that the filtering has removed the remaining vibrations. Additionally, the change of force in z direction due to detachment of the product can be seen.

Figure 3.11: The remaining vibrations of the single mass in a foil gripper. These figures show why filtering is required for the proposed method. It was assumed that the addition of product to the gripper would not affect the behavior of the robot. In reality, the addition of the product to the gripper has a damping effect on the vibration of the robot structure, as can be seen in Figure 3.11a. Taking the difference between the load case with and without product will no longer result in a fair comparison. Therefore, filtering is used to remove the vibrations. A limitation introduced by filtering is the fact that the forces induced by the robot vibration are no longer taken into account.

3.5 Interpretation of the results

Before discussing the findings of this study the results will be interpreted and compared to the current understanding of the grasping strength of suction cup grippers. The load at which failure occurs can be found in Figures 3.7b, 3.8b, 3.9b, and 3.10b and is of interest for industrial application. For a better understanding of the dynamical behavior of suction cup grippers a more general understanding of the different failure modes is valuable. The interpretation leading to a description of failure modes of the stiff and compliant gripper is also presented in this section. The results will be interpreted in the same order as they are presented in section 3.4.

3.5.1 Method validation measurements

The robot acceleration path presented in Figures 3.5a and 3.6a in combination with the unfiltered and uncorrected load measurements presented in Figures 3.5b and 3.6b are considered first. These load and acceleration measurements were used to validate the measurement procedure.

The motion planner always planned a path within the set motion constraints shown

in table 3.1. However, for certain combinations of dynamic constraints the acceleration path showed steps and peaks. The steps and peaks were not investigated further because they did not occur at the product detachment point from the gripper.

In addition, the shape of the measured loads resembles the shape of the acceleration path well. By comparing Figure 3.5b to 3.6b it can be seen that increasing the acceleration simultaneously increases the load on the sensor as expected. However, the force in the z direction is in the wrong direction. Since the suction cup exerts the force required to accelerate the product, the force on the suction cups is expected to be in the opposite direction of the robot's acceleration. To correct for this misalignment in the reference frame of the sensor and the robot, R_1 , also presented in Figure 3.4a, was introduced.

Furthermore, the point of detachment is well captured by the sensor. In Figure 3.6b it can be seen that after the product detaches from the gripper, indicated by the line with label 2, the measurement with and without product overlap. This is expected because there is no difference between the two load cases after product detachment from the gripper.

3.5.2 Expected point of insufficient dynamic holding strength

To emphasize the findings of this study it is important to understand where the current models and their validation measurements predict the occurrence of product detachment from the gripper. As stated in section 3.4, the line labelled 1 is used to indicate this position in the force and acceleration plots. For the explanation, Figure 3.5a will be used. For the other figures showing acceleration of force plots the same reasoning holds.

In the current models the acceleration of a robot, as shown in Figure 3.5a, is directly used to determine the point of lowest dynamic grasping strength. With the path planner used in this study, the maximum acceleration in z and x direction is the same. Since the in plain force that a suction cup can withstand is depended on the normal force exerted on the suction cup, a combined acceleration in z and x will result in the lowest dynamic grasping strength. Only in the corners of the robot path, shown in Figure 3.2, there is a combined loading in theory. In the first corner, the robot accelerates upwards while simultaneously accelerating in horizontal direction. This results in a combined loading of an axial pulling and in plane force on the suction cup. In the second corner, the object is accelerated downwards while simultaneously decelerating in horizontal direction. This results in a combined loading of an axial pushing and in plane force on the suction cup.

The loading in the first corner will in theory result in the lowest dynamic grasping strength. However, in practise, product detachments are seen at the second corner. This point is labelled 2 in all figures showing a force or acceleration plot.

The current models and their validation measurements not only wrongly estimate the acceleration at which detachment of the product from the gripper occurs, but also incorrectly estimate the location of this detachment.

3.5.3 Soup grippers

In this section the measurement results from the stiff and compliant soup gripper, shown in Figures 3.7 and 3.8, will be interpreted and their main differences will be

discussed. The transition from the sub- to supercritical motion path will be the center of the measured load interpretation. This transition captures the point where the dynamic gripping strength becomes insufficient.

When comparing Figure 3.7a to 3.7b and Figure 3.8a to 3.8b it can be seen that the measured load for the supercritical motion path is higher than that of the subcritical motion path. The entire motion path seems to be scaled by the same factor, with the exception of the load at the detachment point. At the point of detachment, labelled 2 in Figures 3.7 and 3.8, the load increases more compared to the rest of the measurement.

Furthermore, for the supercritical load cases shown in Figures 3.7a and 3.7b the detachment of the product can be seen as an increase of load in the z direction. The load is increased because the load is set to 0 at the beginning of the load measurement.

Stiff soup gripper

Considering the stiff soup gripper in more detail, the transition from acceleration to deceleration in x is most interesting. Before the change of acceleration to deceleration the load follows the same shape as the set acceleration. At the same time, the product rotates slightly, as can be seen in the picture labelled 1 in Figures 3.7a and 3.7b. When the robot starts decelerating, the force in x direction and the moment around the y axis rapidly change direction. During this change from acceleration to deceleration the product rotates from one end of the gripper to the other end. This rotation can be seen in the picture labelled 3 in Figures 3.7a and 3.7b. Due to the stiffness of the suction cup the product suddenly stops rotating as the foil is pulled tight. This impulse loading causes a peak in the force in x direction and moment around the y axis.

This peak occurs before the second corner, while the robot is not accelerating in the z direction. This can best be seen in Figure 3.3a.

Compliant soup gripper

For the compliant soup gripper a few key differences can be seen. The dynamic grasping strength is significantly better. The compliant soup gripper is able to achieve higher accelerations while still holding the product. The transition from sub- to supercritical is much larger than for the stiff soup gripper. This will later be explained when considering the difference in failure mode.

The differences between the stiff and compliant gripper start in the first corner. For the compliant gripper, the suction cups grasping plane can rotate, resulting in a higher normal load in z direction and a smaller load in x direction. This is beneficial for holding the object because the friction coefficient is smaller than 1.

Another effect of this compliance is a greater rotation of the product. This can be seen in the pictures labelled 2 in Figure 3.8a and Figure 3.10b. The rotation of the product is limited, once the bellows of the suction cups compress together the compliance is decreased, limiting further rotation.

The second difference can be seen when looking at the change from acceleration to deceleration in the x direction. For the compliant soup gripper this change is much more gradual compared to that of the stiff suction cup. Due to the compliance of the gripper, no peaks in the force in x direction or moment in y direction can be seen

right after the start of the deceleration. The picture labelled 2 in Figure 3.8a shows the product orientation at this point.

The point of failure for the compliant gripper is different than that of the stiff gripper and can be explained by considering two observations. Firstly, the downwards acceleration starts while the product is still oriented as shown in the picture labelled 2 in Figure 3.8a. In this orientation, the center of mass is left of the center line of the gripper. Secondly, the gripper has lost its rotational compliance due to a compression of the suction cup bellows caused by the previous deceleration. This combination results in an increase in moment around the y on the suction cups as can be seen in the line labelled 2 in Figure 3.8a and Figure 3.10b, causing the failure of the compliant soup gripper and placing the point of detachment of the product from the gripper at the start of the second corner.

Because of the failure is depended on the product orientation when entering the second corner a large difference in acceleration between a sub- and supercritical path is explained.

3.5.4 Single serve ice cream gripper

Stiff ice cream grippers

For the stiff ice cream gripper the same behavior as for the stiff soup gripper is seen. The peaks in the force in the x direction and the moment around the y axis are even more clearly visible in Figures 3.9a and 3.9b. Right before and right after the peaks, the force in x direction is the same as in the first half of the motion cycle. This can be seen before and after the line labelled 2 in Figure 3.9a

For the supercritical load case the peaks of force in the x direction and the moment around the y axis are also seen in the first corner, right after the point labelled 1 in Figure 3.9b.

Compliant ice cream gripper

Similar to the soup grippers, the compliant gripper also performs better than the stiff gripper for the single serve ice cream. Table 3.1 shows that the compliant ice cream gripper achieves the same maximum acceleration as the stiff ice cream gripper. The maximum acceleration is a direct indication of cycle speed, which is the most important performance criteria for high-speed case packing. However, the compliant gripper achieves this performance with a smaller surface area. Therefore, the compliant gripper performs better than the stiff gripper for single serve ice cream. However, due to the single row of suction cups the product has reaming motion after the pick and place cycle has finished. This is a large downside creating a trade of between holding capabilities and position certainty.

The behavior of the compliant ice cream gripper also resembles that of the compliant soup gripper. Because of the larger rotational freedom, the measured load plots look different. The most notable difference is the low load in x direction after the first corner, which can be seen in Figure 3.10a. The low load in the x direction is a direct effect of the suction cup rotation. When the acceleration changes to deceleration in the x direction, the product swings to the other side, causing an increase of load in the x direction. When the motion in the z direction is finished there are still load forces measured in x and z direction. These forces are the damped oscillation of the

mass-spring-damper formed by the suction cup and the gripped product. When comparing Figure 3.10a and Figure 3.10b it can be seen that the failure mode of the compliant ice cream grippers is the same as the failure mode of the compliant soup gripper. The downward acceleration of the second corner causes an increase in moment perpendicular to the plane of motion.

3.6 Discussion

Besides, finding the load case that leads to product detachment and interpreting the results explaining the failure mode of stiff and compliant suction cups, other interesting observations were also made during this study. These observations, the limitation of the proposed method, and the recommendations for future work are discussed in this section.

The proposed method worked well to find the load at which product detachment of the suction cup grippers occurred. However, a significant limitation of this method is the fact that the data has to be filtered before the first eigenfrequency of the robot. The load on the suction cups is considered as the difference between the measurement with and without an attached product. This assumes that the addition of the product to the gripper does not change the behavior of the robot. In reality, this is not the case, during measurements it was noted that the vibrations of the robots structure were damped due to the addition of a product to the suction cup. The effects of this damping and filtering are shown in Figure 3.11. Since the two load cases are coupled, subtracting the measurements will not result in a fair comparison. To remove the vibration all together, a low pass filter was added. However, in reality, the product will experience the loads induced by the vibrations of the robot structure as well. These loads are not taken into account using this method. With the current state-of-the-art understanding of the dynamic gripping strength, the neglected forces only pose a minor error.

In the proposed method, the synchronisation of the load measurements, video frames and acceleration profiles was all done manually. This is a time consuming process prone to human errors. For future studies it is recommended to synchronise all measurements with one start button.

The final improvement concerns the robot control and acceleration measurement. In this study, the motion planning and acceleration measurement are handled by the Beckoff motion controller. The source code for the motion planner and acceleration measurements are not available. This results in a "black box" in the measurement setup.

The motion planner is simple to use, but provides limited freedom in the design of the acceleration path. Furthermore, the acceleration calculated by the motion planner using the motor encoders is expected to be strongly filtered. The measured acceleration profiles presented in Figure 3.6a and Figure 3.5a show smooth lines. On the other hand, the measured load shows vibrations in a fixed frequency range. When directly measuring the output of the motor encoders, vibrations at the same frequency can be seen. After further investigation it was determined that the measured frequency was the eigenfrequency of the case packing robot. The measured frequency is depended on the location of the robot in its working space. During the load measurements, eigenfrequencies around 30 Hz were found. To gain more

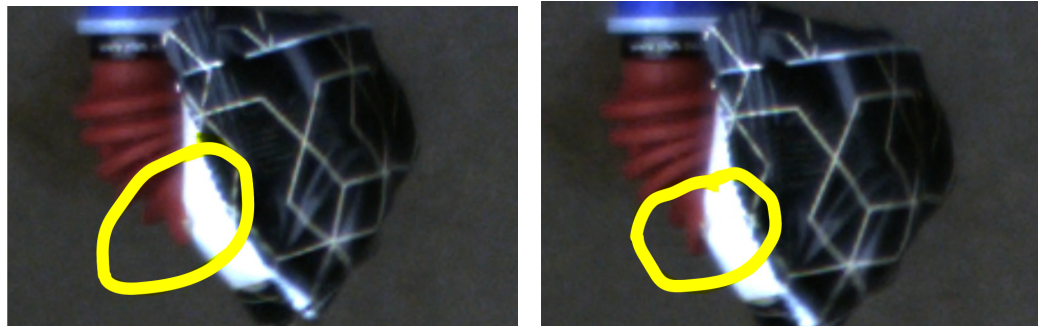
design freedom in the acceleration path and to obtain a better acceleration measurement of the robot platform, it is recommended to design these parts separately from software packaged provided by Beckoff.

During the dynamic grasping strength measurements, some interesting observations were made. Firstly, during the measurements with a supercritical acceleration path, the product detached at the back of the gripper first. The reason for this trend is hypothesized to be caused by an uneven distribution of mass and volume in the foil. Soup is packaged in a tapered pouch placing most of the mass on the front half of the gripper. Single serve ice cream has a popsicle stick on one end of the ice cream, which was always placed in the same direction during measurements, placing its mass and volume continuously on the front half of the gripper.

Considering the failure modes found for stiff and compliant grippers the detachment of the product at the back of the grippers can be explained. As example, the reasoning is given for the stiff ice cream gripper. The failure mode of the stiff grippers was a sudden stop of the angular motion, leading to a peak of force in the horizontal direction and in the moment perpendicular to the plane of motion. The volume of the single serve ice cream is located at the front of the gripper. When this part of the ice cream hits the stiff suction cup a small moment is also measured around the axis in the direction of horizontal motion. This moment is counteracted by a pushing force at the front of the gripper and a pulling force at the back of the gripper. The point of highest pulling load is in that case located at the back of the gripper. A similar reasoning can be made for the other gripper-product combinations.

These observations lead to the recommendation to reconsider the grasping position of the product. Now, the gripper is always placed centred of the product's surface. The throughput could possibly be increased when the gripper is placed above the center of mass of the product.

Secondly, the compliant suction cups showed the ability to re-seal the suction cups after a partial detachment of the product. This observation was made while reviewing the high-speed footage. The re-sealing effect is explained by the idea that a small leak in the seal of a compliant suction cup will cause a rapid increase in airflow. This flow sucks the foil and the compliant suction cup rim back together, closing the seal again. Different frames from the high-speed recording show the re-sealing effect presented in Figure 3.12. The re-sealing effect could be part of the reason that compliant suction cups outperform stiff suction cups.



(A) In this frame a leak starts to form at the front of the compliant suction cup gripper. The leak is encircled in yellow.

(B) The following frames show that the gap slowly grows. One of these frames is shown in this picture.



(C) In this frame the suction cup gripper has re-gripped the products. This is remarkable because the product has continued to move in the direction that originally caused the leak. The rotation of the product did not assist in the re-sealing of the product to the suction cup.

FIGURE 3.12: Three pictures showing the re-sealing capabilities of the compliant suction cups. This video was taken using 800 frames per second using the same camera as for the force measurements. By reducing the amount of pixels that are captured per frame, the frame rate was increased.

Also worth mentioning, in this study only suction cups based grippers were considered. However, the setup and measurement procedures could also be used to study other gripper classes or hybrid grippers. The airflow integration into the sensor structure could be used for the actuation of any pneumatic based gripper. For compliant or underactuated finger based grippers an additional change should be taken into account. When a product is added to the gripper the grasp changes compared to the situation where no product is added to the gripper. The loads induced by the acceleration of the robot will exaggerate this difference. For these type of grippers the method proposed in this work has to be extended. Finally, two type of suction cups and two products have been considered in this study. For future research it is recommended to use the improved method to extend the study including a wider variety of products and grippers.

3.7 Conclusion

In this study, the dynamic grasping strength of suction cup grippers while handling flexible products was measured in an experimental setting. The robot paths and

products used in the measurements of the dynamic grasping strength were picked to resemble high-speed case packing for packaged food. The considered products consisted of soup in a pouch and single serve ice cream. Both products were packed using compliant and stiff suction cup grippers, which was done to identify the difference in their behavior.

For the measurement of the load, the six-axis force moment sensor from chapter 2 that passes airflow through the sensor structure is used. Passing the airflow through the sensor structure eliminates the parasitic forces coming from the stiff vacuum hose.

By taking the difference from a measurement with and without a product attached to the gripper the load on the suction cups was calculated. For this calculation a calibration, rotation and translation matrix were used to transform the load measured at the sensor to the load on the suction cup. To also take the time varying position and angle of the compliant suction cups into account, Apriltag tracking was performed on recorded high-speed videos.

From the calculated loads on the suction cups, the failure mode of compliant and stiff suction cups were determined. The failure modes found were not influenced by the gripped product. For stiff suction cups the failure load is a peak of force in horizontal direction and a moment around the axis perpendicular to the plane of motion. These peaks are caused by an impulse loading when the foil of the product is pulled tight right after the robot path changes from acceleration to deceleration. Compliant suction cups accelerating downwards, while the product is not centred on the gripper, causes the detachment of the product. Accelerating downwards while the product is not centered at the gripper causes an increase in moment perpendicular to the plane of motion, the suction cups are not able to withstand this moment loading.

Interestingly, the moment around the axis perpendicular to the plane of motion is influential for both the stiff and compliant gripper. Literature has not considered this moment before, when measuring the load at which detachment occurs between the product and a suction cup.

Furthermore, the models currently found in literature predict that a product detaches from the gripper in the first corner of the robot path. In reality, the detachment of the product from the suction cups occurs in the second corner. The current models not only predict the acceleration at which a product detaches wrongly, but also predict the location of product detachment incorrectly. This illustrates the lack of understanding of the dynamic grasping strength of suction cups. Finally, compliant bellow suction cups outperform stiff suction cups and are able to hold product at higher accelerations. At this higher throughput the product has a large remaining damped vibration. Because of the remaining vibrations a product can not be placed in a container, leading to the observation that further improvement of suction cups based grippers is limited because there seems to be a trade-off between holding capabilities and position certainty.

For future research it is recommended to change the measurement process by creating a single start button for the load, acceleration and high-speed video measurement. This button will automatically synchronise all the measured data, speeding up the measuring process significantly. Automatic synchronisation will also reduce the change of human errors during the now manually performed data synchronisation process.

After speeding up the measurement process the conclusions presented here should be validated by extending the study to include more products and grippers.

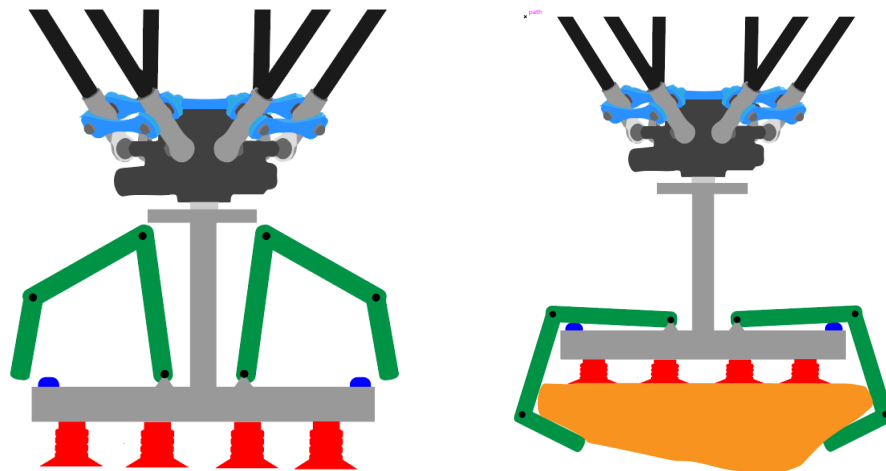
Discussion

The aim of this study is to gain a better understanding of product detachment from suction cups, an effect observed in the high-speed case packing for packaged food. Detachment of products is defined by the loss of contact between the robotic suction cup gripper and the gripped object.

Besides the conclusions drawn in the separate chapters, other chapter overlapping conclusions and insights were also gained.

Combining the knowledge gained from the three chapters two gripper designs are proposed. The first design is a hybrid gripper as shown in Figure 3.13. This design uses suction cups combined with an under actuated gripper. These gripper classes showed to complement each other, which is described in chapter 1. The under actuated gripper will limit the range of motion of the product, thereby eliminating the impulse loading that causes the foil to suddenly pull on the suction cup. For this gripper design, the actuation speed of the under actuated gripper is the main concern.

Low inertia design, high actuation power, low joint friction and gripper-robot synchronisation should be considered to obtain lower actuation times. For the mechanical design, inspiration can be taken from the 100g gripper, designed to catch object using a robot hand [168]. High actuation power could for example be achieved by storing energy in a spring using a lower power actuator, which can store energy during the robot motion that is then released at the pick and place location. An example for such a design can be found in the design of an aerial gripper [99]. Finally, from chapter 3 it is concluded that the second corner in the robot path contains the main limitation. The vertical acceleration and the beginning of the first corner in the robot path can be used as extra time to fully close the gripper. This requires a good synchronisation between the robot and the gripper.



(A) The proposed hybrid gripper design using under actuated gripping with suction cups gripping in the open position

(B) The proposed hybrid gripper design using under actuated gripping with suction cups gripping in the closed position

FIGURE 3.13: The proposed hybrid gripping design combining under actuated gripping with suction cups

The second proposed gripper design uses the observations of rotational freedom that is paramount for better holding capabilities. This design is shown in Figure 3.14 and has the necessary rotational joint added close to a stiff suction cup. All rotational freedom is caused by the added joint for stiff suction cups, resulting in a well defined pendulum. This pendulum will show significant remaining vibrations after a motion cycle. However, because the pendulum is well known, the input shaping can be used to suppress its eigenfrequency reducing the residual motion at the end of a motion cycle. The sensor presented in chapter 2 can be used to determine the input shaping parameters.

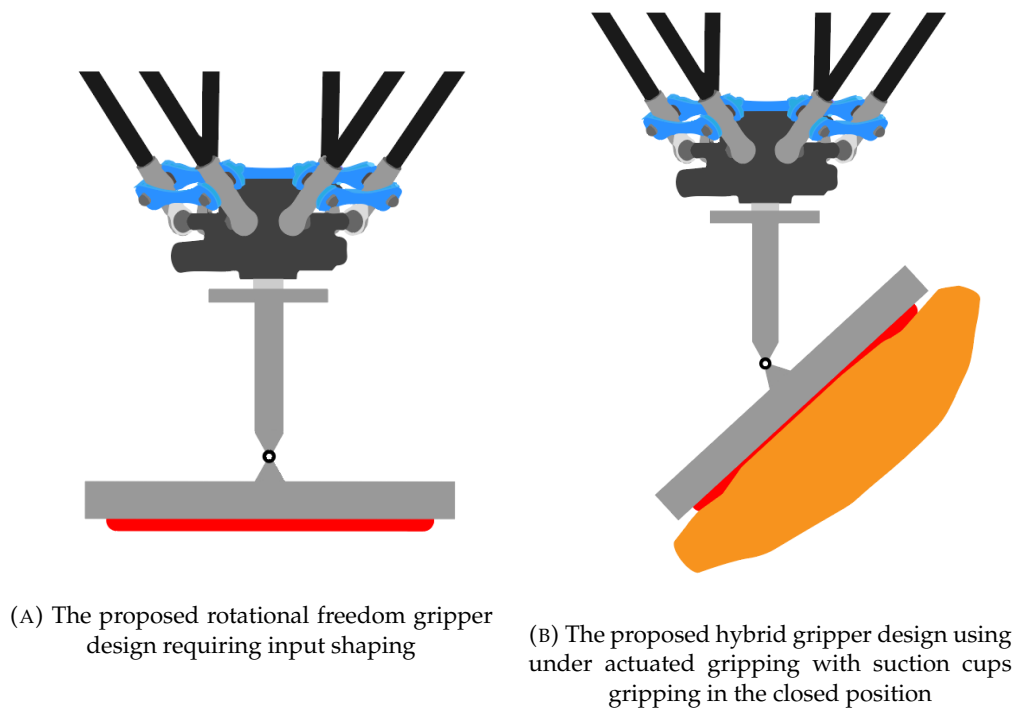


FIGURE 3.14: The proposed rotational freedom gripper design requiring input shaping during motion

Additionally, with the designed sensor, other fields of research such as critical load path planning, suction cup model validation and suction cup hybrid gripper validation have also been enabled. Critical load path planning has already been proven to work for parallel robots [5]. In this study, solid objects are bin picked at a critical speed using a single suction cup. In this work the critical speed was defined as the speed at which either sliding or full detachment of the object from the suction cup occurred. By including a model of the grasping strength limit to the path planner, the suction cup was never loaded supercritically. Using the designed sensor and measurement procedure proposed in chapter 3 this work could also be extended to include the limit of the dynamic grasping strength for flexible products. This will ensure the suction cups are always critically loaded for any motion path, improving the certainty in the path planning.

The more advanced grasping strength suction cup models in literature lack the ability to validate the proposed models. Using the sensor from chapter 2 and the method from 3 the more sophisticated models from literature, lacking validation, can now be validated. It is recommended to first validate the position at which detachment occurs before validating the exact load at product detachment. The currently validated models also predict the location of failure wrongly. Checking the point of failure is easier than checking the exact load, which already improves the current models.

Finally, the validated sensor and proposed method can also be used to validate the grippers proposed in this section. When the dynamic failure load of the proposed grippers has been measured, the amount of improvement can be quantified. With this newly gained knowledge the design can be improved upon again, resulting in a method for the structured improvement of grippers in the high-speed case packing industry. A particular challenge that remains for studying finger based grippers is the change in orientation of the product during the high-speed case packing motion. The measurement without a product will not suffer from the same change in

gripper orientation. However, when this technical challenge has been dealt with the structured improvement of hybrid finger based grippers is made possible.

Conclusion

In the high-speed case-packing of prepackaged food the detachment of products from the suction cup gripper has recently become a prominent challenge. This study consisted of three parts which all aimed to increase the understanding of the product detachment from suction cups.

In chapter 1 the state-of-the-practice in the case-packing for packed food and state-of-the-art of robotic gripping was reviewed. From this review a classification was made, which was followed by a gripper grading used to determine the limiting factors of all gripper classes for the high-speed case packing considering packaged food. It was concluded that actuation time, holding capabilities and operating in confined space formed 65% of the limitations. Interestingly, the research into reducing actuation time of grippers is very limited. Furthermore, suction cups showed to be the overall best gripper for the packaged food industry. However, the data available for the grading was found to be limited.

Chapter 2 set out to fill this literature gap. In this chapter a six-axis force moment sensor capable of passing airflow without influencing the measurement capabilities of the sensor was designed. The design, fabrication, and validation of the sensor resulted in a sensor with sufficient performance for usage in measuring loads during high-speed case packing. The maximum measurement error of the sensor was found to be 8% in the F_z direction.

In Chapter 3 the validated sensor was used to measure the dynamic grasping strength of stiff and compliant suction cups. These measurements showed that the moment perpendicular to the plane of motion are the leading limitation of the dynamic grasping strength of suction cups. For stiff suction cups this moment is caused by an impulse loading when the foil is suddenly pulled after a change in acceleration. For compliant suction cups this moment is induced by accelerating downward while the product is not centered under the gripper.

Combining the knowledge of the three chapters, two gripper designs were proposed to directly improve the end effectors in the high-speed case packing of packaged food. Furthermore, future research suggestions were done, it is recommended to look into expanding the considered product and suction cups, load critical path planning, improving actuation time of mechanical grippers and hybrid gripper design.

Appendix A

Grading data

A.1 Data collected for gripper grading

To allow for grading of the different gripper classes appropriate data was required. The reviewed literature was searched for the required data. During this search it became evident that researchers do not publish all the values that were of interest for this study into gripping. To still obtain a reliable data pool the author further filtered the set of selected papers that were obtained during the literature search. To only include grippers which were deemed to have a size suitable for high speed case packing. This gives a more fair comparison between the gripper classes for the application in this field. Table A.1 shows a summary of the collected data. The table shows the source, the gripper class, the pull out force, the actuation speed the range of products, the contact pressure type and a note. The note gives important information which was noted for the source.

TABLE A.1: A summary of the data used to perform the gripper grading

Gripper class	Pull out	Actuation	Weight (kg)	Range of	Contact	Note	Source
		Force (N)	speed (ms)	Products (mm)		Pressure	

TABLE A.1: A summary of the data used to perform the gripper grading

Gripper class	Pull out	Actuation	Weight (kg)	Range of	Contact	Note	Source	
							Force (N)	Products (mm)
[62]	Bernoulli gripper	0.5	X	X	42	Contact surface	Upper limit Range of Products not given	Pull out force only provided in normal direction
[169]	Bernoulli gripper	X	X	X	19-49.2	Contact surface		
[170]	Bernoulli gripper	0.2	X	X	43	Contact surface	Upper limit Range of Products not given	
[171]	Bernoulli gripper	0.7	X	X	17-70	Contact surface		
[79]	Pressurized bellows	28	see note	X	X	Contact line	Actuation time presented as "1.3 times faster than standard"	Pull out force only provided as a maximum lifting force
[65]	Pressurized bellows	2.5	X	X	0-100	Contact line	Pull out force as a maximum lifting force during a pinch grasp	
[80]	Pressurized bellows	5.5	X	X	0-190	Contact line	Pull out force only provided as a maximum lifting force	
[66]	Pressurized bellows	10	X	0.43	0-120	Contact line		
[172]	Pressurized bellows	6	4E+02	0.44	0-138	Contact line		
[173]	Pressurized bellows	89	X	0.594	0-110	Contact line	Maximum lifting force 200 N	

TABLE A.1: A summary of the data used to perform the gripper grading

Gripper class	Pull out	Actuation	Weight (kg)	Range of	Contact	Note	Source
[174]	Pressurized bellows	4-12	1.6E+03	X	0-170	Contact line	Pull out force given as a function of the object size
	Pressurized bellows	15	6E+02	X	X	Contact line	Source Direct correspondence Soft Robotics
[105]	Suction cups	50-350	X	X	X	Contact surface	Pull out force linear with area and pressure
[103]	Suction cups	100-600	X	0.07	110	Contact surface	Weight of connecting tool not provided Upper limit Range of Products not given Large suction cups measured for pull out force
[175]	Suction cups	35	X	X	X	Contact surface	small suction cup measured for pull out force
BPA	Suction cups	X	20-60	0.6		Contact surface	
BPA	Suction cups	X	20-60	1.87	X	Contact surface	
[176]	Suction cups	X	20-60	X	X	Contact surface	A micro scale suction cup actuation time not used
[177]	Suction cups	70-100	80		80	Contact surface	Upper limit Range of Products not given Normal size suction cups measured

TABLE A.1: A summary of the data used to perform the gripper grading

Gripper class	Pull out	Actuation	Weight (kg)	Range of	Contact	Note	Source
[178]	Structure jamming	10	X	1.1	70-95	Contact surface	
[179]	Structure jamming	44	2.50E+02	1.1	27-63	Contact surface	time vary (100 ms pick 150 ms place) Pull out force in normal direction (tangential 89N)
[179]	Structure jamming	89	1.70E+03	2.9	49.7-115.5	Contact surface	P&P time vary (100 ms pick 150 ms place) Pull out force in normal direction (tangential 178N)
[180]	Structure jamming	100	1.00E+03	X	0-30	Contact surface	
[54]	Distributed compliance	95	X	1.2	0-140	Contact line	Pull out force in normal direction
	Distributed compliance	>27	60	1.5	30-60	Contact surface	Actuation time considers a pinch grasp very close to the object Pull out force measured was to validate design criteria
[181]	Distributed compliance	X	X	X	0-100	Contact line	Contact force was measured instead of pull out (3.7 N)
[182]	Distributed compliance	X	X	X	0-75	Contact line	Contact force was measured instead of pull out (10.5 N)
[183]	Distributed compliance	40	X	X	0-50	Contact line	Tendon force was measured instead of pull out (10.1 N)

TABLE A.1: A summary of the data used to perform the gripper grading

Gripper class	Pull out	Actuation	Weight (kg)	Range of	Contact	Note	Source
[184]	Lumped Compliant	X	2.40E+03	0.23	0-70	Contact points	
[99]	Lumped Compliant	56	2.00E+02	0.5	X	Contact points	
[84]	Rigid 1 DOF	200	2.60E+02	1	0-20	Contact point	Actuatin time of median presented average 0.23 sec
[185]	Rigid 1 DOF	X	3.60E+02	0.72	0-140	Contact point	Pinch force measured at 20N
[186]	Rigid 1 DOF	10-450	20-6.00E+2	1.285	0-15.0	Contact point	
[187]	Rigid 1 DOF	19-500	32-1.69E2	1.05	0-35	Contact point	Range of Products determined by angular range of motion all metal Gripper fingers included in presented mass
[188]	Rigid 1 DOF	X	5.00E+01	X	60	Contact point	All metal Gripper fingers included in presented mass
[189]	Rigid fully actuated gripper	X	1.00E+03	4.2	0-100	Contact points	Auction time limited to 1 s because of a safety concerns
[190]	Rigid fully actuated gripper	X	1.00E+02	1.2	X	Contact points	Platform weight not included in original publication
[37]	Rigid fully actuated gripper	X	X	1.5	X	Contact points	

TABLE A.1: A summary of the data used to perform the gripper grading

Gripper class	Pull out	Actuation	Weight (kg)	Range of	Contact	Note	Source	
							Force (N)	Speed (ms)
[191] Rigid fully actuated gripper		X	1.05E+02	1.95	X	Contact points		
[40] Rigid fully actuated gripper		X	1.00E+03	0.6	X	Contact points		
[192] Rigid fully actuated gripper		65	2.00E+03	0.4	X	Contact points		
[37] Rigid fully actuated gripper		100	X	X	X	Contact points		
[193] Rigid Underactuated gripper		50	3.0E+03	0.75	0-100	Contact points		
[37] Rigid Underactuated gripper		20	X	0.65	X	Contact points		Platform weight not included in original publication
[37] Rigid Underactuated gripper		35.6	X	0.651	X	Contact points		Platform weight not included in original publication
[37] Rigid Underactuated gripper		102	X	0.6	X	Contact points		Platform weight not included in original publication

TABLE A.1: A summary of the data used to preform the gripper grading

Gripper class	Pull out	Actuation Force (N)	Weight (kg)	Range of speed (ms)	Contact Products (mm)	Note	Source
[43]	Rigid Underactuated gripper	107	8.60E+02	0.73	0-120	Contact points	Platform weight not included in original publication
[194]	Rigid Underactuated gripper	20	2.00E+03	X	0-110	Contact points	
[195]	Rigid Underactuated gripper	70	7.20E+02	0.99	X	Contact points	Maximum actuation speed not reported
[195]	Rigid Underactuated gripper	63	7.0E+02	0.638	X	Contact points	Platform weight not included in original publication
[196]	Rigid Underactuated gripper	25	4.00E+02	0.695	0-100	Contact points	Platform weight not included in original publication
[197]	Rigid Underactuated gripper	15	X	X	X	Contact points	Platform weight not included in original publication
[198]	Rigid Underactuated gripper	50	1.6E+03	0.73	X	Contact points	

Appendix B

Gripper Classification

B.0.1 Gripper classification

In this appendix the gripper classification is discussed in full detail. The main content is the same as presented in chapter 1, some sections are even identical. This appendix is only intended to give a more detailed explanation.

Current gripper literature already presented some classifications, however for our purpose a new adjusted overview is made to serve the application-field [20], [26]–[29]. Therefore, a new classification considering high speed P&P for the packaged food industry is made and is shown in figure B.1. The classification consists of 5 main branches: rigid mechanical grippers, compliant grippers, pneumatic grippers, hybrid grippers and infeasible gripper. A main branch has sub-branches leading to gripper classes. The gripper classification is discussed in further detail below.

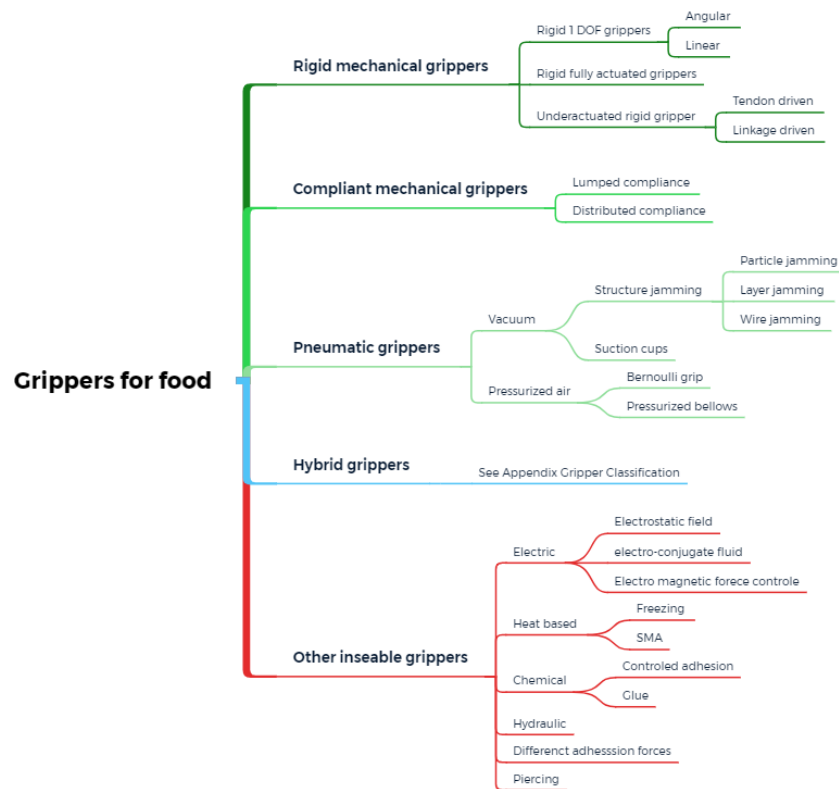


FIGURE B.1: An overview of the presented gripper classification

1. *Rigid mechanical grippers*

All robotic grippers consisting of rigid links and non-compliant parts are placed under this classification. Most traditional robotic grippers fall under this category and are well established in industry due to their predictability, reliability and availability [33]–[35]. Knowledge and literature on this type of grippers is readily available, due to the many years of research that have already been performed [36]. This gripper type can be further subdivided in three gripper classes: fully rigid 1 DOF (degree of freedom) grippers, fully rigid actuated grippers and under actuated rigid grippers.

- a *Rigid 1 DOF grippers*, this gripper class is the simplest rigid gripper and is defined by having one actuated degree of freedom and no compliant parts. This degree of freedom can be achieved by linear or rotational motion, shown in figure B.2a and B.2b respectively [34]. The path this gripper takes is well defined, features simple control and can be bought "off-the-shelf" [33]. A fully rigid 1 DOF gripper could be classed as a fully rigid actuated gripper, but since its design and defining features are very different its deserving of a separate class.
- b *Fully rigid actuated grippers*, grippers in this class have multiple DOF which are each individually controllable. This defining feature results in high adaptability, each phalanx of the gripper can be adjusted as desired. This

however requires as much actuators as DOF and often many more sensors. Making this gripper class heavy, challenging to control and expensive [37]. Reducing weight, cost and control complexity are therefore one of the main focus areas of research topics for the fully rigid actuated grippers [38]–[40]. Figure B.2c shows a gripper form this class.

- c *Underactuated rigid grippers*, grippers with rigid links and more DOF than degrees of actuation (DOA) are placed in this class. Grippers in this class are not able to actuate each phalanx of the gripper individually. However when a phalanx comes in contact with the object a DOF is constrained by the object, the phalanx in contact with the object stops moving while the other phalanges remain in a closing motion. The grasp is completed when all phalanges are constrained in some way. This behavior gives underactuated gripper the ability to grasp around an object, with only limited actuators and no sensors. To maximize the gained benefit from removing the actuators designs often strive to use only one DOA [23], [41]–[43]. Under actuation can be achieved by a linkage driven design as shown in figure B.2e or by a nature inspired tendon driven hand shown in figure B.2d.

2. *Compliant mechanical grippers*

Compliant mechanical grippers consist of one single compliant structure and do not contain any traditional rotational or linear joints. In the general classification of compliant mechanisms two main classes are distinguished, lumped and distributed compliance [44].

- a *Lumped compliance*, for lumped compliance the deformations take place locally in a structural member and is often used to replace traditional rotational joints [44]–[51]. This way rigid mechanical grippers can be transformed to compliant grippers. A lumped compliant gripper is shown in figure B.2f.
- b *Distributed compliance*, for distributed compliance the deformation takes place in a larger region of the structural member [52]–[56]. When neglecting the mass of a the gripper and only considering external loading strain energy can be used as a measure for stiffness [199], [200]. Distributed compliant mechanisms generally have a large strain energy compared to similar size lumped compliant mechanisms, resulting in a higher stiffness. An example of a distributed compliant gripper is shown in figure B.2g.

3. *Pneumatic grippers*

Grippers relying on pneumatics yet not requiring a mechanical support structure to connect to the object, are gathered in this class. This definition was picked to exclude all mechanical grippers using pneumatic cylinders as their actuator is from this class. This gripper type is further divided in vacuum grippers and pressurized air grippers.

- a *Vacuum gripping: suction cups*, the most common vacuum gripper which is often used in industry, is the suction cup [26]. By applying a negative pressure difference inside a volume enclosed, a force is exerted on the object. This working principle is the unifying feature of this gripper class. Their grasp for radial forces and axial moments is based on friction.

- b *Vacuum gripping: structure jamming*, structure jamming grippers are made by loosely packing powder, layers or wires in a deformable enclosed volume. By reducing the volume in which the jamming material is enclosed the jamming material is compressed and does not allow for free movement of the particles anymore [58], [59]. This gripper class must be pre-shaped before actuation, usually done by firmly pressing the jamming gripper against the object to be picked. When a loose shape has been formed the gripper is actuated jamming the particles, increasing the stiffness and gripping of the object. Actuating the gripper can result in a 180 times increase in stiffness [60], [61]. Figure B.2i and B.2h, show layer jamming and particle jamming respectively.
- c *Pressurized air gripping: Bernoulli*, Bernoulli grippers use high speed airflow around an object to generate a lifting force. A lower velocity air stream has a relatively higher static pressure compared to a high velocity air stream [64]. By careful design, the air stream above the object is forced to have a higher velocity creating a lifting force. There is no contact because of the airflow. Delicate, clean or sterile object such as silicon wafers, solar panel cells and sliced fruit or vegetables are best suited for Bernoulli grippers [62], [63]. Figure B.2k shows a Bernoulli gripper.
- d *Pressurized air gripping: Pressurized bellows*, Pressurized bellows consist of a bellow with a semi-rigid spine. By applying pressure inside the bellow the semi-rigid spine bends due to a difference in material extension. Pressurized bellows are designed for the handling of fragile and delicate objects such as fruit, pastries or meat [67]. This type of gripper has been a research topic of great interest in recent years [20]–[22], [65], [66]. Especially hybrid grippers using pressurized bellows see a large research effort [76]–[82]. Furthermore pressurized bellow grippers are readily available on the market at companies such as, Soft Robotics and SoftGripping. Figure B.2l show a typical pressurised bellow gripper.

4. Hybrid grippers

The goal of a hybrid gripper is to counteract the weak points of one gripper class by combining it with another gripper class. The field of hybrid grippers is rapidly growing and is deserving of a more detailed look. Furthermore in grading the gripper classes a hybrid gripper can not be placed in one of the other gripper classes.

While studying literature it became evident hybrid gripping is a well established method to improve the performance of a gripper performing a predefined task. It is also noted all hybrid gripping solutions yielding a feasible combination of gripper classes have been tried already. The main trends for combating the limitation are presented here.

a *Increasing holding capabilities*

The limiting factor for holding capabilities for some gripper classes such as compliant grippers, pressurized bellows and underactuated grippers can be contributed to limited stiffness. A solution to this would be increasing the joints or structure stiffness of the gripper. Considering the same actuator this however also increases the closing time. To maintain the original closing time an actuatable or highly non-linear stiffness

change is desired. With a low stiffness in the open position and a high stiffness in the closed position. In hybrid gripping this is often done by combining a gripper that needs improvement with structure jamming [60], [77], [78], [81], [201], [202]. The original gripper class is used to pre-shape the structure jamming gripper, which is then either locked actively or passively increasing the stiffness tremendously. An increase of stiffness of 180 times and a load capacity increase of 30 times has been achieved using active stiffening of a lumped compliant gripper [60]. Using passive stiffening a 6 fold stiffness increase has been achieved using a particle jamming and pressurized bellow hybrid gripper [77]. The holding capabilities of suction cups considering axial forces have also been increased using a suction cup layer jamming gripper, increasing the normal pull of force by a factor of 5.8 [96].

b *Working in confined spaces*

Grippers sometimes are used in confined spaces when performing bin picking tasks, placing products into a box or when harvesting fruit and vegetables. In confined spaces a suction cup hybrid gripper is often used to make contact and hold the object at a fixed position in the confined space. The second part of the gripper then slowly closes around the pre-fixed object completing the grasp. This is a slow but reliable method for gripping for example fruits and vegetables when harvesting.

A gripper with the ability to grip any object, is created using hybrid combination. Using the suction cup to pick smooth objects or to reach into a confined space and using the other gripper to pick all other objects. This type of hybrid gripper excels at bin picking tasks [203]–[205].

c *Redesign for a compliant gripper*

Finally a trend can be seen where traditional rigid mechanical gripper typologies are converted into compliant grippers. By using lumped compliant joints to replace traditional pin joints. This is done to profit from the benefits of a compliant mechanisms. Such as low backlash, less parts and no joint wear. There exist several extensive and well decontamination methods for the design of compliant mechanism. These methods are also applicable for the designing grippers [206].

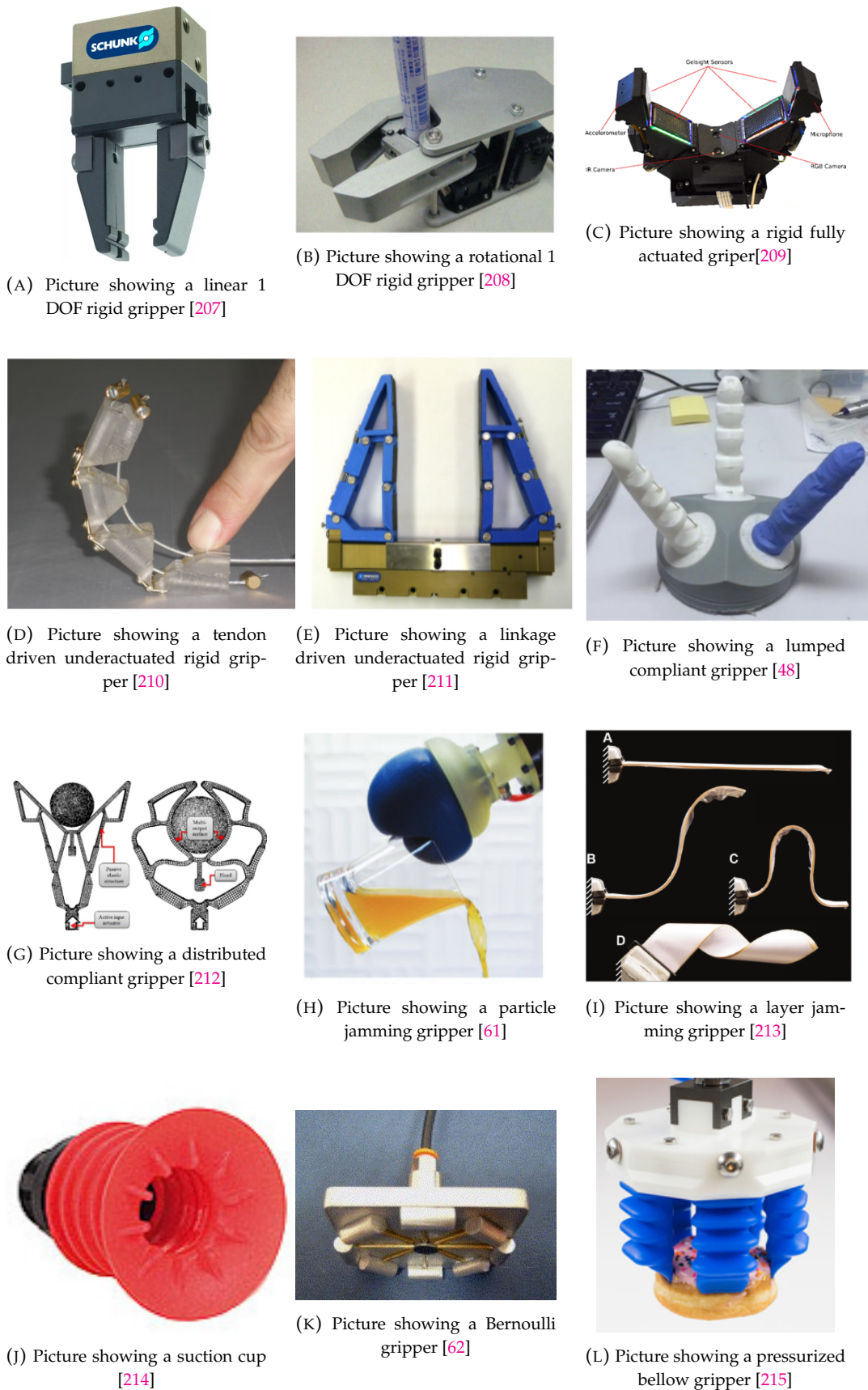
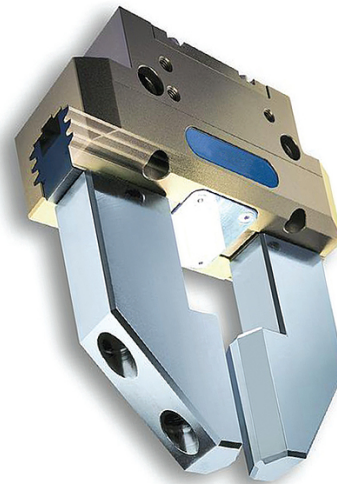


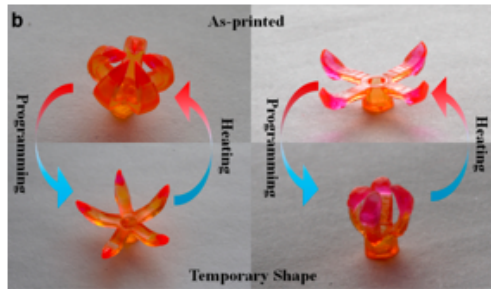
FIGURE B.2: Showing a picture overview of the gripper classification. Figure B.2a and B.2b show rigid 1 DOF grippers. Figure B.2c shows a rigid fully actuated gripper. Figure B.2d and B.2e show a rigid underactuated gripper. Figure B.2f and B.2g show compliant grippers. Figure B.2h through B.2l show pneumatic grippers



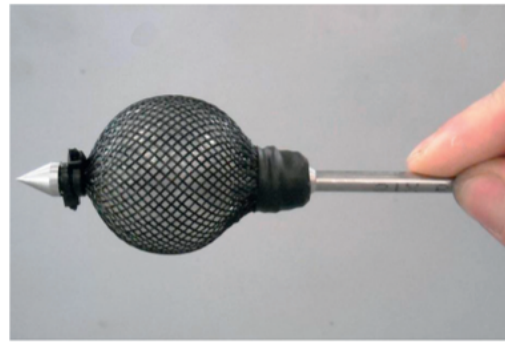
(A) an infeasible electro-magnetic gripper [70]



(B) an infeasible hydraulic gripper [73]



(C) an infeasible heat based SMA gripper [216]



(D) an infeasible piercing gripper [75]

FIGURE B.3: Showing some examples of grippers in the infeasible grippers class

5. Infeasible grippers

The literature available on gripping and end effectors is more extensive than the gripper classes shown previously. Other grippers that were deemed infeasible for high speed case packing are listed below and shown in figure 6.

- a Electro-magnetic grippers, the experience of BPA showed that adding a electrical wire to the fast moving end effector will lead to failure of the wire shielding due to wear. Grippers based on electro-magnetism, using operating principles such as electrostatic attraction, electro-conjugate fluid or ferrofluid grippers were not considered [68]–[70]. Grippers based on magnetism, for example using ferro fluid could strictly speaking be used without requiring electricity by only using permanent magnets. Controlling the gripper would become a cumbersome process resulting in a complex control system not desired for high speed case packing. For inspirational proposes grippers using electromotor as there actuator were still considered.

- b Heat based grippers, such as cryogenic gripper or shape memory alloy grippers have a to slow actuation and risk damaging the packaging. A actuation time of 5-6 seconds is to be expected for these grippers [71].
- c Grippers based on chemical or nano-scale adhesion were not considered because the adhesive material will transfer to the food product, this contamination is not allowed.
- d Hydraulics, grippers using fluid pressure instead of pressurized air were not considered [73], [74]. These type of grippers are more suited for high load, quasi-static operation.
- e Piercing grippers, grippers that pierce the object to grip the object have not been considered because they damage the product and foil [75].

Appendix C

Gripper Grading

In the appendix the grading scheme is elaborated in more detail. The reasoning and calculations performed are presented so future research can build upon the ideas presented here.

To answer the research question a grading of the different grading classes will be presented here. Important performance criteria noted in literature are: actuation speed, holding capabilities, mass, grasping range and product damage as important performance criteria for grippers [83].

Many gripper development and validation studies do not report on all performance criteria, potential due to focusing on gripper specific metrics rather than a standardised approach.

While searching literature for the required values to complete the grading. It was surprisingly noted that not all performance criteria are considered during design or even during validation of the gripper. This could be explained by the fact that dependent on the application some performance criteria are more important than others. Less important criteria are mentioned but not considered during design and often also not tested during the validation phase. This makes comparing a gripper presented in literature for a different gripper field challenging.

Ideally all grippers will be validated using the same or comparable performance metrics. Some steps towards generalizing performance metrics have already been taken [84]. However, this has currently not developed far enough to create a grading of the gripper classes based on the same or even similar performance metrics.

Therefore, the grading will require some approximations and engineering judgement. Where possible the grading will be based on data available in literature. Improvements for the grading will be discussed in section 1.5.

An asterisk is used to show the grading criteria which required the authors engineering's judgement or an approximation. Furthermore different pieces of literature have to be combined to create a full picture of the performance of a gripper class. Only literature presenting grippers deemed capable of handling a product of typical size for the packaged food industry were considered. This was done to try to eliminate the effects of scaling in gripper performance.

Appendix A.1 shows the data set that was made for the grading. For the gripper grading a four point, Harris profile like grading system is used [85], [86].

The gripper classes were graded based on a Harris profile rather than a quantitative point based grading. Since there is a lack of common metric to make a general quantitative comparison. This usually is a downside and introduces the authors bias and

judgement, in this case the authors judgement is required regardless of what grading scheme is picked.

The four points on the scale were graded divided as follows:

1. ++, Exceeds what is required for high-speed case packing considering packaged food
2. +, Meets what is required for high-speed case packing considering packaged food
3. -, Requires a slight improvement to meet what is required for high-speed case packing considering packaged food
4. --, Does not meet what is required for high-speed case packing considering packaged food

For any significant improvement of the current system, the amount of robots required to do a task should be reduced with at least one. The maximum P&P speed of one robot with an easy product is 120 PPM as shown in chapter 1. Achieving the same speed for most challenging products limited to 40 PPM due the end effector limitations, requires 3 robots. A significant improvement could be made if two robots operating at 60 PPM could be used to achieve the same result. This would require an increase of 20 PPM. This train of thought will be the leading consideration in the grading. In studying the state of the art it was also noted. Most case packing line also use three or more robots. BPA has vast order history on case packing lines build using Delta robots. This history was used to determine that three or more delta robots in a case packing line is a common sight. The proposed minimal amount of improved thus has practical relevance.

Grading criteria

A Actuation time (ms)

The actuation time of the gripper is graded as the sum of the opening and closing time of the gripper. Since the robot performance is known and will not be altered in this research, the actuation time determines theoretical the maximum P&P speed of the robot considering a perfectly connected load.

This definition was picked because firstly the the opening and closing time of a gripper does not have to be the same. Secondly during a P&P operation the gripper has to open and close once. This definition of actuation time (t_{act}) allows for the easy and intuitive definition of the cycle time of one P&P operation as the sum of the actuation time and the path time (t_{path}), as seen in equation C.1. The path time is the time the robot takes to move from a pick location to a place location and back to a pick location again. During the literature study it was noted that suction cups have the lowest actuation time of all gripper classes, see appendix A.1 for the used data. Changing to a different gripper class or designing a hybrid gripper will therefor always increase the actuation time. Here the question arises what is the maximum performance increase that can be achieved given a certain actuation time?

This can be determined by looking at the P&P speed presented in chapter 1. For the solid products the maximum P&P speed V_{picks} of 120 picks/min is achieved. This speed is know to be only limited by the robots performance and

not by detachment of the objects from the end effector. Equation C.2 shown how the cycle time can be determined from the P&P speed (v_{picks}). Combining equation C.1 and C.2 with the actuation time found for suction cups in literature 50 ms [176]. The path time at maximum operating speed can easily be determined Equation C.3 shows the final calculation to obtain the path time at maximum operating speed.

$$t_{cycle} = t_{act} + t_{path} \quad (C.1)$$

$$t_{cycle} = \frac{60}{v_{picks}} \quad (C.2)$$

$$t_{path} = t_{cycle} - t_{act} = \frac{60}{v_{picks}} - t_{act} \quad (C.3)$$

$$t_{path} = \left(\frac{60}{120} \cdot 10^3 - 50 \right) ms = 450ms$$

The final assumption that has to be made is that the considered gripper will fully eliminate the product detachment as the limitation. The robot will become the limiting factor as is also the case for the solid products. For this limiting case the path time is known to be 450ms as was calculated by equation C.3. Path time will be used during the determination of the grading intervals. Considering this assumption equation C.1 can be used to determine the allowable actuation time to achieve a certain P&P speed. For the grading 4 separate grading intervals have to be determined. The path time, C.3, is set constant according to the speed required to achieve 120 PPM, the actuation time has become the variable which determines the throughput in this calculation.

Firstly the most ideal gripper which is able to fully remove detachment limitation for more channeling products and shift the limitation back to the robot again. This would require an actuation speed currently found for suction cups of 50ms.

- 1) All grippers achieving an actuation speed of 50ms or faster will be graded ++. to achieve 60 PPM an actuation time of 550ms or lower is required according to equation C.1.
- 2) Gripper classes achieving an actuation time between 50ms and 550ms are graded + According to equation C.1 an actuation speed of 1050ms will have the robot operating at maximum operating speed yet no improvement in P&P speed will be made. 40 PPM was used as the current limiting P&P speed.

- 3) Gripper classes achieving an actuation time between 550ms and 1050ms are graded –
Gripper classes with a actuation time of larger than 1050ms can not achieve the current worse performance.
- 4) Gripper classes with an actuation time of larger than 1050ms will be graded – –

Searching literature the actuation speed for all gripper classes with the exception of Bernoulli grippers and distributed compliant grippers were found, this data is provided in appendix A.1. Bernoulli gripper under performed on the other grading criteria and is not considered a good solution for high-speed P&P in food. The actuation time of this gripper class was therefore not approximated. For the distributed compliant grippers some actuation times were found in literature but with such a large variation that they were deemed not usable. To still consider this gripper in grading its strain energy was considered for approximation of the operating speed. Strain energy is often used in typology optimization as a measure for stiffness [199], [200]. A stiffer compliant gripper considering the same actuator power will result in a slower gripper. Distributed compliant gripper have a higher strain energy than lumped compliant grippers and will be graded 25% slower.

This results in the following grading for the **actuation time**:

- **Rigid 1 DOF (+)**, From the data in appendix A it can be seen that in some cases the rigid 1 DOF grippers achieve a actuation time below 50ms. In reality these grippers are too small to be reliably used in the case packing industry. A actuation time of 200ms to 300ms is to be expected.
- **Rigid fully actuated (+)**, for this gripper class the action time has a large range and is often defined as the time it takes for the hand to fully open and fully close. This is often not required to pick an object. The object limits the required amount of motion. When considering the full extension of the hand this gripper class would be graded –. More reasonably, considering a limited required range of motion a gripping speed lower than 550ms is to be expected. Leading to a + grading.
- **Underactuated rigid (–)**, for this gripper class plenty of action speed data is available. In general a action speed of 700ms is expected. The fastest under actuated gripper found in literature however achieve around 50ms actuation time [168], [188]. This is not the expected speed and requires special spring loaded action.
- **Lumped Compliant (–)**, actuation speed measurements in this gripper class are limited. With the data available a grading of – – or + could be justifiable. The gripper scoring + used a special high power spring loaded action mechanism. The gripper graded – – fully disregarded the actuation speed during the design. This leads to a average grading of –. Considering the fact that compliant grippers have more stiffness than rigid grippers a slight slower actuation time is to be expected.
- **Distributed compliance (–)**, actuation speed measurements in this gripper class are unreliable or lacking in literature. Therefore the grading is determined 25% slower than lumped compliant grippers. This still resulted in a – grading.

- **Suction cups (++)**, this is the benchmark speed set to ++.
- **Structure Jamming (--)**, Structure jamming grippers with sufficient size achieve an actuation time of more than 1050ms. Smaller structure jamming grippers a significantly faster. This because the actuation time is depended on the volume which has to be vacuum sealed. Considering the design of a hybrid gripper this difference is notable. Structure jamming and stiffening effects should not be disregarded for hybrid gripper design.
- **Bernoulli (++)**, **Not data available**, but is near instant, when the air flow is established the lifting force is generated. The expectancy is that the actuation time is the same as that of suction cups
- **Pressurized bellows (-)**, A decent size pressurized bellow achieves an action speed of around 600ms

B Gripping range (mm)

The grasping range in this works is considered as the theoretical maximum object range that can be picked by the gripper. This is calculated as the difference of the maximum and minimum object size that can be picked.

In the packaged food industry it is common to pack multiple products using one case packing line. A gripper with a large gripping range could be used for multiple products not requiring to swap the end effector when picking a different product. This train of thought is in line with the view of a large gripping range that can be found in literature. However grippers only work well for one design point, products outside this design point will have a lower gripper performance.

This raises the question, what performance decrease is acceptable before swapping to a gripper specifically designed for the new products becomes more beneficial? Financial cost of making a new gripper could also be a reason to design one gripper for multiple object. Since the cost of a gripper is low compared to the cost of the rest of the case packing line this reason will not be coincided in this paper, the focus will be purely on performance.

Considering the time it takes to swap an end effector and the operating time of the next case packing operation, the allowable performance decrease can be estimated. This consideration concluded that for a typical use case a performance decrease of less than 0.1% is allowable before swapping to a new end effector will become more beneficial. Further details can be found in appendix ???. Contrary to many other fields of gripping, such as prostheses and bin picking grippers. Using the same gripper to pick multiple objects is not beneficial for the high speed case packing industry from a performance point of view and will not be used to determine the grading scheme.

Equation C.4 can be used to determine what performance decrease of the gripper performance is still allowed before swapping to a new gripper is more beneficial. When equation C.4 is true swapping to the new gripper will result in packing more products in the same time. Here it is assumed that the grippers specifically designed for the product have the same performance for their designed product.

$$P_{dec} > \left(1 - \frac{t_{run}}{t_{run} + t_{swap}}\right) \cdot 100 \quad (C.4)$$

Here:

P_{dec} = The relative throughput decrease
when not swapping to a new gripper (%)

t_{swap} = The time required to switch to a new
end effector (s)

t_{run} = The time the new product will be packed (s)

To minimize down time the switching of an end effector is currently done using a quick change mechanism. Using this system an end effector can be swapped in less than 30 *sec*. Assuming the new product will be packed for only half a day, 12 hours. At a P_{dec} of merely 0.07% swapping to a new end effector is already more beneficial. From this calculation it can be reasoned that a larger grasping range is often not beneficially for using one gripper for multiple products in the high-speed case packing for the packaged food industry.

Another benefit of a large gripping range is that possible errors in robot accuracy can be corrected for. The robots at BPA enter an error mode when the measured and expected position deviate more than 5*mm*. This value is used for grading the grippers. Positioning errors can be on both sides of the object. Thus a gripping range of 10*mm* is required to ensure any rigid object can be picked. All gripper classes are able to achieve a gripping range of 10*mm*. Therefor all gripper classes will be graded ++.

C Operating in a confined space * To achieve a faster P&P speed products are often not placed inside a box but dropped as the robot hovers above the box. This is only possible for impact resistant objects. Not all packaged food products are impact resistant, some packaged food products will break or crack when dropped. These products need to be carefully placed inside the box instead. This in turn means the end effector has to be able to operate in the confined space of a box.

All grasp type grippers are assumed to use an enveloping grasp during the holding phase. A pinch type grasp does not give the required holding force during the holding phase. In the grasp phase a pinch grasp is allowed since the forces are significantly lower compared to the holding phase. This reasoning results in the following grading. A gripper class not able to reconfigure from an enveloping grasp type to a pinch grasp will be graded --. A gripper class able to reconfigure form an enveloping grasp to a pinch type grasp will be graded -. A gripper class using the top edges to grip a product and having no parts located outside of the gripper surface will be graded +. A gripper class which does not have any parts located outside of product surface will be graded ++.

This results in the following grading

- **Rigid 1 DOF** (--), this gripper is a grasp type gripper without the ability to reconfigure its grasp, resulting in a -- grading
- **Fully actuated rigid** (-), this gripper is a grasp type gripper. Due to the control of all DOF it gains the ability to reconfigure its grasp to a pinch grasp, resulting in a - grading

- **underactuated rigid** (–), this is a grasp type gripper. Literature has shown that reconfiguring its grasp type to a pinch type grasp is possible [24], [43]
- **Lumped Compliant** (–), since the underactuated rigid gripper class can be converted to a lumped compliant gripper this gripper class will also be able to reconfigure its grasp type.
- **Distributed compliance** (– –), this gripper class is a grasp type and has not shown the ability to reconfigure from an enveloping grasp to a pinch grasp.
- **Suction cups** (++), this gripper only uses the top surface of the product
- **Structure Jamming** (+), this gripper class uses the top edge to grip a product, it could use more but at least the top edge is required.
- **Bernoulli** (++), only top surface is used by this gripper. More correct this gripper does not even make contact with the gripper product.
- **Pressurized bellows** (– –), this gripper grips around the product without the ability to reconfigure its grasp type reliably.

D Holding Force (N)

When the the maximum acceleration and product mass are known the maximum holding force can be determined. An object with a mass of 600g was found to be the heaviest object still handled at high-speed by case packing robot. Including the mass of a standard the P&P tool this results in a mass of 1.050kg. At this load the robot is able moving at peak accelerations of $120 \frac{m}{s^2}$. For the calculations of holding force newtons second law of motion is used, shown in equation C.5.

$$F = m \cdot a \quad (C.5)$$

here:

- F = The force required to accelerate the rigid object in N
- m = The mass of the accelerating object in kg
- a = The acceleration of the object in m/s^2

To achieve the maximum robot acceleration of $120 \frac{m}{s^2}$ with a object mass of 0.6kg a force of 72N is required according to equation C.5. This pull out force will shift the limiting factor for this grading criteria for the end effector back to the robot again.

For the next grading interval the minimal holding force to achieve 60 PPM has to be determined, this will be done according to equation C.5. To use equation C.5 the maximum acceleration of the path achieving 60 PPM has to be determined. This was done by modeling the path, in this model the control was assumed to be jerk and acceleration limited. The path is also assumed to be have rounded corners. Figure C.1 gives a visual overview of the acceleration profile.

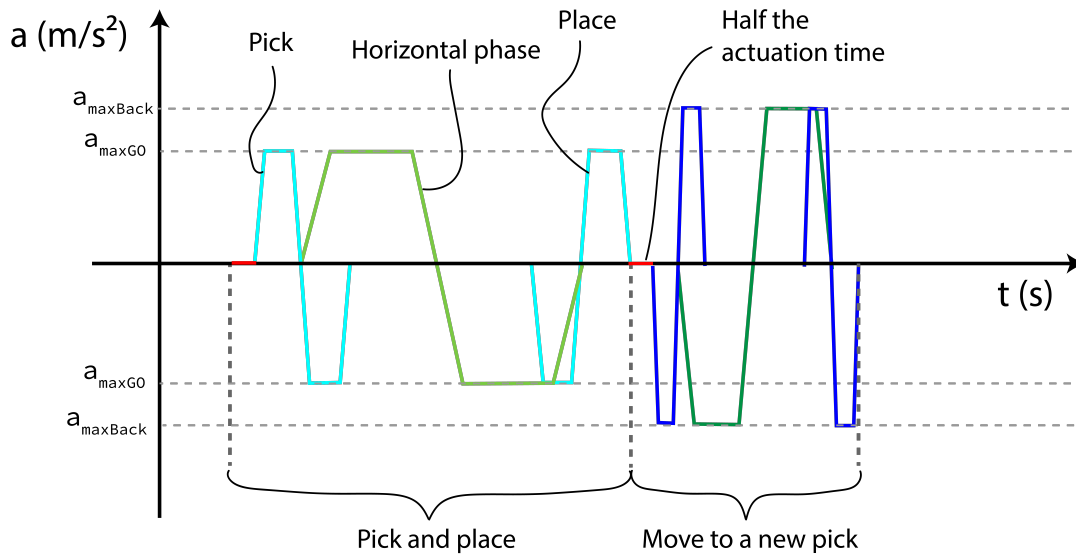


FIGURE C.1: An overview of the acceleration path for a full P&P cycle

In practice there are two ideas for setting the return acceleration. The first idea sets the acceleration equal to the maximum robot acceleration. This maximizes throughput, however the wear of the robot will increase and more expensive components are required. The second idea is to set it equal to the acceleration limit of the pick and place motion. The robot will move with the same limits with and without product. In practise a middle ground between the two ideas is often picked.

For the calculations, the maximum acceleration in the case pack step is set equal to the maximum acceleration in the return trip. This will lead to an overestimating of the peak acceleration. Overestimating the peak acceleration will ensure the grading is on the safe side.

Finally it is assumed that every increase or decrease in acceleration will be performed in 5% of the total path time. This assumption enforces that 80% of each motion step will be spend with a constant acceleration. This method was picked over considering maximum jerk for each motion path because in practice challenging products need to be placed with limited jerk. Although this does not directly follow from the model, since jerk limited control is used to combat vibrations. It is implemented in this manor to stay closer to reality.

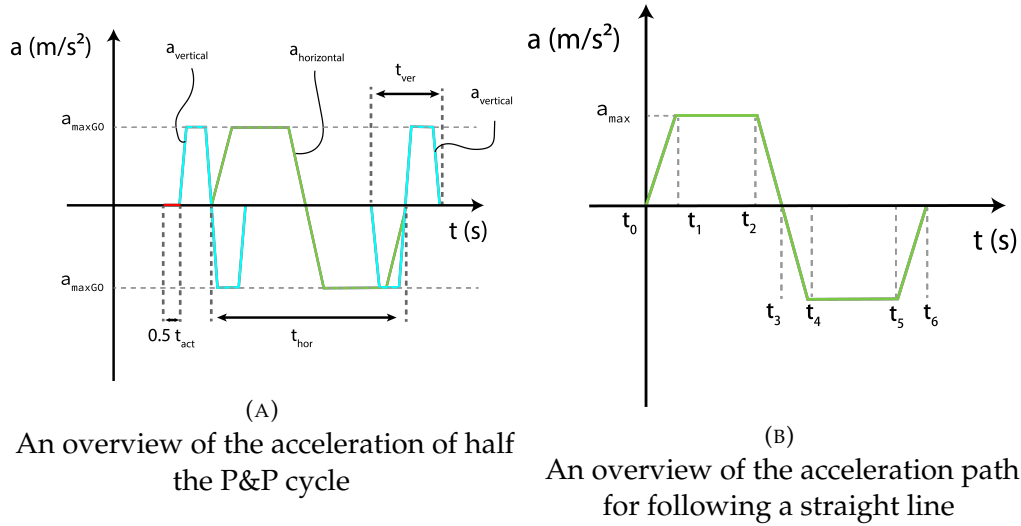


FIGURE C.2: Overview of acceleration paths used in the modeling of the robot motion

Equation C.7 through C.11 give a mathematical description of the acceleration path. The time used stamps refer to the time stamps in figure C.2b. The aim of this model is to find the required maximum acceleration for any desired P&P speed. Therefore the input of the model should be desired P&P speed, giving the output required maximum acceleration.

$$a_1(t) = J \cdot t \quad t_0 < t < t_1 \quad (C.6)$$

$$a_2(t) = a_{max} \quad t_1 < t < t_2 \quad (C.7)$$

$$a_3(t) = a_{max} - J \cdot (t - t_3) \quad t_2 < t < t_3 \quad (C.8)$$

$$a_3(t) = a_{max} - J \cdot (t - t_3) \quad t_3 < t < t_4 \quad (C.9)$$

$$a_5(t) = -a_{max} \quad t_4 < t < t_5 \quad (C.10)$$

$$a_6(t) = J \cdot (t - t_5) - a_{max} \quad t_5 < t < t_6 \quad (C.11)$$

The complete P&P motion consist of 6 similarly shaped acceleration profiles. Firstly a product is lifted vertical to clear other products on the conniver belt, secondly the product is moved horizontally to a place location, finally the product is moved down vertically to place the product. These three steps are repeated to move the end effector to a new pick location.

Since rounded corners are assumed the complete time of a pick motion can be determined by a simple addition the time of the horizontal motion and one vertical motion. See subsection A for the definition of path time. Figure C.2b shows the acceleration profile of one of the sub steps. Integrating this graph once will result in the velocity profile during the motion step. Integrating the velocity profile will result in the distance traveled as a function of time. These steps are shown in equations C.13 and ?. The constants of integration can be determined by considering the next sub step has to start where the previous sup step ended, mathematically shown in equation C.14 and C.15.

$$v_i(t) = \int_{t_{i-1}}^{t_i} a_i dt + C_{v_i} \quad (C.12)$$

$$s_i(t) = \int_{t_{i-1}}^{t_i} v_i dt + C_{s_i} \quad (C.13)$$

$$C_{v_i} = v_{i-1}(t_{i-1}) \quad C_{v_0} = v(t_0) \quad (C.14)$$

$$C_{s_i} = s_{i-1}(t_{i-1}) \quad C_{s_0} = s(t_0) \quad (C.15)$$

Following the presented acceleration profile the jerk can be determined based on the maximum acceleration and the time of the segment of the path. This is shown in equation C.16 and the result of this model is shown in figure C.2.

$$J = \frac{a_{max}}{t_6 \cdot 0.05} \quad (C.16)$$

Now the jerk limit is known the total time of the path can be calculated as the sum of the actuation time t_{act} , the time spend in horizontal motion (t_{hor}) and the time spend in vertical motion t_{ver} . The vertical motion consists of two identical paths to P&P the product respectively. To calculate t_{hor} and t_{ver} it is assumed that the maximum acceleration for horizontal and vertical direction is set equal.

The calculation of path time has to be preformed twice, once for path taken to P&P an object ($t_{path,Place}$) and again for the path taken to return to a new pick location ($t_{path,Return}$). In this model these paths are assumed to be identical in shape. In reality the distance traveled will slightly differ based of the location of the object on the conniver belt. Nonetheless, taking the average path length will give a good estimation. When the robot moves from a place location to a new pick location there is no product attached to the end effector. The described steps are shown in equations C.17, C.18 and C.19.

$$t_{path,Place} = t_{hor,Go} + t_{ver,Go} \quad (C.17)$$

$$t_{path,Return} = t_{path,Place} \cdot t_{ver,Return} \quad (C.18)$$

$$t_{path} = t_{path,Place} + t_{path,Return} \quad (C.19)$$

By picking a similar path as used in practical application and setting the desired PPM the distance traveled and available time to move trough the path are known. Now t_{hor} and t_{ver} are expressed as a function of only a_{max} . Solving equation C.19 will yield a_{max} . The path time t_{path} is determined using equation C.3. Because the full motion cycle is twitch the considered path only half this time is taken.

The actuation time of the end effector should be taken into account when determining the path time for the desired P&P speed as shown in equation C.2. In case of suction cups the actuation time is $50ms$ according to the literature presented in appendix A.1. In the calculations the path was considered to be $75mm$ in vertical direction and $700mm$ in horizontal direction. The height of the path is the height without the curvature.

' The validity of the model was checked by calculating the required acceleration for a pick and place speed for a known situation. This situation is the maximum operating speed of $120m/s^2$ for which 120 PPM are achieved. Plugging 120 PPM into the model a required acceleration of $131.5m/s^2$ is determined. As expected the required acceleration is slightly overestimated. C.5 the minimum pull out force was determined.

- 1) Grippers with a pull out force of $72N$ or higher will be graded ++. These grippers are in theory able to withstand $120m/s^2$ of acceleration
Determining the maximum acceleration for a desired P&P speed of 60 PPM. The required maximum acceleration is calculated to be $30m/s^2$. Following equation C.5 a
- 2) Grippers with a pull out force lower than $72N$ and higher than $18N$ graded +
The current maximum P&P speed for the most challenging products was determined to be 40 PPM. The pull out force required to achieve this acceleration was set as the grading bound for the following grading interval. Grippers achieving this pull out force would not currently not be able to improve the performance. Further research would be required to gain an improvement. According to the model an acceleration of $13 m/s^2$ is already sufficient to achieve 40 PPM
- 3) Grippers with a pullout force lower than $18N$ with higher than $8N$ are graded –
Lastly grippers with a pull out force lower than $8N$ will achieve a P&P speed lower than the current lower bound. These gripper do not meet what is required for high-speed case packing for the packaged food industry.
- 4) Grippers with a pullout force lower than $8N$ are graded –

All gripper classes were graded according to literature, for which a summary can be found in A.1. The pull out force in the weakest direction of the gripper was used to grade this criteria.

This results in the following **Holding capabilities for forces**

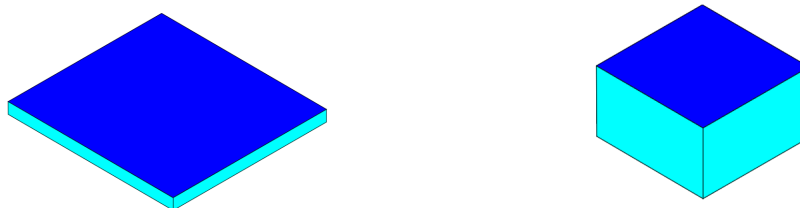
- **Rigid 1 DOF (++)**
- **Rigid fully actuated (++)**, Weaker grippers exist but $72N$ should be obtainable with ease.
- **underactuated rigid (+)**
- **Lumped Compliant (+)**
- **Distributed compliance (+)**
- **Suction cups (++)**, if there is sufficient surface area otherwise +
- **Structure Jamming (+)**
- **Bernoulli (--)**
- **Pressurized bellows (-)**

E Holding capabilities: moment*

In the dynamic load case found in high-speed case packing the moment a gripper can withstand around any axis becomes of importance. First of all objects have to be rotated 180° during the pick and place motion, which requires considerable angular acceleration. Further more if there is any eccentricity between the objects center of mass and the center of the gripping location a purely translational acceleration will also include a moment. If the maximum holding moment of a gripper is exceeded the gripped product breaks free from the grasp. The moments a gripper can hold are not well documented in literature. For suction cups, models considering the moments leading to failure were found [217]. The validation of these models however only considered one moment, namely the moment perpendicular to the gripping plane [104]. For all other gripper classes no measurements were found for the holding capabilities for moments. When considering the use case and working principles of the gripper classes. It can be explained why the holding capabilities of moments are often not considered.

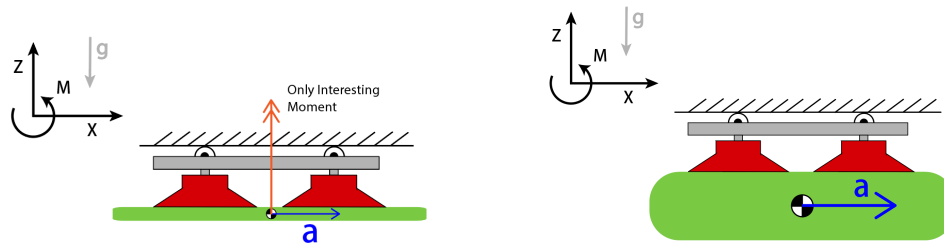
Suction cups are traditionally used for the handling of thin sheet material such as glass, sheet metal or cardboard [218]. A schematic overview of a typical P&P product is shown in figure C.3a. In the case packing for the packaged food industry thin sheets are rarely encountered. Objects displaced in this industry are generally much higher as shown in figure C.3b. This leads to two major performance decreasing aspects compared to moving thin sheet material.

Firstly the surface area to volume ratio is much lower. Figure C.3 shows this difference graphically. Considering weight scale according to volume and for suction cups generated force scales according to surface area. Also following Newton's second law the force required to accelerate an object scales linearly with mass. Therefore the ratio of surface area to volume is a measure for generated force compared to required force. For the same material and volume a sheet like material is able to generate more force than an object found in food industry. Whilst the same force is required to accelerate the object.



(A) schematic overview of a traditional sheet like object (B) schematic overview of an easy object in the case packing industry

FIGURE C.3: Schematic overview different objects in P&P



(A) Overview of studied acceleration for a thin sheet (B) Overview of studied acceleration for a object of P&P

FIGURE C.4: Overview of horizontal accelerating objects

Secondly a thin object has its center of mass close to the suction cup gripping plane as illustrated in figure C.4a. Studying the force required to accelerate a thin object the moment required to ensure no angular acceleration is negligible. Only the moment perpendicular to the suction cup grasp plain are of interested in this case. This is also the only moment studied in [102], [103], [217], and is illustrated in figure C.4a by an orange arrow. Object displaces in the the high-speed case packing for the packaged food industry have a much lager height, as shown in figure C.4b. This height adds a required holding moment to ensure no angular acceleration of the object. This addition to the load case becomes more significant for higher accelerations. Figure C.5 and C.6 show the free body diagrams of the a thin sheet and packaged food object respectively. considering an pure horizontal (in the x y plane) acceleration. Adding an additional acceleration in vertical (z) direction will introduce an extra force required for this acceleration reducing the holding capabilities even further.

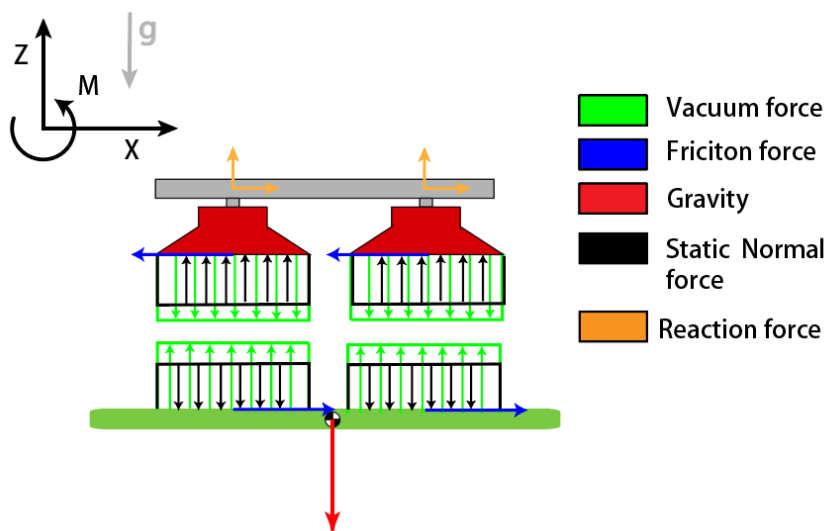


FIGURE C.5: Force analysis of the studied horizontal acceleration considering a sheet like object

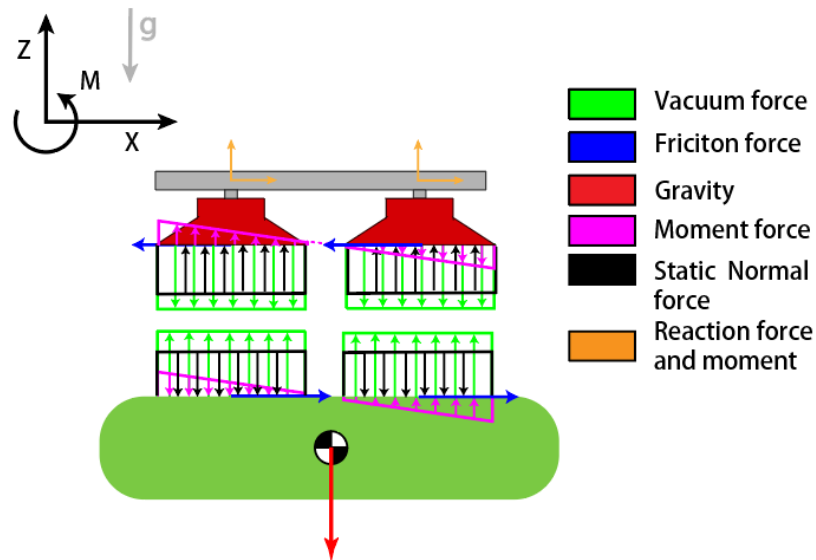


FIGURE C.6: Force analysis of the studied horizontal acceleration considering a packaged food object

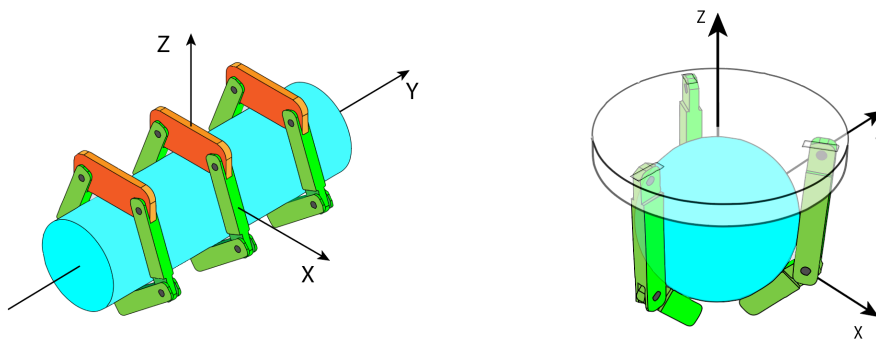
For any load case on suction cups there are two main and theoretical simple failure modes. The first failure mode is the sliding of a product with respect to the suction cups. This failure mode occurs when the friction required to accelerate the object is insufficient. This failure mode is seen for sheet like objects. The second failure mode is the angular acceleration of the object. This occurs when the moment required to ensure no-angular acceleration can not be exerted by the suction cups. This is the expected failure mode for products with a larger height. Other failure modes such as damaging the product, buckling of the suction cups or plastic deforming the foil will not be considered and are assumed to be met *a priori* in this analysis. For typical objects in the food industry the second failure mechanism is far more prominent. Therefore measurements considering the maximum moment a suction cup can withstand is of interest in this field. Yet these measurements have not been documented in literature. A theoretical analysis can be made identifying when which failure mode is expected.

For finger based grippers no moments are measured typically, this can also be explained when looking at their working principle. Finger based gripper typically only grip objects from two sides and are often designed in a 2D plane. Figure C.7a shows the schematic overview of a finger based gripper holding a cylindrical object. The 3D implementation of such a gripper requires stacking multiple planes of the 2D designed gripper, this is shown in figure C.7a. Imagine a moment was acting about the y axis in figure C.7a, the failure mode would be slipping of the object inside the fingers of the gripper. Noting finger based grippers are often designed to grip a cylinder. Slipping inside the grasp of the gripper does not change the gripper's configuration at all. This failure mode is thus not of interest for researchers in the field of finger based grippers.

Now imagine a moment acting about the x axis in figure C.7a, a moment acting in this direction will be countered by forces acting in the z direction. The maximum value of this force is often measured as the pull out force in z direction. Since pull out force is graded separately the moment about the x will not be

considered during the grading. Also studying this moment will in theory not lead to any new interesting information. Moreover placing the 2d finger gripper planes further apart will also increase the capabilities to hold a moment about the x axis.

Finally imagine a moment around the Z axis, the moment direction of interest for suction cups. A moment around this axis will lead to deformation of the fingers. Testing this load case could lead to damaging or breaking a gripper. In a research setting, where only one gripper is available, this is an undesirable outcome. This moment could lead to failure and is not graded simultaneously at another grading criteria. This moment will be the focus



(A) A schematic overview of a finger based gripper designed in a 2D plane

(B) A schematic overview of a typical finger based gripper designed in 3D

Not all finger based grippers are designed in a 2D plane. For the gripper designed in 3D space the common trend is to design the gripper such that 3 fingers are spaced out at 120 degrees apart around a sphere. Figure C.7b schematically shows a gripper from such a design. These gripper are often design to grasp a sphere instead of a cylinder. For this gripper design a moment around any axis will lead to slipping inside the fingers. Assuming a non-spherical object plastic deformation would be required to break an object free for a moment around any action.

To still allow for grading of this important grading criteria an approximation based on the authors judgement has to be made. Firstly it is reasoned that finger based type gripper are more suited to withstand moments. This is because this type of gripper envelops the object. Either plastic deformation or elastic deformation is required to detach an object from the gripper in this case. Considering plastic deformation requires more force than elastic deformation. This distinction results in the two first two grading intervals.

- 1) Graps type grippers requiring plastic material deformation before leading to holding failure due to an exerted moment were grade ++.
- 2) Grasp type Grippers requiring elastic deformation before leading to holding failure a product were graded +.

Part of the desirable performance of enveloping grippers for holding moment can be explained by the fact that they do not require friction force to hold the object. This observation leads to the next grading interval,

which is valid for any gripper class. If a certain enveloping gripper class requires friction force to work it will be graded according to this interval

- 3) Grippers capable of an holding exerted moments requiring friction forces were graded $-$.
Final gripper classes not able to withstand any moment at all were graded lowest.
- 4) Grippers not capable of holding an exerted moment were graded $--$.

This resulted in the following grading:

- **Rigid 1 DOF (++)**, this gripper class could be made to envelop the object with rigid beaks. To break an object free from this grasp plastic deformation is required.
- **Rigid fully actuated (++)**, this gripper class can envelope a grasped object and requires plastic deformation to break an object free from a grasp considering a moment loading.
- **Underactuated Rigid (++)**, this gripper class can envelope a grasped object and requires plastic deformation to break an object free from a grasp considering a moment loading.
- **Lumped Compliant(++)**, this gripper class can envelope a grasped object and requires plastic deformation to break an object free from a grasp considering a moment loading. For some grippers in the class elastic deformation might already lead to loss of the object. Yet since most grippers are expected to require plastic deformation it is graded according to that result.
- **Distributed compliance (++)**, this gripper class can envelope a grasped object and requires plastic deformation to break an object free from a grasp considering a moment loading.
- **Suction cups(-)**, this working of this gripper class is explained to require friction force as shown in figure C.5 and C.6.
- **Structure Jamming(-)**, this gripper class can either work enveloping or based on friction. To pick up object used in the packed food industry the friction based grasp is required.
- **Bernoulli (--)**, this gripper can not withstand moment, if an object tilt ever so slightly due to acceleration of the object the air flow gets interrupted losing the object. This gripper class typical is also exclusively used to handle thin objects [63]. a special gripper geometry has to be designed to grip non flat object [59].
- **Pressurized bellows(-)**, grippers in this class consist of very flexible bellows. Under a moment loading a gripped object will be lost by elastic deformation.

F Gripper mass

The gripper mass is defined as the mass of the gripper measured in kg , measured under standard condition. The gripper mass is a important measure for

the dynamic response of the system. Further, the mass of the gripper will determine what object mass can still be packed at maximum operating speed. The three actuators form the delta robot have to provide the power required to accelerate the gripper and the object. The mass of the gripper will determine what object mass can still be packed at maximum operating speed. The mass is a very important property considering dynamic behavior of a system. Nevertheless even something as simple as the mass of a gripper is not always presented in literature. In other cases a robot platform is included in the presented mass. This makes a gripper seem significantly heavier than it is in reality. To correct for this difference the mass of the current robot platform at BPA is added to any gripper measured not including its robot platform. The mass attached to the robot platform gives a limitation on the maximum accelerations the robot can still achieve.

Following a similar reasoning as in section A. Gripper mass is used as a grading metric for this grading criteria. The author also considered using a dimensionless grading criteria applicable to any gripper class. Equation C.20 shows this grading metric, where $m_{gripper}$ is the mass of the gripper and $m_{payload}$ is the mass of the payload.

$$\lambda_{mass} = \frac{m_{gripper}}{m_{payload}} \quad (C.20)$$

This metric was not picked because the apparent payload changes under dynamic condition. Further more including a load in the grading of the gripper mass would lead to a double grading of the holding capabilities

- A gripper class with an average mass of $0.6kg$ or lower, still allowing for maximum robot speed will be graded ++.
- A gripper mass between $0.6kg$ and $1.5kg$ able to achieve 60 PPM will be graded +.
- A gripper class with a mass between $1.5kg$ and $2.0kg$, able to achieve the current limiting acceleration of $40m/s^2$ will be graded –.
- A gripper class heavier than $2.0kg$ will be graded ––.

For this grading criteria sufficient literature was found which was used for the grading. A summary of the literature used for grading is given in appendix A.1.

- **Rigid 1 DOF (+)**, all considered gripper fall in the + grading range
- **Fully actuated rigid (–)**, some lighter grippers have been found. These gripper used external actuators not included in the mass. This is not possible for case packing.
- **underactuated rigid (+)**
- **Lumped Compliant (++)**, Compliant grippers are often made of lighter compliant materials

- **Distributed compliance (+)**, Distributed compliant gripper often need more material to function properly.
- **Suction cups (++)**
- **Structure Jamming (+)**
- **Bernoulli (++)**
- **Pressurized bellows (++)**

G Contact pressure

The contact pressure would be an ideal measure for estimating product damage and is also used in other fields to estimate wear or failure [88], [89]. The maximum contact pressure of a gripper is of interest when handling fragile products. However measurements of contact pressure were only available for some gripper classes. The available data in literature was not sufficient to make a grading based on literature. Similarly to point E the authors judgements is required to give a fair grading.

It was decide grade according to the contact type. Distinguishing four contact types: A contact with three or less contact points, multiple point contacts, a contact line or a contact surface. The size of the force required to hold an object is assumed to be similar for all gripper, the amount of contact points or area is in that case a measure for the contact pressure.

The larger the contact area the lower the chance of damaging the product. Grippers with a higher contact surface will be graded better. For this grading the object to be picked is considered to be a rigid beam, resulting in the grading. Contact surface is graded ++. Line contact is graded +, a contact consisting of multiple point is graded -, A contact with only three or less contact points --.

- **Rigid 1 DOF (--)**, two contact points of a hard object
- **Fully actuated rigid (-)**, multiple contact points on different phalanges
- **Underactuated rigid (-)**, multiple contact points on different phalanges
- **Lumped Compliant (-)**, multiple contact points on different phalanges
- **Distributed compliance (+)**, a contact line due to the a fully deformable structure is expected. An example would be gripper using the finray effect [219]. Could also achieve a surface contact in specific cases.
- **Suction cups (++)**, a contact surface
- **Structure Jamming (++)**, a contact surface
- **Bernoulli (++)**, a contact surface
- **Pressurized bellows (++)**, a contact surface due to softness of the bellows.

H Life time

An good measure for the life time of a gripper the is the amount of operational hours 99% of the grippers are expected to achieve. If a gripper breaks during operation the case packing line has to be stopped to replace the end effector.

As the case packing procedure stops a part of the food processing step also needs to be halted. The production process of the food to be packed can not simply be halted without consequence however. For example cookies that are baked in an industrial setting have to be removed from the oven at a specific time. If the processing step is halted for only a few minutes these cookies will burn and have to be discarded.

A solution for this problem such as replacing the end effector primitively or a regular maintenance interval will also increase the cost. Life time could be considered as part of a financial cost. In this study it is however viewed separately because the costs are indirect instead of direct and more factors such as customer satisfaction play a role as well.

For too many gripper classes the lifetime is unknown, this makes grading this criteria based on literature impossible. More research considering lifetime has to be performed before a good grading can be made for this grading criteria. This testing is time consuming and often out of the scope of a research paper. The grading of life time will be completely done based on the authors' engineering judgment.

- **Rigid 1 DOF (++)**, known for a long life time
- **Fully actuated rigid (--)**, many actuators and sensors resulting in a larger chance of failure.
- **Underactuated rigid (+)**, industrial applicable grippers exist, yet not particularly known for high life time.
- **Lumped Compliant (-)**, life time is mentioned as a large challenge in literature [48].
- **Distributed compliance (+)**, Distributed compliant grippers are expected to achieve a better life time. This is because the same amount of deformation is caused by a larger part of the structure. Resulting in lower stress in the material.
- **Suction cups (-)**, life time a main design challenge for BPA.
- **Structure Jamming (-)**, Wear of the deformable required enclosure is not well known. It is a material similar to that of suction cups. Thus the same grading is given.
- **Bernoulli (+)**, industrial applicable grippers exist, yet not particularly known for high life time.
- **Pressurized bellows (+)**, life time data available from soft robotics. Design to withstand normal industrial loading conditions

I Financial cost*

The financial cost of a gripper is defined as the financial investment that has to be made to obtain a certain gripper. The financial cost is firstly interesting from a business point of view. A cheaper gripper with the same performance will result in higher profits. Moreover considering replacing human case packing lines the cost of the robotic case packing line and its end effector become important. If a robotic line would be more expensive than a human operated line for the same performance. Investing in a robotic line would not be beneficial. In such a cost estimation many factors play a role, too many factors to consider

in this grading. In literature the cost per pick has been used as a grading criteria for financial cost. This however considers lifetime or operating time as part of the consideration of cost. In this grading scheme life time is considered separately. Including it here would result in a double grading of the grading criteria life time. Therefore the financial cost in euros of a gripper class is considered a good grading metric.

Data on financial cost is sometimes accessible for commercially available grippers. For state of the art robotic grippers as found in literature it is however not available. Research is generally not concerned about the financial cost of a gripper. The lack of data for certain gripper classes makes this a challenging criteria to grade.

Furthermore determining a grading interval is also not trivial here. Since the gripper is an integral part of the robot's performance, a grading based on a certain percentage of robot cost was deemed best. However robot manufacturers do not provide the price of a robot general publicly, a price arrangement is a confidential agreement between a company and its customer. The same goes for certain gripper manufacturers. Similarly to the moment holding capabilities the of financial cost will be grading using 4 grading questions, because insufficient literature is available.

Grippers widely available on the market. Having a large catalog with different tested models are graded ++. Grippers used by industry and available from some vendors are graded +. Grippers available at some vendors, yet still requiring improvement for wide spread application are graded -. Grippers not available on the market or explicitly known for their high cost are graded --. This cost estimation is based on the idea that proven and mass produced grippers are generally cheaper than less developed or even state-of-the-art grippers.

- **Rigid 1 DOF (++)**, this gripper class is commonly used by industry, and is available from many vendors such as FESTO and SCHUNK to name a few. Having large catalogs of tested grippers.
- **Fully actuated rigid (--)**, this gripper is known for its high cost because of the requirement of many actuators and sensors.
- **underactuated rigid (+)**, some underactuated grippers are available on the market which achieve acceptable performance. Nonetheless these are also still part of active research.
- **Lumped Compliant (--)**, no industrial applicable lumped compliant grippers are available on the market. Literature states there are still remaining issues such as control, service life and grasping efficiently that have to be solved for wider application [48].
- **Distributed compliance (--)**, Distributed compliant grippers have seen less research effort than lumped compliant grippers leading to the same and lowest grading.
- **Suction cups (++)**, this gripper class is commonly used by industry, and is available from many vendors such as FESTO, Piab, SCHUNK or Coval to name a few. Having large catalogs of tested suction cups.

- **Structure Jamming (+)**, some grippers are available on the market which work as expected and are well validated [179].
- **Bernoulli (-)**, this gripper class is available on the market, however there usage is limited and active research is still required for broader implementation.
- **Pressurized bellows (++)**, for this gripper class the same reasoning as the underactuated grippers holds.

J Control complexity*

When building a case packing line every extra control variable will lead to a more complex and error sensitive fine-tuning and adjustment step. The adjustment and fine-tuning of variables is required to get optimal performance for the specific food product. Less control variables of a boolean data type are desired.

A gripper class using a specialized control loop requiring non boolean control signals and sensors is the most undesirable. In this case the robot control and gripper control have to be properly synchronised to work correctly, this will add a new level of complexity to an already tedious fine tune process. Therefore a grippers class using a specialized control loop requiring non boolean control signals and sensors will be graded --. A slightly less complex scenario is a gripper class requiring a specialized control loop yet only using boolean control and sensor signals, these gripper classes will be graded -. Even simpler is a gripper class not requiring any sensors to function. Thus a gripper class requiring multiple control inputs and no sensors will be graded +. Finally a gripper class requiring one boolean control input and no sensors will be graded ++.

- **Rigid 1 DOF (++)**, this gripper class is known for its easy on-off control.
- **Fully actuated rigid (--)**, this gripper is known for its complex control and the requirement of sensory feedback.
- **underactuated rigid (++)**, this gripper is often actuated with one degree of freedom. This could be a simple on off control, leading to a ++ grading.
- **Lumped Compliant (++)**, the same reasoning as for the underactuated rigid grippers hold here.
- **Distributed compliance (++)**, the same reasoning as for the underactuated rigid grippers hold here.
- **Suction cups (++)**, this gripper class is known for its easy on-off control.
- **Structure Jamming (+)**, this gripper requires pre-shaping before actuation of the vacuum system. This could for example be done by having the robot press into the product. This has to be tuned to the right amount therefore this is viewed as an extra control variable
- **Bernoulli (++)**, this gripper induces a force by airflow around a product. This airflow just has to be turned on and off.
- **Pressurized bellows (++)**, the pressurized bellows can be used using simple on of control. Other more complex pressure gradient control schemes could also be used however are not required.

C.0.1 Weight factors

Before finalizing the grading it is important to determine the importance of each grading criteria. This will be done by introducing weight factors. To ensure all grading results will yield a positive value the 4 point grading scheme is ranged from 0 to 3. By using normalized weight factors the score ranges from 0 to 3, low to high respectively.

No literature on grading criteria and weight factors for high-speed case packing is available. Therefore a set of grading factors will be proposed in this appendix. The well known Analytical Hierarchy Process (AHP) was used to determine the weight factors [90]. The AHP method was picked because of its . This method has also re-sevide some citrique in literature which has also been disputed by others [91], [100]. No grading method is perfect but this method was picked because it gave a simple, justifiable, appropriate and efficient grading method [91]. When considering the opinion of mutiple people also mechanics with a lot of hands on experience but limited academic education these points are of importance.

The limited academic education of some hands on experts in this field was also the reason to consolidate holding moment and holding forces into one grading criteria during the AHP method. A clear understanding of the moment around the Cartesian reference frame was limited, both force holding and moment holding were viewed being identical.

The weight factors presented here are set up in correspondence with engineers working in the high-speed case packing industry. The average grading is presented in Figure C.10, the overall consciences was calculated to be 75%. There individual response is shown in table C.2 trough C.8.

For the AHP method all criteria are compared pairwise. Firstly it is determined which of the two criteria is more important. Secondly the amount of difference in importance is set using a number ranging form 1 to 9. The meaning of the grading intervals is shown in table C.1.

Intensity	Definition	Explanation
1	Equal impotence	Two elements contribute equally to the objective
3	Equal impotence	Experience and judgment slightly favor one element over another
5	Strong Impotence	Experience and judgment strongly favor one element over another
7	Very strong impotence	One element is favored very strongly over another, it dominance is demonstrated in practice
9	Extreme impotence	The evidence favoring one element over another is of the highest possible order of affirmation

TABLE C.1: The grading scores and the meaning used in the AHP method. A score could also be in between two grading scores

After answering the grading question the grading criteria and consistency the the answers can be calculated [220]. When the answers are not consistent this is an indication that insufficient thought was been put into the grading. A inconsistency of 10% is generally viewed as acceptable [90]. To help review the consistency, other answer review metrics and to combine the different grading answers the excel sheet presented by K. Goepel was used [220].

When the answers are sufficiently consistent the grading criteria are calculate in the excel sheet. This can also be done manually the math used to calculate the grading criteria and constituency index is well documented in literature [90], [220]. The grading results form the engineers in the field of high-speed cases packing is presented in the grading matrix form and shown in table C.2 trough C.8. The average grading is shown in table C.9

Matrix Author	Actuation time	Grasping range	Confined space	Load holding	Gripper mass	Contact pressure	Life time	Financial cost	Control complexity	
	1	2	3	4	5	6	7	8	9	
Actuation time	1	1	6	2	2/3	2	3	2	6	4
Grasping range	2	1/6	1	1/4	1/8	1/4	1/2	1/4	1	1/2
Confined space	3	1/2	4	1	1/2	1	2	1	5	3
Load holding	4	1 1/2	8	2	1	3	3	3	7	6
Gripper mass	5	1/2	4	1	1/3	1	2	1 1/2	4	2
Contact pressure	6	1/3	2	1/2	1/3	1/2	1	2/3	3	1 1/2
Life time	7	1/2	4	1	1/3	2/3	1 1/2	1	4	2
Financial cost	8	1/6	1	1/5	1/7	1/4	1/3	1/4	1	1/2
Control complexity	9	1/4	2	1/3	1/6	1/2	2/3	1/2	2	1

TABLE C.2: The AHP grading results of the author

Matrix Engineer 1	Actuation time	Grasping range	Confined space	Load holding	Gripper mass	Contact pressure	Life time	Financial cost	Control complexity	
	1	2	3	4	5	6	7	8	9	
Actuation time	1	1	3	1/3	1/5	3	1/7	3	2	3
Grasping range	2	1/3	1	1/7	1/5	1/5	1/5	1/2	1/5	1/2
Confined space	3	3	7	1	2	2	1/3	3	3	7
Load holding	4	5	5	1/2	1	3	1	5	2	5
Gripper mass	5	1/3	5	1/2	1/3	1	1/3	5	2	3
Contact pressure	6	7	5	3	1	3	1	5	6	5
Life time	7	1/3	2	1/3	1/5	1/5	1/5	1	1	2
Financial cost	8	1/2	5	1/3	1/2	1/2	1/6	1	1	3
Control complexity	9	1/3	2	1/7	1/5	1/3	1/5	1/2	1/3	1

TABLE C.3: The AHP grading results of the first interviewed engineer

Matrix Engineer 2	Actuation time	Grasping range	Confined space	Load holding	Gripper mass	Contact pressure	Life time	Financial cost	Control complexity	
	1	2	3	4	5	6	7	8	9	
Actuation time	1	1	9	5	1	5	5	2	3	4
Grasping range	2	1/9	1	1/4	1/9	1	1/2	1/5	1/7	1/6
Confined space	3	1/5	4	1	1/5	4	1/7	1/3	1/2	1/4
Load holding	4	1	9	5	1	9	2	5	7	2
Gripper mass	5	1/5	1	1/4	1/9	1	1/5	1/4	1/3	1/6
Contact pressure	6	1/5	2	7	1/2	5	1	3	2	1/2
Life time	7	1/2	5	3	1/5	4	1/3	1	1/3	1/5
Financial cost	8	1/3	7	2	1/7	3	1/2	3	1	1/3
Control complexity	9	1/4	6	4	1/2	6	2	5	3	1

		Actuation time	Grasping range	Confined space	Load holding	Gripper mass	Contact pressure	Life time	Financial cost	Control complexity
Matrix Engineer 3		1	2	3	4	5	6	7	8	9
Actuation time	1	1	3	1/3	1/5	3	1/3	2	3	1/3
Grasping range	2	1/3	1	1/9	1/8	1/4	1/7	1/7	1/3	1/3
Confined space	3	3	9	1	1	1	1/5	2	3	2
Load holding	4	5	8	1	1	4	1/4	2	7	3
Gripper mass	5	1/3	4	1	1/4	1	1/4	1	2	1/3
Contact pressure	6	3	7	5	4	4	1	7	8	6
Life time	7	1/2	7	1/2	1/2	1	1/7	1	2	1/3
Financial cost	8	1/3	3	1/3	1/7	1/2	1/8	1/2	1	1/6
Control complexity	9	3	3	1/2	1/3	3	1/6	3	6	1

TABLE C.4: The AHP grading results of the third interviewed engineer

		Actuation time	Grasping range	Confined space	Load holding	Gripper mass	Contact pressure	Life time	Financial cost	Control complexity
Matrix Engineer 4		1	2	3	4	5	6	7	8	9
Actuation time	1	1	5	3	1	4	3	5	6	6
Grasping range	2	1/5	1	1/2	1/6	1/2	1/5	1/3	4	1/3
Confined space	3	1/3	2	1	1/3	3	1/3	3	5	4
Load holding	4	1	6	3	1	2	1/3	1	6	2
Gripper mass	5	1/4	2	1/3	1/2	1	1/3	1	5	2
Contact pressure	6	1/3	5	3	3	3	1	1	5	3
Life time	7	1/5	3	1/3	1	1	1	1	3	3
Financial cost	8	1/6	1/4	1/5	1/6	1/5	1/5	1/3	1	1/2
Control complexity	9	1/6	3	1/4	1/2	1/2	1/3	1/3	2	1

TABLE C.5: The AHP grading results of the fourth interviewed engineer

		Actuation time	Grasping range	Confined space	Load holding	Gripper mass	Contact pressure	Life time	Financial cost	Control complexity
Matrix Engineer 5		1	2	3	4	5	6	7	8	9
Actuation time	1	1	5	3	1	4	3	5	6	6
Grasping range	2	1/5	1	1/2	1/6	1/2	1/5	1/3	4	1/3
Confined space	3	1/3	2	1	1/3	3	1/3	3	5	4
Load holding	4	1	6	3	1	2	1/3	1	6	2
Gripper mass	5	1/4	2	1/3	1/2	1	1/3	1	5	2
Contact pressure	6	1/3	5	3	3	3	1	1	5	3
Life time	7	1/5	3	1/3	1	1	1	1	3	3
Financial cost	8	1/6	1/4	1/5	1/6	1/5	1/5	1/3	1	1/2
Control complexity	9	1/6	3	1/4	1/2	1/2	1/3	1/3	2	1

TABLE C.6: The AHP grading results of the fifth interviewed engineer

		Actuation time	Grasping range	Confined space	Load holding	Gripper mass	Contact pressure	Life time	Financial cost	Control complexity
Matrix Engineer 6		1	2	3	4	5	6	7	8	9
Actuation time	1	1	5	1/3	3	5	1/5	7	3	1
Grasping range	2	1/5	1	1/3	1/5	1/5	1/5	1/3	1/3	1/5
Confined space	3	3	3	1	5	5	1	7	5	1
Load holding	4	1/3	5	1/5	1	2	1/5	3	1/3	1/5
Gripper mass	5	1/5	5	1/5	1/2	1	1/5	3	3	1/5
Contact pressure	6	5	5	1	5	5	1	5	7	3
Life time	7	1/7	3	1/7	1/3	1/3	1/5	1	1/3	1/5
Financial cost	8	1/3	3	1/5	3	1/3	1/7	3	1	1/3
Control complexity	9	1	5	1	5	5	1/3	5	3	1

TABLE C.7: The AHP grading results of the sixth interviewed engineer

		Actuation time	Grasping range	Confined space	Load holding	Gripper mass	Contact pressure	Life time	Financial cost	Control complexity
Matrix Engineer 3		1	2	3	4	5	6	7	8	9
Actuation time	1	1	3	1/3	1/5	3	1/3	2	3	1/3
Grasping range	2	1/3	1	1/9	1/8	1/4	1/7	1/7	1/3	1/3
Confined space	3	3	9	1	1	1	1/5	2	3	2
Load holding	4	5	8	1	1	4	1/4	2	7	3
Gripper mass	5	1/3	4	1	1/4	1	1/4	1	2	1/3
Contact pressure	6	3	7	5	4	4	1	7	8	6
Life time	7	1/2	7	1/2	1/2	1	1/7	1	2	1/3
Financial cost	8	1/3	3	1/3	1/7	1/2	1/8	1/2	1	1/6
Control complexity	9	3	3	1/2	1/3	3	1/6	3	6	1

TABLE C.8: The AHP grading results of the sixth interviewed engineer

Matrix Average	Actuation time	Grasping range	Confined space	Load holding	Gripper mass	Contact pressure	Life time	Finacial cost	Control complexity	
	1	2	3	4	5	6	7	8	9	
Actuation time	1	1	4 3/4	1 2/9	1/2	3 1/3	6/7	2 4/5	3 2/5	2 7/9
Grasping range	2	1/5	1	1/4	1/7	1/3	1/4	2/7	2/5	1/3
Confined space	3	5/6	4 2/7	1	5/8	2 1/8	2/5	1 5/8	2 4/7	2
Load holding	4	1 8/9	7	1 3/5	1	3 4/5	1	3 4/9	4	2 7/8
Gripper mass	5	1/3	2 5/6	1/2	1/4	1	1/3	1 1/7	1 5/7	4/5
Contact pressure	6	1 1/6	3 5/7	2 1/2	1	2 7/9	1	2 5/7	4 1/2	2 2/5
Life time	7	1/3	3 2/5	5/8	2/7	7/8	3/8	1	1 1/7	1
Finacial cost	8	2/7	2 1/2	2/5	1/4	3/5	2/9	7/8	1	2/3
Control complexity	9	1/3	2 3/4	1/2	1/3	1 2/9	3/7	1	1 1/2	1

TABLE C.9: The AHP grading results of the average results

C.0.2 Grading

Combing the weight factors and grading criteria the gripper classes were graded using data obtained from the state-of-the-art literature. Appendix A.1 shows the data set that was made for the grading. The result of this grading is shown in table C.10. Considering the definition of the four points of the grading scale presented in section 1.4, each minus or double minus sign indicates a limitation. For example a limitation caused by the grading criteria financial cost indicates that the financial cost of the gripper class is too high limiting its application in the field of high speed case packing. More specifically the columns of table C.10 show the degree of limitation stemming for each grading criteria. Additionally considering the rows of table C.10 the limitations for the specific gripper classes can be seen.

	Actuation time	Grasping Range	Operating in confined space	Force holding	Moment Holding	Gripper mass	Contact pressure	Life time	Financial cost	Control complexity	Weight average gripper score
WF	0.138	0.024	0.102	0.181	0.181	0.055	0.162	0.055	0.425	0.060	
Rigid 1 DOF	+	++	--	++	++	+	--	++	++	++	2.0
Rigid fully actuated	+	++	-	++	++	-	-	--	--	--	1.8
Under actuated rigid	-	++	-	+	++	+	-	+	+	++	1.9
Lumped compliant	-	++	-	+	++	++	-	-	--	++	1.8
Distributed compliant	-	++	--	+	++	+	+	+	--	++	1.8
Suction cups	++	++	++	++	-	++	++	-	++	++	2.5
Structure jamming	--	++	+	+	+	+	++	-	+	+	1.9
Bernoulli	++	++	++	--	--	++	++	+	-	++	1.8
Pressurized bellows	-	++	--	-	-	++	++	+	++	++	1.6

TABLE C.10: The results of the gripper grading showing the weight factors in the second row from the top and the average gripper score in the final row

To draw any more meaningful conclusions a numerical value describing limitation has to be determined. This value is named the weight limitation score (WLS) and is calculated according to equation C.21. When the gripper scores ++ or 3 points there is no limitation posed by that grading criteria, in this case the WLS is 0.

$$WLS(i, j) = W(j) \cdot (3 - GS(i, j)) \quad (C.21)$$

Here:

$$W(j) = \text{The weight factor of the } j\text{'th grading criteria}$$

$$GS(i, j) = \text{The considered gripper class (i) and grading criteria (j)}$$

From the WLS the degree of limitation for the different grading criteria can be calculated for each gripper class. This is done by dividing the WLS by the total WLS for that gripper class. This calculation is mathematically shown in equation C.22.

$$\text{degree of limitation}(i, j) = \frac{WLS(i, j)}{\sum_{k=1}^{10} WLS(i, k)} \cdot 100 \quad (\text{C.22})$$

The degree of limitation is presented in table C.11 in the bottom row of table C.11 the average of the calculated limitation is shown.

Limitation for	Actuation time(%)	Grasping Range (%)	Operating in confined space (%)	Force holding (%)	Moment Holding (%)	Gripper mass(%)	Contact pressure (%)	Life time (%)	Financial cost (%)	Control complexity (%)
Rigid 1 DOF	14.0	0.0	31.1	0.0	0.0	5.6	49.3	0.0	0.0	0.0
Rigid fully actuated	14.4	0.0	0.0	0.0	0.0	11.5	0.0	26.2	19.7	28.2
Underactuated rigid	32.9	0.0	12.2	32.3	0.0	3.3	19.3	0.0	0.0	0.0
Lumped compliant	16.8	0.0	12.4	22.0	0.0	0.0	19.7	13.6	15.3	0.0
Distributed compliant	20.8	0.0	23.0	27.3	0.0	12.5	12.2	4.2	0.0	0.0
Suction cups	0.0	0.0	0.0	0.0	82.9	0.0	0.0	17.1	0.0	0.0
Structure jamming	43.5	0.0	10.7	19.0	6.3	5.8	0.0	3.9	4.4	6.3
Bernoulli	0.0	0.0	0.0	45.3	45.3	0.0	0.0	2.3	7.0	0.0
Pressurized bellows	44.6	0.0	49.4	0.0	0.0	0.0	0.0	6.0	0.0	0.0
Average limitation	20.8	0.0	15.4	16.2	15.0	4.3	11.2	8.2	5.2	3.8

TABLE C.11: The degree limitation calculated for each gripper class

Appendix D

Sensor Selection

in this appendix the sensor selection process is discussed in great detail. Firstly the design requirements and sensor placement are discussed, secondly the transducer selection is reasoned. Following the transducer selection the sensor structure is picked using the available literature on multi-axis F/M design. Finally the picked sensor structure are considered in more detail. A more detailed discussion of the sensor selection process can be found in appendix. A summary and brief explanation of all the design requirements is provided in the main text.

D.1 Measurement set up

Figure [D.1a](#) gives a schematic overview of robot set up that will be used in this design. The reference frame shown in this figure will be used throughout this work. This robot was provided by BPA and is usually utilized to perform test on new concepts or ideas. This setup resembles the delta robots that can be found at BPA's customers closely. The main difference are that the test robot contains new and improved components increasing the stiffness of the delta robot. The delta robot is also fitted with more powerful actuators reducing the limitations posed by the actuators of the delta robot. These improvements permit the addition of extra mass during a test, without reducing the performance of the robot. Finally the test set up does not use a conveyor belt and vision system to achieve a continuous product flow, pick and place operations can only be added manual. Since this research is interested in the detachment of products from the end-effector, zooming in on the critical part of one pick and place motion. A vision system and a continuous product flow is not required.

The test setup is already able to measure many desired quantities such as acceleration, velocity and position of the robot platform, but also air flow and pressure in the vacuum tubes. By design a F/M sensor for this test setup the load on the system can additionally be measured, giving more insight in the failure of grippers under dynamic loading.

D.2 Selection considerations

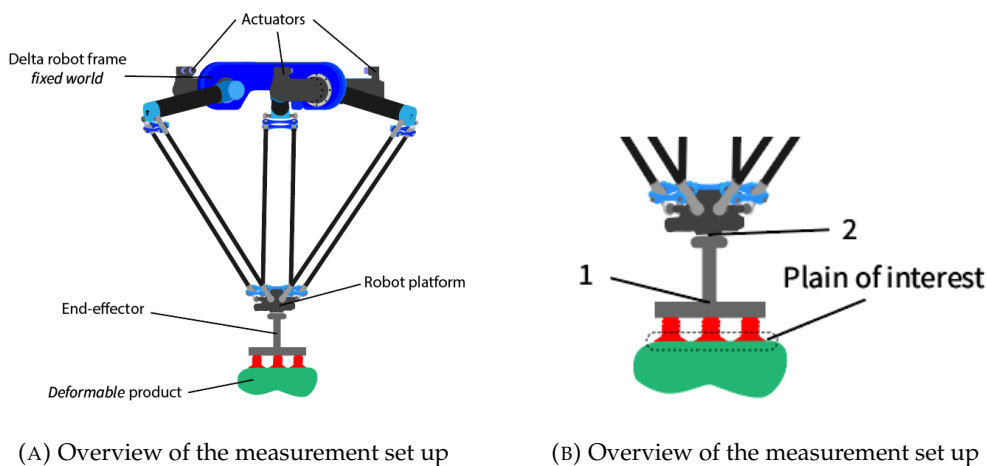
This section will only consider sensor structures relying on strain gauges as transducers for a multi-axis F/M sensor. Strain gauges essentially measure deformation to determine an applied load, see section [D.4.1](#) for more details. Therefore the structure of any n axis force and or torque sensor, requires n unique deformation modes. This limits n to 6, in that case 3 orthogonal forces and 3 orthogonal moments are measured. Many different structures can obtain n desired deformation modes, selecting

the correct sensor structure for the application is essential to ensure the desired performance. Since this section only considers multi-axis F/M sensor, the word sensor will be used with the same meaning.

perform

D.2.1 Sensor placement

The placement of the F/M sensor should be taken into careful consideration. Ideally the sensor should be placed directly at the point where the load needs to be known. This plain of interest is between the gripper and the product, as shown in figure D.1b. Measuring directly at this interface is challenging and no sensor capable of performing such measurements was found available on the market or in literature. Therefore, another measuring location has to be picked. Placing the sensor at another location requires the addition of a correction factor for this displacement. There are two logical location to place the sensor, the first location is labeled 1 in figure D.1b. This location places the sensor as close as possible to the suction cup grasp plane. This minimizes the correction that has to be made for the sensor displacement. The second location, labeled 2 in figure D.1b places the sensor directly under the robot platform, this location minimizes the additional load added by the mass of the sensor during acceleration, another benefit is the fact that the sensor can be designed as an extension of the robot platform. Any previously designed grippers can in that case be connected to the sensor. Location 2 was picked because studding and extending upon previous works was deemed more important than having a smaller correction.



(A) Overview of the measurement set up

(B) Overview of the measurement set up

D.2.2 Expected load

For the selection of a well suited sensor the maximum load on the sensor should be determined. From an analysis of the BPA case packing lines the maximum load on the sensor was determined. The delta robots in a case packing line are at most able to achieve 120 m/s^2 along the x , y and z axis for a load of 1.0kg . The mass of the sensor should also be included for the determination of the moving mass during a measurement. The sensor mass is estimated to be 0.5kg at this stage of the design. To ensure the sensor does not fail because of unexpected behavior such as a robotic crash or emergency stop a safety factor (SF) of two was introduced.

As shown in equation D.1 newtons second law was used to determine the minimum force the sensor needs to be able to withstand. This force is the same in x, y and z direction and was calculated as 360 N.

To determine the determine the minimum moment the sensor needs to be able to withstand the center of mass of a standard end-effector has to be determined. In the redesign of BPA's delta platform a limit to the location of the center of mass was set. For high-speed applications the center of mass needs to be with in 100mm (r_{max}) from the robot platform. Using this distance and the previously determined force the maximum moment around the x and y axis can be determined. This moment is determined to be 36N, as shown in equation D.2. The moment around z is limited to the the torque the motor integrated in the delta platform can provide, which is 2 Nm. Designing a sensor according to these specifications will result in a sensor well suited for only this application. After a sensor structure is picked this required load will be compared to the typical design load found in literature and a final maximum design load will be picked in section D.4.

$$F_{req} = m_{a_{max}} \cdot a_{max} \cdot SF = 360N \quad (D.1)$$

$$F_{x_{req}} = F_{y_{req}} = F_{z_{req}} = F_{req}$$

$$M_{x_{req}} = M_{y_{req}} = r_{max} \cdot F_{req} = 36Nm \quad (D.2)$$

D.2.3 Coupled and decoupled sensors

In literature multi-axis F/M sensors are general divided in two types, mechanically coupled and mechanically decoupled sensor. This classification is applicable to any sensor structure or transducer choice and is based on the relation ship of the measured strain and applied load [108], [110], [139].

Mechanical decoupled sensors measure stain in only one transducer bridge when a pure load is applied in one of the principle measuring directions. Mechanically coupled sensors on the on the other hand measure strain in multiple bridges if a load is applied in one of the principle measuring directions. Mechanically coupled sensors often have more transducer bridges than measurement direction. Measuring bridges will be explained further in section D.4.1. Both categories have there advantages and disadvantages. Mechanically decoupled sensors do not require complicated decoupling algorithms to translate the measured strain into an applied load, making there usage and calibration process much more intuitive [108], [139]. Furthermore removing a measurement direction is relatively simple and low cost. However their structural design process is more complex and their cross-coupling error tends to be to large to truly be decoupled [108], [139], [140].

Because of the remaining issues industrial available multi-axis force torque sensor are usually designed to be strongly coupled [139]. In research on the other hand the desire for a decoupled sensor applicable for industrial purposes remains strong [108]–[110], [118], [120], [124], [137], [139], [221]–[223]. This is because for most sensor structures based on strain gauges the cross coupling error is by far the largest error, much larger than for example non-linearity errors, hysteresis or non-repeatability [109]. The main focus of recent research into multi axis F/M sensors is therefor combating and eliminating cross coupling.

Combating cross coupling

Two main methods for combating the issues faced by coupling errors are observed in this field [109], [139]. The first method uses signal processing without changing the mechanical structure of the sensor. This method relay on decoupling algorithms to reduce the effects of cross-coupling errors. The most commonly used decoupling algorithm is the least squares (LS) method [108], [110], [114], [115], [117], [150], [224]. But more complex algorithms achieving better performance have also been used such as neural networks [123], [225]–[227], shape-form-motion [155], [228] and support vector regression [229], [230].

The second method focuses on changing the sensors mechanical structure and strain gauge placement to achieve a mechanically decoupled sensor structure. This method aims to remove the cross coupling by picking a smart and novel sensor structure in the design stage which is intended to minimize the internal cross coupling. Many different sensor structures using strain gauges have been designed, fabricated and validated. The list of considered sensor structures consist of E-type membrane structure [123], H-shaped beams on a Steward platform [124], a circular spoke membrane structure [126], a parallel plate structure [127], [128], a parallel beam structure [129], a stack of multiple load cells [130], [131], T-shaped bars [132], commercially available 3 beam structure [133] and the Maltese cross structure [136], [137].

Some researchers in this field critically observe a division in research goals concerning the structural design of the multi-axis F/M sensors. They classify two groups of research [109], [124], [139]. The first groups considers case specific designs following a trail-and-error design strategy based on the designers experience. Resulting in a sensors with a high production cost, which is not or hardly generalize for other fields.

The second group aims to create a general and structured design method, aiming to create a generally applicable sensor with low production cost. Other researches and industries can follow the proposed to design methods to create a sensors fitting there needs. A sensor structure contain literature in the second group is highly preferably for the design of a new structure. A summary of the trends seen in literature is shown in figure D.2

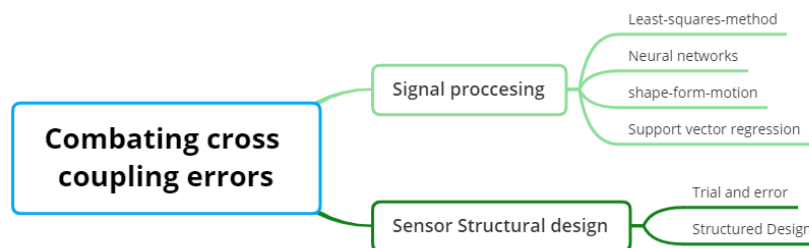


FIGURE D.2: A visual overview of the structure in the multi-axis sensor design literature

D.3 Sensor selection

The selection of the designed sensor consisted of three structured steps. Firstly the measurement principle was selected by picking the most suitable transducer. A transducer is as a device which converts a physical property into a measurable voltage or current signal. Several transducer usable for the design of a load sensor were considered, the one best suited for application in the high speed case packing industry was selected. Secondly different sensor structures using the selected transducer were considered and one was selected for the design.

D.3.1 Transducer selection

The transducers used to measure force do often not measure force directly, but instead measure the elastically deformation of a structure. Since this deformation is driven by an external load this method can be used to measure this applied load. The considered transducers have at least a proof of principle of design presented in literature. For each transducer a short description and a reasoning for there suitability is provided.

Infeasible transducers

1. **Force sensitive resistor (FSR)**, using an FSR it is possible to directly measure force as a change in resistance [111]. This transducer type has not yet been used to create a multi-axis force torque sensor and is lacking in performance compared to the other measurements techniques. Most problematic are a low force measurement range, large error and measuring moments [112]. Because of these limitations the FSR transducer was discarded.
2. **Capacitance**, the change in capacitance between two parallel plates has been used to measure the force on a deformable structure. This method is most often used and is most feasible on micro and nano scale [113]–[115]. However some attempt of a sensor on an industrially applicable scale was found in literature [116], [117]. This sensor under performed compared to sensors made using other transducers. For example the achieved error was twice as large as other sensors. Furthermore the maximum moment was 20 to 40 times smaller compared to other sensors, while a similar maximum force was achieved. For application in high speed pick and place industry measuring moments under dynamic load is a clear literature gap. This transducer can therefore not be used in the high speed case packing industry.
3. **Optical**, by placing a light emitter and a receiver on a deforming structure the load on a structure has been measured [118]. This novel design requires a flexible sensor structure to function. Which in turn causes very low load measuring ranges, a factor 200 smaller compared to that is minimally required for the high speed case packing industry. Furthermore this sensor has hysteresis of over 20%, which is highly undesirable.
4. **Fluid Pressure**, In literature a sensors using fluid pressure to measure an applied load have been designed and validated [119]. This sensors showed outstanding performance, yet is too heavy and large to be applied in a highly dynamic environment. Furthermore this design process started with the intention to eliminate tubes from the system, which are required for this sensor.

This transducer type could on the other hand be used excellently to calibrate other F/M sensors.

Feasible transducers

1. **Material deformation**, Strain gauges have a slight change in resistance when there subjected to a strain. By measuring the strain of a loaded structure, stain gauges can be used to determine an external load. Strain gauges are a well developed and accepted in industry due to there ability to be applied in dynamic and static load cases, repeatability, smallness, low hysteresis and low cost [109]. All other considered transducers were lacking performance or sufficient proof of principle compared to stain gauges. Therefor strain gauges were picked as the transducer for the force torque sensor that will be developed. Section D.4.1 will go into more depth about the working principle and usage of strain gauges.
2. **Piezoelectric**, Piezoelectric materials generate a voltage when compresses, this effect has been used to design a multi axis F/M sensor [120]. The resulting sensor achieves a decoupled behaviour measuring all the load 6 axis, the degree of remaining coupling or error in the sensor is not mentioned. Further more it is state that this transducer type does, as apposed to other transducers, not fail under high loads [120]. In the high speed case packing industry measuring in the kN range is not required, therefor this feasible transducer type was not picked.
3. **Piezoresistive**, piezoresistive transducers behave similar to stain gauges, when they experience a strain their resistance changes. They can therefor be used as a replacement for strain gauges, however in they performing slightly worse than traditional strain gauges in this use case [122]. Piezoresistive transducers can however also be used at a much smaller scale not interesting for the high speed case packing industry. However this application field ensures piezoresistive transducers remain part of active research, possibly increasing the performing in the near future [112], [121].

D.3.2 Sensor structure determination

Sensor structure selection

From the considered sensor structure one has to be picked for a further detailed design. The considered sensor structures were reviewed on 5 criteria and one was selected for further design. The review of the sensor structures was done using simple binary questions, a full grading scheme was not required because the Maltese cross sensor structure clearly outperformed the other sensor structures. The 5 review points are explained below and the review of the sensor structures can be found in table D.1. The 6'th column provides information on the publishing year of the most recent publication for each sensor structure.

1. Passing air flow

passing air flow trough the sensor structure is the unique feature of the sensor that will be designed. This feature has to the best of the authors knowledge not yet been implemented in a multi-axis F/M sensor and can therefore not be directly reviewed from literature. The authors engineer judgement will be used label this criteria either likely of unlikely. Where likely means the sensor

structure is expected to be modifiable to allow the passage of airflow, unlikely indicates the opposite.

2. Coupling

The coupling review criteria checks whether a sensor structure is slightly or strongly mechanically coupled. Mechanically decoupled or slightly coupled sensors are preferred over strongly mechanically coupled sensors.

Mechanical decoupled sensors measure strain in only one transducer bridge when a pure load is applied in one of the principle measuring directions. Mechanically coupled sensors on the other hand measure strain in multiple bridges if a load is applied in one of the principle measuring directions. Mechanical decoupled sensors require less complex calibration procedures, however have more complex mechanical designs [108], [139]. The remaining cross-coupling of mechanically decoupled sensors tends to be too large to truly be decoupled, making them slightly coupled [108], [139], [140].

3. Design method

For the review of this criteria literature was studied looking for a structured and proven design method for each sensor structure. The availability of a structured and proven design method will lead to an easier and more feasible design.

Some researchers in this field critically observe a division in research goals concerning the structural design of the multi-axis F/M sensors. They classify two groups of research [109], [124], [139]. The first group considers case specific designs following a trial-and-error design strategy based on the designers experience. Resulting in sensors with a high production cost, which is not or hardly generalizable for other fields.

The second group aims to create a general and structured design method, aiming to create a generally applicable sensor with low production cost. Other researchers and industries can follow the proposed design methods to create sensors fitting their needs. A sensor structure containing literature in the second group is highly preferable for the design of a new structure.

4. P&P compatible

This review criteria considers if the sensor structure is compatible for usage during high speed pick and place. The main consideration of this review criteria is the design goal of the sensor structure. Sensors that are designed to be attached to or integrated in a robot are labeled compatible. While sensor structures designed to function as a multi-axis scale are labeled incompatible. The stiffness of the sensor which is required to withstand the dynamic loading is not considered here because this data is often not provided in literature.

5. Error

Commercially available multi-axis sensors are expected to measure loads with a maximum error of 3-5% at their rated load [107], [109]. This review criteria will look at the maximum measurement error for each sensor structure. A sensor is deemed usable if the maximum error is below 5%, this error included cross coupling errors. Therefore this criteria is labeled larger or smaller than 5%. This is a very simple review of measurement error, not considering non-linearity's, hysteresis or drift.

Further more a cross coupling error 3 -5% could in specific load cases lead to much larger errors, this is one of the driving factors for active research into multi-axis F/M sensor [109]. Take for example a perfectly linear 2 axis F/M sensor measuring a force in the y direction and a moment around the x axis, F_y and M_x respectively. The rate load of this sensors is $F_y = 400N$ and $M_x = 40Nm$, both measuring $1000 \mu st$ strain at the rated load ($\mu st = 10^{-6} \frac{mm}{mm}$). When the sensor is subjected to its rate M_x load, the F_y direction also measures some unintended signal, for example $25\mu st$. The cross coupling of a sensors is often determined at the rated load and is defined as the fraction of the unintended and the intended signal. This results in a cross coupling error of $(\frac{25\mu st}{1000\mu st} \cdot 100) = 2.5\%$. Now consider the same sensor loaded at $F_y = 40N$ and $M_x = 40Nm$, the unintended signal due to the cross coupling caused by the M_x load remains $30\mu st$. However the intended signal in the F_y direction has reduced to $100\mu st$. When the cross coupling error is calculated again, $(\frac{25\mu st}{100\mu st} \cdot 100) = 25\%$, it can be seen that the error has increased by a factor of 10. The cross coupling error is therefore most meaning full when the sensor is subjected to its rated load.

Nevertheless, 3-5% cross coupling error is what is can be expected form a fully developed commercially available multi-axis F/M sensor. Design a sensor better than this industrial standard is highly unlikely and is not expected for this design.

Sensor Structure	Coupling	Design method	passing air flow	P&P compatible	Error	Year
E-type membrane	Slight	available	likely	yes	>5%	2010
Platform	Strong	available	unlikely	no	>5%	2016
circular spoke	Strong	available	unlikely	yes	>5%	2014
parallel plate	Slight	available	unlikely	yes	>5%	2002
parallel beam	Slight	Available	unlikely	yes	>5	2007
load cell stack	Unknown	available	unlikely	yes	>5	2005
T-shaped bars	Strong	available	unlikely	yes	Unknown	2002
3 beam structure	Strong	available	likely	yes	>5%	2021
Multi spoke wheel	Strong	available	likely	yes	>5%	2016
Maltese cross	Slight	available	likely	yes	>5%	2021
Sliding joint Maltese cross	Near perfect	available	unlikely	no	>5%	2021

TABLE D.1: A summary of the considered sensor structures and there consideration criteria

The Maltese cross structure is expected to be modifiable to pass air flow, has a small build volume and is still part of active research. All other considered sensor were either not suited to pas air flow, to large to be added to a dynamical moving robot platform or stopped seeing research effort in favor for other better performing sensor structures.

D.4 Maltese cross sensor

A Maltese cross sensor structure as shown in figure D.3, was first proposed by B.Shimano V. Scheinman in 1971 [141]. In 1977 B.Shimano and B. Roth further extended on the previous work outlining the mathematics and calibration process of a maltheses cross sensor sensor. [110]. This sensor structure is very close to being mechanically decoupled and inherently has a high sensitivity for forces and a low cross coupling. The sensors structure consists of 4 strain measuring beams, 4 thin plates a central connection block and a connection rim. By measuring the strain of the strain measuring beams the applied force can be determined. A more detailed

explanation of the working principle of the sensor can be found in section D.4.1. In research structural changes have been made to this general Maltese sensor structure in an attempt to increase sensitivity and reduce cross coupling [139]. This research is as mentioned in section D.2.3, based on the researchers experience and does not result in a structured design method that can be used by other researchers.

Another group of research aims present structured design methods for the different Maltese cross variations, which are intended to be more widely applicable. These works will serve as the inspiration and guide lines for the sensor designed and presented in this work.

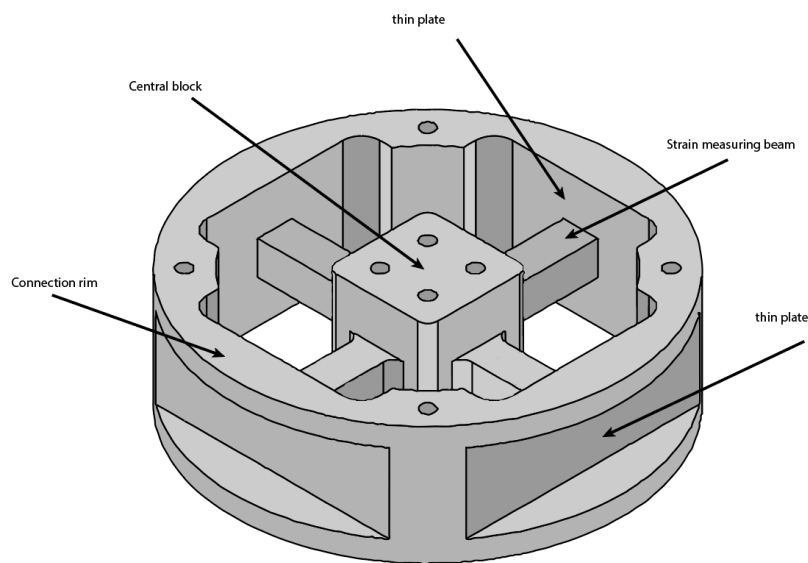


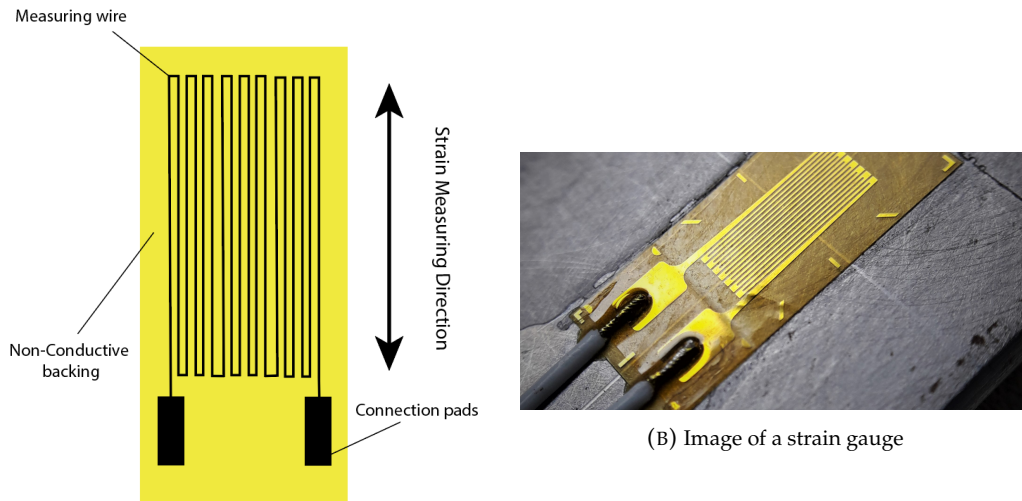
FIGURE D.3: An overview of a maltheses cross sensor structure

D.4.1 Measuring principle

Strain gauges

The core measuring principle of the Maltese cross sensor is based on strain gauge. Strain gauges are transducers that are used to measure strain of a piece of material. A strain gauge consist of one long folded wire, placed inside a thin flexible restive foil. By applying a deformation in the longitudinal direction of a strain gauge, the folded wire inside the stain elongates. This elongation changes the resistance of the wire. When elongated the resistance increases and when compressed the resistance decreases. Strain gauges can therefore be used as deformation measuring resistors. The stain of a piece of material, usually metal, can be measured by gluing the strain gauge to the surface of the material.

Since the deformations are very small, the change in resistance is also very small. To measure this small resistance change special measuring circuitry is needed. The most commonly used circuit is known as the Wheatstone bridge and gives an output voltage related to the strain of the strain gauges.



(A) Schematic overview of a strain gauge glued to a piece of metal

FIGURE D.4: Figures showing strain gauges

Wheatstone bridge

The Wheatstone bridge circuit can be used to measure a relative change in resistance. This allows for measurements with great accuracy, measuring resistance changes of the order of 10^{-4} to 10^{-2} can usually be obtained. The most simple version of a Wheatstone bridge used to measure strain, the quarter bridge, is shown in figure D.5a. When there is no deformation the resistors R_1 through R_4 have the same value, typically 350Ω , this results in an output voltage, U_o of $0V$. When the strain gauge deforms, its resistance changes resulting in a change in U_{out} . This circuit has one major drawback, when the temperature changes the strain gauge will deform due to expansion or contraction of the material it is attached to. Since the measured strain is used to determine the applied load, a relationship between applied load and temperature exists.

To manage this issue, and gain a more sensitive measurement a full or half bridge circuit can be used using replacing half of the resistors of all of the resistors with active strain gauges respectively. In these measuring circuits the two strain gauges in one leg of the bridge circuit are placed such that they measure equal but opposite strains. A change in temperature will result in an equal strain in both strain gauges. This will not result in a relative change in resistance, not altering the output voltage.

This work will consider the usage of a full bridge circuit, to gain the maximum sensitivity, as shown in figure D.5b. Half bridge circuits have been used in literature before and provide a less cumbersome manufacturing process [231].

Using a calibration process further explained in section ??, this circuit provides a method to measure an applied load determined according to the measured voltage.

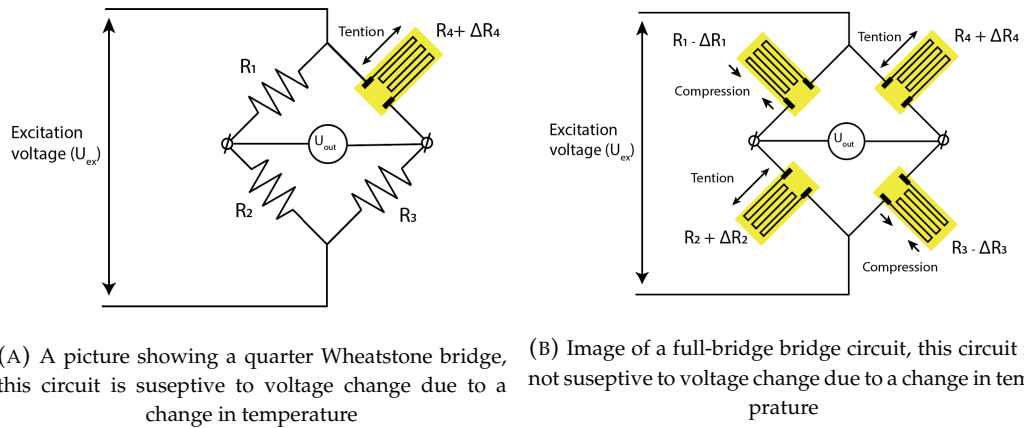
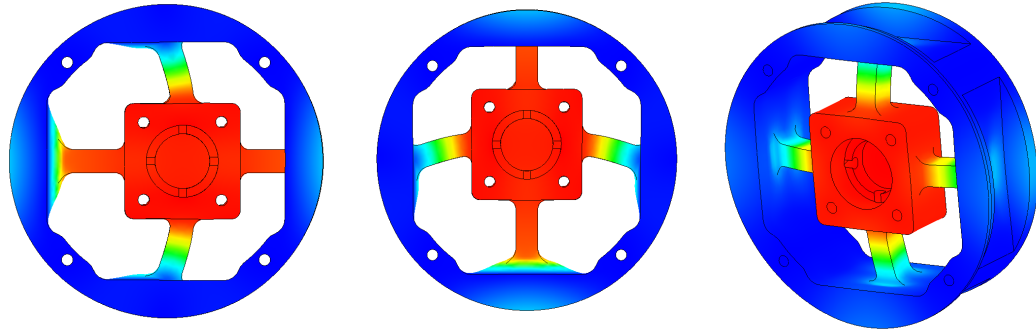


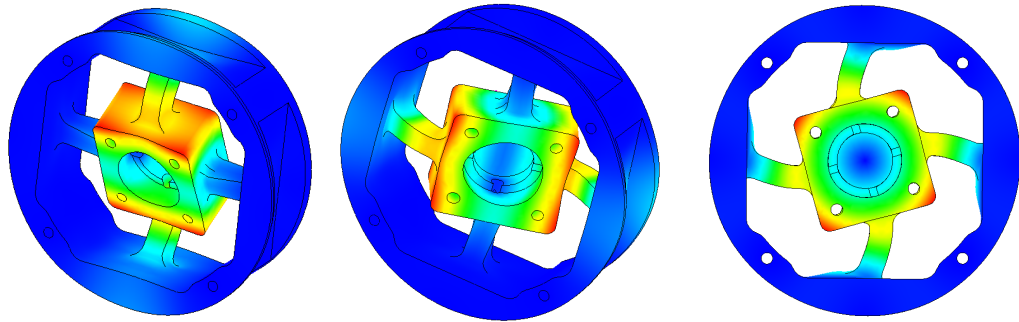
FIGURE D.5: Figures showing strain gauges

Deformation modes

Figure D.6 shows the six deformation modes of the sensor. The decoupled behaviour of the sensor is obtained through these distinct deformation modes. The strain gauge measuring circuits should be placed such that strain is only measured for one of the six deformation modes. This is only possible if the sensor has a distinct deformation mode for each pure external load. Viewing the sensor body as a mechanical structure, the thin plates labeled in figure D.6 can be viewed to act as linear guides. The thin plates should only allow one degree of freedom, this requires infinite stiffness in all other directions. This is physically impossible and a reason for the introduction of cross coupling even for this sensor structure.



(A) The displacement of the central block due to a pure force in the F_x direction (B) The displacement of the central block due to a pure force in the F_y direction (C) The displacement of the central block due to a pure force in the F_z direction



(D) The rotation of the central block due to a pure moment around the x axis (E) The rotation of the central block due to a pure moment around the y axis (F) The rotation of the central block due to a pure moment around the z axis

FIGURE D.6: The six deformation modes of the sensor body

Design load

As mention in section D.2.2 the required load has to be compared to the typical design load found in literature. Picking the load similar to what is found in literature the design could be applicable to other use cases as well. Further more comparison of the results with results from literature becomes more meaning full. This reasoning only holds if the maximum load considered in literature is higher than what is required for this use case. Table D.2 shows the design loads of different Maltese cross sensor design in literature. According to these load case the maximum design load was picked as $\vec{F}_{max} = [F_{x_{max}}, F_{y_{max}}, F_{z_{max}}, M_{x_{max}}, M_{y_{max}}, M_{z_{max}}]^T = [400N, 400N, 800N, 40Nm, 40Nm, 40Nm]^T$

Load direction	Max load [139]	Max load [108]	Max load [109]	Max load [109]
$F_x(N)$	400	400	330	400
$F_y(N)$	400	400	330	400
$F_z(N)$	800	800	990	1000
$M_x(Nm)$	40	40	30	20
$M_y(Nm)$	40	40	30	20
$M_z(Nm)$	40	40	30	10

TABLE D.2: Maximum loads found in literature

Relationship between applied load and output voltage

A multi-axis F/T sensor converts the linear deformation of a mechanical structure caused by an applied load in a measurable output voltage. In this simple analysis the load is considered to be applied at the origin of the sensors measuring frame of reference. In reality this is rarely the case and extra correction matrices have to be used to convert the measured load to the point of application [110]. Finally this section will consider any general F/M sensor measuring in n load direction using m transducer bridges. This results in the force and voltage vectors as shown in equation D.3 and D.4 respectively

$$\vec{F} = \begin{bmatrix} F_1 \\ F_2 \\ \vdots \\ F_n \end{bmatrix} \quad (\text{D.3})$$

$$\vec{V} = \begin{bmatrix} V_1 \\ V_2 \\ \vdots \\ V_m \end{bmatrix} \quad (\text{D.4})$$

Since the strain gauges are attached to a linearly deforming structure the output voltage is expected to show a linear behavior with respect to the applied load. This notion leads to the relationship between voltage and applied load as shown in equation D.5. In stead of the voltage vector the strain vector is also often used in equation D.5, the C matrix entries will change accordingly.

$$\vec{F} = C^{-1} \cdot \vec{V} \quad (\text{D.5})$$

Here C is a m by n matrix as shown in equation D.6, named the compliance matrix.

$$C_{ij} = \begin{bmatrix} C_{11} & C_{12} & \dots & C_{1n} \\ C_{21} & \ddots & & \\ \vdots & & \ddots & \\ C_{m1} & & & C_{mn} \end{bmatrix} \quad (\text{D.6})$$

In case of a decoupled sensor C would be a diagonal matrix. In this case the force in the F_x direction is nothing more than a the scaled output V_1 . This makes the interpretation of the sensor data very intuitive.

Due to for example placement errors in the strain gauges no sensor is truly decoupled, to improve the sensor performance a simple leas-squares correction is usually sufficient for structurally decoupled sensors. This correction is performed by the of diagonal term in the C matrix.

Cross Coupling

One of the main performance metrics of a Maltese cross structure sensor is its cross coupling. During the design process and sensor validation the determination is of importance. For the determination of the cross-coupling the strain matrix has to be introduced first [139]. Considering a n axis F/M sensor with m transducer bridges. The strain matrix gives the relationship between applied force and measured strain. The n 'th column of the matrix contains the measured strain in the m strain gauge bridges for a pure load in the n 'th direction. Considering an 6 axis F/M sensor containing 6 measurement bridges, as will be designed in chapter 2. The strain matrix is a 6×6 matrix, where the first column \vec{S}_1 , contains the strain measured for an applied load in the F_x direction. The strain matrix is filled by applying n independent pure loads and measuring the m strains on the strain gauge bridges. The complete strain matrix for an general and the proposed F/M sensor are shown in equation D.7 and D.8 respectively.

$$S = \begin{bmatrix} \vec{S}_1 & \vec{S}_2 & \dots & \vec{S}_n \end{bmatrix} = \begin{bmatrix} S_{11} & S_{12} & \dots & S_{1n} \\ S_{21} & \ddots & & \\ \vdots & & \ddots & \\ S_{m1} & & & S_{mn} \end{bmatrix} \quad (D.7)$$

$$S = \begin{bmatrix} \vec{S}_1 & \vec{S}_2 & \vec{S}_3 & \vec{S}_4 & \vec{S}_5 & \vec{S}_6 \end{bmatrix} = \begin{bmatrix} S_{11} & S_{12} & S_{13} & S_{14} & S_{15} & S_{16} \\ S_{21} & S_{22} & S_{23} & S_{24} & S_{25} & S_{26} \\ S_{31} & S_{32} & S_{33} & S_{34} & S_{35} & S_{36} \\ S_{41} & S_{42} & S_{43} & S_{44} & S_{45} & S_{46} \\ S_{51} & S_{52} & S_{53} & S_{54} & S_{55} & S_{56} \\ S_{61} & S_{62} & S_{63} & S_{64} & S_{65} & S_{66} \end{bmatrix} \quad (D.8)$$

The cross-coupling is defined as the amount of undesired strain with respect to desired the strain at maximum load. This is mathematically shown in equation D.9. In a practical application using Wheatstone bridges, the measured output voltage is linearly related to the strain. Therefore the cross-coupling can also be directly computed for the measured output voltages at maximum load [109]. This observation also yields a method to calculate the cross coupling directly from the compliance matrix, as shown in equation D.9.

$$(CC)_{ij} = \frac{S_{ij}}{S_{ii}} = \frac{F_j^{max} \cdot C_{ij}}{F_i^{max} \cdot C_{ii}} \quad (D.9)$$

From literature it is known that this cross coupling term is low in comparison to other sensor structures. A maximum cross coupling of about 10 % is to be expected for the maltese cross sensor as apposed to 25-30% which is found for other sensor structures [108], [123], [139], [225]. Kang et al. was the first to note that the main cross coupling terms for the Maltese cross sensor are CC_{15} , CC_{24} [108], [139]. Only these principle cross coupling term require extra design effort to further reduce the remaining errors. Some studies report very low cross coupling. These designs however often consider a low moment to force (M to F) ratio, $0.005 - 0.05Nm/N$, which makes them not applicable for use in general industry [129], [132], [140], [221]. The trend seen in literature is that a higher M to F ratio will result in more cross coupling [139]. $0.1Nm/N$ is generally seen as a high M to F ratio and will also be considered

in this design [109].

Another sensor design which did not deliver a proof of concept and only considered the result of the optimization algorithm have obtained even lower near perfect cross coupling errors [109]. Since this work did not manufacture a sensor and prove the results of the optimization its hard to tell if these results are obtainable in reality. The results of this work will therefor not be considered when setting the constraints for the optimizer.

Appendix E

Sensor optimization and FEM model validation

In this appendix the optimization scheme and the FEM model validation are discussed in more detail.

E.0.1 Optimization scheme

In this sub section the optimization scheme used in this work is described. Firstly the design variables are explained, secondly the optimization problem is set up and finally the optimization implementation is described.

Design variables

The preparation step of the optimization scheme starts with the parametric design of the sensor structure in Solidworks. The parametric variables will be used to perform the parametric optimization. Some designs in literature have considered nearly every possible parameter as a design variable, other designs only consider a few variables [109],[139]. Choosing more design variables is expected to result in a better functioning sensor since more aspects of the sensor can be optimized, however this will drastically increase the computational effort of the optimization scheme. Due to the available manufacturing method of CNC milling as opposed to EDM wire cutting some curvatures were set a priori. In this work only the most influential design parameters were considered as shown in figure E.1, these parameters directly influence the stiffness of the sensor.

1. strain measuring beam length (L), the first design variable is the length of the strain measuring beams. This variable is constrained between 13mm and 25mm . The lower bound is set to ensure the strain gauge fits the beam. The upper bound is set to limit the searching range of the optimizer.
2. strain measuring beam height (h), the second design variable is the height of the strain measuring beams. This variable is constrained between 8mm and 21mm . The lower bound is set to the width of the strain gauges, the upper bound is set to ensure no geometrical errors in the sensor shape.
3. strain measuring beam width (b), the third design variable is the width of the strain measuring beams. This variable is constrained between 8mm and 15mm . The lower bound is set to the width of the strain gauges, the upper bound is set to ensure no geometrical errors in the sensor shape.

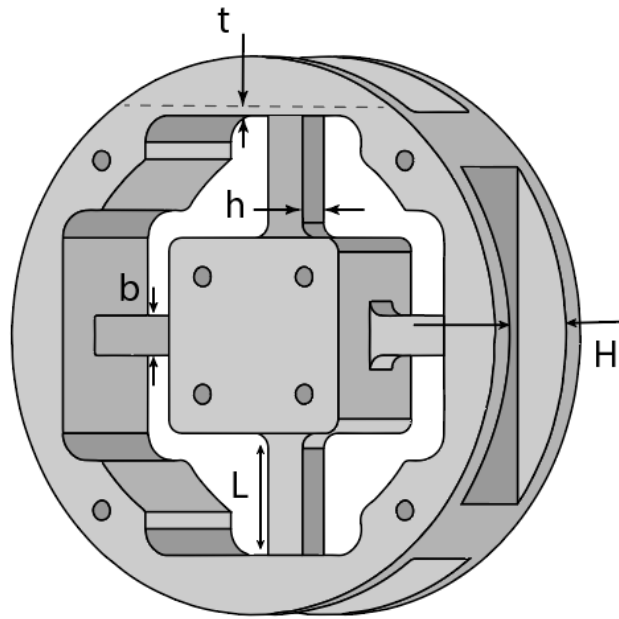


FIGURE E.1: A visual overview of dimensions of the mechanical sensor design

4. Thin plate height (H), the fourth design variable is the height of the thin plate plates this variable is constraint between 15mm and 25mm these bounds are set to limit the range of the optimizer.
5. Thin plate thickness (t), the fifth and final design variable is the thickness of the thin plates this variable is constraint between 0.7mm and 3mm the lower bound is set according to literature [139] the upper limit is set to limit the range of the optimizer

All design variables that were set to limit the range of the optimizer were not picked according to a physical limitation, if the optimizer hits one of these bounds the bounds should be adjusted accordingly. The design variables are grouped in a vector $\vec{X} = [b, h, H, L, t]$

Optimization method

The work flow of the optimization scheme is shown in figure E.2. The optimization scheme used in the works is inspired by the successfully designs presented in literature. Some changes have been made to have an easier implementation in industry. For example Solidworks was used to model the sensor structure, The software package COMSOL was used for FEM analysis, finally Matlab was used for the optimization scheme. These software packages offer training and customer support, are well established in industry and offer many options for extension on the optimization scheme. By using the appropriate professional software packages the optimization scheme is applicable in a wider part of industry the without requiring extensive knowledge of mechanical design theory or optimization.

This method used the software packages in there strength. Solidworks is mainly used for computer aided design (CAD) but also offers limited FEM analysis options,

on the other hand COMSOL also offers the option to draw model structures, yet is known for its FEM analysis of multi-physics problems. Finally COMSOL and Solidworks also both have integrated optimization abilities but do not offer as much selection freedom and options as Matlab. For the communication between the different software packages COMSOL's livelink feature was used.

An optimization sequence starts by picking a set of starting dimensions stored in COMSOL. The model is built accordingly by Solidworks and passed on to COMSOL. COMSOL runs the FEM analysis and determines the quantities required to calculate the cost function and constraints. These values are passed on to MATLAB which calculates the cost function and constraints, if the optimization stop criteria are not met Matlab updates the design variables which are passed to COMSOL, which updates the Solidworks model and starts the next optimization loop.

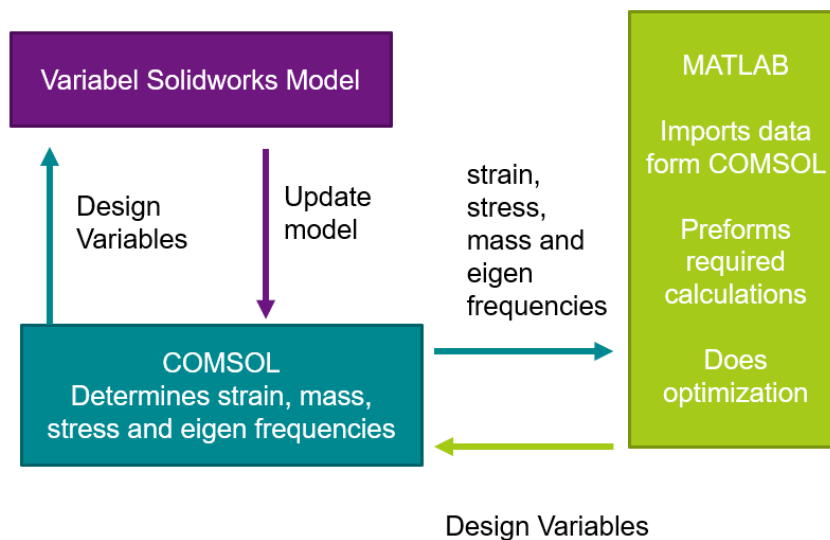


FIGURE E.2: Overview of the optimization method

Optimization problem

To perform the optimization in Matlab the optimization problem should be fully determined. This is done by determining the cost function and constraints. This sensor is intended to be used in industry and is not meant to prove mechanically decoupled Maltese cross sensors are possible. Therefore the optimization goal will be defined as the average sensor sensitivity over six measuring bridges when the combined maximum load is applied. This choice is in line with the vision of some researchers in this field [142], [143]. The combined maximum is defined as the load case where all 6 load directions are at their maximum. The cost function is physical defined as the negative average absolute strain measured at the maximum load, this mathematical shown in equation E.1. The minimization of f will maximize the average measured strain at combined maximum load. To limit the size of $f(\vec{X})$ to be around one. $f_{physical}(\vec{X})$ was divided by 200 to obtain $f_{opt}(\vec{X})$, which was used during optimization.

$$f_{physical}(\vec{X}) = - \frac{|\epsilon_{Fx}| + |\epsilon_{Fy}| + |\epsilon_{Fz}| + |\epsilon_{Mx}| + |\epsilon_{My}| + |\epsilon_{Mz}|}{6} \quad (E.1)$$

$$f_{opt}(\vec{X}) = - \frac{|\epsilon_{Fx}| + |\epsilon_{Fy}| + |\epsilon_{Fz}| + |\epsilon_{Mx}| + |\epsilon_{My}| + |\epsilon_{Mz}|}{6 \cdot 200}$$

In this calculation it is assumed that the coupling effects are small compared to true measured strain. The measured strain in one bridge under the combined maximum load will be nearly identical to the measured strain in this bridge if a pure load in its measuring direction was applied.

Next to the cost function constraints are added to the design to take into account other important design considerations. These design criteria are deliberately not added to the cost function to prevent any priority issues in a combined cost function. The considered constraints can be divided in two groups design constraints and physical constraints. The design constraints are set as part of the design, the physical constraints are set to ensure no rebuild errors will occur during the optimization.

1. Cross coupling, The cross coupling of the sensor is not used as an optimization criteria but remains of importance. To keep the cross coupling sufficiently small a constraint is added. To limit the computational effort one of the two main cross coupling terms, CC_{15} and CC_{24} , as explained in section D.4.1 are considered. The research proposing the novel strain gauge arrangement, that was used in this work achieved a cross coupling error of 10-11% in the design phase [108]. Following this result the cross coupling constraint was set lower to the same value as shown in equation E.2 and E.3.

$$CC_{15} < 5\% \quad (E.2)$$

$$CC_{24} < 5\% \quad (E.3)$$

2. Minimum strain, The cost function considers the average over all strains. If one direction would measure near 0 strain while another direction measures a very large strain the cost function indicates this as a good design. However this is not a desirable sensor design. Every measurement direction is of importance and should measure a minimal amount of strain. The minimum strain constraint is used to ensure this happens. The minimum strain ϵ_{min} is set to $300 \frac{\mu m}{m}$ slightly lower than values also used in literature [139]. Since more constraints are added compared to other design less strict bounds have to be set to find a design meeting all constraints. This constraint is set for all 6 measuring bridges and is shown in equation E.4.

$$\epsilon_{F(i)} > \epsilon_{min} \quad i = 1, \dots, 6 \quad (E.4)$$

$$\vec{F} = [F_x \quad F_y \quad F_z \quad M_x \quad M_y \quad M_z]$$

3. Maximum strain, the life time of a strain gauge is effected by the strain at which is periodically loaded. To provide sufficient life time a maximum strain was set, a life time of $1 \cdot 10^8$ load cycles was deemed sufficient. According to the

data sheet a maximum cyclic strain of $\pm 1000 \frac{\mu m}{m}$ is allowed for the desired fatigue life [152]. It is assumed that all 4 strain gauges in the Wheatstone bridge measure about the same strain. Following this reasoning, this constraint is set for all 6 measurement bridges and not for each strain gauge individually. Equation E.5 shows the constraints.

$$\epsilon_{F(i)} < \epsilon_{max} \quad i = 1, \dots, 6 \quad (E.5)$$

4. Sensor mass, because of the highly dynamic motion of case packing robot the mass of the sensor needs to be sufficiently small. The maximum mass (m_{max}) was set to 450 grams, similar to commercially available 6 axis F/T sensors [107]. To save computational effort it is advantageous to not include the part required to pass airflow in the FEM model. These parts however do have a mass which changes as the length of the strain measuring beams changes. For the minimal beam length till the maximum length with steps of 1mm the mass of the additional parts ($m_{additional}$) was determined. By linear interpolation between these points the additional mass is estimated. The change in mass of the air flow parts due to a change in the other design variables is negligible. Equation E.6 show the described constraint on the sensor mass.

$$m_{max} < m + m_{additional} \quad (E.6)$$

5. Tool tip displacement, Due to the flexibility of the sensor the gripper will displace and rotate. If this displacement is too large the sensor will influence the behavior of the gripper and the product. The robot used for this research will enter an error state if the expected and measured position of the platform differs by 5mm. 25% of this range was deemed to be acceptable for this constraint. The longest tool that has been attached to the robot platform is 420mm. The displacement at the tip of this gripper was considered when determining this constraint.

The displacement of the tool tip was determined by drawing a vector starting at the center of the central block, with a length equal to the length of the longest gripper. The end point of this vector is the location of the tool tip of the longest gripper. The location before deformation can easily be determined, since the vector is aligned with the z axis. By taking the displacement of 3 points on the top face of the central block from COMSOL the displacement and orientation of the vector can be found after deformation. Again determining the location of the tip of the vector gives the location of the tool tip after deformation. The magnitude of the difference between these two vectors yields the displacement. Equation E.7 shows this mathematically. R_0 is used to indicate the vector before deformation, R_{def} is used to indicate the vector after deformation and Δr is used to indicate the displacement of the tool tip.

$$\Delta r = | R_{def} - R_0 | \quad (E.7)$$

6. Natural frequency, during high speed motion it is essential that the natural frequency of the sensor is not excited. Setting an exact requirement for this constraint is challenging. Commercially available sensors and measurements of the dynamic response of 6 axis F/M sensors in literature have been used as

a reference to set a value for this constraint [146],[126]. Values ranging from 1.0 to 2.6kHz were found, 2.0kHz was set as the constraint value. Equation E.8 shows the constraint mathematically. In the FEM model used for optimization the parts used for the air flow are not considered to save computational effort. These parts are not expected to change the sensor stiffness significantly. However they will add mass to the sensor decreasing the eigenfrequency. The eigenfrequency of the full section will be analysed in section E.1 and needs to be above 1.0kHz, the lowest bound found acceptable in literature.

$$\omega_n > 2000\text{Hz} \quad (\text{E.8})$$

7. Absolute design variable limits, the design variables have a limited range as explained in section E.0.1. This leads to the constraint as shown in equation E.9.

$$\begin{aligned} 8 \text{ mm} < b < 15 \text{ mm} \\ 8 \text{ mm} < h < 21 \text{ mm} \\ 15 \text{ mm} < H < 25 \text{ mm} \\ 15 \text{ mm} < L < 25 \text{ mm} \\ 0.7 \text{ mm} < t < 3 \text{ mm} \end{aligned} \quad (\text{E.9})$$

8. Relative design variable limit, the height of the strain measuring beams may not exceed the height of the thin plates. If this happens the sensor geometry will become invalid. To ensure a sufficiently large difference the constraint shown in equation E.10 is used

$$H > 0.9 \cdot h \quad (\text{E.10})$$

E.0.2 Optimizer

An optimizer changes the design variables $\vec{X} = [b, h, H, L, t]$ until a local minimum of the cost function is found. Many different methods of optimization are available, to obtain a trustworthy optimization result the optimizer should be determined with consideration. In this case the optimization problem is constrained and expected to be non-linear. For such problems sequential quadratic programming SQP is often used. SQP a gradient based optimizer which is known for its robustness and fast convergence [148].

In literature the (SQP) has also proven to be well suited for this type of optimization problem [108], [109], [139]. This optimization algorithm is also available in Matlab and will be used in this work.

The SQP method determines the design improvement direction of the design variables by sequentially solving quadratic programming (QP) sub-problems. Each iteration the gradient of the cost function and constraints is determined. This is done using a numerical approximation, equation E.11 shows the gradient of the cost function is determined, ΔX_j is a small perturbation of the j 'th design variable.

$$\frac{\partial f}{\partial X_j} \approx \frac{f(X_j + \Delta X_j) - f(X_j)}{\Delta X_j} \quad (\text{E.11})$$

To determine these gradients the FEM model has to be calculated several times each iteration of the optimization scheme. Using the gradient information the direction of fastest improvement, meeting the constraints, is determined. If the stop conditions are not met Matlab changes the design variables and a new iteration starts.

Optimizer setting

The settings of the optimizer have to be set specifically for this optimization problem. The most important settings contain the stop conditions, the optimizer step size and the finite difference step size.

The optimizer told to stop under two conditions. Firstly if objective function does not decrease more than 0.01 for one iteration to the next. Secondly if 50 optimization cycles are reached, in literature optimizes find there optimum ranging form 5 to 40 iterations [109], [156].

The minimum step the design variables have to make is set to 0.05mm. This step size was set in consultation with the CNC workshop at the TU Delft responsible for the milling of the sensor structure. Picking a smaller step in design variables will lead to design with a higher level of detail than is allowed by the manufacturer. This setting also helps avoid the optimizer getting stuck in very shallow local minimal

Finally the finite difference step size has to be set courser than standard. During the optimization runs it was noted that the optimizer had trouble finding the direction of fastest decrease of the optimization function is the finite difference step size was set to small. This is likely because there are many local minima on the cost function, taking a larger step size will result in studding the global trend more than the local trend.

FEM and mesh setting

Similarly to picking the correct optimization algorithm and setting, the FEM analysis should should also be considered carefully. Firstly the correct material and boundary conditions have to be selected. The material 7075 T6 aluminium, is part of the standard COMSOL material library. For the boundary conditions either the central block of the outer rim has to be fixed. The part that is not fixed is used to applied the external load.

The connection rim was constrained using a fixed boundary condition. The central block is used to exert the external loads. This is because in COMSOL only forces can be applied, moments have to be created by applying two anti parallel forces. As the length of the strain measuring beam changes the position of the mounting holes in the connection rim change accordingly. The location of the connection holes in the central block do however not change position. The holes in the central block provide a constant moment arm for the anti parallel forces.

Secondly a proper mesh should be created. The model is changing in size and shape each iteration of the optimizer. The mesh needs to be automatically generated for any set of design variables. If a to course mesh is picked the results of the FEM analysis are not trustworthy. On the other hand if a to fine mesh is picked the FEM calculation will be come very computationally expensive. The mesh was design for the most demanding set of design variables $\vec{X} = [b, h, H, L, t] = [8, 8, 25, 0.7, 25] \text{ mm}$. The strain measuring beams and thin plates are taken as small as possible requiring a

finer mesh. The thin plate height and the strain measuring beam length were picked as large as possible. This creates a larger thin plate and slender longer beams which are harder geometries to mesh properly. A mesh sufficient for the most design variables structure will also achieve the desired performance on less demanding design variables.

To mesh the sensor structure the sensor was divided in 6 domains. Each domain has its own mesh size. Areas requiring more detail are meshed finer than areas which do not require the same level of detail. In this manor each domain can be meshed with just the right amount of detail. The selected domains from fine to course are, the thin plate, the strain gauge surface, the milled corners, the strain measuring beams, the central block and the connection rim.

To study which level of detail was required a mesh convergence study was performed. In this study the mesh is iterative refined. At each iteration the strain matrix was determined. If the mesh is sufficiently fine further refinement will not change the calculated strain. By iteration number against the measured strain this point can be identified. Figure E.3a shows the results of the mesh convergence study. For easy comprising for the relative change, the y-axis of figure E.3a shows the measured strain with respect to the measured strain of the first refinement step cycle. In E.3a it can be seen that the calculated strain barley change after point refinement step 6. This mesh size was picked for all future calculations.

COMSOL also offers a mesh quality statistic, this was used as a second check for the selected mesh. To determine the mesh quality a quality measure has to be picked. For this work the standard skewness measure was picked, however other quantities can also be used [154]. The skewness measure ranges form 0 to 1, a score of 1 indicates the optimal element according the skewness quality measure. A low quality is indicated with a score near 0. For most application a quality measure score below 0.1 is seen as a poor quality [154]. If the quality score of any of the elements is below 0.1 the mesh setting, mesh size or domain selection has to be reviewed again and changed until the quality improves sufficiently. Figure E.3b shown the mesh quality study for all elements and the lowest element score. A performance score near one is indicate in green, a performance score near zero is indicated in red. For the designed mesh and determined mesh size the lowest mesh element scores is 0.44. The lowest element scores above 0.1, the mesh design and size is picked good enough according to this performance measure.

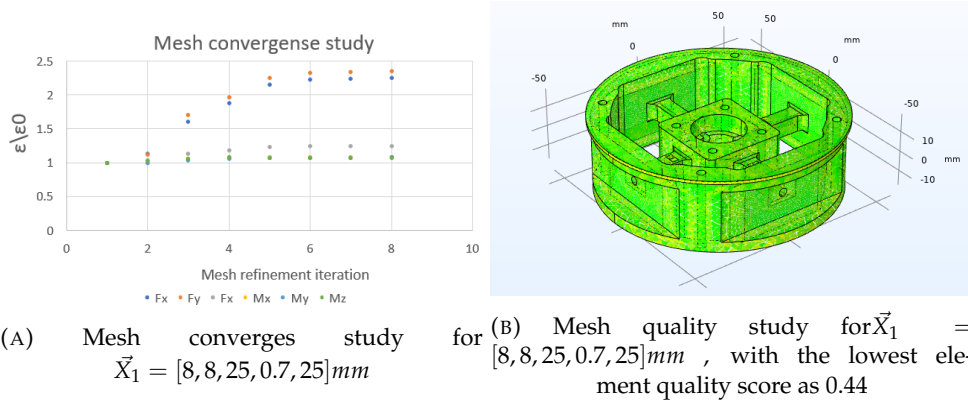


FIGURE E.3: Mesh convergence and mesh quality study for the sets of design variables $\vec{X}_1 = [8, 8, 25, 0.7, 25] mm$

Lastly the measured strain can be compared to designs found in literature. If the strain found in the FEM calculation is similar to that is found in literature the model is likely correct and the mesh is sufficient. The strain found during this calculations compared to those found in literature are shown in table E.1. For this comparison only the diagonal terms of the strain matrix were considered. The load applied and dimensions to the sensor were similar to the load applied in literature. It is concluded that the result of the simulation is likely to be correct because the calculated strain and the strain from literature are in the same order of magnitude.

Measuring direction	strain from design $\frac{\mu m}{m}$	strain from [139] $\frac{\mu m}{m}$	strain from $\frac{\mu m}{m}$ [143]
ϵ_{Fx}	429.1	350.0	174
ϵ_{Fy}	428.1	350.1	174
ϵ_{Fz}	301.3	437.8	1872
ϵ_{Mx}	1302.3	859.9	1375
ϵ_{My}	1302.1	859.9	1375
ϵ_{Mz}	734.26	486.2	1486

TABLE E.1: Comparing the diagonal elements of the strain matrix strain

As an extra conformation the mesh quality and the convergence study were also studied for several different sets of design variables. Figure E.4a and E.4c shows the results of mesh convergence studied for two other sets of design variables $\vec{X}_2 = [11.5, 14.5, 20, 1.5, 20] mm$ and $\vec{X}_3 = [15, 21, 25, 3, 25] mm$ respectively. Figure E.4b and E.4d shows the mesh quality for these design variables. All studied cases showed a good quality mesh and convergence at the selected mesh size. Therefore the mesh is suited to be used during the optimization scheme.

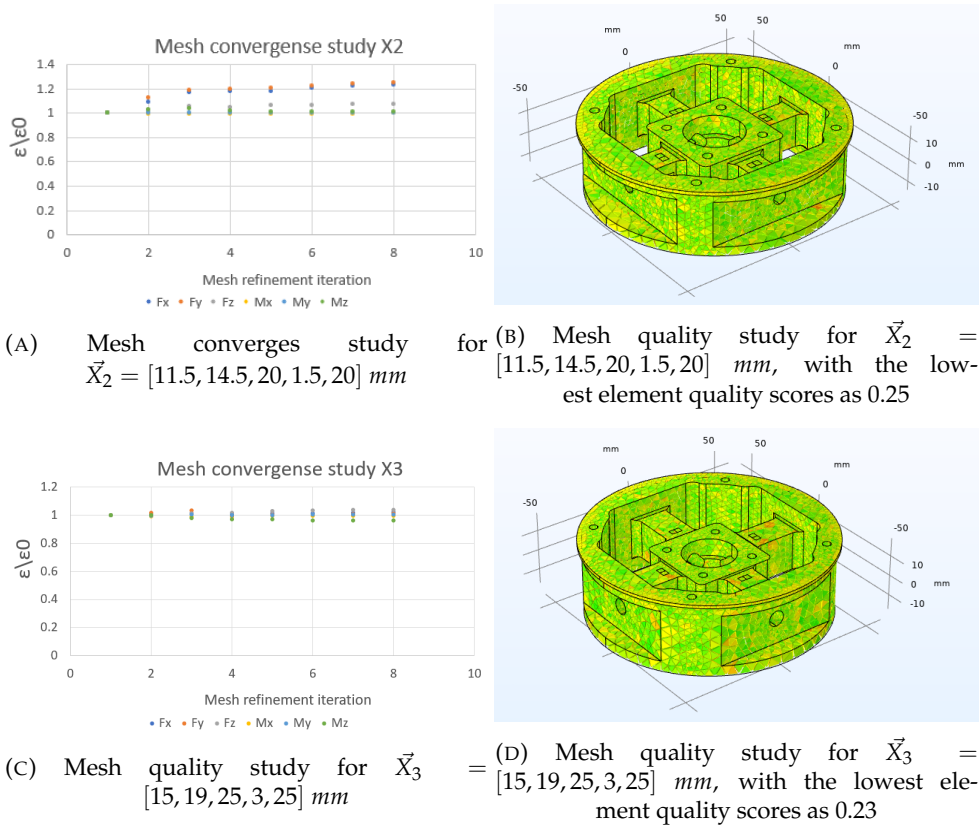


FIGURE E.4: Mesh convergence and mesh quality study performed for conformation for the sets of design variables $\vec{X}_2 = [11.5, 14.5, 20, 1.5, 20] \text{ mm}$ and $\vec{X}_3 = [15, 19, 25, 3, 25] \text{ mm}$

E.0.3 Optimization results

The described optimization scheme was calculated for several different starting condition. During these calculations a few key observations were made which were used to reduce the computational time by change the optimization scheme. Firstly it was noted that the Von Mises stress constraint was never violated. This observation was validated by calculating the maximum Von Mises stress for the most compliant version of sensor structure. Secondly it was observed that the design variables b and t converged to there lower bound for every optimization run that was preformed. The change of b and t for three different sets of starting design variables are shown in figure E.5 Since the design variables b and t are optimal at there upper and lower bound, these design variables can be made fixed in the optimization scheme. Removing two out the five design variables is expected to reduce the computational time by 40%.

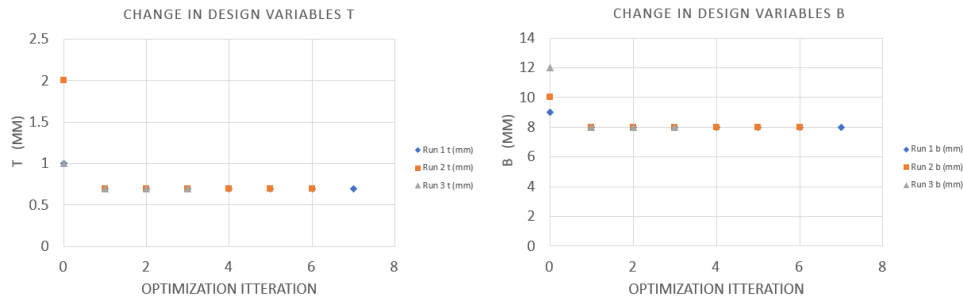
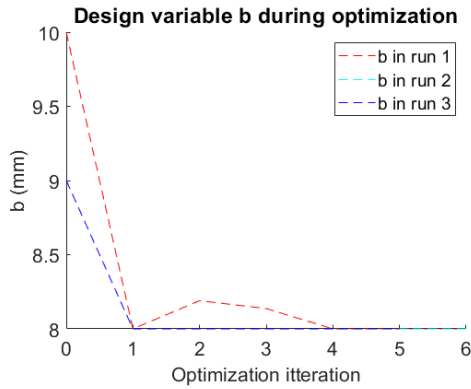
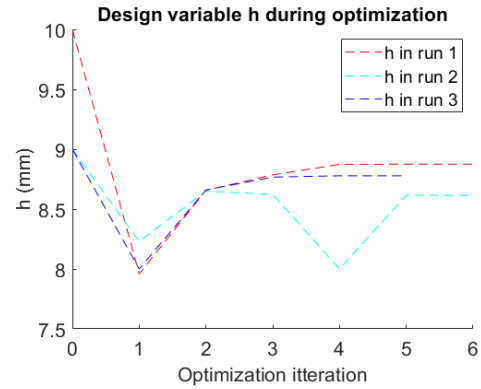


FIGURE E.5: Plots showing the change in design variables b and t for three different starting points

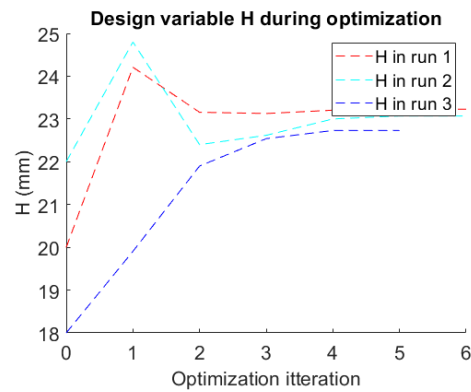
After setting b and t constant and equal to their lower bound the optimization scheme was computed again for a larger set of starting points to increase the odds of finding the global minimum. Figure E.6 shows the results of 5 optimization calculations all considering different starting variables. From these calculations the final sensor dimensions were picked as $X_{final} = [8, 8.75, 23.25, 19.5, 0.7]$ mm, the sensor was made according to these design variables.



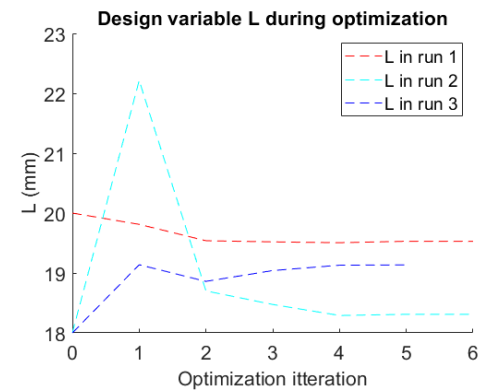
(A) The change of the design variable b for five different optimization runs. A different set of design variables is used each optimization run



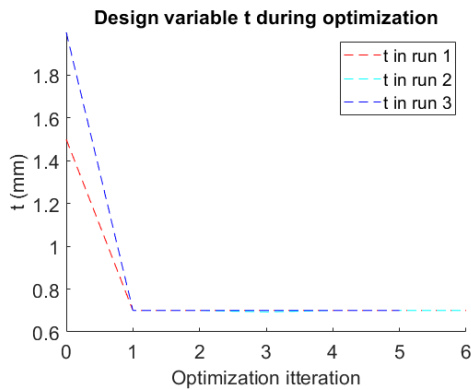
(B) The change of the design variable h for five different optimization runs. A different set of design variables is used each optimization run



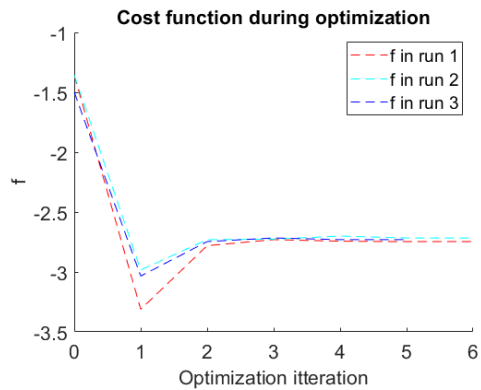
(C) The change of the design variable H for five different optimization runs. A different set of design variables is used each optimization run



(D) The change of the design variable L for five different optimization runs. A different set of design variables is used each optimization run



(E) The change of the design variable t for five different optimization runs. A different set of design variables is used each optimization run



(F) The change of the cost function for five different optimization runs. A different set of design variables is used each optimization run

FIGURE E.6: Results of the optimization runs

E.1 Analysis of the final design

For comprising to the fabricated sensor and to verify if the most important constrains were met the final design was analysed to determine mass, eigenfrequency, strain matrix and cross coupling matrix.

E.1.1 Mass and eigenfrequency

The mass of the sensor is constant and is computed by the volume integral of the density 7075-T6 aluminum in COMSOL. This results in a total sensor mass of 449.6g, this is equal to the maximum constraint that was set. This constraint is therefore an active constraint limiting further decrease of the cost function.

The eigenfrequency of the sensor is highly dependent of the way it is constraint. To perform a measurement either the connection rim or the central block is constraint to be fixed. The stiffness of the measuring part of sensor is independent of this choice, however the amount of moving mass does change according to this choice. When the connection rim is constraint to be fixed the moving mass only consists of the central block and the strain measuring beams. This will result in the lowest moving mass with an eigenfrequency of 2511Hz as shown in figure E.7a. This value is approaching the higher values found in literature. If the central block is constraint to be fixed the moving mass consists of the strain measuring beams, the connecting rim and all the air flow passage parts. This is the intended use case while performing measurement during case packing and will result in a lower eigenfrequency of 1092Hz as shown in figure E.7c. This eigenfrequency is sufficient as stated in section E.0.1.

If the sensor would be used without the airflow integration parts the shape and frequency of the first eigenmode change. Firstly the frequency is much higher at 1892Hz because the moving mass is decreased. Secondly the connection rim will start to deform non-uniformly as shown in figure E.7c. This can be explained by the stiffness added by bottom plate of the air flow passing parts. This eigenmode does however not strain the strain gauges and will not directly influence the measurements. The second eigenmode directly influence the measurements and has a frequency of 2006Hz

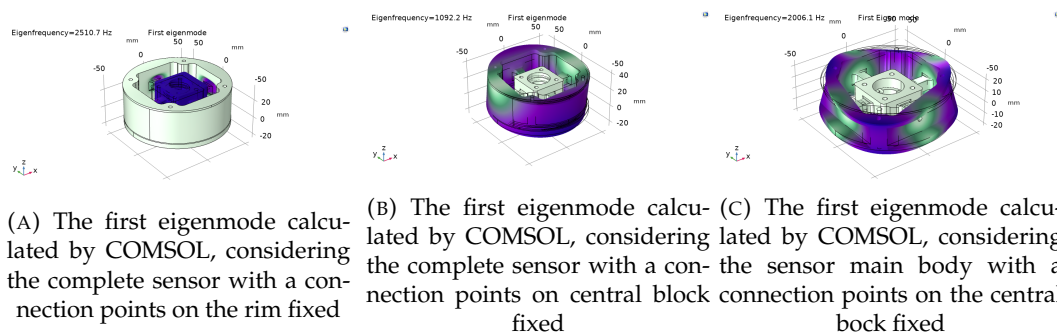


FIGURE E.7: Showing the effect of the air flow passage parts and constraint points on the determined eigenfrequency

Bibliography

- [1] F. Castellano, *Future of the agrifood industry*, Feb. 2020. [Online]. Available: <https://www.toptal.com/finance/market-research-analysts/agrifood-industry>.
- [2] *AgFunder AgriFood Tech Investing Report - 2018*, 2018. [Online]. Available: <https://agfunder.com/research/agrifood-tech-investing-report-2018/>.
- [3] *AgFunder Agri-FoodTech Investing Report - 2019*, 2019. [Online]. Available: <https://agfunder.com/research/agfunder-agrifood-tech-investing-report-2019/>.
- [4] L. Searby, "Automatic moves," *Packing News*, pp. 52–52, 2006. [Online]. Available: www.scopus.com.
- [5] H. Pham and Q. C. Pham, "Critically fast pick-and-place with suction cups," *Proceedings - IEEE International Conference on Robotics and Automation*, vol. 2019-May, pp. 3045–3051, 2019, ISSN: 10504729. DOI: 10.1109/ICRA.2019.8794081.
- [6] L. Berkel, *BPA NEEMT ACTIVITEITEN RACUPACK OVER*, Jul. 2013. [Online]. Available: <https://www.packonline.nl/nieuws/bpa-neemt-activiteiten-racupack-over>.
- [7] *IRB 360 Data - IRB 360 FlexPicker (Robots industriels)*, 2020. [Online]. Available: <https://new.abb.com/products/robotics/fr/robots-industriels/irb-360-flexpicker/irb-360-data>.
- [8] T. M. Huh, K. Sanders, M. Danielczuk, M. Li, K. Goldberg, and H. S. Stuart, "A Multi-Chamber Smart Suction Cup for Adaptive Gripping and Haptic Exploration," 2021. [Online]. Available: <http://arxiv.org/abs/2105.02345>.
- [9] J. IQBAL, Z. H. KHAN, and A. KHALID, "Prospects of robotics in food industry," *Food Science and Technology*, vol. 37, pp. 159–165, 2017, ISSN: 0101-2061. [Online]. Available: http://www.scielo.br/scielo.php?script=sci_arttext&pid=S0101-20612017000200159&nrm=iso.
- [10] C. Connolly, "Feature ABB high-speed picking robots establish themselves in food packaging," vol. 4, pp. 281–284, 2007. DOI: 10.1108/01439910710749591.
- [11] V Nabat, M. D. L. O. Rodriguez, S. Krut, and F. Pierrot, "Par4: Very High Speed Parallel Robot for Pick-and-Place," in *IEEE/RSJ International Conference on Intelligent Robots and Systems*, 2005, pp. 553–558. DOI: 10.1109/IR0S.2005.1545143.
- [12] P. Y. Chua, T. Ilschner, and D. G. Caldwell, "Robotic manipulation of food products – a review," vol. 30, no. 4, pp. 345–354, 2003. DOI: 10.1108/01439910310479612.
- [13] J. de Jong, "Delft Center for Systems and Control,"

- [14] Z. Pan, J. Polden, N. Larkin, S. Van Duin, and J. Norrish, "Recent progress on programming methods for industrial robots," *Robotics and Computer-Integrated Manufacturing*, vol. 28, no. 2, pp. 87–94, 2012, ISSN: 07365845. DOI: [10.1016/j.rcim.2011.08.004](https://doi.org/10.1016/j.rcim.2011.08.004). [Online]. Available: <http://dx.doi.org/10.1016/j.rcim.2011.08.004>.
- [15] B. Fu, L. Chen, Y. Zhou, D. Zheng, Z. Wei, J. Dai, and H. Pan, "An improved A* algorithm for the industrial robot path planning with high success rate and short length," *Robotics and Autonomous Systems*, vol. 106, pp. 26–37, 2018, ISSN: 09218890. DOI: [10.1016/j.robot.2018.04.007](https://doi.org/10.1016/j.robot.2018.04.007). [Online]. Available: <https://doi.org/10.1016/j.robot.2018.04.007>.
- [16] H. Mikami, "Historical Evolution of Motor Technology," 2010.
- [17] W. Zhang, J. Mei, and Y. Ding, "Design and Development of a High Speed Sorting System Based on Machine Vision Guiding," *Physics Procedia*, vol. 25, pp. 1955–1965, 2012, ISSN: 1875-3892. DOI: [10.1016/j.phpro.2012.03.335](https://doi.org/10.1016/j.phpro.2012.03.335). [Online]. Available: <http://dx.doi.org/10.1016/j.phpro.2012.03.335>.
- [18] V. Shah, N. Gilke, V. Dhore, C. Phutane, and B. Kondhol, "Design of Gripper and Selection of Robotic Arm for Automation of a Pick and Place Process," in *Advances in Manufacturing Systems*, S. Kumar and K. P. Rajurkar, Eds., Singapore: Springer Singapore, 2021, pp. 95–107, ISBN: 978-981-33-4466-2.
- [19] N. P. Mahalik and A. N. Nambiar, "Trends in food packaging and manufacturing systems and technology," *Trends in Food Science and Technology*, vol. 21, no. 3, pp. 117–128, 2010, ISSN: 09242244. DOI: [10.1016/j.tifs.2009.12.006](https://doi.org/10.1016/j.tifs.2009.12.006). [Online]. Available: <http://dx.doi.org/10.1016/j.tifs.2009.12.006>.
- [20] B. Zhang, Y. Xie, J. Zhou, K. Wang, and Z. Zhang, "State-of-the-art robotic grippers, grasping and control strategies, as well as their applications in agricultural robots: A review," *Computers and Electronics in Agriculture*, vol. 177, p. 105694, 2020, ISSN: 0168-1699. DOI: <https://doi.org/10.1016/j.compag.2020.105694>. [Online]. Available: <http://www.sciencedirect.com/science/article/pii/S0168169920311030>.
- [21] Y. Kuriyama, Y. Okino, Z. Wang, and S. Hirai, "A Wrapping Gripper for Packaging Chopped and Granular Food Materials," 2019, pp. 114–119. DOI: [10.1109/ROBOSOFT.2019.8722745](https://doi.org/10.1109/ROBOSOFT.2019.8722745).
- [22] Z. Wang and S. Hirai, "A Soft Gripper with Adjustable Stiffness and Variable Working Length for Handling Food Material," 2018, pp. 25–29. DOI: [10.1109/RCAR.2018.8621676](https://doi.org/10.1109/RCAR.2018.8621676).
- [23] C. Gosselin, F. Pelletier, and T. Laliberte, "An anthropomorphic underactuated robotic hand with 15 dofs and a single actuator," in *2008 IEEE International Conference on Robotics and Automation*, 2008, pp. 749–754. DOI: [10.1109/ROBOT.2008.4543295](https://doi.org/10.1109/ROBOT.2008.4543295).
- [24] Y. J. Kim, H. Song, and C. Y. Maeng, "Blt gripper: An adaptive gripper with active transition capability between precise pinch and compliant grasp," *IEEE Robotics and Automation Letters*, vol. 5, no. 4, pp. 5518–5525, 2020, ISSN: 23773766. DOI: [10.1109/LRA.2020.3008137](https://doi.org/10.1109/LRA.2020.3008137).
- [25] H. S. Stuart, M. Bagheri, S. Wang, H. Barnard, A. L. Sheng, M. Jenkins, and M. R. Cutkosky, "Suction helps in a pinch: Improving underwater manipulation with gentle suction flow," *IEEE International Conference on Intelligent Robots and Systems*, vol. 2015-Decem, pp. 2279–2284, 2015, ISSN: 21530866. DOI: [10.1109/IR0S.2015.7353683](https://doi.org/10.1109/IR0S.2015.7353683).

- [26] G. Fantoni, M. Santochi, G. Dini, K. Tracht, B. Scholz-Reiter, J. Fleischer, T. Kristoffer Lien, G. Seliger, G. Reinhart, J. Franke, H. Nørgaard Hansen, and A. Verl, "Grasping devices and methods in automated production processes," *CIRP Annals*, vol. 63, no. 2, pp. 679–701, 2014, ISSN: 0007-8506. DOI: <https://doi.org/10.1016/j.cirp.2014.05.006>. [Online]. Available: <http://www.sciencedirect.com/science/article/pii/S0007850614001887>.
- [27] J. Walker, T. Zidek, C. Harbel, S. Yoon, F. S. Strickland, S. Kumar, and M. Shin, "Soft Robotics: A Review of Recent Developments of Pneumatic Soft Actuators," *Actuators*, vol. 9, no. 1, 2020, ISSN: 2076-0825. DOI: [10.3390/act9010003](https://doi.org/10.3390/act9010003). [Online]. Available: <https://www.mdpi.com/2076-0825/9/1/3>.
- [28] J. Shintake, V. Cacucciolo, D. Floreano, and H. Shea, "Soft Robotic Grippers," *Advanced Materials*, vol. 30, no. 29, p. 1707035, 2018. DOI: <https://doi.org/10.1002/adma.201707035>. [Online]. Available: <https://onlinelibrary.wiley.com/doi/abs/10.1002/adma.201707035>.
- [29] P. Boyraz, G. Runge, and A. Raatz, "An Overview of Novel Actuators for Soft Robotics," *Actuators*, vol. 7, p. 48, 2018. DOI: [10.3390/act7030048](https://doi.org/10.3390/act7030048).
- [30] S. H. Park, W. J. Chung, H. G. Hwang, H. R. Kim, M. J. Jee, and W. C. Hong, "ANSYS®-Based Gear Stress Analysis of a Lightweight 3-DOF Wrist Mechanism for a Parallel Robot with Expanded Workspace," *2020 IEEE International Conference on Mechatronics and Automation, ICMA 2020*, pp. 750–755, 2020. DOI: [10.1109/ICMA49215.2020.9233768](https://doi.org/10.1109/ICMA49215.2020.9233768).
- [31] Marel, *Marel's new RoboBatcher Box is the world's leading intelligent robotic solution for fish packing*, Feb. 2021. [Online]. Available: <https://marel.com/en/news/marel-s-new-robobatcher-box-is-the-world-s-leading-intelligent-robotic-solution-for-fish-packing>.
- [32] A. Robotics, *Meat Gripper*, 2008. [Online]. Available: <https://www.appliedrobotics.com/products/automation/grippers/meat-gripper/>.
- [33] L. Birglen and T. Schlicht, "A statistical review of industrial robotic grippers," *Robotics and Computer-Integrated Manufacturing*, vol. 49, pp. 88–97, Feb. 2018. DOI: [10.1016/j.rcim.2017.05.007](https://doi.org/10.1016/j.rcim.2017.05.007). [Online]. Available: <https://www.sciencedirect.com.tudelft.idm.oclc.org/science/article/pii/S0736584516304240>.
- [34] W. Chen, S. Zhao, and S. L. Chow, "Grippers and End Effectors," in *Handbook of Manufacturing Engineering and Technology*, A. Nee, Ed., London: Springer London, 2013, pp. 1–32, ISBN: 978-1-4471-4976-7. DOI: [10.1007/978-1-4471-4976-7_96-1](https://doi.org/10.1007/978-1-4471-4976-7_96-1). [Online]. Available: https://doi.org/10.1007/978-1-4471-4976-7_96-1.
- [35] S. M. G. GmbH, *No Title*. [Online]. Available: <https://schunk.com/fileadmin/pim/docs/IM0019885.PDF>.
- [36] G. Carbone, "No Title," in *Grasping in robotics*, Springer, 2013, pp. 110–135.
- [37] D. R. R. Rebollo, P. Ponce, and A. Molina, "From 3 fingers to 5 fingers dexterous hands," *Advanced Robotics*, vol. 31, no. 19-20, pp. 1051–1070, 2017. DOI: [10.1080/01691864.2017.1393349](https://doi.org/10.1080/01691864.2017.1393349). [Online]. Available: <https://doi.org/10.1080/01691864.2017.1393349>.
- [38] M. Quigley, C. Salisbury, A. Ng, and J. Salisbury, "Mechatronic design of an integrated robotic hand," *The International Journal of Robotics Research*, vol. 33, pp. 706–720, 2014.

- [39] F. III, J. Weisz, A. de la Llera, P. Allen, and R. Howe, "Towards a design optimization method for reducing the mechanical complexity of underactuated robotic hands," *Proceedings - IEEE International Conference on Robotics and Automation*, pp. 2843–2850, 2012. DOI: [10.1109/ICRA.2012.6225010](https://doi.org/10.1109/ICRA.2012.6225010).
- [40] Z. Xu, V. Kumar, and E. Todorov, "A low-cost and modular, 20-DOF anthropomorphic robotic hand: Design, actuation and modeling," *IEEE-RAS International Conference on Humanoid Robots*, vol. 2015, pp. 368–375, 2015. DOI: [10.1109/HUMANOIDS.2013.7030001](https://doi.org/10.1109/HUMANOIDS.2013.7030001).
- [41] R. A. J. Stavenuiter, L. Birglen, and J. L. Herder, "A planar underactuated grasper with adjustable compliance," *Mechanism and Machine Theory*, vol. 112, pp. 295–306, 2017, ISSN: 0094-114X. DOI: <https://doi.org/10.1016/j.mechmachtheory.2016.08.001>. [Online]. Available: <http://www.sciencedirect.com/science/article/pii/S0094114X16301690>.
- [42] D. Esposito, S. Savino, C. Cosenza, G. D. Gargiulo, A. Fratini, G. Cesarelli, and P. Bifulco, "Study on the Activation Speed and the Energy Consumption of "Federica" Prosthetic Hand," in *XV Mediterranean Conference on Medical and Biological Engineering and Computing – MEDICON 2019*, J. Henriques, N. Neves, and P. de Carvalho, Eds., Cham: Springer International Publishing, 2020, pp. 594–603, ISBN: 978-3-030-31635-8.
- [43] G. A. Kragten, "Underactuated hands: fundamentals, performance analysis and design," Ph.D. dissertation, Delft University of Technology, 2011, 131–131. [Online]. Available: <http://resolver.tudelft.nl/uuid:e6e4b937-08ef-48d7-b380-03eaa98fbca8>.
- [44] J. Gallego Sanchez and J. Herder, "Synthesis Methods in Compliant Mechanisms: An Overview," in *Proceedings of the ASME Design Engineering Technical Conference*, vol. 7, 2009. DOI: [10.1115/DETC2009-86845](https://doi.org/10.1115/DETC2009-86845).
- [45] B. Belzile and L. Birglen, "A compliant self-adaptive gripper with proprioceptive haptic feedback," *Autonomous Robots*, vol. 36, pp. 79–91, 2014.
- [46] H. Zhou, A. Mohammadi, D. Oetomo, and G. Alici, "A Novel Monolithic Soft Robotic Thumb for an Anthropomorphic Prosthetic Hand," *IEEE Robotics and Automation Letters*, vol. 4, no. 2, pp. 602–609, 2019. DOI: [10.1109/LRA.2019.2892203](https://doi.org/10.1109/LRA.2019.2892203).
- [47] N. Mouazé and L. Birglen, "Deformation Modeling of Compliant Robotic Fingers Grasping Soft Objects," *Journal of Mechanisms and Robotics*, vol. 13, no. 1, 2020, ISSN: 1942-4302. DOI: [10.1115/1.4047988](https://doi.org/10.1115/1.4047988). [Online]. Available: <https://doi.org/10.1115/1.4047988>.
- [48] R. Mutlu, G. Alici, M. in het Panhuis, and G. Spinks, "3D Printed Flexure Hinges for Soft Monolithic Prosthetic Fingers," *Soft Robotics*, vol. 3, pp. 120–133, 2016. DOI: [10.1089/soro.2016.0026](https://doi.org/10.1089/soro.2016.0026).
- [49] M. Manti, T. Hassan, G. Passetti, N. d'Elia, M. Cianchetti, and C. Laschi, "An Under-Actuated and Adaptable Soft Robotic Gripper," in *Biomimetic and Biohybrid Systems*, S. P. Wilson, P. F. M. J. Verschure, A. Mura, and T. J. Prescott, Eds., Cham: Springer International Publishing, 2015, pp. 64–74, ISBN: 978-3-319-22979-9.
- [50] T. Hassan, M. Manti, G. Passetti, N. d'Elia, M. Cianchetti, and C. Laschi, "Design and development of a bio-inspired, under-actuated soft gripper," in *2015 37th Annual International Conference of the IEEE Engineering in Medicine and Biology Society (EMBC)*, 2015, pp. 3619–3622. DOI: [10.1109/EMBC.2015.7319176](https://doi.org/10.1109/EMBC.2015.7319176).

- [51] G. Hao, H. Li, A. Nayak, and S. Caro, "Design of a Compliant Gripper With Multimode Jaws," *Journal of Mechanisms and Robotics*, vol. 10, 2018. DOI: [10.1115/1.4039498](https://doi.org/10.1115/1.4039498).
- [52] C. Blanes, M. Mellado, and P. Beltran, "Novel Additive Manufacturing Pneumatic Actuators and Mechanisms for Food Handling Grippers," *Actuators*, vol. 3, no. 3, pp. 205–225, 2014, ISSN: 2076-0825. [Online]. Available: <https://www.mdpi.com/2076-0825/3/3/205>.
- [53] C.-H. Liu, G.-F. Huang, C.-H. Chiu, and T.-Y. Pai, "Topology Synthesis and Optimal Design of an Adaptive Compliant Gripper to Maximize Output Displacement," *Journal of Intelligent & Robotic Systems*, vol. 90, 2018. DOI: [10.1007/s10846-017-0671-x](https://doi.org/10.1007/s10846-017-0671-x).
- [54] C. H. Liu, F. M. Chung, Y. Chen, C. H. Chiu, and T. L. Chen, "Optimal Design of a Motor-Driven Three-Finger Soft Robotic Gripper," *IEEE/ASME Transactions on Mechatronics*, vol. 25, no. 4, pp. 1830–1840, 2020. DOI: [10.1109/TMECH.2020.2997743](https://doi.org/10.1109/TMECH.2020.2997743).
- [55] P. Steutel, G. Kragten, and J. Herder, "Design of an Underactuated Finger With a Monolithic Structure and Largely Distributed Compliance," vol. 2, 2010. DOI: [10.1115/DETC2010-28127](https://doi.org/10.1115/DETC2010-28127).
- [56] M Netzev, A Angleraud, and R Pieters, "Soft Robotic Gripper With Compliant Cell Stacks for Industrial Part Handling," *IEEE Robotics and Automation Letters*, vol. 5, no. 4, pp. 6821–6828, 2020. DOI: [10.1109/LRA.2020.3020546](https://doi.org/10.1109/LRA.2020.3020546).
- [57] Y.-C Chiu, P. Y. Yang, and S Chen, "Development of the end-effector of a picking robot for greenhouse-grown tomatoes," *Applied Engineering in Agriculture*, vol. 29, pp. 1001–1009, 2013. DOI: [10.13031/aea.29.9913](https://doi.org/10.13031/aea.29.9913).
- [58] J. M. Krahn, F Fabbro, and C Menon, "A Soft-Touch Gripper for Grasping Delicate Objects," *IEEE/ASME Transactions on Mechatronics*, vol. 22, no. 3, pp. 1276–1286, 2017. DOI: [10.1109/TMECH.2017.2663322](https://doi.org/10.1109/TMECH.2017.2663322).
- [59] R Mukaide, M Watanabe, K Tadakuma, Y Ozawa, T Takahashi, M Konyo, and S Tadokoro, "Radial-Layer Jamming Mechanism for String Configuration," *IEEE Robotics and Automation Letters*, vol. 5, no. 4, pp. 5221–5228, 2020. DOI: [10.1109/LRA.2020.2983679](https://doi.org/10.1109/LRA.2020.2983679).
- [60] Y. Gao, X. Huang, I. S. Mann, and H.-J. Su, "A Novel Variable Stiffness Compliant Robotic Gripper Based on Layer Jamming," *Journal of Mechanisms and Robotics*, vol. 12, no. 5, 2020, ISSN: 1942-4302. DOI: [10.1115/1.4047156](https://doi.org/10.1115/1.4047156). [Online]. Available: <https://doi.org/10.1115/1.4047156>.
- [61] J. Amend, N. Cheng, S. Fakhouri, and B. Culley, "Soft Robotics Commercialization: Jamming Grippers from Research to Product," *Soft Robotics*, vol. 3, no. 4, pp. 213–222, 2016. DOI: [10.1089/soro.2016.0021](https://doi.org/10.1089/soro.2016.0021). [Online]. Available: <https://doi.org/10.1089/soro.2016.0021>.
- [62] S Davis, J. O. Gray, and D. G. Caldwell, "An end effector based on the Bernoulli principle for handling sliced fruit and vegetables," *Robotics and Computer-Integrated Manufacturing*, vol. 24, no. 2, pp. 249–257, 2008, ISSN: 0736-5845. DOI: <https://doi.org/10.1016/j.rcim.2006.11.002>. [Online]. Available: <http://www.sciencedirect.com/science/article/pii/S0736584506001347>.
- [63] X. F. Brun and S. N. Melkote, "Evaluation of Handling Stresses Applied to EFG Silicon Wafer using a Bernoulli Gripper," in *2006 IEEE 4th World Conference on Photovoltaic Energy Conference*, vol. 2, 2006, pp. 1346–1349. DOI: [10.1109/WCPEC.2006.279680](https://doi.org/10.1109/WCPEC.2006.279680).

- [64] V. Savkiv, R. Mykhailyshyn, F. Duchon, and O. Fendo, "Justification of design and parameters of Bernoulli–vacuum gripping device," *International Journal of Advanced Robotic Systems*, vol. 14, no. 6, p. 1729881417741740, 2017. DOI: [10.1177/1729881417741740](https://doi.org/10.1177/1729881417741740). [Online]. Available: <https://doi.org/10.1177/1729881417741740>.
- [65] W Park, S Seo, and J Bae, "A Hybrid Gripper With Soft Material and Rigid Structures," *IEEE Robotics and Automation Letters*, vol. 4, no. 1, pp. 65–72, 2019. DOI: [10.1109/LRA.2018.2878972](https://doi.org/10.1109/LRA.2018.2878972).
- [66] H. G. El Bana and A Abbas, "A Novel Design of the Utilisation of Soft Grippers in Loading and Unloading Applications," in *2020 International Conference on Innovative Trends in Communication and Computer Engineering (ITCE)*, 2020, pp. 158–163. DOI: [10.1109/ITCE48509.2020.9047779](https://doi.org/10.1109/ITCE48509.2020.9047779).
- [67] S. R. Inc., *Solving Difficult Applications with Soft Robotics*. [Online]. Available: <https://www.youtube.com/watch?v=mfa7LQ5CW20>.
- [68] J. Shintake, S. Rosset, B. Schubert, D. Floreano, and H. Shea, "Versatile Soft Grippers with Intrinsic Electroadhesion Based on Multifunctional Polymer Actuators," *Advanced materials (Deerfield Beach, Fla.)*, vol. 28, 2015. DOI: [10.1002/adma.201504264](https://doi.org/10.1002/adma.201504264).
- [69] A. Yamaguchi, K. Takemura, S. Yokota, and K. Edamura, "A robot hand using electro-conjugate fluid," in *Proceedings - IEEE International Conference on Robotics and Automation*, 2011, pp. 5923–5928. DOI: [10.1109/ICRA.2011.5979691](https://doi.org/10.1109/ICRA.2011.5979691).
- [70] T. Nishida, Y. Okatani, and K. Tadakuma, "Development of Universal Robot Gripper Using MR α Fluid," *International Journal of Humanoid Robotics*, vol. 13, p. 1650017, 2016. DOI: [10.1142/S0219843616500171](https://doi.org/10.1142/S0219843616500171).
- [71] P. Motzki, J Kunze, A. York, and S Seelecke, "Energy-efficient SMA Vacuum Gripper System," 2016. DOI: [10.13140/RG.2.2.25486.97609](https://doi.org/10.13140/RG.2.2.25486.97609).
- [72] P. van Assenbergh, K. Zhang, J. G. Buijnsters, and D. Dodou, "Effect of lateral reinforcements on the adhesion and friction of micropillar adhesives," *Applied Physics A: Materials Science and Processing*, vol. 126, no. 10, pp. 1–9, 2020, ISSN: 14320630. DOI: [10.1007/s00339-020-03947-y](https://doi.org/10.1007/s00339-020-03947-y). [Online]. Available: <https://doi.org/10.1007/s00339-020-03947-y>.
- [73] *What are Hydraulic Grippers*, Sep. 2013. [Online]. Available: <https://www.mobilehydraulicstips.com/hydraulic-grippers/>.
- [74] K. Galloway, K. Becker, B. Phillips, J. Kirby, S. Licht, R. Wood, and D. Gruber, "Soft Robotic Grippers for Biological Sampling on Deep Reefs," *Soft Robotics*, vol. 3, 2016. DOI: [10.1089/soro.2015.0019](https://doi.org/10.1089/soro.2015.0019).
- [75] J. Tilli, A. Brando, and G. Fantoni, "Gripping Device for Heavy and Deformable Materials Handling: Concept, Design, Selection and Test," *Procedia CIRP*, vol. 21, pp. 373–378, 2014. DOI: [10.1016/j.procir.2014.03.166](https://doi.org/10.1016/j.procir.2014.03.166).
- [76] X.-Y. Guo, W.-B. Li, Q.-H. Gao, H. Yan, Y. Fei, and W Zhang, "Self-locking mechanism for variable stiffness rigid-soft gripper," *Smart Materials and Structures*, vol. 29, 2020. DOI: [10.1088/1361-665X/ab710f](https://doi.org/10.1088/1361-665X/ab710f).
- [77] Y. Li, Y. Chen, Y. Yang, and Y. Wei, "Passive Particle Jamming and Its Stiffening of Soft Robotic Grippers," *IEEE Transactions on Robotics*, vol. PP, pp. 1–10, 2017. DOI: [10.1109/TR0.2016.2636899](https://doi.org/10.1109/TR0.2016.2636899).

- [78] Y. Li, Y. Chen, Y. Yang, and Y. Li, "Soft Robotic Grippers Based on Particle Transmission," *IEEE/ASME Transactions on Mechatronics*, vol. 24, 2019. DOI: [10.1109/TMECH.2019.2907045](https://doi.org/10.1109/TMECH.2019.2907045).
- [79] Z. Wang, K. Or, and S. Hirai, "A dual-mode soft gripper for food packaging," *Robotics and Autonomous Systems*, vol. 125, p. 103427, 2020. DOI: [10.1016/j.robot.2020.103427](https://doi.org/10.1016/j.robot.2020.103427).
- [80] Y. Sun, Q. Zhang, and X. Chen, "Design and analysis of a flexible robotic hand with soft fingers and a changeable palm," *Advanced Robotics*, vol. 34, pp. 1–14, 2020. DOI: [10.1080/01691864.2020.1777197](https://doi.org/10.1080/01691864.2020.1777197).
- [81] Y. Yang, Y. Zhang, Z. Kan, J. Zeng, and M. Y. Wang, "Hybrid Jamming for Bioinspired Soft Robotic Fingers," *Soft Robotics*, vol. 7, no. 3, pp. 292–308, 2020. DOI: [10.1089/soro.2019.0093](https://doi.org/10.1089/soro.2019.0093). [Online]. Available: <https://doi.org/10.1089/soro.2019.0093>.
- [82] Z. Tang, J. Lu, and Z. Wang, "The development of a new variable stiffness soft gripper," *International Journal of Advanced Robotic Systems*, vol. 16, p. 172988141987982, 2019. DOI: [10.1177/1729881419879824](https://doi.org/10.1177/1729881419879824).
- [83] C Blanes, M Mellado, C Ortiz, and A Valera, "Technologies for robot grippers in pick and place operations for fresh fruits and vegetables [Tecnologías en garras robotizadas para operaciones de coger y dejar productos hortofrutícolas frescos]," *Spanish Journal of Agricultural Research*, vol. 9, no. 4, pp. 1130–1141, 2011. DOI: [10.5424/sjar/20110904-501-10](https://doi.org/10.5424/sjar/20110904-501-10). [Online]. Available: <https://www.scopus.com/inward/record.uri?eid=2-s2.0-82755163752&doi=10.5424%2Fsjar%2F20110904-501-10&partnerID=40&md5=fcdc1c87653ca19a82c2a555aa0dbb>.
- [84] L. Birglen and T. Schlicht, "A statistical review of industrial robotic grippers," *Robotics and Computer-Integrated Manufacturing*, vol. 49, pp. 88–97, 2018, ISSN: 0736-5845. DOI: <https://doi.org/10.1016/j.rcim.2017.05.007>. [Online]. Available: <http://www.sciencedirect.com/science/article/pii/S0736584516304240>.
- [85] J. S. Harris, "New Product Profile Chart," *Chemical and Engineering News*, vol. 39, no. 16, 110–119, Apr. 1963.
- [86] *Harris profile*, Apr. 2011. [Online]. Available: http://wikid.io.tudelft.nl/WikID/index.php/Harris_profile.
- [87] J. Falco, K. V. Wyk, and E. Messina, "No Title," *Performance Metrics and Test Methods for Robotic Hands*, Oct. 2018. DOI: <https://doi.org/10.6028/NIST.SP.1227-draf>.
- [88] R. Attota and S. Jahanmir, "Effect of Contact Pressure and Load on Wear of Alumina," *Wear*, vol. 251, pp. 980–984, 2001. DOI: [10.1016/S0043-1648\(01\)00739-6](https://doi.org/10.1016/S0043-1648(01)00739-6).
- [89] B Alfredsson, "A Study on Contact Fatigue Mechanisms," 2000.
- [90] T. L. Saaty, "How to make a decision: The analytic hierarchy process," *European Journal of Operational Research*, vol. 48, no. 1, pp. 9–26, 1990, ISSN: 0377-2217. DOI: [https://doi.org/10.1016/0377-2217\(90\)90057-I](https://doi.org/10.1016/0377-2217(90)90057-I). [Online]. Available: <http://www.sciencedirect.com/science/article/pii/S037722179090057I>.
- [91] K. Venkatesan, "A Comparison of Strengths and Weaknesses for Analytical Hierarchy Process," vol. 9, no. July, pp. 12–15, 2019.

- [92] C. C. Chen and C. C. Lan, "An Accurate Force Regulation Mechanism for High-Speed Handling of Fragile Objects Using Pneumatic Grippers," *IEEE Transactions on Automation Science and Engineering*, vol. 15, no. 4, pp. 1600–1608, 2018, ISSN: 15455955. DOI: [10.1109/TASE.2017.2757527](https://doi.org/10.1109/TASE.2017.2757527).
- [93] A. Koivikko, D. M. Drotlef, M. Sitti, and V. Sariola, "Magnetically switchable soft suction grippers," *Extreme Mechanics Letters*, vol. 44, p. 101 263, 2021, ISSN: 23524316. DOI: [10.1016/j.eml.2021.101263](https://doi.org/10.1016/j.eml.2021.101263). [Online]. Available: <https://doi.org/10.1016/j.eml.2021.101263>.
- [94] M. Maggi, G. Mantriota, and G. Reina, "Introducing POLYPUS: A novel adaptive vacuum gripper," *Mechanism and Machine Theory*, vol. 167, no. August 2021, p. 104 483, 2022, ISSN: 0094114X. DOI: [10.1016/j.mechmachtheory.2021.104483](https://doi.org/10.1016/j.mechmachtheory.2021.104483). [Online]. Available: <https://doi.org/10.1016/j.mechmachtheory.2021.104483>.
- [95] Y. h. Li, Q. j. Lei, C. Cheng, G. Zhang, W. Wang, and Z. Xu, "A review: machine learning on robotic grasping," no. March 2019, p. 54, 2019, ISSN: 1996756X. DOI: [10.1117/12.2522945](https://doi.org/10.1117/12.2522945).
- [96] Y. Gao, X. Huang, I. Mann, and H.-J. Su, "A Novel Variable Stiffness Compliant Robotic Gripper Based on Layer Jamming," *Journal of Mechanisms and Robotics*, vol. 12, pp. 1–10, 2020. DOI: [10.1115/1.4047156](https://doi.org/10.1115/1.4047156).
- [97] Z. Wang, H. Furuta, S. Hirai, and S. Kawamura, "A Scooping-Binding Robotic Gripper for Handling Various Food Products," *Frontiers in Robotics and AI*, vol. 8, no. March, pp. 1–13, 2021, ISSN: 22969144. DOI: [10.3389/frobt.2021.640805](https://doi.org/10.3389/frobt.2021.640805).
- [98] Y. Miao and J. Zheng, "Optimization design of compliant constant-force mechanism for apple picking actuator," *Comput. Electron. Agric.*, vol. 170, p. 105 232, 2020.
- [99] A. McLaren, Z. Fitzgerald, G. Gao, and M. Liarokapis, "A Passive Closing, Tendon Driven, Adaptive Robot Hand for Ultra-Fast, Aerial Grasping and Perching," 2019. DOI: [10.1109/IRoS40897.2019.8968076](https://doi.org/10.1109/IRoS40897.2019.8968076).
- [100] R. Whitaker, "Criticisms of the Analytic Hierarchy Process: Why they often make no sense," *Mathematical and Computer Modelling*, vol. 46, no. 7-8, pp. 948–961, 2007, ISSN: 08957177. DOI: [10.1016/j.mcm.2007.03.016](https://doi.org/10.1016/j.mcm.2007.03.016).
- [101] G. Mantriota, "Optimal grasp of vacuum grippers with multiple suction cups," *Mechanism and Machine Theory*, vol. 42, no. 1, pp. 18–33, 2007, ISSN: 0094114X. DOI: [10.1016/j.mechmachtheory.2006.02.007](https://doi.org/10.1016/j.mechmachtheory.2006.02.007).
- [102] —, "Optimal grasp of vacuum grippers with multiple suction cups," *Mechanism and Machine Theory*, vol. 42, no. 1, pp. 18–33, 2007, ISSN: 0094-114X. DOI: <https://doi.org/10.1016/j.mechmachtheory.2006.02.007>. [Online]. Available: <http://www.sciencedirect.com/science/article/pii/S0094114X06000541>.
- [103] G. Mantriota and A. Messina, "Theoretical and experimental study of the performance of flat suction cups in the presence of tangential loads," *Mechanism and Machine Theory*, vol. 46, no. 5, pp. 607–617, 2011, ISSN: 0094-114X. DOI: <https://doi.org/10.1016/j.mechmachtheory.2011.01.003>. [Online]. Available: <http://www.sciencedirect.com/science/article/pii/S0094114X11000139>.

- [104] M. M. Rutkowski, P. J. Smolinski, and M. C. Miller, "The geometry of vacuum assisted interface adhesion: Resistance to axial moment," *Vacuum*, vol. 83, no. 5, pp. 869–872, 2009, ISSN: 0042-207X. DOI: <https://doi.org/10.1016/j.vacuum.2008.09.004>. [Online]. Available: <http://www.sciencedirect.com/science/article/pii/S0042207X08004661>.
- [105] —, "The geometry of vacuum assisted interface adhesion: Resistance to axial moment," *Vacuum*, vol. 83, no. 5, pp. 869–872, 2009, ISSN: 0042-207X. DOI: <https://doi.org/10.1016/j.vacuum.2008.09.004>. [Online]. Available: <http://www.sciencedirect.com/science/article/pii/S0042207X08004661>.
- [106] G. Mantriota and A. Messina, "Theoretical and experimental study of the performance of flat suction cups in the presence of tangential loads," *Mechanism and Machine Theory*, vol. 46, no. 5, pp. 607–617, 2011, ISSN: 0094114X. DOI: [10.1016/j.mechmachtheory.2011.01.003](https://doi.org/10.1016/j.mechmachtheory.2011.01.003). [Online]. Available: <http://dx.doi.org/10.1016/j.mechmachtheory.2011.01.003>.
- [107] OnRobot, *Datasheet Hex-e/h qc*.
- [108] G. A. Kebede, A. R. Ahmad, S. C. Lee, and C. Y. Lin, "Decoupled six-axis force–moment sensor with a novel strain gauge arrangement and error reduction techniques," *Sensors (Switzerland)*, vol. 19, no. 13, 2019, ISSN: 14248220. DOI: [10.3390/s19133012](https://doi.org/10.3390/s19133012).
- [109] H. Akbari and A. Kazerooni, "Improving the coupling errors of a Maltese cross-beams type six-axis force/moment sensor using numerical shape-optimization technique," *Measurement: Journal of the International Measurement Confederation*, vol. 126, 2018, ISSN: 02632241. DOI: [10.1016/j.measurement.2018.05.074](https://doi.org/10.1016/j.measurement.2018.05.074).
- [110] B Shimano and B Roth, "On Force Sensing Information and Its Use in Controlling Manipulators," *IFAC Proceedings Volumes*, vol. 10, no. 11, pp. 119–126, 1977, ISSN: 14746670. DOI: [10.1016/S1474-6670\(17\)66591-1](https://doi.org/10.1016/S1474-6670(17)66591-1). [Online]. Available: [http://dx.doi.org/10.1016/S1474-6670\(17\)66591-1](http://dx.doi.org/10.1016/S1474-6670(17)66591-1).
- [111] A. S. Sadun, J Jalani, and J. A. Sukor, "Force Sensing Resistor (FSR): a brief overview and the low-cost sensor for active compliance control," *First International Workshop on Pattern Recognition*, vol. 10011, no. December, p. 1 001 112, 2016, ISSN: 1996756X. DOI: [10.1117/12.2242950](https://doi.org/10.1117/12.2242950).
- [112] E. I. Velásquez, V. Gómez, L. Paredes-Madrid, and H. A. Colorado, "Error compensation in force sensing resistors," *Sensing and Bio-Sensing Research*, vol. 26, no. April, p. 100 300, 2019, ISSN: 22141804. DOI: [10.1016/j.sbsr.2019.100300](https://doi.org/10.1016/j.sbsr.2019.100300). [Online]. Available: <https://doi.org/10.1016/j.sbsr.2019.100300>.
- [113] F Beyeler, S Muntwyler, and B. J. Nelson, "Design and calibration of a micro-fabricated 6-axis force-torque sensor for microrobotic applications," *Proceedings - IEEE International Conference on Robotics and Automation*, pp. 520–525, 2009, ISSN: 10504729. DOI: [10.1109/ROBOT.2009.5152253](https://doi.org/10.1109/ROBOT.2009.5152253).
- [114] K. Kim, Y. Sun, R. M. Voyles, and B. J. Nelson, "Calibration of multi-axis MEMS force sensors using the shape-from-motion method," *IEEE Sensors Journal*, vol. 7, no. 3, pp. 344–351, 2007, ISSN: 1530437X. DOI: [10.1109/JSEN.2006.890141](https://doi.org/10.1109/JSEN.2006.890141).

- [115] U. Kim, Y. B. Kim, D. Y. Seok, J. So, and H. R. Choi, "A surgical palpation probe with 6-axis force/torque sensing capability for minimally invasive surgery," *IEEE Transactions on Industrial Electronics*, vol. 65, no. 3, pp. 2755–2765, 2018, ISSN: 02780046. DOI: [10.1109/TIE.2017.2739681](https://doi.org/10.1109/TIE.2017.2739681).
- [116] D.-h. Lee, U. Kim, H. Jung, and H. R. Choi, "A Capacitive-Type Novel Six-Axis Force / Torque Sensor for Robotic Applications," vol. 16, no. 8, pp. 2290–2299, 2016.
- [117] U. Kim, D. H. Lee, Y. B. Kim, D. Y. Seok, and H. R. Choi, "A novel six-axis force/torque sensor for robotic applications," *IEEE/ASME Transactions on Mechatronics*, vol. 22, no. 3, pp. 1381–1391, 2017, ISSN: 10834435. DOI: [10.1109/TMECH.2016.2640194](https://doi.org/10.1109/TMECH.2016.2640194).
- [118] Y. Noh, J. Bimbo, S. Sareh, H. Wurdemann, J. Fraš, D. S. Chathuranga, H. Liu, J. Housden, K. Althoefer, and K. Rhode, "Multi-Axis force/torque sensor based on Simply-Supported beam and optoelectronics," *Sensors (Switzerland)*, vol. 16, no. 11, 2016, ISSN: 14248220. DOI: [10.3390/s16111936](https://doi.org/10.3390/s16111936).
- [119] B. Huang, X. Wang, C. Li, J. Yi, R. Lu, and J. Tao, "Development and calibration of an air-floating six-axis force measurement platform using self-calibration," *Review of Scientific Instruments*, vol. 87, no. 9, 2016, ISSN: 10897623. DOI: [10.1063/1.4962042](https://doi.org/10.1063/1.4962042). [Online]. Available: <http://dx.doi.org/10.1063/1.4962042>.
- [120] Y. jun Li, C. Yang, G. cong Wang, H. Zhang, H. yong Cui, and Y. liang Zhang, "Research on the parallel load sharing principle of a novel self-decoupled piezoelectric six-dimensional force sensor," *ISA Transactions*, vol. 70, pp. 447–457, 2017, ISSN: 00190578. DOI: [10.1016/j.isatra.2017.07.008](https://doi.org/10.1016/j.isatra.2017.07.008). [Online]. Available: <http://dx.doi.org/10.1016/j.isatra.2017.07.008>.
- [121] F. Becker, R. Jäger, F. Schmidt, B. Lapatki, and O. Paul, "Miniaturized six-degree-of-freedom force/moment transducers for instrumented teeth," *IEEE Sensors Journal*, vol. 17, no. 12, pp. 3644–3655, 2017, ISSN: 1530437X. DOI: [10.1109/JSEN.2017.2696035](https://doi.org/10.1109/JSEN.2017.2696035).
- [122] C. Jacq, B. Lüthi, T. Maeder, O. Lamercy, R. Gassert, and P. Ryser, "Thick-film multi-DOF force/torque sensor for wrist rehabilitation," *Sensors and Actuators, A: Physical*, vol. 162, no. 2, pp. 361–366, 2010, ISSN: 09244247. DOI: [10.1016/j.sna.2010.01.014](https://doi.org/10.1016/j.sna.2010.01.014). [Online]. Available: <http://dx.doi.org/10.1016/j.sna.2010.01.014>.
- [123] Q. Liang, D. Zhang, Q. Song, Y. Ge, H. Cao, and Y. Ge, "Design and fabrication of a six-dimensional wrist force/torque sensor based on E-type membranes compared to cross beams," *Measurement: Journal of the International Measurement Confederation*, vol. 43, no. 10, pp. 1702–1719, 2010, ISSN: 02632241. DOI: [10.1016/j.measurement.2010.09.010](https://doi.org/10.1016/j.measurement.2010.09.010).
- [124] N. Krouglicof, L. M. Alonso, and W. D. Keat, "Development of a mechanically coupled, six degree-of-freedom load platform for biomechanics and sports medicine," *Conference Proceedings - IEEE International Conference on Systems, Man and Cybernetics*, vol. 5, pp. 4426–4431, 2004, ISSN: 1062922X. DOI: [10.1109/ICSMC.2004.1401228](https://doi.org/10.1109/ICSMC.2004.1401228).
- [125] Y. Zhao, C. Zhang, D. Zhang, Z. Shi, and T. Zhao, "Mathematical model and calibration experiment of a large measurement range flexible joints 6-UPUR six-axis force sensor," *Sensors (Switzerland)*, vol. 16, no. 8, 2016, ISSN: 14248220. DOI: [10.3390/s16081271](https://doi.org/10.3390/s16081271).

- [126] F Ballo, M Gobbi, G Mastinu, and G Previati, "Advances in Force and Moments Measurements by an Innovative Six-axis Load Cell," *Experimental Mechanics*, vol. 54, no. 4, pp. 571–592, 2014, ISSN: 17412765. DOI: [10.1007/s11340-013-9824-4](https://doi.org/10.1007/s11340-013-9824-4).
- [127] J. W. Joo, K. S. Na, and D. I. Kang, "Design and evaluation of a six-component load cell," *Measurement: Journal of the International Measurement Confederation*, vol. 32, no. 2, pp. 125–133, 2002, ISSN: 02632241. DOI: [10.1016/S0263-2241\(02\)00002-7](https://doi.org/10.1016/S0263-2241(02)00002-7).
- [128] T Yoshikawa and T Miyazaki, "A six-axis force sensor with three-dimensional cross-shape structure," in *Proceedings, 1989 International Conference on Robotics and Automation*, 1989, 249–255 vol.1. DOI: [10.1109/ROBOT.1989.99997](https://doi.org/10.1109/ROBOT.1989.99997).
- [129] G. S. Kim, "Design of a six-axis wrist force/moment sensor using FEM and its fabrication for an intelligent robot," *Sensors and Actuators, A: Physical*, vol. 133, no. 1, pp. 27–34, 2007, ISSN: 09244247. DOI: [10.1016/j.sna.2006.03.038](https://doi.org/10.1016/j.sna.2006.03.038).
- [130] J.-J. Park and G.-S. Kim, "Development of the 6-axis force/moment sensor for an intelligent robot's gripper," *Sensors and Actuators A: Physical*, vol. 118, no. 1, pp. 127–134, 2005, ISSN: 09244247. DOI: [10.1016/j.sna.2004.07.013](https://doi.org/10.1016/j.sna.2004.07.013).
- [131] T. Liu, Y. Inoue, and K. Shibata, "Wearable force sensor with parallel structure for measurement of ground-reaction force," *Measurement*, vol. 40, no. 6, pp. 644–653, 2007, ISSN: 0263-2241. DOI: <https://doi.org/10.1016/j.measurement.2006.08.008>. [Online]. Available: <https://www.sciencedirect.com/science/article/pii/S0263224106001692>.
- [132] S. A. Liu and H. L. Tzo, "A novel six-component force sensor of good measurement isotropy and sensitivities," *Sensors and Actuators A: Physical*, vol. 100, no. 2-3, pp. 223–230, Sep. 2002, ISSN: 09244247. DOI: [10.1016/S0924-4247\(02\)00135-8](https://doi.org/10.1016/S0924-4247(02)00135-8). [Online]. Available: <https://linkinghub.elsevier.com/retrieve/pii/S0924424702001358>.
- [133] A. Parmiggiani, M. Maggiali, L. Natale, F. Nori, A. Schmitz, N. Tsagarakis, J. S. Victor, F. Becchi, G. Sandini, and G. Metta, "The design of the iCub humanoid robot," *International Journal of Humanoid Robotics*, vol. 9, no. 4, 2012, ISSN: 02198436. DOI: [10.1142/S0219843612500272](https://doi.org/10.1142/S0219843612500272).
- [134] L. Feng, G. Lin, W. Zhang, H. Pang, and T. Wang, "Design and optimization of a self-decoupled six-axis wheel force transducer for a heavy truck," *Proceedings of the Institution of Mechanical Engineers, Part D: Journal of Automobile Engineering*, vol. 229, no. 12, pp. 1585–1610, 2015, ISSN: 09544070. DOI: [10.1177/0954407014566439](https://doi.org/10.1177/0954407014566439).
- [135] J. Yao, H. Zhang, X. Xiang, H. Bai, and Y. Zhao, "A 3-D printed redundant six-component force sensor with eight parallel limbs," *Sensors and Actuators, A: Physical*, vol. 247, pp. 90–97, 2016, ISSN: 09244247. DOI: [10.1016/j.sna.2016.05.041](https://doi.org/10.1016/j.sna.2016.05.041). [Online]. Available: <http://dx.doi.org/10.1016/j.sna.2016.05.041>.
- [136] C. Yuan, L. P. Luo, Q. Yuan, J. Wu, R. J. Yan, H. Kim, K. S. Shin, and C. S. Han, "Development and evaluation of a compact 6-axis force/moment sensor with a serial structure for the humanoid robot foot," *Measurement: Journal of the International Measurement Confederation*, vol. 70, pp. 110–122, 2015, ISSN: 02632241. DOI: [10.1016/j.measurement.2015.03.027](https://doi.org/10.1016/j.measurement.2015.03.027). [Online]. Available: <http://dx.doi.org/10.1016/j.measurement.2015.03.027>.

- [137] C. Y. Lin, A. R. Ahmad, and G. A. Kebede, "Novel mechanically fully decoupled six-axis force-moment sensor," *Sensors (Switzerland)*, vol. 20, no. 2, 2020, ISSN: 14248220. DOI: [10.3390/s20020395](https://doi.org/10.3390/s20020395).
- [138] B. Wu and P. Cai, "Decoupling analysis of a sliding structure six-axis force/torque sensor," *Measurement Science Review*, vol. 13, no. 4, pp. 187–193, 2013, ISSN: 13358871. DOI: [10.2478/msr-2013-0028](https://doi.org/10.2478/msr-2013-0028).
- [139] M.-K. Kang, S. Lee, and J.-H. Kim, "Shape optimization of a mechanically decoupled six-axis force/torque sensor," *Sensors and Actuators A: Physical*, vol. 209, pp. 41–51, Mar. 2014, ISSN: 09244247. DOI: [10.1016/j.sna.2014.01.001](https://doi.org/10.1016/j.sna.2014.01.001). [Online]. Available: <https://linkinghub.elsevier.com/retrieve/pii/S092442471400003X>.
- [140] L. P. Chao and K. T. Chen, "Shape optimal design and force sensitivity evaluation of six-axis force sensors," *Sensors and Actuators, A: Physical*, vol. 63, no. 2, pp. 105–112, 1997, ISSN: 09244247. DOI: [10.1016/S0924-4247\(97\)01534-3](https://doi.org/10.1016/S0924-4247(97)01534-3).
- [141] V. D. Scheinman and B Shimano, *A preliminary work on implementing a manipulator force sensing wrist*, 1971.
- [142] A. R. Ahmad, T. Wynn, and C.-y. Lin, "A Comprehensive Design of Six-Axis Force / Moment Sensor," pp. 1–18, 2021.
- [143] Y. Wang, G. Zuo, X. Chen, and L. Liu, "Strain Analysis of Six-Axis Force/Torque Sensors Based on Analytical Method," *IEEE Sensors Journal*, vol. 17, no. 14, 2017, ISSN: 1530437X. DOI: [10.1109/JSEN.2017.2703160](https://doi.org/10.1109/JSEN.2017.2703160).
- [144] J. Ma and A. Song, "Fast estimation of strains for cross-beams six-axis force/torque sensors by mechanical modeling," *Sensors (Switzerland)*, vol. 13, no. 5, pp. 6669–6686, 2013, ISSN: 14248220. DOI: [10.3390/s130506669](https://doi.org/10.3390/s130506669).
- [145] J. Huang, C. Y. Wong, D. T. Pham, Y. Wang, C. Ji, S. Su, W. Xu, Q. Liu, and Z. Zhou, "Design of a novel six-axis force/torque sensor based on optical fibre sensing for robotic applications," *ICINCO 2018 - Proceedings of the 15th International Conference on Informatics in Control, Automation and Robotics*, vol. 1, no. Icinco, pp. 517–524, 2018. DOI: [10.5220/0006911705170524](https://doi.org/10.5220/0006911705170524).
- [146] L. Fu and A. Song, "Dynamic characteristics analysis of the six-axis force/torque sensor," *Journal of Sensors*, vol. 2018, 2018, ISSN: 16877268. DOI: [10.1155/2018/6216979](https://doi.org/10.1155/2018/6216979).
- [147] Y. Sun, Y. Liu, and H. Liu, "Temperature Compensation for a Six-Axis Force/Torque Sensor Based on the Particle Swarm Optimization Least Square Support Vector Machine for Space Manipulator," *IEEE Sensors Journal*, vol. 16, no. 3, pp. 798–805, 2016, ISSN: 1530437X. DOI: [10.1109/JSEN.2015.2485258](https://doi.org/10.1109/JSEN.2015.2485258).
- [148] Shih-Ping Han, "SUPERLINEARLY CONVERGENT VARIABLE METRIC ALGORITHMS FOR GENERAL NONLINEAR PROGRAMMING PROBLEMS*," *Mathematical Programming*, vol. 11, pp. 263–282, 1976.
- [149] Y. Sun, Y. Liu, M. Jin, and H. Liu, "Design of a novel six-axis force/torque sensor based on strain gauges by finite element method," *Proceedings of the World Congress on Intelligent Control and Automation (WCICA)*, vol. 2015-March, no. March, pp. 3387–3392, 2015. DOI: [10.1109/WCICA.2014.7053277](https://doi.org/10.1109/WCICA.2014.7053277).
- [150] M Uchiyama and E Bayo, "to Minimize a Performance Index for Robot Force Sensors 1," no. 1987, 1991.

- [151] E. Bayo and J. Stubbe, "Six-axis force sensor evaluation and a new type of optimal frame truss design for robotic applications," *J. Field Robotics*, vol. 6, pp. 191–208, 1989.
- [152] *Series Y, Strain gages, Data sheet, B4709*.
- [153] E. Zalnezhad, A. A. D Sarhan, M. Hamdi Abd Shukor, A. A. Sarhan, M. Hamdi, and B. Asri, "A Fuzzy Logic Based Model to Predict the Fretting Fatigue Life of Aerospace Al7075-T6 Alloy," *Caspian Journal of Applied Sciences Research*, no. 12, pp. 39–48, 2012. [Online]. Available: <http://www.cjasr.com>.
- [154] H. Gothäll, *How to Inspect Your Mesh in COMSOL Multiphysics*, 2017. [Online]. Available: <https://www.comsol.com/blogs/how-to-inspect-your-mesh-in-comsol-multiphysics/>.
- [155] R. M. Voyles, J. D. Morrow, and P. K. Khosla, "The shape from motion approach to rapid and precise force/torque sensor calibration," *Journal of Dynamic Systems, Measurement and Control, Transactions of the ASME*, vol. 119, no. 2, pp. 229–235, 1997, ISSN: 15289028. DOI: [10.1115/1.2801238](https://doi.org/10.1115/1.2801238).
- [156] C. G. Kang, "Performance improvement of a 6-Axis force-torque sensor via novel electronics and cross-shaped double-hole structure," *International Journal of Control, Automation and Systems*, vol. 3, no. 3, pp. 469–476, 2005, ISSN: 15986446.
- [157] G.-s. Kim, "Design and fabrication of a six-component force r moment sensor," 1999.
- [158] M. Glaskin, "Climbing the walls," *Engineering (London)*, vol. 239, no. 10, p. 38, 1998, ISSN: 00137782. DOI: [10.5749/j.ctvf34hkf.5](https://doi.org/10.5749/j.ctvf34hkf.5).
- [159] M. Rachkov and V. Bebenin, "Automatic two-stage vacuum gripper system," *Proceedings - 2018 International Conference on Industrial Engineering, Applications and Manufacturing, ICIEAM 2018*, pp. 27–30, 2018. DOI: [10.1109/ICIEAM.2018.8728733](https://doi.org/10.1109/ICIEAM.2018.8728733).
- [160] X. Cheng, Y. Hou, and M. T. Mason, "Manipulation with Suction Cups using External Contacts," *International Symposium on Robotics Research*, pp. 1–16, 2019.
- [161] J. Schmalz, L. Giering, M. Hölzle, N. Huber, and G. Reinhart, "Method for the Automated Dimensioning of Gripper Systems," *Procedia CIRP*, vol. 44, pp. 239–244, 2016, ISSN: 22128271. DOI: [10.1016/j.procir.2016.02.106](https://doi.org/10.1016/j.procir.2016.02.106). [Online]. Available: <http://dx.doi.org/10.1016/j.procir.2016.02.106>.
- [162] G. J. Monkman, S. Hesse, R. Steinmann, and H. Schunk, *Robot grippers*. John Wiley & Sons, 2007.
- [163] G. Mantriota, "Theoretical model of the grasp with vacuum gripper," *Mechanism and Machine Theory*, vol. 42, no. 1, pp. 2–17, 2007, ISSN: 0094114X. DOI: [10.1016/j.mechmachtheory.2006.03.003](https://doi.org/10.1016/j.mechmachtheory.2006.03.003).
- [164] A. J. Valencia, R. M. Idrovo, A. D. Sappa, D. P. Guingla, and D. Ochoa, "A 3D vision based approach for optimal grasp of vacuum grippers," *Proceedings of the 2017 IEEE International Workshop of Electronics, Control, Measurement, Signals and their Application to Mechatronics, ECMSM 2017*, 2017. DOI: [10.1109/ECMSM.2017.7945886](https://doi.org/10.1109/ECMSM.2017.7945886).

- [165] J. Mahler, M. Matl, X. Liu, A. Li, D. Gealy, and K. Goldberg, "Dex-Net 3.0: Computing Robust Vacuum Suction Grasp Targets in Point Clouds Using a New Analytic Model and Deep Learning," *Proceedings - IEEE International Conference on Robotics and Automation*, pp. 5620–5627, 2018, ISSN: 10504729. DOI: [10.1109/ICRA.2018.8460887](https://doi.org/10.1109/ICRA.2018.8460887).
- [166] A. Betnardin, C. Duriez, and M. Marchal, "An Interactive Physically-based Model for Active Suction Phenomenon Simulation," *IEEE International Conference on Intelligent Robots and Systems*, pp. 1466–1471, 2019, ISSN: 21530866. DOI: [10.1109/IRoS40897.2019.8967526](https://doi.org/10.1109/IRoS40897.2019.8967526).
- [167] F. Gabriel, M. Fahning, J. Meiners, F. Dietrich, and K. Dröder, "Modeling of vacuum grippers for the design of energy efficient vacuum-based handling processes," *Production Engineering*, vol. 14, no. 5-6, pp. 545–554, 2020, ISSN: 18637353. DOI: [10.1007/s11740-020-00990-9](https://doi.org/10.1007/s11740-020-00990-9). [Online]. Available: <https://doi.org/10.1007/s11740-020-00990-9>.
- [168] M. Higashimori, M. Kaneko, A. Namiki, and M. Ishikawa, "Design of the 100G capturing robot based on dynamic preshaping," *International Journal of Robotics Research*, vol. 24, no. 9, pp. 743–753, 2005, ISSN: 02783649. DOI: [10.1177/0278364905057058](https://doi.org/10.1177/0278364905057058).
- [169] R. Sam and N. Buniyamin, "A Bernoulli principle based flexible handling device for automation of food manufacturing processes," in *2012 International Conference on Control, Automation and Information Sciences, ICCAIS 2012*, 2012, pp. 214–219, ISBN: 978-1-4673-0812-0. DOI: [10.1109/ICCAIS.2012.6466590](https://doi.org/10.1109/ICCAIS.2012.6466590).
- [170] R. Sam and S. Nefti-meziari, "A novel, flexible and multi-functional handling device based on Bernoulli principle," 2011. DOI: [10.1109/ICSEngT.2011.5993443](https://doi.org/10.1109/ICSEngT.2011.5993443).
- [171] A. Petterson, T. Ohlsson, D. G. Caldwell, S. Davis, J. O. Gray, and T. J. Dodd, *SURFconext - Select an institution to login to the service TU Delft Library EZProxy server hosted by OCLC*, Oct. 2010. [Online]. Available: <https://www-emerald-com.tudelft.idm.oclc.org/insight/content/doi/10.1108/01439911011081669/full/html>.
- [172] *ROCHU: Soft Robotics Gripper Factory*. [Online]. Available: <https://www.softroboticgripper.com/gripper-combination-1/heavy-type-soft-robotic-gripper>.
- [173] G. Miron, B. Bédard, and J.-S. Plante, "Sleeved Bending Actuators for Soft Grippers: A Durable Solution for High Force-to-Weight Applications," *Actuators*, vol. 7, p. 40, 2018. DOI: [10.3390/act7030040](https://doi.org/10.3390/act7030040).
- [174] Y. Hao, Z. Gong, Z. Xie, S. Guan, X. Yang, T. Wang, and L. Wen, "A Soft Bionic Gripper with Variable Effective Length," *Journal of Bionic Engineering*, vol. 15, pp. 220–235, 2018. DOI: [10.1007/s42235-018-0017-9](https://doi.org/10.1007/s42235-018-0017-9).
- [175] J. F. G. Poovathy, S Sahoo, S Eswaramoorthy, M Gopalan, U Ramachandraiab, and A. R. Rao, "Modeling of a Suction Chamber based Wall Climbing Robot for Angular Stability," in *2020 IEEE International Instrumentation and Measurement Technology Conference (I2MTC)*, 2020, pp. 1–6. DOI: [10.1109/I2MTC43012.2020.9128606](https://doi.org/10.1109/I2MTC43012.2020.9128606).
- [176] h. Bingshan and H. Yu, "Optimal Design and Simulation of a Microsuction Cup Integrated with a Valveless Piezoelectric Pump for Robotics," *Shock and Vibration*, vol. 2018, pp. 1–16, 2018. DOI: [10.1155/2018/7987502](https://doi.org/10.1155/2018/7987502).

- [177] Festo, "Brief overview and basic principles of vacuum technology," *Whitepaper*, p. 54, 2012.
- [178] J. M. Krahn, F Fabbro, and C Menon, "A Soft-Touch Gripper for Grasping Delicate Objects," *IEEE/ASME Transactions on Mechatronics*, vol. 22, no. 3, pp. 1276–1286, 2017. DOI: [10.1109/TMECH.2017.2663322](https://doi.org/10.1109/TMECH.2017.2663322).
- [179] L. Al Abeach, S. Nefti-meziari, T. Theodoridis, and S. Davis, "A Variable Stiffness Soft Gripper Using Granular Jamming and Biologically Inspired Pneumatic Muscles," *Journal of Bionic Engineering*, vol. 15, pp. 236–246, 2018. DOI: [10.1007/s42235-018-0018-8](https://doi.org/10.1007/s42235-018-0018-8).
- [180] J. R. Amend, E Brown, N Rodenberg, H. M. Jaeger, and H Lipson, "A Positive Pressure Universal Gripper Based on the Jamming of Granular Material," *IEEE Transactions on Robotics*, vol. 28, no. 2, pp. 341–350, 2012. DOI: [10.1109/TR0.2011.2171093](https://doi.org/10.1109/TR0.2011.2171093).
- [181] Z Dong, G Gao, H Wang, and Y Du, "Study on Deformation and Contact Force Stability of a Novel Flexible Self-Adaptive Picking Manipulator," in *2018 2nd IEEE Advanced Information Management, Communicates, Electronic and Automation Control Conference (IMCEC)*, 2018, pp. 759–763. DOI: [10.1109/IMCEC.2018.8469512](https://doi.org/10.1109/IMCEC.2018.8469512).
- [182] D. Aukes, B. Heyneman, J. Ulmen, H. Stuart, M. Cutkosky, S. Kim, P. Garcia, and A. Edsinger, "Design and testing of a selectively compliant underactuated hand," *The International Journal of Robotics Research*, vol. 33, pp. 721–735, 2014. DOI: [10.1177/0278364913518997](https://doi.org/10.1177/0278364913518997).
- [183] H. K. Yap, H. Ng, and R. C.-H. Yeow, "High-Force Soft Printable Pneumatics for Soft Robotic Applications," *Soft Robotics*, vol. 3, pp. 144–158, 2016. DOI: [10.1089/soro.2016.0030](https://doi.org/10.1089/soro.2016.0030).
- [184] A Mohammadi, J Lavranos, Y Tan, P Choong, and D Oetomo, "A Paediatric 3D-Printed Soft Robotic Hand Prosthesis for Children with Upper Limb Loss," in *2020 42nd Annual International Conference of the IEEE Engineering in Medicine Biology Society (EMBC)*, 2020, pp. 3310–3313. DOI: [10.1109/EMBC44109.2020.9176848](https://doi.org/10.1109/EMBC44109.2020.9176848).
- [185] Wei-chen Lee and Chih-Wei Wu, "A novel design of a prosthetic hand," in *2010 IEEE International Conference on Systems, Man and Cybernetics*, 2010, pp. 1821–1824. DOI: [10.1109/ICSMC.2010.5642290](https://doi.org/10.1109/ICSMC.2010.5642290).
- [186] FESTO, "Parallel gripper DHPS," 2021, [Online]. Available: https://www.festo.com/cat/nl_nl/data/doc_engb/PDF/EN/DHPS_EN.PDF.
- [187] —, "Angle grippers DHWS," 2021, [Online]. Available: https://www.festo.com/cat/nl_nl/data/doc_engb/PDF/EN/DHWS_EN.PDF.
- [188] H Frank, D Barteit, N Wellerdick-Wojtasik, T Frank, G Novak, and S Mahlknecht, "Autonomous Mechanical Controlled Grippers for Capturing Flying Objects," in *2007 5th IEEE International Conference on Industrial Informatics*, vol. 1, 2007, pp. 431–436. DOI: [10.1109/INDIN.2007.4384796](https://doi.org/10.1109/INDIN.2007.4384796).
- [189] Shadow Robot, "Shadow Dexterous Hand E1 Series (E1M3R, E1M3L, E1P1R, E1P1L)," no. January, pp. 1–14, 2013. [Online]. Available: http://www.shadowrobot.com/wp-content/uploads/shadow_dexterous_hand_technical_specification_E1_20130101.pdf.

- [190] A Namiki, Y Imai, M Ishikawa, and M Kaneko, "Development of a high-speed multifingered hand system and its application to catching," in *Proceedings 2003 IEEE/RSJ International Conference on Intelligent Robots and Systems (IROS 2003) (Cat. No.03CH37453)*, vol. 3, 2003, pp. 2666–2671. DOI: [10.1109/IROS.2003.1249273](https://doi.org/10.1109/IROS.2003.1249273).
- [191] SCHUNK, "Modular and Mobile Gripping Systems through Modularity," [Online]. Available: <https://schunk.com/fileadmin/pim/docs/IM0019885.PDF>.
- [192] I. N. Gaiser, C. Pylatiuk, S. Schulz, A. Kargov, R. Oberle, and T. Werner, "The FLUIDHAND III: A Multifunctional Prosthetic Hand," *JPO Journal of Prosthetics and Orthotics*, vol. 21, no. 2, 91–96, Apr. 2009. DOI: [10.1097/jpo.0b013e3181a1ca54](https://doi.org/10.1097/jpo.0b013e3181a1ca54).
- [193] PRENSILA, "Multipurpose platform EH1 MILANO series," 2010, [Online]. Available: http://mindtrans.narod.ru/pdfs/EH1_Milano_Hand.pdf.
- [194] M. Ciocarlie, F. M. Hicks, R. Holmberg, J. Hawke, M. Schlicht, J. Gee, S. Stanford, and R. Bahadur, "The Velo gripper: A versatile single-actuator design for enveloping, parallel and fingertip grasps," *The International Journal of Robotics Research*, vol. 33, no. 5, pp. 753–767, 2014. DOI: [10.1177/0278364913519148](https://doi.org/10.1177/0278364913519148). [Online]. Available: <https://doi.org/10.1177/0278364913519148>.
- [195] I. Vujaklija, D Farina, and O Aszmann, "New developments in prosthetic arm systems," *Orthopedic Research and Reviews*, vol. 8, pp. 31–39, 2016.
- [196] R Werink, *Design and realization of a gripper for the SHERPA robotic arm*, Jul. 2016. [Online]. Available: <http://essay.utwente.nl/81333/>.
- [197] D. Aukes, B. Heyneman, J. Ulmen, H. Stuart, M. Cutkosky, S. Kim, P. Garcia, and A. Edsinger, "Design and testing of a selectively compliant underactuated hand," *The International Journal of Robotics Research*, vol. 33, pp. 721–735, 2014. DOI: [10.1177/0278364913518997](https://doi.org/10.1177/0278364913518997).
- [198] Y. Kamikawa and T. Maeno, "Underactuated Five-Finger Prosthetic Hand Inspired by Grasping Force Distribution of Humans," in *2008 IEEE/RSJ International Conference on Intelligent Robots and Systems, IROS*, vol. 74, 2008, pp. 717–722. DOI: [10.1109/IROS.2008.4650628](https://doi.org/10.1109/IROS.2008.4650628).
- [199] W. Zhang, G. Dai, F. Wang, S. Sun, and H. Bassir, "Using strain energy-based prediction of effective elastic properties in topology optimization of material microstructures," *Acta Mechanica Sinica*, vol. 23, no. 1, 77–89, 2007. DOI: [10.1007/s10409-006-0045-2](https://doi.org/10.1007/s10409-006-0045-2).
- [200] L. Yin and G. K. Ananthasuresh, "Design of Distributed Compliant Mechanisms," *Mechanics Based Design of Structures and Machines*, vol. 31, no. 2, pp. 151–179, 2003. DOI: [10.1081/SME-120020289](https://doi.org/10.1081/SME-120020289). [Online]. Available: <https://doi.org/10.1081/SME-120020289>.
- [201] E Fox and F. L. Hammond, "Soft Variable Stiffness Joints for Controllable Grasp Synergies in Underactuated Robotic Hands," in *2020 3rd IEEE International Conference on Soft Robotics (RoboSoft)*, 2020, pp. 586–592. DOI: [10.1109/RoboSoft48309.2020.9115995](https://doi.org/10.1109/RoboSoft48309.2020.9115995).
- [202] P. Jiang, Y. Yandong, M. Chen, and y. Chen, "A variable stiffness gripper based on differential drive particle jamming," *Bioinspiration & Biomimetics*, vol. 14, 2019. DOI: [10.1088/1748-3190/ab04d1](https://doi.org/10.1088/1748-3190/ab04d1).

- [203] H Nakamoto, M Ohtake, K Komoda, A Sugahara, and A Ogawa, "A Gripper System for Robustly Picking Various Objects Placed Densely by Suction and Pinching," in *2018 IEEE/RSJ International Conference on Intelligent Robots and Systems (IROS)*, 2018, pp. 6093–6098. DOI: [10.1109/IROS.2018.8593887](https://doi.org/10.1109/IROS.2018.8593887).
- [204] L. Kang, J.-T. Seo, S.-H. Kim, W.-J. Kim, and B.-J. Yi, "Design and Implementation of a Multi-Function Gripper for Grasping General Objects," *Applied Sciences*, vol. 9, p. 5266, 2019. DOI: [10.3390/app9245266](https://doi.org/10.3390/app9245266).
- [205] C. Hernández Corbato, M. Bharatheesha, W. Ko, H. Gaiser, J. Tan, K. Deurzen, M. Vries, B. Mil, J. Egmond, R. Burger, M. Morariu, J. Ju, X. Germann, R. Ensing, J. Frankenhuyzen, and M. Wisse, "Team Delft's Robot Winner of the Amazon Picking Challenge 2016," 2016.
- [206] H. Soemers, *Design principles for precision mechanisms*, Feb. 2015. [Online]. Available: <http://cds.cern.ch/record/1995001>.
- [207] *An image of a 1 DOF rigid gripper made by schunk*. Schunk, Nov. 2020. [Online]. Available: https://www.hmkrobotics.com/accessories_and_plug-ins/grippers/pneumatic-grippers/schunk/mpg-gripper/.
- [208] W.-c. Lee and C.-W. Wu, "A novel design of a prosthetic hand," in *Conference Proceedings - IEEE International Conference on Systems, Man and Cybernetics*, 2010, pp. 1821–1824. DOI: [10.1109/ICSMC.2010.5642290](https://doi.org/10.1109/ICSMC.2010.5642290).
- [209] A. Wilson, S. Wang, B. Romero, and E. Adelson, "Design of a Fully Actuated Robotic Hand With Multiple Gelsight Tactile Sensors," *CoRR*, vol. abs/2002.0, 2020. [Online]. Available: <https://arxiv.org/abs/2002.02474>.
- [210] C. Rossi, S. Savino, V. Niola, and S. Troncone, "A study of a robotic hand with tendon driven fingers," *Robotica*, vol. 33, pp. 1–15, 2014. DOI: [10.1017/S0263574714001179](https://doi.org/10.1017/S0263574714001179).
- [211] L Birglen, "Enhancing versatility and safety of industrial grippers with adaptive robotic fingers," in *2015 IEEE/RSJ International Conference on Intelligent Robots and Systems (IROS)*, 2015, pp. 2911–2916. DOI: [10.1109/IROS.2015.7353778](https://doi.org/10.1109/IROS.2015.7353778).
- [212] D Petkovic, N. D. Pavlovic, S. Shamshirband, and N Anuar, "Development of a new type of passively adaptive compliant gripper," *Ind. Robot*, vol. 40, pp. 610–623, 2013.
- [213] Y. S. Narang, J Vlassak, and R Howe, "Mechanically Versatile Soft Machines through Laminar Jamming," *Advanced Functional Materials*, vol. 28, p. 1707136, 2018.
- [214] *Image of the PIAB BL40-4*. [Online]. Available: <https://www.piab.com/Products/suction-cups/shape/multibellows/bl-4---bellows-long-30-50-mm/bl40-4/>.
- [215] J. Sprovieri, *Picture of a Soft Robotics gripper picking a donut*. Soft Robotics Introduces Modular, Flexible Gripper for UR Cobots, Nov. 2019. [Online]. Available: <https://www.assemblymag.com/articles/95318-soft-robotics-introduces-modular-flexible-grip>.
- [216] Q. Ge, A. H. Sakhaei, H. Lee, C. K. Dunn, N. X. Fang, and M. L. Dunn, "Multimaterial 4D Printing with Tailorable Shape Memory Polymers," *Scientific Reports*, vol. 6, no. 1, 2016. DOI: [10.1038/srep31110](https://doi.org/10.1038/srep31110).

- [217] G. Mantriota, "Theoretical model of the grasp with vacuum gripper," *Mechanism and Machine Theory*, vol. 42, no. 1, pp. 2–17, 2007, ISSN: 0094-114X. DOI: <https://doi.org/10.1016/j.mechmachtheory.2006.03.003>. [Online]. Available: <http://www.sciencedirect.com/science/article/pii/S0094114X06000577>.
- [218] K. Korane, *Vacuum cups: Key uses*, Feb. 2016. [Online]. Available: <https://www.pneumatictips.com/how-are-vacuum-cups-used/#:~:text=Vacuumcups%2CORSUCTIONCUPS,metal%2CPIPESANDGLASSWINDOWS..>
- [219] "No Title,"
- [220] K. D. Goepel, "METHOD FOR MULTI-CRITERIA DECISION MAKING IN CORPORATE 2 . AHP Spreadsheet Template 3 . Experiences in the practical application of AHP," *Proceedings of the International Symposium on the Analytic Hierarchy Process*, vol. 2, no. 10, pp. 1–10, 2013.
- [221] A. Song, J. Wu, G. Qin, and W. Huang, "A novel self-decoupled four degree-of-freedom wrist force/torque sensor," *Measurement: Journal of the International Measurement Confederation*, vol. 40, no. 9-10, pp. 883–891, 2007, ISSN: 02632241. DOI: [10.1016/j.measurement.2006.11.018](https://doi.org/10.1016/j.measurement.2006.11.018).
- [222] H. Weiyi, J. Hongming, and Z. Hanqing, "Mechanical analysis of a novel six-degree-of-freedom wrist force sensor," *Sensors and Actuators: A. Physical*, vol. 35, no. 3, pp. 203–208, 1993, ISSN: 09244247. DOI: [10.1016/0924-4247\(93\)80153-8](https://doi.org/10.1016/0924-4247(93)80153-8).
- [223] Y. Zhao, L. Jiao, D. Weng, D. Zhang, and R. Zheng, "Decoupling principle analysis and development of a parallel three-dimensional force sensor," *Sensors (Switzerland)*, vol. 16, no. 9, 2016, ISSN: 14248220. DOI: [10.3390/s16091506](https://doi.org/10.3390/s16091506).
- [224] Y. Sun, Y. Liu, T. Zou, M. Jin, and H. Liu, "Design and optimization of a novel six-axis force/torque sensor for space robot," *Measurement: Journal of the International Measurement Confederation*, vol. 65, pp. 135–148, 2015, ISSN: 02632241. DOI: [10.1016/j.measurement.2015.01.005](https://doi.org/10.1016/j.measurement.2015.01.005). [Online]. Available: <http://dx.doi.org/10.1016/j.measurement.2015.01.005>.
- [225] D. Chen, A. Song, and A. Li, "Design and Calibration of a Six-axis Force/torque Sensor with Large Measurement Range Used for the Space Manipulator," *Procedia Engineering*, vol. 99, pp. 1164–1170, 2015, ISSN: 18777058. DOI: [10.1016/j.proeng.2014.12.699](https://doi.org/10.1016/j.proeng.2014.12.699). [Online]. Available: <http://dx.doi.org/10.1016/j.proeng.2014.12.699>.
- [226] Q. Liang, W. Wu, G. Coppola, D. Zhang, W. Sun, Y. Ge, and Y. Wang, "Calibration and decoupling of multi-axis robotic Force/Moment sensors," *Robotics and Computer-Integrated Manufacturing*, vol. 49, no. May 2016, pp. 301–308, 2018, ISSN: 07365845. DOI: [10.1016/j.rcim.2017.08.008](https://doi.org/10.1016/j.rcim.2017.08.008).
- [227] H. S. Oh, G. Kang, U. Kim, J. K. Seo, W. S. You, and H. R. Choi, "Force/torque sensor calibration method by using deep-learning," *2017 14th International Conference on Ubiquitous Robots and Ambient Intelligence, URAI 2017*, pp. 777–782, 2017. DOI: [10.1109/URAI.2017.7992824](https://doi.org/10.1109/URAI.2017.7992824).
- [228] Y. Sun, Y. Li, Y. Liu, and H. Liu, "An online calibration method for six-dimensional force/torque sensor based on shape from motion combined with complex algorithm," *2014 IEEE International Conference on Robotics and Biomimetics, IEEE ROBOT 2014*, no. April, pp. 2631–2636, 2014. DOI: [10.1109/ROBOT.2014.7090739](https://doi.org/10.1109/ROBOT.2014.7090739).

- [229] J. Ma, A. Song, and J. Xiao, "A robust static decoupling algorithm for 3-axis force sensors based on coupling error model and -SVR," *Sensors (Switzerland)*, vol. 12, no. 11, pp. 14 537–14 555, 2012, ISSN: 14248220. DOI: [10.3390/s121114537](https://doi.org/10.3390/s121114537).
- [230] Y. Ma, S. Xie, X. Zhang, and Y. Luo, "Hybrid calibration method for six-component force/torque transducers of wind tunnel balance based on support vector machines," *Chinese Journal of Aeronautics*, vol. 26, no. 3, pp. 554–562, 2013, ISSN: 10009361. DOI: [10.1016/j.cja.2013.04.056](https://doi.org/10.1016/j.cja.2013.04.056). [Online]. Available: <http://dx.doi.org/10.1016/j.cja.2013.04.056>.
- [231] L. Schickl, K. Dorer, L. Schickl, K. Dorer, W Michael, Y. D. Antilio, and U. Hochberg, "Development of a Six-Axis Force and Torque Sensor for the Humanoid Robot Sweaty 2 . 0 Development of a Six-Axis Force and Torque Sensor for the Humanoid," no. November, 2016.